Mechanisms, influencing factors and manufacturing implication of prepreg tack in automated fiber placement

DOCTORAL THESIS

(Dissertation)

to be awarded the degree
Doctor of Engineering (Dr.-Ing.)

submitted by

Dennis Budelmann

from Bremen

approved by the Faculty of Natural and Material Science,
Clausthal University of Technology

Date of oral examination:
4 December 2024

Dean

Prof. Dr. René Wilhelm

Chairperson of the Board of Examiners

Prof. Dr.-Ing. Babette Tonn

Supervising tutor

Prof. Dr.-Ing. Dieter Meiners

Reviewers

Prof. Dr.-Ing. Axel S. Herrmann

Prof. Dr.-Ing. Martin Wiedemann

Acknowledgements

This doctoral thesis was prepared while working as a research assistant at the Institute of Polymer Materials and Plastics Engineering (Clausthal University of Technology) and has benefited in various ways from the support of a large number of people.
A special thanks goes to my academic supervisor Prof. Dr.-Ing. Dieter Meiners who assiduously mentored me throughout my studies while giving me the space to implement my own ideas. Thanks are also due to Prof. Dr.-Ing. Axel Herrmann and Prof. Dr.-Ing. Martin Wiedemann for agreeing to co-review this thesis.
I would like to thank Dr.-Ing. Carsten Schmidt who has been instrumental in developing the great working environment I found in the research group 'HP CFK'. It was a pleasure to work with the many colleagues both in Stade and Clausthal and I would like to thank all of them for their help and encouraging discussions. Special gratitude is expressed towards Tim Tiemann for helping me out with the lay-up simulation in conjunction with the case study.
I am deeply grateful to my fiancée Lisa Schmitz for her patience and everlasting loving support. A special thanks goes to my parents who unconditionally supported and believed in me at all time.
Lastly, I acknowledge the financial support by Deutsche Forschungsgemeinschaft (DFG) granted for the research project 'TackTIC' (Tack of Thermoset Impregnated Carbon Fibers, project number 458900231) as well as by the European Regional Development Fund (ERDF) and the federal state of Lower Saxony for the interdisciplinary research project 'FlexProCFK'.

Abstract

In an effort to tackle the technological and economical challenges linked to cost-effective production of composite parts in high-wage countries, automated manufacturing technologies have been established in different industries over the last decades. In the aviation sector, automated fiber placement (AFP) is a driving technique to efficiently manufacture large-scale, high-performance composite parts from carbon fiber/epoxy prepregs. Despite being industry standard since the late 1980s, the process is prone to manufacturing defects which result from insufficient adhesion of prepregs, commonly related to as prepreg tack.

In literature, prepreg tack has historically been investigated from segregated perspectives utilizing both diverse materials and measurement techniques eventually resulting in a lack of comparableness and transferability. There is evidence, however, to suggest that tack is a complex phenomenon that demands holistic consideration. This thesis therefore explores the involved mechanisms (surface wetting, contact formation, autohesion), process and environmental influencing factors (compaction pressure, lay-up speed, ageing, temperature), material criteria (resin type, B-staging, toughening), measurement effects (probe, peel testing) and manufacturing implication of prepreg tack in AFP.

Prepreg tack was found to be sensitive to all investigated influencing factors which could be ascribed to changes in material properties examined by comprehensive complementary material analysis. The employed measurement techniques were demonstrated to be suitable for prepreg tack measurement in terms of reproducibility and the ability to disclose adhesive mechanisms but were partially limited in terms of AFP process parameter representation. Therefore, the manufacturing implication of prepreg tack in AFP was assessed by utilizing a semi-empirical process model which was demonstrated to successfully replicate the characteristic bell-shaped tack curves plotted as a function of prepreg temperature for different lay-up scenarios. Experimentally founded and model-based recommendations are furthermore proposed to tailor formulations of thermoplastic toughened epoxy-based prepreg resins with regard to tackiness. The presented outcomes of this thesis provide an informed basis for process adjustment to meet manufacturing demands in terms of prepreg tackiness and therefore reduce the risk of laminate defects during automated prepreg lay-up.

Zusammenfassung

Im Bestreben, technologische und wirtschaftliche Herausforderungen im Zusammenhang mit der kosteneffizienten Produktion von Faserverbundbauteilen in Hochlohnländern zu bewältigen, wurden in den letzten Jahrzehnten automatisierte Fertigungstechnologien in einer Vielzahl von Branchen eingeführt. Im Luftfahrtsektor ist das Automated Fiber Placement (AFP) eine etablierte Fertigungstechnologie zur effizienten Herstellung von großformatigen, hochbelasteten Faserverbunden aus Kohlefaser/Epoxid-Prepregs. Obwohl das Verfahren seit den späten 1980er Jahren den Stand der Technik im Flugzeugbau darstellt, ist es anfällig für Fertigungsfehler, die häufig auf eine unzureichende Haftung der Prepregs zurückzuführen sind – eine Materialeigenschaft, die gemeinhin als Prepreg-Tack bezeichnet wird.

In der Forschungsliteratur wurde die Klebrigkeit von Prepregs in der Vergangenheit aus verschiedenen Blickwinkeln untersucht, wobei sowohl unterschiedliche Materialien als auch Messverfahren zum Einsatz kamen. In der Folge ist ein Vergleichbarkeits- und Übertragbarkeitsdefizit zu verzeichnen, während es Hinweise dafür gibt, dass es sich bei Prepreg-Tack um ein komplexes Phänomen handelt, welches holistische Betrachtung erfordert. In dieser Arbeit werden daher die zugrundeliegenden Mechanismen (Oberflächenbenetzung, Autohäsion, Kontaktausbildung), prozess- und umweltbedingte Faktoren (Alterung, Kompaktierungsdruck, Legegeschwindigkeit, Temperatur), Materialkriterien (Harztyp, Zäh-modifizierung, B-Staging), messtechnische Effekte (Stempel- und Schältest) sowie fertigungsrelevante Implikationen des Prepreg-Tacks im AFP eingehend untersucht.

Es wurde festgestellt, dass die Klebeeigenschaften von allen untersuchten Faktoren signifikant beeinflusst werden. Die Einflüsse konnten auf Veränderungen der Prepregeigenschaften zurückgeführt werden, die durch umfassende ergänzende Materialanalyse offengelegt wurden. Die eingesetzten Messverfahren erwiesen sich als geeignet für die Messung der Prepreg-Klebrigkeit in Bezug auf Reproduzierbarkeit und die Fähigkeit, zugrundeliegende Haftmechanismen zu erklären. Einschränkungen ergaben sich jedoch in Hinblick auf die messtechnische Repräsentation der AFP-Prozessparameter. Daher wurde die fertigungstechnische Reichweite des Prepreg-Tacks mithilfe eines semi-empirischen AFP-Prozessmodells

bewertet, das die charakteristischen glockenförmigen Klebrigkeitskurven als Funktion der Materialtemperatur für verschiedene Fertigungsszenarien erfolgreich reproduzierte. Darüber hinaus wurden experimentell begründete und modellgestützte Empfehlungen zur Anpassung von Formulierungen für thermoplastisch schlagzähmodifizierte Prepregs auf Epoxidharzbasis in Hinblick auf die Klebrigkeit erarbeitet. Die in dieser Arbeit vorgestellten Ergebnisse bieten dadurch eine fundierte Grundlage für Prozessanpassungen, um die Anforderungen an die Klebrigkeit von Prepregs zu erfüllen und somit das Risiko von Laminatdefekten während der automatisierten Prepregablage zu reduzieren.

Table of Contents

Acknowledgements II
Abstract IV
Nomenclature XI

1. Introduction 1

2. Thesis outline 5
   2.1 Objective 5
   2.2 Structure 8
   2.3 Publications and authorship contribution 13
      2.2.1 Publication I 14
      2.2.2 Publication II 15
      2.2.3 Publication III 16
      2.2.4 Publication IV 17
      2.2.5 Publication V 18

3. State of technology 19
   3.1 Composites in civil aviation 19
      3.1.1 Economic benefits and drawbacks 22
      3.1.2 Ecological impact 22
   3.2 Automated Fiber Placement (AFP) 24
      3.2.1 Process cycle 25
      3.2.2 Machinery 27
      3.2.3 Potentials and challenges 29
   3.3 Prepregs 31
      3.3.1. Components and composition 31
         3.3.1.1 Matrices 33
         3.3.1.2 Reinforcement fibers 37
      3.3.2 Production and cure process 38
      3.3.3. Tack(iness) 41

4. State of research – Publication I 43
   4.1 Introduction 45
   4.2 Role of prepreg tack in AFP/ATL 46
      4.2.1 General process considerations 46
      4.2.2 Production-induced defects 47
      4.2.3 Manufacturing-relevant factors affecting prepreg tack 49

4.3 Measurement 50
4.3.1 Probe tack test 51
4.3.2 Peel test 53
4.3.3 Other measurement techniques 53
4.4 Experimental studies 55
4.4.1 Process parameters 56
4.4.1.1 Temperature 57
4.4.1.2 Compaction force and time 59
4.4.1.3 Debonding rate 61
4.4.1.4 Contact material 62
4.4.2 Environmental factors 63
4.4.2.1 Ageing and DoC 64
4.4.2.2 Moisture 66
4.4.3 Material properties 68
4.4.3.1 Resin viscosity 68
4.4.3.2 Prepreg arcitecture and fiber volume fraction 71
4.5 Model approaches 72
4.6 Conclusion/future perspective 74
4.7 Research on prepreg tack after 2020 76
4.7.1 ASTM D8336 76
4.7.2 Studies focusing on the lay-up process 77
4.7.3 Studies focusing on materials 78
4.7.4 Studies focusing on tack fundamentals 78

5. Process and environmental parameters – Publication II 79
5.1 Introduction 81
5.2 Experimental 84
5.2.1 Materials 84
5.2.2 Test parameters raised from AFP/ATL and automated draping processes 85
5.2.3 Tack measurement 86
5.2.4 Differential scanning calorimetry 88
5.2.5 Rheology 89
5.3 Results and discussion 89
5.3.1 Prepreg (Material A) 89
5.3.2 Temperature 90
5.3.3 Compaction force 92
5.3.4 Lay-up speed 95
5.3.5 Prepreg ageing 96
5.3.6 Impregnated carbon tape for draping (Material B) 100
5.4 Conclusion 104

6. Adhesive mechanisms – Publication III 107
6.1 Introduction 109
6.2 Materials 112
6.2.1 Prepreg 112
6.2.2 Neat resin 112
6.2.3 Contact materials 113
6.3 Experimental methods and data analysis 114
6.3.1 Tack measurement 114
6.3.2 Wetting analysis 115
6.3.3 Rheology 116
6.3.4 Surface topography 117
6.4 Results and discussion 117
6.4.1 Surface tension (SFT) 117
6.4.2 Substrate wetting analysis of standard test liquids 120
6.4.3 Surface wetting of viscous prepreg resin 123
6.4.4 Role of adhesive attraction for prepreg tack 125
6.4.5 Rheological implication in resin surface wetting 128
6.4.6 Roughness-extended Dahlquist criterion 133
6.5 Conclusion 136

7. Prepreg resin formulation – Publication IV 139
7.1 Introduction 141
7.2 Materials 143
7.2.1 Model resin formulation 143
7.2.2 Sample preparation 144
7.3 Experimental methods 145
7.3.1 Differential scanning calorimetry 145
7.3.2 Cure kinetics 145
7.3.3 Rheology 146
7.3.4 Tack testing 146
7.4 Results and discussion 147
7.4.1 Cure kinetics 147
7.4.2 Influence of epoxy prepolymer on tack 150
7.4.3 Influence of B-staging on tack 153
7.4.4 Influence of toughening on tack 155
7.4.5 Manufacturing implication 156
7.5 Conclusion 158

8. Contact formation and autohesion – Publication V 161
8.1 Introduction 163
8.2 Materials 166
8.3 Experimental methods and data analysis 167
8.3.1 Tack measurement cycles 167
8.3.2 Peel testing procedure 169
8.3.3 Rheology 171
8.3.4 Degree of intimate contact (DoIC) 172
8.4 Results and discussion 173
8.4.1 Contact formation – experiment 173
8.4.2 Contact formation – model 175
8.4.3 Tack measured by standard isothermal peel test 176
8.4.4 Tack of fully contacted ply interfaces 178
8.4.5 Autohesion: Determination of relaxation time 180
8.4.6 Autohesion – model 182
8.4.7 Transfer to AFP scenarios 184
8.4.8 Adhesion-cohesion balance of prepreg tack 189
8.5 Conclusion 191

9. Implications for industrial practice 197
9.1 Case study: Lay-up of an aircraft part using AFP 197
9.1.1 Part geometry & stacking sequence 198
9.1.2 Lay-up simulation 199
9.1.3 Effect of tack control on lay-up time 200
9.2 AFP-oriented tack control of prepreg resins 203
9.3 Recommendations for tack testing in practice 205

10. Conclusion & Outlook 207
10.1 Recapitulation 207
10.2 Key findings 208
10.3 Future work 213

Figures, Tables, References 215
Further publications 215
Figures 216
Tables 225
References 227

Nomenclature

Abbreviations

Abbreviation	Description
AFP	Automated fiber placement
AHEW	Amine hydrogen equivalent weight
AI	Artificial intelligence
ASME	American Society of Mechanical Engineers
ASTM	American Society for Testing and Materials
ATL	Automated tape laying
BMC	Bulk molding compound
BMI	Bismaleimide
BP	Backing paper
CA	Contact angle
CFK	Kohlenstofffaserverstärkter Kunststoff
CFRP	Carbon fiber reinforced plastics
CMC	Ceramic matrix composites
CO_2	Carbon dioxide
CTI	Compression tack index
DDM	Data-driven model
DDS	4,4'diaminodiphenyl sulfone
DETA	Diethylenetriamine
DFG	Deutsche Forschungsgemeinschaft (German Research Foundation)
DGEBA	Bisphenol A diglycidyl ether
DICY	Dicyandiamide
DMA	Dynamic mechanical analysis
DoC	Degree of cure
DOE	Design of experiment
DOF	Degree of freedom
DoIC	Degree of intimate contact

Abbreviation	Description
DSC	Differential scanning calorimetry
EEW	Epoxy equivalent weight
ERDF	European Regional Development Fund
FPP	Fiber patch placement
FRP	Fiber-reinforced plastics
FVF	Fiber volume fraction
FVK	Faserverstärkte Kunststoffe
FW	Filament winding
FWO	Flynn Wall Ozawa (method)
GPC	Gel permeation chromatography
IMF	Intermolecular force
IUPAC	International Union of Pure and Applied Chemistry
LCA	Life Cycle Assessment
LVE	Linear viscoelastic (region)
ML	Machine learning
MMC	Metal matrix composites
NO_x	Nitrogen oxide
OoA	Out-of-autoclave
OWRK	Owens, Wendt, Rabel & Kaeble (method)
PAN	Polyacrylonitrile
PBM	Physics-based model
PEI	Polyetherimide
PES	Polyethersulfone
PI	Polyimide
PMC	Polymer matrix composites
PP	Polypropylene
PSA	Pressure sensitive adhesives
PU	Polyurethane
RH	Relative humidity
RTM	Resin transfer molding

Abbreviation	Description
SAMPE	Society for the Advancement of Materials and Process Engineering
SC	Spreading coefficient
SD	Standard deviation
SFE	Surface free energy
SFT	Surface tension
SiC	Silicon carbide
SMC	Sheet molding compound
ST	(Stainless) steel
ST_{pol}	Polished (stainless) steel
TackTIC	Tack of Thermoset Impregnated Carbon Fibers
Tan δ	Loss factor
T_g	Glass transition temperature
TGAP	Triglycidyl p-aminophenol
TGMDA	Tetraglycidyl-4,4'-methylenedianiline
THF	Tetrahydrofuran
TTS	Time temperature superposition (principle)
UD	Unidirectional
USA	United States of America
VBO	Vacuum bag-only
WLF	William Landel Ferry (equation)

Symbols[1]

Symbol	Description	Unit
a	Transition parameter	-
a_T	Rheological shift factor (TTS)	-
α	Degree of cure	%
β	Heating rate	K min^{-1}
C_1, C_2	Empirical constants (TTS)	-
CTI_σ	Compression tack index	-
$\dot{\gamma}$	Shear rate	s^{-1}
$\dot{\gamma}_c$	Critical shear rate	s^{-1}
d	Displacement	mm
D_a	Degree of autohesion	-
D_b	Degree of bonding	-
D_{ic}	Degree of intimate contact	-
D_{ic0}	Initial degree of intimate contact	-
E_a	Activation energy	J mol^{-1}
ε_a	Peel strain	-
F	Force	N
F_c	Compaction force	N
G	Fracture energy	J m^{-2}
G‘	Storage modulus	Pa
G’$_c$	Critical (storage) modulus	Pa
G“	Loss modulus	Pa
G_{auto}	Fracture energy (autohesion test cycle)	J m^{-2}
G_{fc}	Fracture energy (full contact test cycle)	J m^{-2}
G_p	Plastic portion of fracture energy	J m^{-2}
G_{std}	Fracture energy (standard test cycle)	J m^{-2}
G_∞	Fracture energy of fully healed surfaces	J m^{-2}
η^*	Complex viscosity	Pa s
η_0	Zero shear viscosity	Pa s

[1] The list excludes the nomenclature and indices of chapter 4 (State of research - Publication I)

Symbol	Description	Unit
η_∞	Infinite-shear viscosity	Pa s
h	Peel arm thickness	mm
H_a	Reaction heat of aged material	J g^{-1}
H_f	Reaction heat of fresh material	J g^{-1}
H_{res}	Residual heat of reaction	J g^{-1}
H_t	Total heat of reaction	J g^{-1}
Θ	Contact angle / peeling angle	°
l_r	Measurement length	mm
λ	Relaxation time	s
λ_n	Displacement in test cycle	mm
λ_0	Maximum wavelength in roughness profile	mm
n	Power law exponent	-
P_{app}	Pressure applied by compaction stamp/roller	N mm^{-2}
Q	Heat flux	W m^{-2}
R	Universal gas constant	J K^{-1} mol^{-1}
R_q	Root mean square roughness	mm
R^2	Coefficient of determination	-
S	Areal roughness	µm
σ	Tension	N mm^{-2}
σ_c	Compaction stress	N mm^{-2}
σ_{max}	Maximum stress (tack indicator)	N mm^{-2}
φ	Fiber volume fraction	%
σ_{SG}	(solid) Surface free energy	mN m^{-1}
σ_{SL}	(solid/liquid) Interfacial free energy	mN m^{-1}
σ_{LG}	(liquid) Surface tension	mN m^{-1}
σ_{SG}^d	Dispersive portion of surface free energy	mN m^{-1}
σ_{LG}^d	Dispersive portion of surface tension	mN m^{-1}
σ_{SG}^p	Polar portion of surface free energy	mN m^{-1}
σ_{LG}^p	Polar portion of surface tension	mN m^{-1}
t	Time	s
t_{age}	Storage/ageing time at RT	days

Symbol	Description	Unit
tan δ	Loss factor	-
t_c	Compaction time	s
t_l	Lay-up time	min
t_{lam}	Time of lamination	min
t_{off}	Non-productive process time	min
T	Temperature	°C
T_{ageing}	Ageing temperature	°C
T_c	Temperature at critical modulus	°C
T_{max}	Temperature at maximum tack	°C
T_{proc}	(Prepreg) processing temperature	°C
T_{onset}	Onset temperature	°C
v	Lay-up velocity	m s^{-1}
v_d	Displacement rate	mm s^{-1}
w	Prepreg width	mm
W_{adh}	Work of adhesion (tack indicator)	µJ mm^{-2}
W_{SL}	Thermodynamic work of adhesion	µJ mm^{-2}
W_t	Work of separation (tack indicator)	µJ mm^{-2}

Chapter 1

1. Introduction

Fiber-reinforced plastics (FRP) excel in an outstanding ratio between attainable load capacity and material density. If the material anisotropy is appropriately taken account of in the part design process, composite structures made of FRP exceed the weight-specific properties of conventional construction materials such as steel and aluminum. For this reason, lightweight construction based on composites is gaining increasing interest in more and more industries and already constitutes a key technology for tackling current mobility challenges with social, economic and ecological implication.

The aerospace industry in particular has always been considered a technological pacesetter for the use of FRP with the aim of reducing moved weight and the associated savings in fuel and emissions. The European Commission emphasizes the importance of lightweight construction for achieving its ambitious emission reduction targets of Flightpath 2050 (75 % CO_2 and 90 % NO_x reduction [1]). Over the entire service life of a modern commercial aircraft, there are also economic advantages due to weight savings for holistic cost balances, which take into account both acquisition and operating costs: Four-digit additional investment costs (in US dollars) are usually amortized by reducing a single kilogram of structural weight [2] due to the reduced fuel consumption of an air plane within its expected life span of ~20-30 years. Characteristic composite structures for airplanes are large-scale components with limited geometric complexity such as upper wing shells, fuselage shells or vertical stabilizers made of carbon fiber reinforced plastic (CFRP).

Individual models of the current civil aircraft generation such as the Airbus A350 XWB or the Boeing 787 Dreamliner yet feature a CFRP share of over 50 % in structural weight.

From a manufacturing point of view, CFRP components, which are made from pre-impregnated fibers (prepregs) and subsequently cured in an autoclave at elevated temperatures, represent the state of the art in aircraft manufacturing while at the same time spearheading polymer-based composites in terms of mechanical performance [3]. The ply-wise prepreg lay-up of laminates (**Figure 1-1**, (1)) is performed using robot- or gantry-processes, namely automated fiber placement (AFP) and automated tape laying (ATL), which essentially differ in terms of the prepreg volume laid per time unit and feasible component complexity [4]. A virtually unrestricted laminate design with regard to ply angles, stacking sequence and patch integration allows for adapting to specific load cases and, therefore, making the best possible use of the material's lightweight potential.

The prerequisite for success of the AFP process is a precise positioning of the thin fiber layers (tows) which primarily depends on the stickiness (tack) of the laid prepreg material [5]. Sufficient tack is necessary in order to achieve fixation on the mold or on previously prepreg layers that have already been laid. If the stickiness is

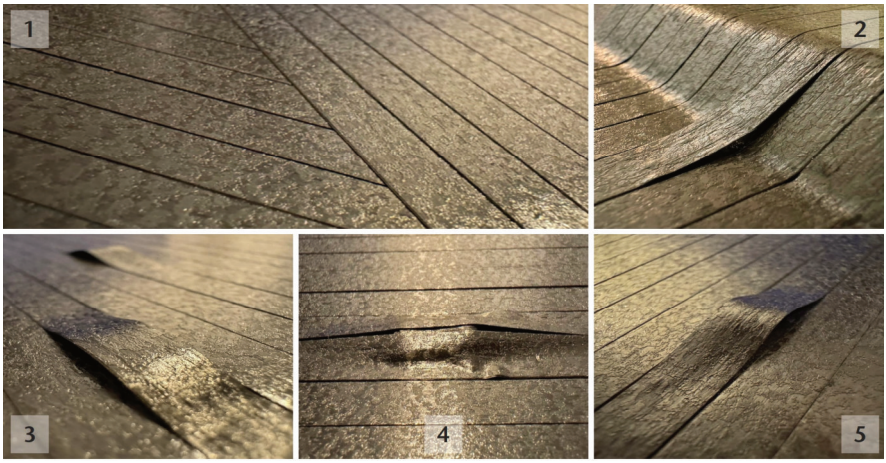

Figure 1-1. Composite laminate manufactured from ¼" carbon fiber/epoxy prepreg slit tapes by automated fiber placement (1) and tack-related laminate defects (2-5).

not adjusted properly during the manufacturing process, laminate defects can occur (**Figure 1-1**, (2-5)) that may prove to be mechanical flaws in the cured structural component [6,7]. At the same time, the material may not stick to machine parts of the placement head or material feed (e.g. the tow guidance or the compaction roller). It turns out that the robustness of automated laying processes employed in the aerospace industry is highly dependent on the insensitivity to fluctuations in prepreg tack.

Although controlling prepreg tack evidently looms large in industrial processing, prepreg suppliers are yet due to quantify the level of stickiness of their products on the corresponding data sheets in the form of numerical data. If anything, ordinal-scaled information such as 'low', 'medium' or 'high tack' is provided so that no comparability between different materials is given. Processors thus struggle to estimate the suitability of the prepreg for their manufacturing systems in advance of material sourcing. In absence of material data, process adjustment is ultimately based on purely heuristic approaches, which usually entails production of waste and numerous iteration loops during material selection.

The portrayed uncertainty of dealing with prepreg tack in an industrial environment may be due to the fact that until 2021, no standardized measuring method for quantifying the tack of fiber-reinforced, pre-impregnated semi-finished products has been available. On the other hand, the deficient and almost exclusively experimental state of research on the topic alludes to prepreg tackiness being a complex material property that is subject to a large number of material, process and environmental influences. Their mutual interdependencies and fundamental mechanisms are not fully understood and require basic research.

This doctoral thesis systematically deals with this challenge. With a view to prepreg-processing advanced composite manufacturing techniques in the aerospace industry, a contribution is made to overcome the prevalent heuristic practices when setting tack-influencing process parameters. Instead, a comprehensive understanding of the tack-determining mechanisms based on material characterization and modelling is developed. The findings are consolidated in the form of recommendations for the control of prepreg tack in automated fiber placement to promote process reliability. In order to achieve this goal, various publications on the subject of prepreg tack have emanated from the author's research at the Institute of Polymer Materials and Plastics Engineering at

Clausthal University of Technology. Five of them yield the basis of this cumulative dissertation and are arranged in **Table 1-1**.

Table 1-1. Published journal articles of the cumulative thesis.

#	Authors	Title	Journal	Type	Word count*
I	D. Budelmann C. Schmidt D. Meiners	Prepreg tack: A review of mechanisms, measurement, and manufacturing implication	Polymer Composites 2020; 41(9):3440-58.	Review article	9,570
II	D. Budelmann H. Detampel C. Schmidt D. Meiners	Interaction of process parameters and material properties with regard to prepreg tack in automated lay-up and draping processes	Composites Part A: Applied Science and Manufacturing 2019; 117:308-16.	Research article	8,002
III	D. Budelmann C. Schmidt D. Meiners	Adhesion-cohesion balance of prepreg tack in thermoset automated fiber placement. Part 1: Adhesion and surface wetting	Composites Part C: Open Access 2021; 6:100204.	Research article	9,032
IV	D. Budelmann C. Schmidt D. Meiners	Tack of epoxy resin films for aerospace-grade prepregs: influence of resin formulation, toughening and B-staging	Polymer Testing 2022; 114:107709.	Research article	5,859
V	D. Budelmann C. Schmidt L. Steuernagel D. Meiners	Adhesion-cohesion balance of prepreg tack in thermoset automated fiber placement. Part 2: Ply-ply cohesion through contact formation and autohesion	Composites Part C: Open Access 2023; 12:100396	Research article	8,658

*excluding figures and references

Chapter 2

2. Thesis outline

The collectivity of the research articles presented in the introduction (**Table 1-1**) comprises the basis for this cumulative doctoral thesis and is subject to a superordinate research objective which is outlined in the following section 2.1. The individual articles are therefore contextualized within the thesis structure in section 2.2 and discussed in terms of their contribution to the thesis objective. A statement with the intention of recognizing the detailed individual author contribution to the articles is eventually added in section 2.3.

2.1 Objective

Prepreg tack in general is a matter of polymer adhesion with direct implication for advanced composite manufacturing techniques. In their recent perspective article, Raos and Zappone [8] point out that despite being ubiquitous in both the natural world and human technology, a lot of questions of polymer adhesion still remain unanswered. The authors designate polymer adhesion “a complex multiscale phenomenon, such that the solution of adhesion problems requires a convergence of chemistry, physics, and engineering”. This conversion of different disciplines undoubtedly applies to the stickiness of prepregs in the same manner.

Therefore, the overarching objective of this thesis is to provide a fundamental and comprehensive understanding of the complex material-process interaction and underlying adhesive/cohesive mechanisms involved the tack of thermoset prepreg materials. Achieving the research objective is reliant on answering the following questions:

Chapter 4: **State of research** (Publication I)

- What are the most relevant but unaccounted influencing factors of prepreg tack in literature?
- Are there any methodical lackings in prepreg tack characterization?

Chapter 5: **Process and environmental factors** (Publication II)

- How does a variation of temperature influence prepreg tack?
- Is there a influence of room temperature ageing on tack and how can it be accounted for in AFP processes? How does the prepreg material change in terms of cure progression?
- In which way do the process/test parameters compaction force and debonding rate generally affect the measured stickiness?

Chapter 6: **Adhesive mechanisms** (Publication III)

- Is there a difference in prepreg adhesion between variable AFP-related surface materials such as polyurethane (compaction roller), backing paper and mold materials (steel)?
- Is prepreg tack on solid surfaces a matter of surface wetting and can it be approached through a wetting analysis based on contact angle measurement?
- Can potential differences in adhesion be related to various types of intermolecular forces such as van der Waals forces, dipole-dipole interaction or h-bonding?
- How does surface topography influence tack?

Chapter 7: **Prepreg resin formulation** (Publication IV)

- Does the use of different epoxy-prepolymers (TGMDA, TGAP and DGEBA) result in diverse levels of initial stickiness?
- Can the prepreg B-staging be tailored to reach desired tack levels based on the correlation between modeled cure stage (OWRK) and tack data?
- Which thermoplastic toughener content is considered favorable for the use in epoxy-based prepregs in terms of tack?

Chapter 8: **Contact formation and autohesion** (Publication V)

- How does experimentally determined intimate ply-ply contact develop as a function of temperature, compaction force and dwell time?
- Is it possible to transfer the autohesion concept known from thermoplastic polymer healing to thermoset prepregs to predict ply-ply bond strength?
- Can contact formation and autohesion submodels be combined and applied to estimate tack as a function of multiple process and material parameters?

Despite the fundamental character of the research presented in the papers for this cumulative thesis, the insights gained from answering the preceding questions comprise valuable implications for advanced composite manufacturing in practice. The lead questions connected to the thesis' applied research on tack and AFP are posed as follows:

Chapter 9: **Implication for industrial practice**

- How big is the economic impact with regard to process times when accounting for prepreg tack during the manufacturing of a close to reality aerospace composite part?
- In which way and to which extent should the prepreg's resin be modified in terms of pre-cure and toughening to meet stickiness requirements in industrial practice?
- What is the preferential test method to quantify the tackiness of prepregs?

2.2 Structure

Figure 2-1 gives an overview of the thesis structure.

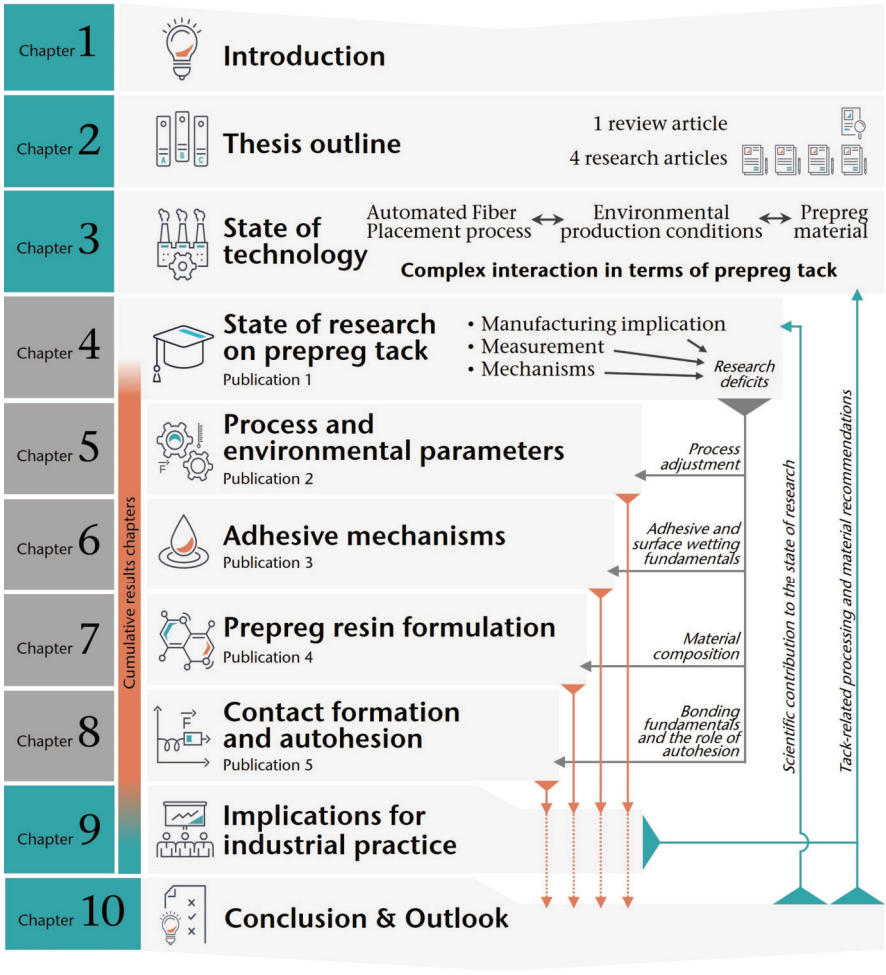

Figure 2-1. Overview of the thesis structure: Chapter sequence and relatedness.

Following an introduction to the topic and an overview of the thesis publications in **chapters 1 and 2**, the state of technology was reviewed in **chapter 3**. Here, the technological context, in which the tack of prepregs is ascribed to its practical

relevance, was outlined. In a first step, reasons for the growing industrial use of composites in civil aviation were discussed from both an economic and ecological perspective (3.1). The predominant manufacturing process of large advanced composite structures for civil airplanes, namely automated fiber placement was introduced (3.2). Herein, the general aspects of the process were presented such as the fundamental production cycle and the deployed machinery. The processed materials of unidirectional epoxy-based, carbon fiber reinforced prepregs were presented in section 3.3 by giving an insight into their composition (3.3.1), production techniques and cure cycles (3.3.2). The following chapter thoroughly records the state of research on the tackiness of thermoset prepreg materials.

In order to identify scientific desiderata, a review article (**Chapter 4, Publication I**) was published in midyear 2020. The journal article is the only available review article on prepreg tack to date. A profound overview of the scientific work on the topic was provided featuring a total of 164 references from multiple fields of the science and technology of composites. In a first step, general process considerations and manufacturing implications of prepreg tack were outlined (4.1 and 4.2). The material tackiness was discussed as the primary cause for the formation of laminate defects (4.2.2) that can have negative impact on post-cure part quality. Manufacturing-relevant factors were categorized in section 4.2.3 before eventually highlighting their precise influence on prepreg tack (4.4.4). Therefore, the extrinsic process (4.4.1) and environmental (4.4.2) influence parameters of temperature, compaction force and time, debonding rate, contact material, ageing and relative humidity as well as material properties (4.4.3) resin viscosity, prepreg architecture, fiber volume fraction and degree of cure were reviewed in detail. A tabular overview over all impactful experimental studies on the topic conducted between 1981 and 2020 was included. In intermediate section 4.3, a discussion of different utilized techniques to determine prepreg tack was provided. Section 4.5 comprises a short representation of model approaches presented in literature. The review article concluded with a future perspective on unsettled issues (4.6) which were partly addressed in this thesis.

Scientific progress made in the field of prepreg tack after publication of the review article was summarized in section 4.8. Therefore, recent studies focusing on the lay-up process (4.8.1), materials (4.8.2) and tack fundamentals (4.8.3) as well as the newly established ASTM standard test method for characterizing tack of prepregs using a continuous application-and-peel procedure (4.7.4) were reviewed.

With the release of **Publication II (chapter 5)** in 2019, the first research article in preparation of the thesis was published. The focus was set on the complex interaction between AFP-related process parameters and material properties to seamlessly satisfy a major research deficit outlined in the state of the research (Publication I). In order to quantify the tackiness of a commercially available aerospace-grade carbon fiber prepreg (5.2.1), a test method developed for pressure sensitive adhesives was adapted to prepreg materials (5.2.3). The standardized ASTM D8336 (4.7.4) has not been available yet at this point of time. Applying the probe test to a rheometer turned out to provide a highly accurate and reproducible method which was thenceforth used in the following studies. The two tack indicators σ_{max} (maximum stress) and W_{adh} (work of adhesion) were extracted from the method's stress-displacement curves and discussed in terms of their suitability to represent prepreg tack. For generating the results presented in this chapter, the method was able to mimic basic AFP-related process parameters such as the compaction force and duration applied by the roller, debonding rate and process temperature (5.2.2). Despite apparatus-related limitations in terms of maximum achievable compaction pressure and lay-up speed, general correlations between process parameters, namely temperature (5.3.2), compaction force (5.3.3) and debonding rate (5.3.4) and tack could be revealed and described. Additional emphasis was put on investigating the influence of a highly manufacturing-relevant aspect that is room-temperature ageing of prepregs. As resin and curing agent are pre-mixed in commercial prepregs, the time and temperature-dependent curing reaction (3.3.2) sets in prior to processing. The evolution of the curing reaction was therefore studied (5.2.4) as a function of prepreg out-time and discussed in conjunction to tack (5.3.5). Oscillatory rheological analysis (5.2.5) revealed tack-contributing changes in viscoelastic parameters.

Both the explorative design and the eventual findings of Publication II however raised additional questions on fundamental tack mechanisms such as the specific adhesive (Publication III, chapter 6) and cohesive (Publication V, chapter 8) contribution. Furthermore, the use of a commercial prepreg system in this study prevented insight into formulation-relevant factors, which led to the idea of investigating tailored epoxy resin formulations with purposive component variation (Publication IV, chapter 7). The research article in this respect laid the methodical foundation and served as an impulse for the research presented in adjacent chapters 6-8.

A key aspect of Publication II was the observation that prepreg tack generally follows bell-shaped curves when being plotted as a function of temperature for isothermal compaction and debonding. In order to examine the nature of the bell shaped curves and their variations, a tow-part paper series was initiated in 2021. In **chapter 6 (Publication III)**, the adhesive portion of the so-called adhesion-cohesion balance was presented. For the first time in literature, probe tack (6.3.1) was correlated to the interfacial, adhesion-governing interaction between prepregs and AFP-relevant substrates by employing a detailed surface wetting analysis (6.3.2). Contact angles were measured between standard test liquids as well as extracted neat prepreg resin (6.2.2) and solid substrate, namely stainless steel of different surface roughness, siliconized backing paper, polyurethane and the prepreg itself (6.2.3). Optical characterization of the surface topographies was performed by laser scanning microscopy (6.3.4) and combined with oscillatory rheology (6.3.3) in order to test the validity of selected contact formation criteria for prepregs that have originally been developed for PSA (6.4.6). The criterion validation was predicated on the previously characterized liquid/solid interaction at the interface based on the wetting properties.

The study presented in **chapter 7 (Publication IV)** was conceptualized as an answer to the prevalent scientific approach of investigating tack exclusively from a perspective of commercially prepreg systems. Following this approach, the prepreg resin that is the key component in terms of tack is a black box and questions on influences of resin formulation on tack remained unanswered. Thus, aerospace-grade model epoxy resins for prepregs were formulated using different multifunctional epoxy-prepolymers and variations of the polyethersulfone (PES) toughener content (7.2.1, 7.2.2). Dynamic DSC measurements (7.3.1) were conducted on the model formulations in order to describe the cure kinetics by means of the model-free Flynn-Wall-Ozawa (FWO) approach (7.3.2). The isoconversional resin cure model was eventually used to adjust the B-stage level of the resin films (7.4.1) prior to further material analysis by oscillatory rheometry (7.3.3). Temperature-dependent tack levels were determined by applying a modified probe tack test (7.3.4) for the resin films varying in terms of used prepolymers (7.4.2), B-staging (7.4.3) and toughener content (7.4.4). The collectivity of findings implied strategies of resin formulation and conditioning to tailor pre-cure properties for epoxy-based prepregs and help to understand the influence of intrinsic properties on prepreg tack for commercial systems (7.5).

Chapter 8 (Publication V) pursued the exploration of the adhesion-cohesion balance as a direct continuation of chapter 6 which covered the adhesive portion of the balance. In chapter 8, the implication of contact formation and autohesion in developing cohesive strength at the interface between two commercial prepreg plies (8.2) was investigated. In an effort to isolate the influences of contact formation and autohesion on prepreg tack, three test cycles were designed (8.3.1). The cycles were implemented as 90° peel tests using in-house designed test fixtures in conjunction with a rheometer (8.3.2). Contact formation was quantified as function of the compaction parameters contact pressure, dwell time and temperature using pressure-sensitive films, image processing and optical analysis (8.4.1). The experimentally determined progression of the degree of intimate contact (DoIC) was eventually used to parametrize a semi-empirical contact formation model (8.4.2). Tack data from the standard isothermal test cycle (8.4.3) and from a test cycle providing fully contacted ply interfaces (8.4.4) was gathered in preparation for the tack process model. Prior to this, rheological analysis (8.3.3) yielded the temperature-dependent relaxation times of neat prepreg resin as a well-accepted viscoelastic measure that determines the rate of autohesion (8.4.5) for the application in an analytical autohesion model (8.4.6). By merging the modelled mechanisms of contact formation and autohesion, tack was estimated for different AFP scenarios (8.4.7). Lastly, the bond strength model was demonstrated to replicate the interaction between the tack-governing mechanisms in the form of bell-shaped tack curves proposed by the adhesion-cohesion balance (8.4.8).
In practice-oriented **chapter 9**, an integration of the fundamental findings from the previous chapters was carried out. A case study was set up to demonstrate the tack implication in the fabrication of a large-scale composite aircraft part using AFP. Here, the impact of tack-related process parameter adjustment on lay-up times was determined and evaluated. Additionally, succinct guidelines for customizing the tack of epoxy-based prepreg resins were provided in section 9.2 and a discussion on the intricacies of informed prepreg tack measurement was presented in section 9.3.
Chapter 10 concludes the thesis with a recapitulation of the conducted research (10.1) and a compilation of the key findings (10.2). The thesis' contribution to the state of research as well as its restrictions were discussed critically. At last, points of contact for future research were proposed (10.3).

2.3 Publications and authorship contribution

The following statement on authorship contribution to the published work for this thesis is based on a suggestion by Brand et al. [9]. The way of categorizing contribution is to assign the author roles, which were addressed in the paper production process, to predefined standardized tasks. This contributor roles taxonomy (CRediT) is currently used by most journals published by Elsevier, including the majority of this thesis' articles.

Table 2-1. CRediT – contributor role taxonomy [9] used for this thesis' research articles.

Term/Task	Definition
Conceptualization	Ideas; formulation or evolution of overarching research goals and aims
Methodology	Development or design of methodology; creation of models
Software	Programming, software development; designing computer programs; implementation of the computer code and supporting algorithms; testing of existing code components
Validation	Verification, whether as a part of the activity or separate, of the overall replication/reproducibility of results/experiments or other research outputs
Formal Analysis	Application of statistical, mathematical, computational, or other formal techniques to analyze or synthesize study data
Investigation	Conducting a research and investigation process, specifically performing the experiments, or data/evidence collection
Resources	Provision of study materials, reagents, materials, patients, laboratory samples, instrumentation, computing resources, or other analysis tools
Data curation	Management activities to annotate (produce metadata), scrub data and maintain research data (including software code, where it is necessary for interpreting the data itself) for initial use and later reuse
Writing – original draft	Preparation, creation and/or presentation of the published work, specifically writing the initial draft (including substantive translation)
Writing – review & editing	Preparation, creation and/or presentation of the published work by those from the original research group, specifically critical review, commentary or revision – including pre- or post-publication stages
Visualization	Preparation, creation and/or presentation of the published work, specifically visualization/data presentation
Supervision	Oversight and leadership responsibility for the research activity planning and execution, including mentorship external to the core team
Project administration	Management and coordination responsibility for the research activity planning and execution
Funding acquisition	Acquisition of the financial support for the project leading to publication.

2.2.1 Publication I

D. Budelmann, C. Schmidt, D. Meiners

Prepreg tack: A review of mechanisms, measurement, and manufacturing implication.

Polymer Composites 41 (2020) p. 3440-3458.

Table 2-2. Individual authorship contribution to publication I (chapter 4).

Author	Contributor role	Specific task performed for the publication
DB	Conceptualization	Idea generation: Identification of a lacking review article on prepreg tack in literature.
	Methodology	Planning of literature research. Identifying and structuring covered topics
	Investigation	Conducting literature research on prepreg tack and related topics of composite manufacturing
	Writing – original draft	Creation of the initial draft including writing, figure/ table preparation, type setting, language editing. Full corresponding author responsibility for submission
	Writing – review & editing.	Implementation of co-authors comments. Manuscript revision according to reviewer comments. Full corresponding author responsibility for revision
CS	Conceptualization	Definition and evolution of overarching research goals for the academic cooperation in branch office
	Resources	Supply of research infrastructure
	Writing – review & editing	Critical manuscript review and commentary before and after revision
	Supervision	Oversight and leadership responsibility for daily research activities in branch office
	Funding acquisition	Contribution to applying for the European Regional Development Fund (ERDF) research grant *FlexProCFK*
DM	Conceptualization	Definition and evolution of overarching research goals for the academic institute
	Resources	Supply of research infrastructure
	Writing – review & editing	Critical manuscript review and commentary before and after revision
	Supervision	Scientific oversight responsibility for the ERDF reseach project *FlexProCFK*
	Project administration	Management and coordination responsibility for the ERDF reseach project *FlexProCFK*
	Funding acquisition	Applying for the ERDF research grant *FlexProCFK*

2.2.2 Publication II

D. Budelmann, H. Detampel, C. Schmidt, D. Meiners

Interaction of process parameters and material properties with regard to prepreg tack in automated lay-up and draping processes.

Composites Part A: Appl. Sci. and Manuf.117 (2019) 308-316.

Table 2-3. Individual authorship contribution to publication II (chapter 5).

Author	Contributor role	Specific task performed for the publication
DB	Conceptualization	Indentification and defining test conditions representing process and environmental factors in AFP
	Methodology	Design and application of fixtures for probe testing prepreg tack in a rheometer. Defining and elaborating periphal testing methods
	Validation	Exploring reproducibility of tack testing method and optimization
	Formal analysis	Implementation, evaluation and optimization of a Matlab scipt
	Investigation	Planning, conducting and evaluation of DSC, rheology, conditioning (prepreg ageing) and tack experiments
	Writing – original draft	Creation of the initial draft including writing, figure/ table preparation, type setting, language editing. Full corresponding author responsibility for submission
	Writing – review & editing.	Implementation of co-authors comments. Revision according to reviewer comments. Corresponding author responsibility
HD	Conceptualization	Indentification and defining test conditions representing process and environmental factors in AFP
	Methodology	Design and application of fixtures for probe tack testing
	Writing – review & editing	Critical manuscript review and commentary before and after revision process
CS	Conceptualization	Definition and evolution of overarching research goals for the academic cooperation in branch office
	Writing – review & editing	Critical manuscript review and commentary before and after revision process
	Supervision	Oversight and leadership responsibility for daily research activities in branch office
	Funding acquisition	Contribution to applying for the research grants *TackTIC* & *Robufil*
DM	Conceptualization	Evolution of overarching research goals for the academic institute
	Resources	Supply of infrastructure and instrumentation (DSC, rheometer)
	Writing – review & editing	Critical manuscript review and commentary before and after revision
	Supervision	Scientific oversight responsibility for reseach projects
	Project administration	Management and coordination responsibility for research projects
	Funding acquisition	Applying for the research grants *TackTIC* & *Robufil*

2.2.3 Publication III

D. Budelmann, C. Schmidt, D. Meiners

Adhesion-cohesion balance of prepreg tack in thermoset automated fiber placement. Part 1: adhesion and surface wetting.

Composites Part C: Open Access 6 (2021) 100204.

Table 2-4. Individual authorship contribution to publication III (chapter 6).

Author	Contributor role	Specific task performed for the publication
DB	Conceptualization	Idea generation: Initiation to separately investigate the adhesive and cohesive contribution to prepreg tack
	Methodology	Application of contact angle measurement as the central analyis method and definition of periphal tests
	Validation	Reproducibility and suitability verification of DSC, contact angle, rheology, topography and tack results
	Formal analysis	Application of OWRK model. Implementation of the Matlab scipt for tack evaluation. Determination of fit parameters for tack curves
	Investigation	Planning, conducting and evaluation of DSC, contact angle, rheology, topography and tack experiments
	Writing – original draft	Creation of the initial draft including writing, figure/ table preparation, type setting, language editing. Full corresponding author responsibility for submission
	Writing – review & editing.	Implementation of co-authors comments. Revision according to reviewer comments. Corresponding author responsibility
CS	Conceptualization	Definition and evolution of overarching research goals for the academic cooperation in branch office
	Resources	Supply of prepregs and instrumentation (3D laser microscope)
	Writing – review & editing	Critical manuscript review and commentary before and after revision
	Supervision	Oversight and leadership responsibility for daily research activities in branch office
	Funding acquisition	Contribution to applying for the research grant *TackTIC*
DM	Conceptualization	Evolution of overarching research goals for the academic institute
	Resources	Supply of research infrastructure and instrumentation (DSC, rheometer, contact angle measurement)
	Writing – review & editing	Critical manuscript review and commentary before and after revision
	Supervision	Scientific oversight responsibility for reseach projects
	Project administration	Management and coordination responsibility for research project
	Funding acquisition	Applying for the research grant *TackTIC*

2.2.4 Publication IV

D. Budelmann, C. Schmidt, D. Meiners

Tack of epoxy resin films for aerospace-grade prepregs: Influence of resin formulation, toughening and b-staging.

Polymer Testing 114 (2022) 107709.

Table 2-5. Individual authorship contribution to publication IV (chapter 7).

Author	Contributor role	Specific task performed for the publication
DB	Conceptualization	Idea generation: Exploring the influence of chemical resin composition and b-staging on prepreg tack
	Methodology	Application of a modified tack testing procedure and definition of periphal testing. Determining chemicals for resin formulation
	Validation	Reproducibility and suitability verification of resin formulation process, DSC, rheology and tack results
	Formal analysis	Application of Flynn-Wall Ozawa (FWO) cure kinetics model for b-staging. Determination of fit parameters for and FWO plots
	Investigation	Formulation of model epoxy resins. Carrying out resin b-staging. Planning, conducting and evaluation of DSC, contact angle, rheology and tack experiments
	Writing – original draft	Creation of the initial draft including writing, figure/ table preparation, type setting, language editing. Full corresponding author responsibility for submission
	Writing – review & editing.	Implementation of co-authors comments. Revision according to reviewer comments. Corresponding author responsibility
CS	Conceptualization	Definition and evolution of overarching research goals for the academic cooperation in branch office
	Resources	Supply of research infrastructure and prepregs
	Writing – review & editing	Critical manuscript review and commentary before and after revision
	Supervision	Oversight and leadership responsibility for daily research activities in branch office
	Funding acquisition	Contribution to applying for the research grant *TackTIC*
DM	Conceptualization	Evolution of overarching research goals for the academic institute
	Resources	Supply of research infrastructure and instrumentation (DSC, rheometer, contact angle measurement)
	Writing – review & editing	Critical manuscript review and commentary before and after revision
	Supervision	Scientific oversight responsibility for reseach projects
	Project administration	Management and coordination responsibility for research project
	Funding acquisition	Applying for the research grant *TackTIC*

2.2.5 Publication V

D. Budelmann, C. Schmidt, L. Steuernagel, D. Meiners

Adhesion-cohesion balance of prepreg tack in thermoset automated fiber placement. Part 2: Ply-ply cohesion through contact formation and autohesion.

Composites Part C: Open Access 12 (2023) 100396.

Table 2-6. Individual authorship contribution to publication V (chapter 8).

Author	Contributor role	Specific task performed for the publication
DB	Conceptualization	Idea generation: Initiation to separately investigate the adhesive and cohesive contribution to prepreg tack
	Methodology	Development of peel tack test method, intimate contact characterization and contact formation/autohesion approach
	Validation	Suitability and reproducibility verification of the novel peel test
	Formal analysis	Application, modification and validation of contact formation/autohesion model
	Investigation	Planning, conducting and evaluation of DSC, rheology, contact analysis and tack experiments
	Visualisation	Preparation and creation of graphs, illustrations and figures
	Writing – original draft	Creation of the initial draft with full corresponding author responsibility for submission
	Writing – review & editing.	Implementation of co-authors comments. Revision according to reviewer comments. Corresponding author responsibility
CS	Conceptualization	Definition and evolution of overarching research goals for the academic cooperation in branch office
	Resources	Supply of research infrastructure and prepregs
	Writing – review & editing	Critical manuscript review and commentary before and after revision
	Supervision	Oversight and leadership responsibility for daily research activities in branch office
	Funding acquisition	Contribution to applying for the research grant *TackTIC*
LS	Resources	Supply of research infrastructure and instrumentation
	Proj. administration	Management and coordination of the research project
	Writing – review & editing	Critical manuscript review and commentary before and after revision
DM	Conceptualization	Evolution of overarching research goals for the academic institute
	Resources	Supply of research infrastructure and instrumentation
	Writing – review & editing	Critical manuscript review and commentary before and after revision
	Supervision	Scientific oversight responsibility for reseach projects
	Proj. administration	Management and coordination responsibility for research project
	Funding acquisition	Applying for the research grant *TackTIC*

Chapter 3

3. State of technology

The following chapter technologically contextualizes the thesis' topic by picturing the industrial significance of prepreg tack for advanced composite manufacturing in the aviation industry. Therefore, a short overview of the use of composite materials in airplanes is provided in section 3.1 including their economic benefits (section 3.1.1) and ecological impact (section 3.1.2) as well as the established manufacturing processes. The process with the highest implication in the material tackiness, namely automated fiber placement (AFP), is described in section 3.2 relating to the underlying process cycle (section 3.2.1), machinery (section (3.2.2) and to its potentials/challenges (section 3.2.3). The herein processed semi-finished products of interest, pre-impregnated reinforcement fibers also known as prepregs, are highlighted in section 3.3. Emphasis is put on tack-relevant aspects such as composition/components (section 3.3.1) and the production/cure process (section 3.3.2). Concluding subsection 3.3.3 leads over to the state of research on prepreg tack, which is reviewed in detail in publication I (chapter 4).

3.1 Composites in civil aviation

The idea of using composites as construction materials for aircrafts is as old as motor-operated aviation itself: Dating back to the early 1900s, the Wright brothers employed spruce and ash wood for the design of the Wright Flyer 1 which is presumed to be the first manned, powered and controlled aircraft in history [10]. As

a ‘ready-to-use natural composite’, wood comprises both features claimed in the definition of composites [11]:

- A combination of two or more components differing in form or composition on a macroscale
- A rise to properties which transcend those of the individual constituents

Composites are an amalgamation of a base material (matrix) and a filler (reinforcement). The reinforcement acts as the strong and stiff load-bearing constituent and is embedded in a matrix which ensures cohesion [12]. The most common approach to classify composites is according to the utilized material group of the matrix component: Ceramic matrix composites (CMC), metal matrix composites (MMC) and polymer matrix composites (PMC) [13]. The latter PMC are considered the most versatile and widespread type with vast usage in various light-weight applications due to enhanced material performance involving high strength/stiffness, toughness, heat resistance, light weight, thermal endurance, stability in the presence of aggressive chemicals and fatigue resistance [14]. Especially for the mobility sector, the desired rise in properties of advanced composites in combination with a low density have led to a persistent trend of composites replacing conventional materials in different industries such as aerospace, automotive, shipbuilding and railway [15]. As shown in **Figure 3-1**, this development trend has particularly been distinctive within the aviation sector. The

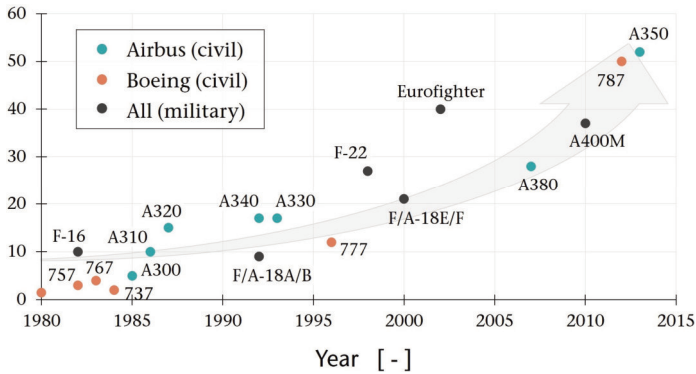

Figure 3-1. Development of the structural weight portion of fiber reinforced plastics in civil and military airplanes. Data adapted from [16].

plotted data pictures the chronological evolution of composite usage in civil and military airplanes between 1980 and 2015.

Initially, composites have been used in single- and twin-aisle passenger airplanes since the late-1960s, with the first applications being in non-safety critical components such as fairings and undercarriage doors [17]. In 1982, the horizontal stabilizer for the Boeing's narrow-body aircraft 737 was certified as the first primary structure made from composite materials and was eventually put into service in 1984 [18]. Almost simultaneously, Airbus developed carbon fiber sandwich composite rudders, airbrakes and spoilers to be introduced for the A310 family. A technological breakthrough in terms of monolithic CFRP construction was achieved shortly after by the introduction of a full composite vertical stabilizer in the A310-200.

The years after were hallmarked by a gradual increase of composite usage in both civil and military aircraft. Despite the vast majority of composites for aerospace applications relying on epoxy-based matrices, Tenax TPCL featuring a polyetheretherketone (PEEK) resin was qualified for the world's first use of thermoplastic CFRP in primary structures [19]. Since 2014, it has been used for clips in the A350 XWB which - together with Boeing's 787 Dreamliner – spearheads in terms of the structural weight portion of FRP in civil aircraft (**Figure 3-1**). For both product families, composite parts like wings, doors, fuselage panels, stringers and others made from monolithic and sandwich CFRP make up more than half of their structural weight (**Figure 3-2**).

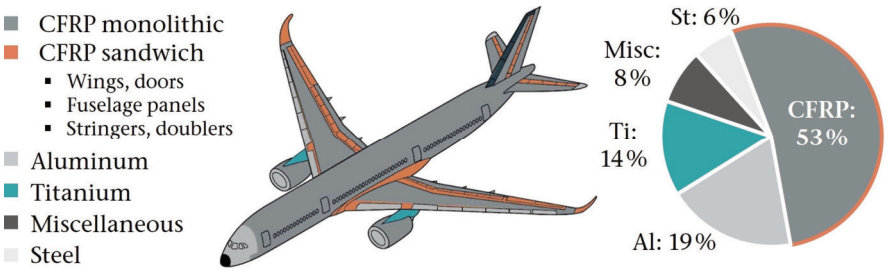

Figure 3-2. Material composition of a modern civil aircraft (Airbus A350XWB). Data and aircraft scheme adapted from [20].

Future builds will undoubtedly continue to deploy composite materials in the next chapter of aviation. Notably, Boeing built a $1 billion, 121,000 m^2 composite wing center for its future wide-body, the 777X. Airbus has also been preparing to work on the deployment of new composite technologies with its next-generation ZEROe hydrogen-propulsion concepts. Therefore, composite materials, especially reinforced by carbon fiber, will play a significant role in future commercial aviation.

3.1.1 Economic benefits and drawbacks

The material costs for carbon fiber-based, aerospace-grade prepregs (section 3.3) are high in comparison to conventional construction metals as prices range from >50 € kg^{-1} for prepreg tape and >100 € kg^{-1} for slit tape [21]. Meanwhile, the investment in automated lay-up technology can easily be a multi-million machine expense (gantry system, placement head, freezer etc., section 3.2). The combination of both factors made AFP-manufactured aerospace composite parts (as finished parts in high volume) sell for 150 USD per pound in 2015 [22], current prizes will be even higher.

Nonetheless, using high-performance advanced composite materials in load-bearing aerospace structures promises an attractive return on investment in the aircraft use phase through reduced fuel consumption. In addition to the growing concern about environmental (see next section) impact of aviation, fuel is the major component in terms of operating costs of an airline. Boeing points out that composite use offers weight savings on average of 20 % compared to more conventional aluminum designs while the frame will need less maintenance when in service due to reduced wear down [23]. Likewise, the Airbus A350 requires 50 % fewer structure maintenance tasks and the schedule for airframe checks for the jetliner is every 12 years [24].

3.1.2 Ecological impact

The light-weighting fuel reduction potential sketched in the previous section directly translates into with greenhouse gas emission savings. Several studies present life cycle assessments (LCA) that demonstrate significant environmental impact reduction through the transition from conventional aluminum fuselage sections to an equivalent made of carbon fiber reinforced plastics [25–27]. E.g.,

Timmis et al. [27] reason that break-even distances for CFRP against aluminum in terms of CO_2 and NO_x are rather short, equaling merely a few long distance flights. Therefore, manufacturing-related emissions can practically be neglected and even the highly energy-consuming production of carbon fibers is of little consequence compared to the emissions caused by fuel consumption. To put this into perspective, Van Grootel et al. [28] established a link between manufacturing variability of CFRP components and environmental impact. The authors estimated that a decrease in variability (mechanical performance of a structural CFRP part) from 14 to 9 % would result in weight savings of 0.12 kg per kg part weight. Over the lifetime of a Boeing 787, the weight reduction would save 8.3 kton of fuel equaling a value of 3.6 million USD in 2020, and would prevent 21.9 kton CO_2 from entering the atmosphere [28].

While the production-related environmental burden of CFRP are quickly amortized in the use phase of airplanes, there is an urgent problem with end of life (EoL) composite parts made from carbon fibers: By 2050, the aviation sector is expected to generate about half a million tons of accumulated carbon fiber reinforced plastic waste from the production and the end-of-life phase of aircrafts [29]. In order to tackle the recycling challenge, Rodrigues Dias et al. [30], who explored the possibilities of circular economy application in the aerospace industry, observed that the components and materials used by the aerospace industry can be reused by other industrial sectors (such as furniture). The feasibility of design processes in complex products, such as the airplane, requires attention to the design for disassembly in the early phases of new product development. Actually, several recycling routes have been proposed, e.g. through pyrolysis [31], (electro)chemical treatment [32] or mechanical grinding [33]. The recycling routes are mostly uneconomical and/or concomitant with downcycling so that recyclates do not achieve the performance levels of virgin materials. The latter restriction to CFRP recycling was strikingly exemplified by the study of Witik et al. [34] who environmentally assessed recycling, energy recovery and landfilling: The presence and extent of ecological benefits from recycling was shown to be strongly linked to the recovery process, the (virgin) materials to be replaced in a secondary application and secondary application itself. A large portion of end of life CFRP parts, however, are still disposed of in landfills [35] and there have been almost no cases where recycled carbon fibers have been used for mass applications until now [29].

3.2 Automated Fiber Placement (AFP)

Soon after the start of implementing composites as secondary and primary structures in civil airplanes in the 1970s and 80s, it became evident that automation will be necessary to meet the growing demand of airplanes by raised production rates – a topic that is still present facing the fast-growing markets in Asia and the Middle East [36]. Today's most common technologies to meet this requirement are Automated Tape Laying (ATL) and Automated Fiber Placement (AFP). The ATL process was developed in the early 1970s with commercially available AFP technology following approximately 10 years later. Both processes are employed to manufacture large advanced composite laminates from mostly unidirectional prepreg material by the automation of prepreg hand lay-up which results in a considerable increase in productivity [37]. The industrially accelerated evolution of process refinement was accompanied by an increasing scientific interest of academic institutions in automated lay-up technologies. It can be retraced consulting **Figure 3-3** which shows the evolution of published research and review articles featuring the keywords 'Automated Fiber Placement' and 'Automated Tape Laying' based on a keyword literature search on Elsevier's research data base ScienceDirect.

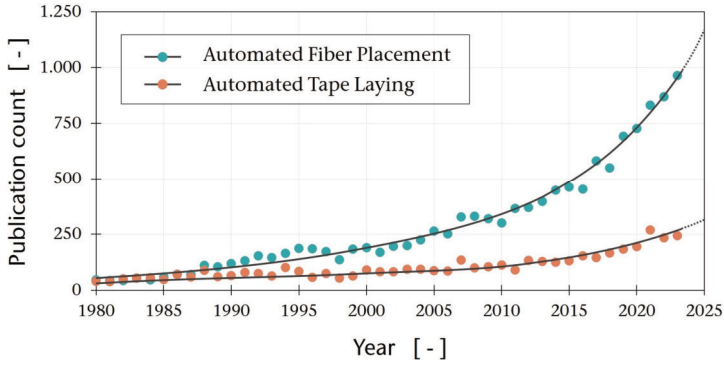

Figure 3-3. Evolution of the scientific interest in Automated Fiber Placement and Automated Tape Laying technology based on publication count.

Since the early 1980s, a considerable amount of research has been published in conjunction with both processes. The number of papers on Automated Fiber Placement is even prospected to double in less than a ten-year span starting in 2015. The enormous amount of progress in this field was recapitulated by researchers who authored multiple review articles featuring the most crucial topics such as general process considerations [4,38–40], materials [41–43], component properties [44,45], defects and their detection techniques [46–50], path planning [51] and prepreg tack [52]. However, the continuous increase in publication output in recent years (**Figure 3-3**), especially for AFP, implicates that the potential of automated lay-up technologies is yet to be fully exploited. Potential reasons for recent diverging interest between AFP and ATL can be presumed based on the benefits and drawbacks both processes entail. In order to understand those, a closer look at both process cycles is necessary.

3.2.1 Process cycle

For composite manufacturing via Automated Tape Laying, which replicates the hand lay-up of wide prepreg sheets in an automated manner, a typically 80-300 mm [53] wide unidirectional prepreg tape is placed on a mold surface by an end effector. Stacking up several plies of material results in a laminate that can be transferred to an autoclave to cure to a final composite part. The material deposition process of ATL places within the value stream of advanced composite manufacturing in the same way as AFP and is presented in **Figure 3-4**. Despite being displayed in the form of a linear work-flow, it has to be pointed out that, according to a recent review article on AFP by Brasington et al. [38], modern advanced composite manufacturing has to include a flow of data that originates from concepts within the manufacturing sector of Industry 4.0. The authors emphasize that 'design is no longer a starting point, but rather a trade in a continuous improvement cycle [...] [with] many challenges remaining within the AFP industry and the composites domain as a whole'.

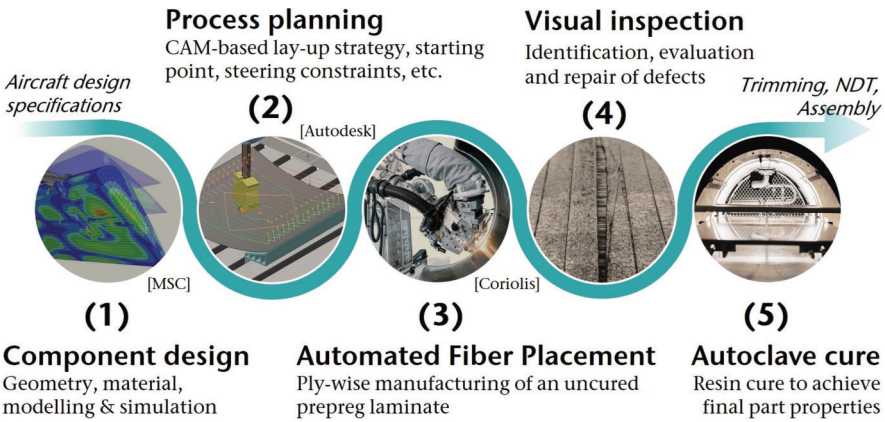

Figure 3-4. Simplified workflow of composite part manufacturing via Automated Fiber Placement in the aerospace industry.

The introduction of composites in civil aircrafts was attended by the need for reviewing and – in many cases – replacing the traditional methodology of aluminum design due to the novel material's anisotropy [54]. Unsophisticated one-to-one replacement of metal alloy by carbon fiber reinforced plastics, also known as the 'black metal'-concept [55], is accepted to not being the go-to strategy but is still prevalent in industrial practice. The component design process for AFP-manufactured CFRP parts (**Figure 3-4**, (1)) especially has to accommodate critical safety issues such as the materials vulnerability and damage tolerance to crash loads and foreign object impacts from bird strike, hail, tire rubber and metal fragments [56]. This also implicates robust, reliable and repeatable structural repair strategies to restore damaged composite components [57].

Process planning (**Figure 3-4**, (2)) in the context of AFP is the stage in which a manufacturing plan based on the working material, component design and manufacturing resources is created [58]. Herein determined course trajectories have to respect the specifications from the component design process in terms of fiber orientation. The definition of the placement path is the most crucial step in process planning while being constrained by a variety of factors, including geometry characteristics of curved surface, prepreg tow deformation performance, compaction roller deformation characteristics and capabilities of AFP machine [59]. A reasonable amount of algorithms to create lay-up strategies in an automated

manner, e.g. for flat panels with and without holes [60–62], cylinders [63] and complex surfaces [64–67] has been presented in literature [51].
Once the lay-up strategy is set, the actual composite part manufacturing takes place via automated fiber placement (**Figure 3-4**, (3)) followed by visual laminate inspection (4) and autoclave cure (5) to gain final part properties. These stages of the work-flow are linked to the thesis topic of prepreg tack and are hence outlined in the following chapters starting with the AFP process and employed machinery.

3.2.2 Machinery

Owing to the niche existence of AFP and ATL technology in the aerospace industry, there is only a handful of companies supplying production systems for automated lay-up worldwide. The core part of AFP hardware setups is the AFP head, a complex end effector which stores and/or centralizes, guides, cuts, preheats and eventually performs lay-up of the prepreg tows. Automated fiber placement heads are set in relative motion to the mold by different types of manipulation, namely gantry-systems (horizontal or vertical) or industrial robots with each having advantages and disadvantages in terms of productivity and geometrical flexibility of the fabricable composite parts.

Figure 3-5. Manufacturing of a CFRP fuselage section by a gantry-attached Automated Fiber Placement head processing thermoset prepregs [Premium AEROTEC].

The larger and less geometrically complex the part is, the more gantry systems stand out in terms of productivity and, thus, economic viability. If high geometrical versatility is demanded, the larger number of degrees of freedom (DOF) of industrial robots are beneficial especially in combination with a rotating tool. **Figure 3-5** shows a CFRP fuselage section that is manufactured by an AFP head placing 16 ½“ thermoset prepreg tows. The placement head is attached to a horizontal portal gantry system.

In order to close in on ATL in terms of productivity, AFP heads were developed, which place up to 32 tows simultaneously. Modular placement systems are available featuring quickly exchangeable (e.g., within 90 seconds [68]) AFP heads which allows for the loading of spools and head maintenance offline. All of this technological evolution is an indicator of AFP having been identified as a high priority research area to target deposition rates of around 100 kg h^{-1} [69] and to thereby match the increasing demand of airplanes.

The key machine parts of an AFP head and their functions in a placement course are schematically shown in **Figure 3-6**. The process starts by unwinding the thin strips of prepreg material from spools which are either attached to the head or reposited in a creel system next to the tool. Carrying the spools close to the deposition point reduces the tow guiding distances and therefore minimizes the risk of undesired tow twists or fuzzball formation [70]. Forwarding the prepreg material is performed by the tow feed after the backing film is removed that prohibits the slit tape from sticking together on the spool. For starting the course (**Figure 3-6**, (a)), the material

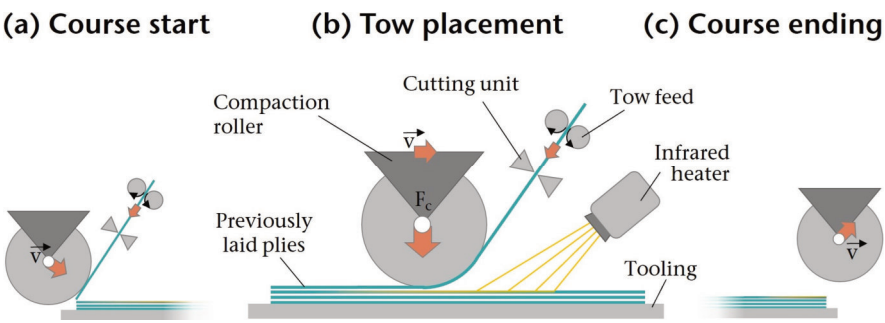

Figure 3-6. Simplified representation of AFP course placement steps and machine hardware used in placement heads.

is forwarded until reaching its initial position at the lower end of the compaction roller. A specific compaction pressure is now applied to consolidate the placed tow on either the mold (first ply) or subsequently placed prepreg material while moving forward.

Throughout the tow placement process (**Figure 3-6**, (b)) the tow is continuously fed at the same speed as the AFP moves over the laminate. The interaction between the compaction roller with respect to its deformation behavior, which has been studied extensively [71–73], the currently deposited prepreg and the previously laid material is of major importance for the success of the automated fiber placement process. Here, the tack of the consolidated prepregs ensures reliable positioning and remaining during the whole manufacturing process.

The ending of each course (**Figure 3-6**, (c)) is initiated with a cut of the prepreg tape by a cutting unit (see [74] for different AFP cutting configurations) shortly before reaching the part boundary. Here, the distance between cutting unit and the lower end of the compaction roller determines the minimal placing length of the system. This distance especially limits the minimum size of local patches which are a simple method for AFP laminate tailoring by adding patches of additional layers with different fiber orientations into the component [75,76]. The whole depicted process (steps a-c) is repeated until a full laminate of multiple layers is deposited which can take last several hours to days depending on the part size and geometric complexity.

3.2.3 Potentials and challenges

As previously stated, AFP and ATL can be considered as the fully automated pendant of manual hand lay-up of prepreg material. However, the automated processes are preferable for large CFRP parts manufactured in high-wage countries due to higher productivity, accuracy and reliability [77]. For exemplification, Lukaszewicz [4] refers to the results from a study of industrial application by Measom and Sewell [78], who reported on the development process of a part originally manufactured by filament winding (FW) and manual lay-up. Process alternation to AFP reduced material wastage rates from 62 to 6 % and increased productivity by 450 %. The downsides are found in the high process and material costs discussed earlier. Disregarding the cost aspects, the process' applicability is limited to parts with low geometric complexity compared to other composite manufacturing techniques used in the aerospace industry such as resin transfer molding (RTM) or hot forming.

One way to overcome the geometric limitations of AFP in terms of complexity and customizability is process combination, e.g. with additive manufacturing technologies [79,80] or processes relying on co-curing [81].
Another challenge to be met when processing thermoset prepregs is the need controlled workshop conditions in terms of temperature and humidity as well as a certain degree of workshop cleanliness [82]. According to Airbus specifications [83], workshop operations including thawing, cutting, placing and shaping of prepregs shall be performed in clean areas with controlled temperature and humidity in the range shown in **Figure 3-7**. For AFP operation, even higher requirements have to be met with a relative humidity in the range of 35 to 40 % and temperature between 18 and 22 °C.

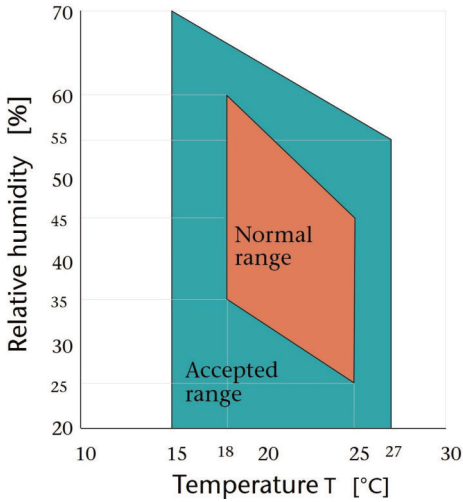

Figure 3-7. Airbus specification [83] for favorable temperature and humidity ranges (workshop conditions) in thermoset prepreg processing.

Lay-up defects that will be discussed in detail in sections 3.3.3 and 4.2 can accumulate when defaulting on the accepted processing range as a result of undesired material alteration. Therefore, it is necessary to pay close attention to the prepreg properties which are the materialized depending on the deployed components (section 3.3.1) and the production and cure process, respectively (section 3.3.2).

3.3 Prepregs

The following section is meant to provide an overview of the composition, production/cure process and tack of the material of interest for this thesis: the prepregs. The term 'prepreg' is a short form of 'pre-impregnated fibers' and describes a two-component semi-finished product for advanced composite production, which is made of reinforcement fibers and a partially cured polymer matrix (section 3.3.1). The major difference and at the same time the most beneficial property in terms of processing in comparison to other composite raw materials lies in the actuality that no additional infusion process of the reinforcement is necessary. Laminates made of thermoset prepregs rather solely have to be cured at elevated temperature and pressure (section 3.3.2) to gain the final high quality part characteristics. The most crucial material property of prepregs on the way to an AFP-manufactured composite part is tack, which is introduced concludingly (section 3.3.3) to round of the state of technology before reviewing the scientific progress on the topic.

3.3.1. Components and composition

Both aforementioned prepreg components, namely matrix and reinforcement fibers, perform specific tasks for the composite in use: While the matrix protects the fibers and transfers loads to the reinforcement, the latter takes up forces and thereby determines the load-bearing capacity of the composite part. Reinforcement fibers in prepregs are continuous by definition [84] and in that differ from other ready-to-mold short fiber-reinforced materials such as bulk molding compounds (BMC) or sheet molding compounds (SMC). Two reinforcement-based types are predominant, that is unidirectional (UD) tape/fabric and bi-directional woven prepregs [85]. For automated lay-up technology such as AFP and ATL, mainly thermoset (epoxy) carbon fiber UD prepregs are processed. These prepregs are deposited either in the form of wide tape material (ATL) or slitted into typically ¼" wide tows (see chapter 3.2.1). Aerospace-grade prepregs have undergone a steady development process to meet the increasing performance requirements of modern aircraft construction. The generational evolution of prepregs can be retraced following the categorization of Lengsfeld [5] shown in **Figure 3-8**.

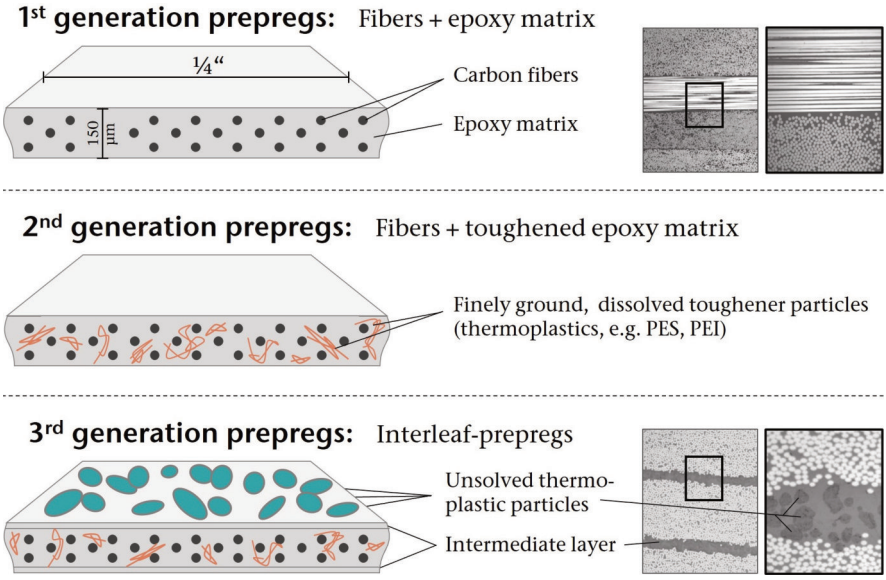

Figure 3-8. Generational evolution of carbon fiber/epoxy prepreg composition and architecture used for aerospace applications. Microscopic images taken from [5].

Early epoxy-based prepregs solely consisted of carbon fibers impregnated by the epoxy resin. The major drawback of this generation of prepregs is the brittleness and sudden/catastrophic failure behavior of the pure epoxy resin which is unfavorable for composites especially when being exposed to impact loading. On this account, matrix resins were mixed with toughening agents (especially with rubber [86–88] or thermoplastic [89–91] particles) which have extensively been demonstrated to enhance the fracture toughness of epoxy resins. For these prepregs, the tougheners are dissolved in the uncured epoxy resin at higher temperatures. A two-phase morphology is then generated during the curing process to reduce crack propagation [92]. For this matter, local shear yielding of the toughening agent around the crack tip was observed to be the dominating toughening mechanism [93]. The latest generation (3rd) of prepregs contain intermediate layers of unsolved thermoplastic particles. Upon curing, an interlaminar toughening layer evolves between two prepreg plies. In addition to the traditional toughening mechanisms involving e.g. crack deflection, plastic deformation and crack pinning [94], hackle marks (comb-like microcracks) are

introduced by shear stresses. Hackle formation in interleaved polymer matrix composites is described in detail and exemplified with literature in the review articles by Shivakumar et al. [95] and Shakil et al. [96].
Despite focusing on the evolution of carbon fiber/epoxy-based prepregs in this chapter due to their widespread application in the aerospace industry, generally, a multitude of both polymer matrices (section 3.3.1.1) and reinforcement fibers (3.3.1.2) are used for prepreg production as outlined in the following.

3.3.1.1 Matrices

Both thermoset and thermoplastic polymers are used as matrix materials for the production of prepregs. Thermoplastics are fully polymerized materials which, for processing, are transferred into a viscous state by the addition of heat and solidify after the forming process when falling below melting temperature. While being available in a wide viscosity range, thermoset polymers are generally supplied in a non-solid state at room temperature and do not gain their final molecular structure until manufacturing. The transformation from viscous to solid is linked to a non-reversible cure process in which macromolecules are built in cross-linking reactions. Direct comparison between both polymer material classes reveals the benefits and drawbacks outlined in **Table 3-1**.

Table 3-1. Comparison of thermosets and thermoplastics used for prepregs.

Category	Thermoset	Thermoplastic
Viscosity during processing	**Low***	High
Weldability	Not weldable	**Weldable**
Recycling	Challenging	**Less challenging**
Mechanical performance	High strength, high modulus	High fracture toughness
Toxicity	Noxious in uncured state	**Harmless**
Shelf life	Typically <12 months	**Unlimited**

*Favorable properties are printed bold type

The property spectrum of thermoplastics, especially linked to meltability and morphology, entails numerous advantages over thermosets. However, the high viscosity of thermoplastic polymers (~10^2-10^4 Pa s) introduces a series of issues when thermoplastic prepregs are stacked and formed, e.g. ply adhesion and void removing during consolidation [97]. These issues have not been overcome for most

manufacturing processes and applications yet, so that thermosets are still oftentimes favored, especially for automated lay-up processes like AFP and ATL.
The most commonly processed polymeric matrices in prepregs are depicted in **Figure 3-9**. The materials used in this doctoral thesis, namely epoxy resins composed of BPA-based multifunctional epoxy monomers and aromatic amine curing agents, are highlighted in blue color.

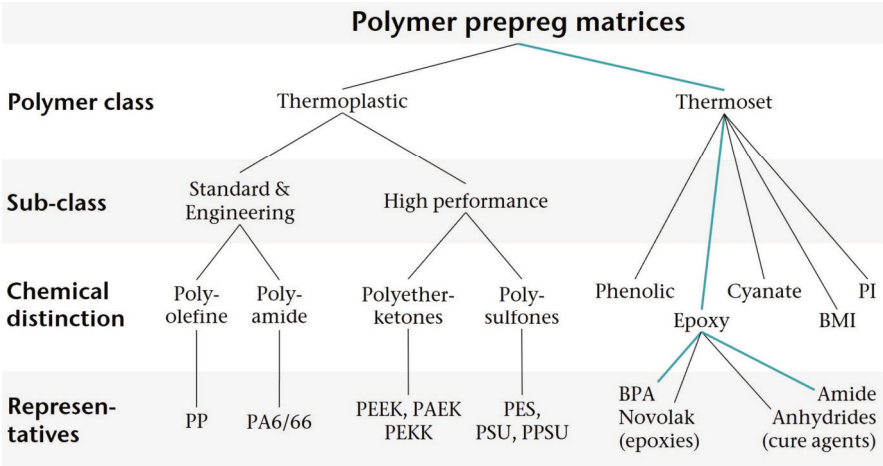

Figure 3-9. Classes and representatives of polymers used as matrix material in commercial prepregs.

As thermoplastics solidify upon cooling, they do not exhibit stickiness (tack) in the same way as thermosets do during AFP. The following discussion is therefore limited to thermoset matrix materials with the focus on epoxy-based polymers. **Table 3-2** summarizes the most common thermoset material groups used for prepreg production.
Since their commercial availability in the 1940s [98], epoxy resins are the most common matrix for advanced composites and a variety of demanding applications [99]. This is mainly due their excellent properties in terms of superior mechanical strength, chemical resistance, adhesion, electrical insolation, commercial availability, low shrinkage on cure and others. However, high costs, brittleness and toxicity in an uncured state limit their use for some applications.

Table 3-2. Characteristic properties of thermoset resins systems used for prepreg production [100].

Resins	Epoxy	Phenolic	Cyanate	BMI	PI
Cure temperature [°C]	120-177	170	177	230	316
Operating temp. [°C]	80-177	200	200	260	371
Processing performance	++	++	++	+	+
Flow ability	+−	+	+−	+−	+−
Wet/hot mechanical	−	−	−	+	+
Fracture toughness	+	−	−	−	−
Flame retardant	−	++	++	++	++

Numerical values are approximate; BMI: Bismaleimide, PI: Polyimide

Chemically, reactive epoxy prepolymers feature at least one epoxide group also known as oxirane according to the IUPAC nomenclature. The functional epoxy group acts as the reactive site in the curse of the curing reaction. Several different curing agents are available for epoxy prepolymers to initiate cross-linking with the most prominent systems being amine, alkali, anhydride and catalytic curing agents [101]. The combination of epoxy prepolymer and curing agent determines both the processing characteristics of the epoxy system as well as its properties in use. Phase transition from a viscous into a solid state involves a three-dimensional network formation into a highly cross-linked macromolecule. **Figure 3-10** shows the network formation of the tetrafunctional epoxy monomer tetraglycidyl-4,4'-methylenedianiline (TGMDA, $C_{25}H_{30}N_2O_4$) and the aromatic amine hardener 4,4'diaminodiphenyl sulfone (DDS, $C_{12}H_{12}N_2O_2S$). Aromatic amines like DDS - in comparison to their aliphatic and cycloaliphatic counterparts - are known to form high-T_g polymers when used as curing agents for epoxy systems [102–104]. Especially in combination with multifunctional epoxy prepolymers such as TGMDA, these systems provide excellent thermomechanical properties due to their highly cross-linked macromolecular network and robust chemical backbone, which make them high-performance matrices in aerospace applications [105–107]. Model epoxy systems for potential use in aerospace-grade prepregs from these categories were also used for investigating the influence of resin formulation on tack in chapter 7.

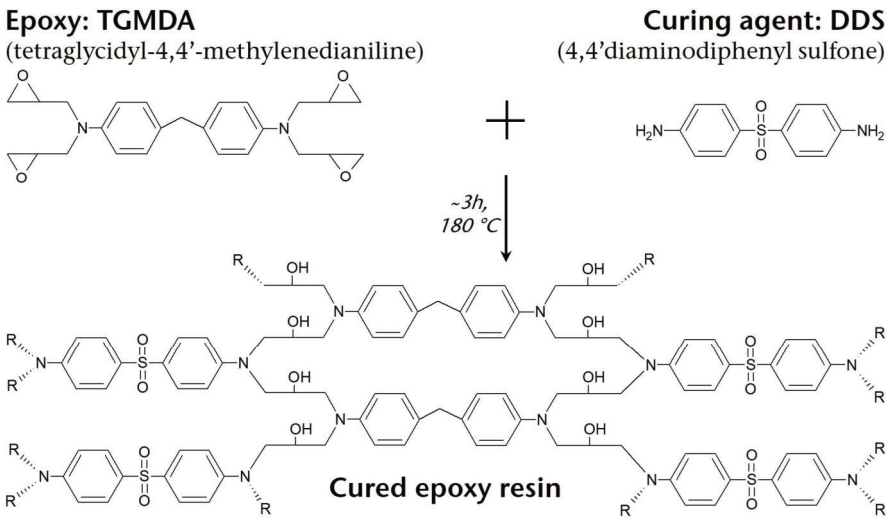

Figure 3-10. Network formation as a result of epoxy cure reaction shown for TGMDA and DDS.

In order to remain load bearing capability even at high temperatures, these systems are cured accordingly at ~180 °C for several hours as depicted in the simplified reaction scheme shown above in **Figure 3-10**. Here, the eponymous four epoxy groups of tetrafunctional TGMDA react with the amine groups in a multi-step autocatalytic reaction which has been the investigated excessively in multiple studies on cure kinetics, e.g. in [108–113]. Knowledge on polymerization reaction kinetics is a crucial aspect in terms of optimizing processing parameters to gain constant part quality or developing new cure cycles [114]. The underlying reaction mechanism of amine-based epoxy curing is shown in **Figure 3-11**.

The autocatalytic and exothermic multistep reaction is initiated by an active hydrogen of the primary amine reacting with a epoxy group in a ring-opening addition reaction leading to the generation of a secondary amine. The formed secondary amine is sterically more hindered and contains only one reactive hydrogen atom left (orange color). At this point, it can react with either another epoxy group to form a tertiary amine or can react at the formed hydroxyl group via etherification. Homopolymerization of epoxides at high temperatures is a possible way of polymerization as well.

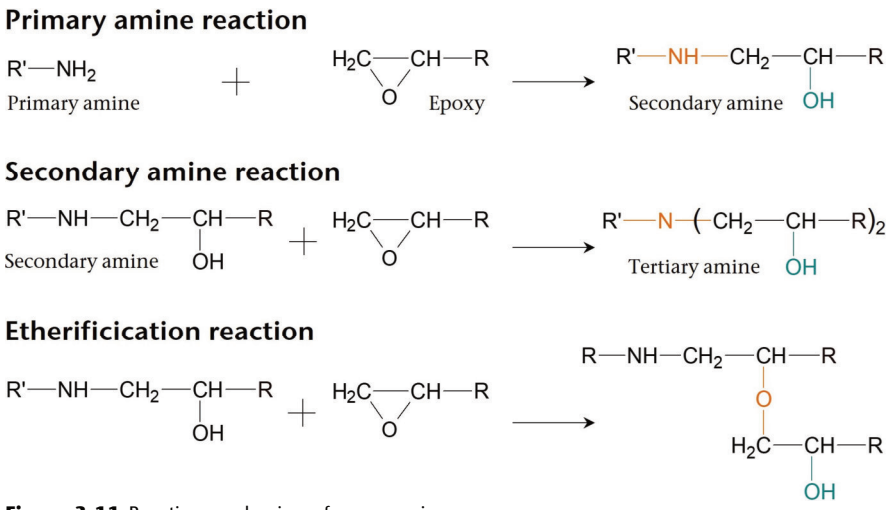

Figure 3-11. Reaction mechanism of epoxy-amine cure.

As monomers react to progressively form longer linear chains and eventually cross-link, the molecular weight and viscosity of the polymer increases rapidly. Fully cross-linked, thermosets are unable to flow but soften when heating above their glass transition temperature T_g. In general, the above-mentioned reactions may occur, either simultaneously or at different stages of the curing process, depending on the relative reactivity of the components, stoichiometry and process temperature [115].

3.3.1.2 Reinforcement fibers

In general, any type of reinforcement fibers can be used for prepreg production. The predominant fiber types, however, are high-performance fibers like carbon, glass and aramid. Recently, the first natural fiber-based prepregs made from flax, hemp or kenaf fibers have come into the market but remain niche products. Selected properties of wide-spread fibers are summarized in **Table 3-3**.

Superior mechanical properties in combination with a low density of 1.8 g cm^{-3} (black highlight box) make carbon an attractive reinforcement fiber for high-load applications where weight-reduction is key. This is why the annual carbon fiber production volume was most lately estimated to having surpassed the milestone of

Table 3-3. Comparison of properties of reinforcing fibers for prepregs production [100].

Reinforcement	E-glass	S-glass	Aramid	Carbon	Boron
Cost	++	+	−	−−	−−
Density	−−	−	++	+	−−
Modulus	−−	−	+	++	++
Strength	−	+	+	++	++
Toughness	+	+	++	−	
Thermal resistance	+	++	−−	−	++
Impact	+	+	++	−−	

100,000 t a^{-1} [116]. However, carbon fiber composites remain a niche material compared to glass fiber reinforced systems which still account for 95 % of the overall market [117]. The reason for this discrepancy is mainly related to the vast difference in pricing of one order of magnitude (~2 \$ kg^{-1} for E-glass fiber vs. ~20 \$ kg^{-1} for carbon fiber [118]).

Typically, carbon fibers are 5-6 µm in diameter and are produced from synthetic polyacrylonitrile (PAN) precursor in order to guarantee consistently high quality. The layered structure of hexagonal graphite is decisive for the carbon fiber's high degree of anisotropy and, hence, for the outstanding strength and stiffness [119]. Different types of carbon fibers are commercially available to match specific applications ranging from high modulus (HM: ~380 GPa) and intermediate modulus (IM: ~290 GPa) to high strength (HS: 4.5 GPa with a modulus ~290 GPa) types [10]. Several thousands of filaments, e.g. 3,000 (3K), 6,000 (6K), 12,000 (12K) or 24,000 (24K), are combined in the form of tows. An overall global share of more than 50 % of all produced carbon fibers are used for prepregs [5] whose production and cure process will be highlighted in the following.

3.3.2 Production and cure process

Unidirectional prepregs in the composite industry are perceived as high-quality semi-finished products which is the result of long-standing production process refinement. The prepregging process can be realized in different ways, the two industrially most relevant processes for thermoset prepregs are [120]:

- Hot-melt impregnation process
- (Solution-) Dipping process

Initially for both processes, collimated carbon fiber tows are unwound from a creel, spread out evenly and parallelized to form a unidirectional aerial entity. If unspread tows are impregnated directly by dip coating, the produced semi-finished products are called towpregs which are inferior quality composite materials compared to prepregs yet considerably cheaper. Towpregs are therefore attractive for cost-sensitive applications [121] but may cause difficulties when being processed by AFP due to reduced dimensional accuracy. Oftentimes, solvents are used to lower the resin viscosity to ensure uniform impregnation with resin that has to be removed by evaporation to sustain the final prepreg/towpreg.
Hot-melt impregnation gets by without solvents but rather relies on transferring a thin resin film to the reinforcement and impregnation under temperature and pressure. In order to produce state-of-the-art interleaf prepregs (section 3.3.1), toughener particles are pre-mixed with the neat resin, followed by a single or double pass impregnation method to create a particle rich surface [122]. After impregnation, the prepregs are cooled down to room temperature and mostly equipped with protective paper or a backing film before coiling. The prepreg coils are immediately put into a freezer to prevent undesired cure.
Most CFRP parts in the aviation industry made from thermoset prepregs are cured in an autoclave (**Figure 3-12**). Autoclaves provide the high temperatures (~200 °C)

Figure 3-12. View out of an industrial autoclave used for curing large-scale aircraft composite parts made from carbon fiber reinforced plastics [Premium AEROTEC].

and pressures (up to 10 bar) needed to cure high-performance parts with claimed porosities >1% [123]. A comprehensive review on autoclave machinery and its technological challenges can be found in [124]. From a manufacturing perspective, autoclave processing of prepreg laminates is an established and well-understood process step with wide industrial use and at the same time the benchmark of CFPR production techniques [125]. For completeness, it has to be noted that so-called out-of-autoclave (OoA) prepregs have been developed which reach acceptable part quality even by vacuum bag-only (VBO) consolidation. A comprehensive review on OoA prepregs was provided by Centea et al. [126]. Despite numerous attempts to improve autoclave curing cycles (e.g. [127,128]), two-step cycles similar to the one shown in **Figure 3-13** have prevailed state of the art in the aviation industry.

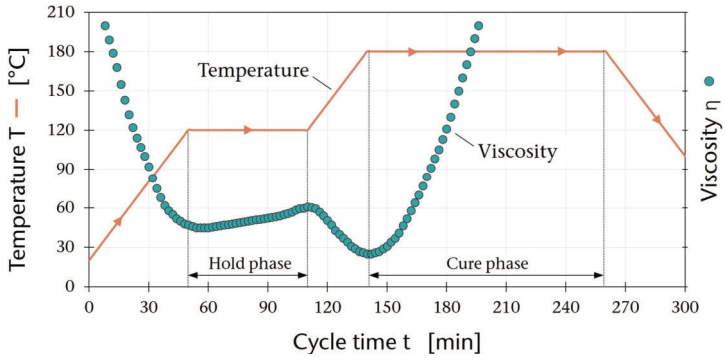

Figure 3-13. Temperature and qualitative viscosity progression during a typical autoclave cure process for thermoset aerospace-grade epoxy prepregs.

The cycle starts with heating up the autoclave from room temperature up to a first hold phase at ~120 °C. The temperature at the first hold phase is a compromise between a desired decreasing of the resin viscosity and a delay of cure because at this point, vacuum is applied to remove volatiles from the laminate. Afterwards, full autoclave pressure of ~7 bar is applied to the laminate while increasing the temperature to 180 °C. Temperature-dependent viscosity will decrease further up until it starts to rise as a result of accretive cross-linking of the polymer matrix. Within a time span of additional 120 min, the part is fully cured and a T_g of ~180 °C will be reached.

3.3.3. Tack(iness)

Historically, the term 'tack' was given distinction within the context of non-reactive adhesives, in particular for pressure sensitive adhesives (PSA). Tack is considered the main property of PSA and is defined as the ability of an adhesive to instantaneously develop interactions with a substrate under light pressure and during short contact time [129]. For prepregs, the term was ultimately adapted due to the similar subjective perception of their stickiness. The ability of thermoset prepregs to develop load-bearing capacity upon cure is similar to structural adhesives. Prepreg tackiness, however, does not rely on cure but is rather a material property solely present in the uncured state. It therefore exclusively affects the built-up stage of the laminate before the autoclave. During the material deposition process, various types of laminate defects may occur as schematically shown in **Figure 3-14** [130]. Especially bonding defects, which result from stresses within the laminate exceeding the tackiness level of the material [131], are related to insufficient tack levels (see **Figure 1-1** for ¼" prepreg bonding defects).

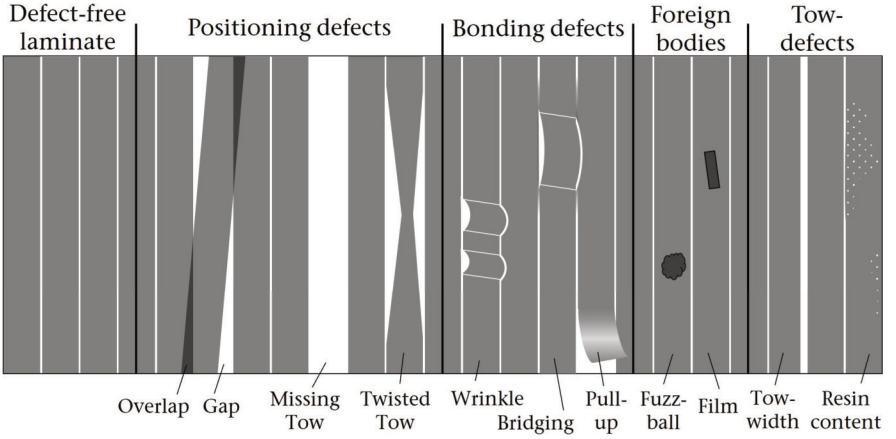

Figure 3-14. Types and categorization of defects in prepreg laminates produced during automated fiber placement. Figure adapted and extended from [130].

The following chapter 4 includes the first thesis' publication that reviews the state of research on prepreg tack in detail. The most recent scientific advances between the paper publication (2020) and present are summarized in section 4.7.

Chapter 4

4. State of research – Publication I

Prepreg tack: A review of mechanisms, measurement, and manufacturing implication

D. Budelmann[a], C. Schmidt[b], D. Meiners[c]

[a]Institute of Polymer Materials and Plastics Engineering, Clausthal University of Technology, Ottenbecker Damm 12, Stade, Germany

[b]Institute of Production Engineering and Machine Tools, Leibniz Universität Hannover, Ottenbecker Damm 12, Stade, Germany

[c]Institute of Polymer Materials and Plastics Engineering, Clausthal University of Technology, Agricolastr. 6, Clausthal-Zellerfeld, Germany

Polymer Composites* 41 (2020) 3440-3458.

*Journal metrics:

CiteScore: **7.5** (Scopus, 2023)
Rank 36/161; 77th Percentile (Material Science: Polymers and Plastics)

Impact factor: **4.8** (Clarivate, 2023)

Abstract

The stickiness of prepregs (tack) is considered a decisive material property for the success of high-quality composite manufacturing by automated lay-up processes such as automated fiber placement (AFP) or automated tape laying (ATL). Adverse control of prepreg tack can easily result in laminate defects or machine breakdown, which are highly undesirable considering the tremendous machinery and material costs of these processes. Prepreg tack is governed by a complex interaction of adhesive and cohesive phenomena that are influenced by machine and environmental parameters of the production process as well as by intrinsic properties of the prepreg material itself. This review aims at providing a condensed insight into the current state of research on prepreg tack. Therefore, experimental studies including the discussion of utilized tack measurement methods as well as model approaches to prepreg tack are reviewed. The findings are discussed against the background of fundamental mechanisms, the strong interdependency of influencing parameters and the challenge of translating measured tack data into an enhanced AFP/ATL process stability by process adjustment.

4.1 Introduction

Lightweight construction based on carbon fiber reinforced plastics has evolved into a key technology to achieve both the economic and ecological mobility goals of modern civil aviation [132,133]. Large-scale composite parts with the highest level of mechanical performance are manufactured by automated lay-up of epoxy pre-impregnated carbon fibers and subsequent autoclave cure [40,134]. The most prevalent processes automated fiber placement (AFP) and automated tape laying (ATL) employ robot- or gantry-attached endeffectors, which build up an uncured laminate ply-by-ply on the surface of a rigid tool [135,136]. Automated lay-up technology has substantial benefits compared to the hand laminating of prepreg material in terms of both the quality and productivity with the most prevalent being higher output volume [37], ply placement accuracy in terms of repeatability [39,68] and uniform laminate compaction [137]. In order to maintain it in the desired position, the material laid must provide a certain level of stickiness [138] commonly referred to as prepreg tack. In combination with drape, tack is the most important material property of the prepreg material for a successful outcome of automated processing using lay-up technology [139].

There is no well-established definition of prepreg tack as a material property specifying its predominating mechanisms or stipulating how to quantify it. Still, it can be generally stated that prepreg tack phenomenologically is not an effect of the epoxy cure reaction forming covalent bonds to a substrate but can rather be understood as an intrinsic stickiness in the absence of any chemical reactions or solvent evaporation. In this regard, it is basically similar to pressure sensitive adhesives (PSA) which have been the target of extensive scientific research for several decades since their economic breakthrough in the late 19th century [140]. For both thermoset prepregs and PSA, tack is a measure of mechanical resistance that needs to be overcome in order to separate the prepreg/adhesive and the substrate. Characteristically, the intimate interfacial contact between both bonding partners is established by applying light pressure over a short period of time compared to most physically or chemically setting structural adhesives [141,142].

Despite all the similarities between prepreg and PSA tack, both the process-related framework of AFP/ATL and the peculiarity of prepregs (presence of reinforcement fibers, B-stage, etc.) must be taken into account for prepreg tack characterization.

This makes prepreg tack a complex phenomenon governed by adhesive and cohesive mechanisms which themselves are strongly affected by a large set of influence parameters. As individual research papers are forced to selectively focus on individual aspects of the topic's complexity (for example, isolated influence parameters), it can be a challenge to fully comprehend the nature of prepreg tack. As well as giving a brief overview of the topic, this article summarizes the fundamentals of prepreg tack by reviewing the most common methods of quantification, results and deductions based on experimental characterization as well as modeling approaches presented in literature. The challenge of transferring both measurement and simulation results into the practice of automated composite manufacturing and, finally, topics to be covered in future research are presented.

4.2 Role of prepreg tack in AFP/ATL

The beginning of scientific research on prepreg tack can be dated back to the early 1980s [143] - a period of time in which AFP and ATL systems gained increasing technical maturity as a consequence of technological innovation [144–146] and, subsequently, established its first industrial relevance. The strong interest in automated lay-up technology from this point in time on can also be retraced to the increasing publication output highlighted in the review article by Lukaszewicz et al. [4]. Evidently, providing robust processes was inevitably linked to the necessity of quantifying prepreg tack from the very beginning of technology refinement.

4.2.1 General process considerations

Figure 4-1 illustrates the ATL process with regard to the adhesive interaction between prepreg material (including backing paper), lay-up surface, and different machine elements. Orange arrows indicate prepreg tack whereas counteracting forces are displayed in white.

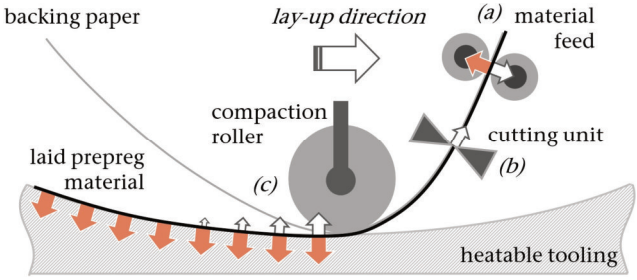

Figure 4-1. Schematic representation of prepreg tack in automated tape laying (ATL) processes. Adapted from [147] with permission from Elsevier, 2012, and extended by authors.

With the help of the simplified force diagram, it makes sense that optimum tack does not equal maximum tack from a processing perspective by any means. Actually, a suitable level of prepreg tack is a sensible balance between partially conflicting requirements: On the one hand, tack needs to be preferably low on its way through the placement head prior to the nip point in order not to adhere to guiding or conveying elements such as the material feed rollers (**Figure 4-1**, A). Resin gradually building up around the cutting unit can also cause material jams because of resin adhering to the blades (**Figure 4-1**, B). On the other hand, high tack is required to keep the laid prepreg material in position by withstanding peel forces that result from the removal of the backing paper (**Figure 4-1**, C). For AFP, the adhesive interaction of the slit tape with the compaction roller is crucial if the release film has been removed before compaction. Successful lay-up at the nip point is achieved for both processes if the adherence of prepreg toward the substrate is higher than towards the backing paper/compaction roller. Otherwise, the material will either be removed right after lay-up by the placement head or defect formation will occur within the laminate.

4.2.2 Production-induced defects

Various types of lay-up defects are known to occur during automated lay-up, namely, positioning defects such as gaps, overlaps or twisted tows [130,148–151] and bonding defects such as wrinkles/buckles, bridging, or pull-ups at tow ends [152,153]. Depending on their occurrence in terms of type, size, and frequency, production-related defects have been found to affect the mechanical properties even after autoclave cure [6,154–157].

If not handled adequately, unfavorable tack, in particular, can be responsible for the formation of the aforementioned bonding defects. One type of defect that has been investigated extensively is out-of-plane wrinkles as a result of tow steering. If prepreg tows are placed along curved paths, a mismatch between fiber length and steering path arises [158]. In-plane compressive stress on the tow inside results in buckling which counteracts the adhesive forces of prepreg tack holding down the tow (**Figure 4-2**, B). Wrinkles can be observed when the steering radius reaches a critical minimum [159]. A number of studies have examined the minimum steering radius of defect-free lay-up experimentally [138,160–162].

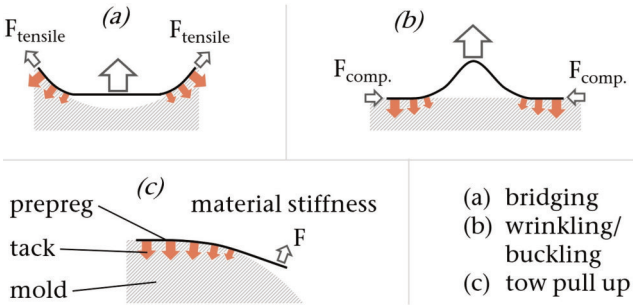

Figure 4-2. Tack-related defect formation in automated lay-up processes.

In some research papers, models are presented that directly include the role of prepreg tack. Bakjshi and Hojjati [160] introduced a time-dependent buckling model for an orthotropic plate resting on a generalized viscoelastic Pasternak foundation. With the help of the model and experimental data from tack measurement, the authors are able to predict the length of wrinkles and their formation as a function of time. Lichtinger et al. [72] use a theoretical relationship between tack and compaction considerations [163] in order to predict gaps and bridging. Bridging occurs in concave mold sections to reach lower energy levels if tensile stress exceeds tack [160] and eventually lifts the material laid (**Figure 4-2**, A). Tensile stress of the material laid can often be controlled as a process parameter or is induced as a result of underdosed material feed and at steering as discussed above. Another bonding defect-inducing scenario becomes a reality when high prepreg stiffness leads to material pull up, for example, on convex surfaces (**Figure 4-2**, C).

For automated prepreg processing by lay-up, both scenarios of machine downtime, manual laminate repair due to defects and or even wastage production are highly undesirable as they have serious economic repercussions given the high machinery (several million dollars [22]) and material costs (>100 dollars kg^{-1} [164]). Productivity issues for AFP are ascribed to machine downtime reported of up to 50 % [165]. The potential of AFP and especially ATL to excel as the most cost-effective automated composite manufacturing processes for selected industries (as demonstrated in refs. [166–168]) is, therefore, highly sensitive to prepreg tack.

4.2.3 Manufacturing-relevant factors affecting prepreg tack

A seemingly practicable way to categorize the different influencing factors on prepreg tack is to classify them into AFP/ATL-related process parameters, environmental aspects of composite production and the prepreg material properties as delivered. **Table 4-1** summarizes the most relevant factors according to the suggested categories. A brief description of the influence parameters in relation to manufacturing and/or the prepreg material has been added.

Table 4-1. AFP/ATL-related influences on prepreg tack.

Category	Influence parameter	Description
Process parameter (extrinsic)	temperature	Prepreg, head and mold temperature
	compaction force	Pressure on material at nip point applied by compaction roller
	compaction time	Duration of compaction (dependent on lay-up speed)
	debonding rate	Defect/lay-up speed-dependent rate of prepreg removal from substrate
	contact material	Surface material in contact with prepreg (mold, roller, backing paper etc.)
Environmental factor (extrinsic)	ageing	Material storage in and out of freezer due to proceeding cure reaction
	relative humidity	Relative humidity in manufacturing environment causing moisture pickup
Material property (intrinsic)	matrix viscosity	Epoxy resin flowability
	Prepreg architecture	Structural composition (impregnation level, tack-enhancing resin layers etc.)
	fiber volume fraction (FVF)	Volumetric fiber/resin ratio
	degree of cure (DoC)	Cured portion in initial B-stage as delivered

Apparently, this suggestion of classification is not and cannot be fully selective as interdependencies have been observed for many of the conceivable factor combinations, for example, increased material temperature at the nip point of the material decreases the prepreg matrix viscosity and will eventually affect the measured tack. The interdependencies are discussed in detail in section 4.4. However, the list illustrates the large variety of influence factors and, therefore, reflects the huge prospect of factor variation when characterizing prepreg tack experimentally. The majority of the depicted process parameters (**Table 4-1**) can be adjusted as test parameters within the measurement techniques for tack testing (section 4.3) itself. Environmental aspects can be simulated artificially, for example, by material storage in climatic chambers prior to tack testing. Both process parameters and environmental factors are extrinsic influences on prepreg tack which are most relevant for prepreg processors in composite manufacturing. Influences of the third category, namely material properties, are considered intrinsic and accessible through standard material characterization in the form of rheological, thermal (cure kinetics, phase transitions, etc.), microscopic or wetting analysis. Prepreg manufacturers, in particular, can benefit from a deep understanding of prepreg tack's dependence on intrinsic material properties in order to supply tailor-made prepreg systems.

4.3 Measurement

Given the high relevance of prepreg tack for advanced composite manufacturing by automated lay-up, it is rather surprising that prepreg data sheets have been providing very sparse information on tack properties to the present day. Information on tack is usually limited to the ordinal scaling of ‘low’, ‘medium’, or ‘high’ and a declaration on how long the material will be sufficiently tacky, commonly referred to as tack life. In industrial practice, the adjustment of prepreg tack is thus mainly based on heuristic methods and experience rather than on measured data. Two aspects of prepreg tack characterization are primarily responsible for this:

– First, there is no standardized measurement technique to quantify the tack of resin impregnated fibers [5]*. This failing seems to have gained recognition recently as two test methods (ASTM WK67852 and WK70428) are being currently developed by the ASTM Committee.
– Second, prepreg tack is a complex phenomenon influenced by a multitude of parameters (see section 4.4) which makes it impossible to break down tack properties to a single value. A whole set of test parameters has to be taken into account for comprehensive quantification.

*this claim is no longer valid since publication of ASTM D8336 in 2021 (see section 4.7.4)

Apart from industrial implications, both of these aspects have likewise been influencing the scientific activities on prepreg tack up to the present day. In order to tackle the first challenge, different measurement methods were utilized in the past. The majority of techniques have been adapted from PSA characterization due to their evident similarities in their fundamental adhesive nature. The methods are either performed according to PSA standards or are adapted and tailored to prepregs and/or lay-up process conditions. The methods utilized most often for experimental prepreg characterization are the probe tack test and peel test. Still, considerable research on comparability between different measuring techniques for tack testing of prepregs has not been conducted yet.

4.3.1 Probe tack test

Probe tack testing is the mechanical simulation of the highly subjective thumb or finger tack test [169]. The test is standardized by ASTM D2979 [170] which was withdrawn without a replacement in April 2019 due to its limited use in industry. However, it has been used extensively in PSA research [171–174] because of its precise control of input variables and high reproducibility [175] as well as its ability to characterize the nature of debonding (cavitation and fibrillation) in detail [176–178]. The test, which is occasionally referred to as the Polyken (probe) test [179], includes two strictly separate phases: During the compression phase, a flat probe is brought into contact with the tested material for a definite period of time (dwell time) under compressive force (**Figure 4-3**, A). When the probe is removed at a controlled rate of separation during the tensile phase (**Figure 4-3**, B), force is recorded as a function of displacement.

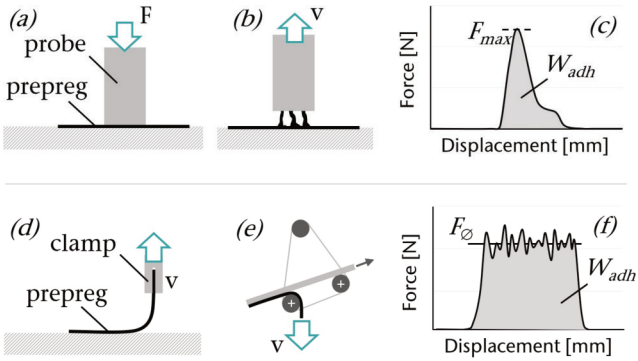

Figure 4-3. Upper figure: Compression (A) and tension/measurement (B) phases in probe tack test; lower figure: 90° (D) and floating roller (E) peel test setups; right figure: Characteristic force/displacement curves (C) and (F).

Two main indicators for tack performance can be obtained from probe testing:

- Maximum force F_{max} during the debonding process, usually measured at low elongation in the early stages of separation [180]. If the separation force is divided by the contact area, a corresponding stress value σ_{max} can be calculated.
- The work of adhesion W_{adh} or fracture energy [181] describes the energy needed to separate the formed interface completely. It is calculated by taking the force integral over the displacement interval from the start of measurement to full separation (F = 0) [182].

The probe tack test is mainly performed by using fixtures mounted to universal testing machines. Heating chambers are applied for temperature-dependent testing. Most recently, rheometers were utilized for probe tack testing of prepreg materials as well [183–185]. Apart from the compression (**Figure 4-3**, A) and tension/debonding phases (measurement, **Figure 4-3**, B), **Figure 4-3** also shows a characteristic force-displacement curve including its quantifiable tack indicators (**Figure 4-3**, C). Dubois et al. [186] investigated the curve shape by probe tack testing prepreg. Phases known from PSA testing, namely cavity formation/ growth and fibrillation [187], were transferred to prepreg material and the differences between both materials were described in detail.

4.3.2 Peel test

Several standards exist for testing the peel resistance of adhesives bonds [188]. Depending on the type of application, the standards differ in the applied peel angle (90° (**Figure 4-3**, D [189]), 180° [190] and T-Peel [191]) and/or in terms of the testing equipment employed, for example, by utilizing a floating roller (**Figure 4-3**, E [192]) or a climbing drum [193]. ASTM 3330 [194] provides several methods particularly designed for PSA tapes. All standards intend to remove progressively the tested material from a substrate or itself under a constant peel angle which results in the characteristic force/displacement curve depicted in the bottom right of **Figure 4-3**, F. The most common approach to tack evaluation is to determine the average load throughout the measurement distance $F_{\varnothing}$. Alternatively or additionally, work of adhesion Wadh can be calculated similarly to the probe test described above. Adhesive peeling in general is a well-understood mechanism which has been the target of experimental and simulative studies for some time [195–198].

4.3.3 Other measurement techniques

Other standardized methods such as the loop tack (ASTM 6195 [199]) or rolling ball method (ASTM D3121 [200]) have not been utilized to quantify prepreg tack yet despite their common use in PSA testing [201–204]. However, efforts have been put into developing measurement techniques that mimic prepreg manipulation during AFP and ATL. Crossley et al. from the University of Nottingham present a modified peel test based on the floating roller method in [205]. The method's applicability to prepreg was discussed in detail [147], repeatedly utilized and refined for further experimental studies [206–209]. A large number of results gained with the help of the Crossley apparatus are compiled in [210], the only doctoral thesis exclusively dealing with prepreg tack known to the authors of this review article.

The utilized test rig (**Figure 4-4**) mounted to a universal testing machine consists of two pairs of rollers with the first guiding the rigid plate. The second pair is spring-loaded and applies compaction force. When removing the prepreg material at a 90° peel angle, dynamic stiffness, and peel force are recorded over a predetermined distance. The authors argue that the measuring method developed reflects the ATL process more accurately than conventional tack testing methods due to the inverse

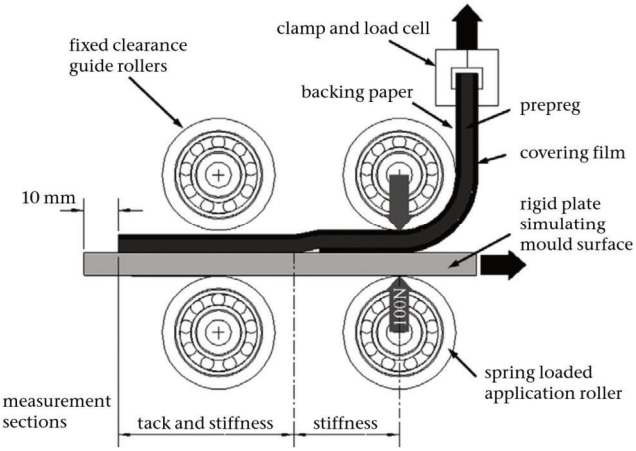

Figure 4-4. Crossley's peel tack and dynamic stiffness measuring equipment. Reprinted from [207] with permission from Elsevier, 2013.

correlation between contact time and peel rate. Furthermore, ATL process conditions are claimed to be simulated closer to reality in terms of lay-up speed and compaction force [147].

Another manufacturing-inspired measurement method for prepreg tack is presented by Boeckl et al. [211,212] who developed an online monitoring system for slit tapes in AFP. The measurement principle differs significantly from conventional testing: The transverse friction force induced by the prepreg being forwarded through a loaded pair of rollers is used as a tack indicator. This way, prepreg tack can be measured continuously as a function of compaction force and the interdependent parameters prepreg velocity/contact time. The method shows the long-term potential of its implementation as an online quality control system in industrial practice due to its continuous mode of operation. It will, however, have to prove its validity by comparison to other methods like probe or peel testing first. Nguyen performed tack characterization by producing overlapping (20 mm) prepreg specimens with the help of a robot-attached AFP head in a first step. The specimens were then tested by using a self-designed lap shear fixture loosely based on ASTM D1002 [213]. Employing the technique presented in [214], testing of AFP-manufactured samples is possible. The method was modified and transferred into a fully robot-based measuring unit [215].

4.4 Experimental studies

Experimental investigation of prepreg tack has been performed scientifically for almost four decades. The topic is still relevant in current research in the field of advanced composite manufacturing indicating that the nature of prepreg tack has not been fully understood yet. The preceding considerations can be retraced when looking at a chronological overview of experimental studies shown in **Table 4-2**. The table summarizes the findings for different input variables categorized according to the classification presented in section 4.2.3. The response of the dependent variable prepreg tack is indicated for an increase in each input variable.

Table 4-2. Overview of experimental studies of ATL/AFP-related influencing factors on prepreg tack.

Ref./ Year	Process parameter					Environmental		Material property				Test
	Tempe-rature	Comp. force	Comp. time	Debonding rate	Contact surface	Ageing	Relative humidity	Viscosity	Archi-tecture	FVF	DoC	
[185] 2019									~	(~)		Probe
[184] 2019	~	+		~	~	~		~			~	Probe
[209] 2018	~	+	~	~	~	-	+	~	~		-	Peel
[183] 2017	~	~	+	0			~					Probe
[215] 2017	(~)		0		~							Lap shear
[208] 2016	~		~	~	~				~			Peel
[216] 2016	+	~	~					~				Peel
[214] 2016	+					~						Lap shear
[207] 2013	~		~	~				~				Peel
[147] 2012	~							~	~	~		Peel
[206] 2011	~		~	~	~			~				Peel
[217] 2011								~			~	Peel
[218] 2011								~			~	Probe
[186] 2010	-	+	+	+		-			~			Probe
[219] 2004								~			~	Peel
[220] 2000							~		~			Probe
[221] 2000						-				-		Probe
[222] 1996	(-*)	(-*)							~			Probe
[223] 1995	(-*)		(-*)						~	-		Probe
[224] 1992	~					~					~	Probe
[225] 1992	~	+	+	+				~	~			Probe
[226] 1992	~	+	+	+		-					~	Probe
[227] 1991						(-)				~		Hold time
[143] 1981	~	+	+	+					(~)			Probe

Key: [+] tack-increasing, [-] tack-decreasing, [~] complex tack response, [0] no significant influence, [( )] limited validity, [ ] not investigated [*] varied during impregnation

Several aspects of experimental prepreg characterization can be deduced from the tabular list. On the one hand, a slight focusing upon the investigation of process parameters is observed especially in the earliest studies. Applied research on finding solutions for processors to run stable processes appears predominant although a shift toward the investigation of prepreg tack fundamentals becomes apparent: Not much time passed until subsequent research started focusing on the more elaborate investigation of intrinsic material parameters on prepreg tack in order to gain a deeper understanding of the process-material interaction in AFP/ATL. In summary, the current state of research is a rather balanced compilation of studies on the influences of process parameters, environmental factors, and material properties on prepreg tack.
On the other hand, the large portion of complex tack responses (indicated by) that were found for the majority of input parameters is significant. For these cases, prepreg tack was found not to follow monotonically increasing/decreasing functions and/or showed significant interdependence with other input variables. The influence of temperature discussed in section 4.4.1.1 can serve as a prime example of this behavior. In this context, Wohl et al. criticize experimental research that is conducted by investigating a single parameter of prepreg tack while the remaining parameters are kept constant. This necessarily eliminates the possibility of quantifying the influence of two (or more) parameters in conjunction with the property of interest [183].

4.4.1 Process parameters

In the following subsections, the influences on prepreg tack are reviewed and discussed in detail. The authors of this review article desist from compiling a tabular overview of numerical prepreg tack data because direct comparison turns out to be problematic due to differences in measurement techniques, test parameters, and materials. If not explicitly stated otherwise, the summarized results have been obtained from the characterization of carbon fiber/epoxy prepreg systems which represent the standard in AFP and ATL manufacturing of large aerospace structures [228].

4.4.1.1 Temperature

Selective adjustment of temperature is the most effective and at the same time workable process-related measure to control prepreg tack [5]. Modern lay-up machines are equipped with infrared heaters or hot air guns to heat up the laminate locally before prepreg placement. Additionally, heated tools can be utilized to enhance tack to the mold or previously laid plies [229]. For industrial application, suitable temperature windows are still defined by trial-and-error approaches [230]. This may contribute to the fact that efforts have been put into the heat transfer simulation to predict temperature distribution in thermoset lay-up processes [231–234]. Although considered a matter of process parameter adjustment, control of temperature strongly governs both environmental and material influences as well. Hence, prepreg tack as a function of temperature has been targeted by several experimental studies with most of them revealing a significant correlation. Ahn et al. found a bell-shaped curve featuring a tack maximum at medium temperatures [224]. The observation has been proven consistent for peel testing by Crossley [147] and in our previous work [184] utilizing a probe test method in a rheometer (see **Figure 4-5**).

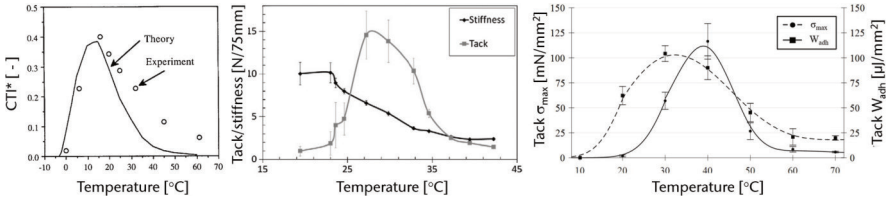

Figure 4-5. Bell-shaped curves of prepreg tack as a function of temperature. Left: reprinted from [225] with permission from Wiley, 1992. Center/right: Reprinted from refs. [147] and [184] with permission from Elsevier, 2012 and 2019.

Prepreg tack is found to be very sensitive to temperature variation: For all three studies, tack rises to a maximum and falls to practically zero within the span of less than 50 K. The temperature of maximum tack deviates around room temperature most likely due to different utilized measurement methods, test parameters, tack indicators, and materials. However, a tack maximum indicates that at least two contrasting temperature-dependent mechanisms have to prevail. In all of these studies, evidence was found that for low temperatures poor tack values are achieved

due to insufficient interface wetting resulting in adhesive failure between prepreg and substrate. For higher temperatures, wetting improves while the epoxy matrix is not able to provide high shear resistance during debonding due to a temperature-dependent decrease in viscosity (see section 4.4.3.1 for more details). Here, matrix fibrillation and residue on the substrate can be observed which indicates cohesive failure within the bulk material. Bringing both temperature-dependent mechanisms together, maximum tack performance can be achieved in the transition region from adhesive to cohesive failure [207,209]. The adhesion-cohesion balance [235] is described as a tradeoff between providing sufficient adhesive interaction at the material-substrate interface and cohesive strength. This observation is considered a PSA fundamental [236] and seems to determine the nature of prepregs in the same matter. The adhesive properties of PSA are traditionally divided into tack, peel adhesion, and shear strength [237–239]. According to this differentiation, tack is the ability to adhere quickly, peel adhesion is the resistance against peel removal and shear strength is a measure to hold the adhesive in position when shear forces are applied [240]. The categorization appears to be reasonable when taking the adhesion-cohesion balance into consideration. For prepregs, however, this distinction has not asserted itself substantially (yet). All adhesive influences are rather combined in the term prepreg tack with very limited differentiation made.

Other studies on the temperature dependence of prepreg tack found that prepreg tack follows monotonic functions. Putnam et al. [223] report a decrease in tack for elevated temperatures. The quantitative results from probe tack testing are correlated to a perceived qualitative rating provided by Boeing manufacturing personnel. Dubois et al. [186] found tack to exponentially decrease as a function of probe temperature within the investigated temperature range. Other studies revealed an increase in prepreg tack performance when raising the temperature [214,215]. These findings are neither contradictory to each other nor to the bell-shaped curves in **Figure 4-5**. Instead, test conditions are most likely chosen in a way that the results display one side of the bell-shaped curve. Extending the investigated temperature range would have most likely revealed a tack maximum as a result of temperature dependent improved wetting and decreased cohesive strength.

4.4.1.2 Compaction force and time

The manufacturing aspects of AFP and ATL presented in Section 4.4.2 illustrate that prepreg tack depends on a sequence of both the bonding and the debonding processes. In order to achieve optimum bonding conditions, intimate contact of the prepreg material toward the substrate is crucial. Process-related factors, which determine the true contact area, are the compaction force/stress applied by the consolidation roller as well as the time of compaction also known as dwell time. **Figure 5-6** shows tack of prepreg measured by Dubois [186] with the help of a probe test setup.

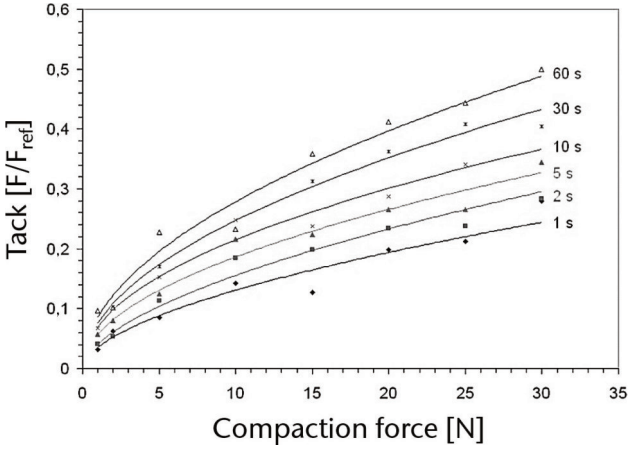

Figure 4-6. Tack as a function of compaction force and compaction time at 30 °C probe temperature. Reprinted from [186] with permission from Springer Nature, 2009. Labels were renewed for improved readability.

Prepreg tack is found to increase as a function of both compaction force and time. The results are supported by several studies utilizing different test methods [143,209,224,225]. Hence, the influence seems to be independent of the measurement technique. **Figure 5-6** evidently showcases that a lack of tack due to insufficient compaction force can be countervailed by an increase in dwell time. This measure, however, conflicts with a productive lay-up process as compaction time is inversely proportional to the lay-up speed in AFP and ATL processes [241]. Experimental results from some studies on compaction force and pressure are

subject to restrictions in terms of manufacturing transferability. Test parameters often do not reflect lay-up conditions adequately [205] as, for example, compaction time is limited to a few milliseconds depending on lay-up speed and compact roller dimensions [242].

The aforementioned true contact area describes the actual area that is wetted by the adhesive or the prepreg resin respectively during the bonding process [187,243,244]. The concept was adapted by Gillanders [143] (probe test) and Endruweit [208] (Crossley apparatus) who both determined the true contact area of prepreg resin to glass plates after defined compaction. The results were correlated with results from tack measurement and a correlation between the true contact area and prepreg tack was found: True contact area as function of compaction force converges a maximum logarithmically indicating 100 % intimate contact. Tack follows compaction force in the same way (also see **Figure 4-6**) which entails linear relationship between prepreg tack and true contact area. Consequently, maximum prepreg tack in terms of the bonding process is achieved when the substrate is fully wetted. The influence of the compaction roller (stiff vs compliant roller) on prepreg tack was also studied [209]. Differences in tack were observed and attributed to differences in pressure distribution and contact time between both rollers. The actual deformation behavior of the investigated rollers remained unknown in the study.

Although considered an intrinsic material property to be discussed in detail in Section 4.4.3.1, resin viscosity is crucial when discussing contact formation. Dahlquist, in this context, made a proposal on what a PSA has to fulfill in terms of flow to efficiently make contact to substrates [245]: Storage modulus G' measured by dynamic mechanical analysis (DMA) or oscillatory rheology has to be below $3*10^6$ dyne cm^{-2} or 0.3 MPa, respectively. Despite its simple nature, the proposal has proven to be surprisingly applicable independent of the utilized adhesive or substrate [246,247]. The validity of the Dahlquist Criterion for the viscoelastic and tack properties of prepregs was eventually tested by Crossley et al. [147]. The authors found prepreg tack to generally follow the criterion's principle of improved contact for lower moduli but numerical values differ from the 0.3 MPa proposed by Dahlquist. The discrepancy is credited to prepreg-characteristic features such as fiber surface pattern and impregnation conditions discussed in Section 4.4.3.2.

4.4.1.3 Debonding rate

The debonding rate is perceived as the velocity of material removal during prepreg-substrate separation and is highly dependent on the individual defect (section 4.2.2). Instantaneous peeling of laid prepreg by the placement head will, for example, occur at much higher debonding rates (approximately at lay-up speed) than for the rather slow prepreg detachment due to bridging. The debonding rate has a significant influence on the measured stress-strain curves and, therefore, on the final tack performance as reviewed in the following.

Most of the studies which targeted the influence of debonding rate on prepreg tack found an increasing tack response when the prepreg-substrate interface is broken up at higher rates [143,183,184,186,226]. It has to be noted, however, that especially for probe testing, the shapes of the stress-strain curves change drastically when varying the debonding rate as pointed out by Dubois et al. [186] When comparing the stress-strain curves of different studies in literature, high-rate curves show a more surface-near, adhesion-controlled fracture (with little or no fibrillation) resulting in a high tack value of F_{max} and lower W_{adh}, respectively. Hence, the dependency of tack on the debonding rate is highly contingent on the used tack indicator. Böckl et al. [212] report a decrease in transverse friction force as a function of velocity. Still, the applied measurement technique differs fundamentally from peel or probe testing which may explain the discrepancy.

Observations similar to the depicted probe testing results have been made employing peel testing methods such as the Crossley apparatus: In [206], an inverse logarithmic relationship between the debonding rate and temperature is reported. This has led to the suggestion that the time-temperature superposition principle (TTS) may be applicable toward prepreg tack which has been confirmed repeatedly for peel testing in subsequent studies [147,207–209]. Here, dynamic prepreg stiffness was found to increase monotonically as a function of feed rate while bell-shaped curves are determined experimentally for tack. The rate dependency of tack, for example, for PSA, has traditionally been explained based on viscoelastic behavior exhibited by polymers during the debonding process.[128] The role of prepreg resin viscosity and TTS are discussed in detail elsewhere (section 4.4.3.1).

4.4.1.4 Contact material

Following the prepreg material on its way through AFP or ATL heads, it makes contact to different tack-exhibiting surfaces such as the compaction roller, guiding elements, backing paper and eventually the mold or previously laid plies (see section 4.2.1). Generally, most experimental studies resort to only one material which the tack of a single layer of prepreg material is measured toward. The most commonly used material combinations are prepreg-steel and prepreg-prepreg. In addition, research was conducted to selectively quantify the influence of different surface combinations. These studies yield a common result: Whenever tack between two prepreg layers was determined and compared to other material combinations, tack was found to be highest for the prepreg-prepreg combination. Endruweit et al. [209] report the adhesive performance of the prepreg-prepreg combination to be 2.5 to 5.5 higher than for prepreg-steel depending on the face. No effective tack toward fluorinated ethylene propylene representing the surface coating of the compaction roller was detected. The findings from tack measurement can serve as a quantitatively based explanation for the first-ply tack problem which estimates that a successful lay-up of the first ply on the mold as being the most difficult [70,248]. Crossley et al. [206] compared the peel tack of ATL prepreg tape toward stainless steel and composite tool with/without a mold release agent. The experimentally determined tack responses, which were rudimentarily validated by subsequently performed ATL trials, are shown in **Figure 4-7**.

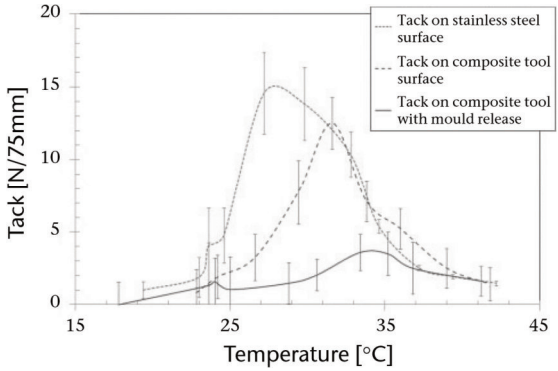

Figure 4-7. Peel tack of automated tape laying (ATL) prepreg tape toward different contact materials. Reprinted from [206] with permission from Taylor & Francis, 2011. Figure labels were renewed for improved readability.

A significant influence of the contact material is reported with the release agent eliminating the largest portion of prepreg tack toward the composite tool surface. In this context, Nguyen [215] performed first ply tack tests with various types of release films aiming at reliable process conditions for vertical tow placement. Differences between the release films were observed as a function of temperature. According to **Figure 4-7**, stainless steel exhibits highest tack among the investigated materials of the study. However, it must be noted that the prepreg-prepreg combination was not investigated at this point and tack tests on stainless steel were limited to a single level of surface roughness [206]. The latter aspect may be of importance for prepreg tack as the effect of surface roughness on the tackiness of soft adhesives has been demonstrated for PSA [249,250]. This may contribute to physical adhesion mechanisms such as mechanical interlocking [251].
Previous considerations in combination with the influence of compaction force and dwell are the basis for the adhesive portion of bonding between prepreg resin and the substrate of interest. Interfacial interaction with the substrate is most likely caused by intermolecular forces (IMFs), namely different types of van der Waals forces and H-bonding [252]. These interactions are known to range roughly two magnitudes below covalent bonds in terms of bond energies (1-25 kJ mol^{-1} vs >200 kJ mol^{-1} [253]) which account for the low separation energies of prepreg tack compared to physically or chemically curing adhesives. Although the epoxy matrix is evidently able to chemically react (for final autoclave cure), prepreg tack is not determined by covalent bond formation toward the substrate but is rather a matter of the aforementioned IMF. The intermolecular adhesive interaction between prepreg resin and substrate has not been investigated despite its very probable crucial role. This should be encountered by further research efforts – for example, in the form of analyzing the temperature-dependent wetting behavior of different surfaces by epoxy resin using contact angle measurement. Potential results would contribute to the fundamental understanding of prepreg tack mechanisms.

4.4.2 Environmental factors

The time-temperature dependent curing and moisture pickup process of prepreg material progresses primarily in the time span of ambient environment exposure between freezing and AFP/ATL processing [254]. There is an interdependency between both factors as moisture absorption by epoxy resin has been shown to

accelerate the curing reaction [255]. However, for their influence on prepreg tack, both aspects have mostly been investigated independently as reviewed in the following.

4.4.2.1 Ageing and DoC

The fact that targeted ageing of prepreg material is occasionally performed in industrial practice in order to control prepreg tack prior to lay-up highlights the crucial role of this environmental factor. It is represented on data sheets in the form of tack life which indicates the time span of suitable tack properties after removal from the freezer. Thermoanalytical methods have been combined with tack measurement in order to investigate the influence of ageing-related cure behavior on prepreg tack. In their early study on the topic, Ahn et al. [224] report a temperature-dependent tack maximum which decreases for increasing storage times. Tack of fresh prepregs was compared to the adhesive properties of prepreg material which was stored at -18 °C for 46 months and an additional exposure to 75 °C for 3 hours, respectively. The tack maximum, however, remains constant at temperatures 20 °C to 25 °C above the glass transition temperature T_g shifting toward higher temperatures with increasing ageing times. The same phenomenon but for slightly different temperatures (40 °C-45 °C above T_g) is reported in [184]. The temperature difference between both studies may be attributed to diverse ageing temperatures and times (46 months at -18 °C vs 5-60 days at room temperature). The shift of maximum tack as a consequence of progressive material ageing was also substantiated by results from TTS for peel testing (see section 4.4.3.1 for details) performed in [209]. It was deduced from these studies that a certain flowability is necessary for surface wetting and, consequently, for a considerable tack to be measured. Matrix vitrification when tack measurement temperature is set below T_g, therefore, appears to greatly restrain surface wetting. In this case, the aged prepreg's bending stiffness increases drastically resulting in deteriorated drape. This issue is reflected in **Figure 4-8** which shows the ageing-related evolution of DoC and T_g for a carbon fiber/epoxy prepreg measured by differential scanning calorimetry.

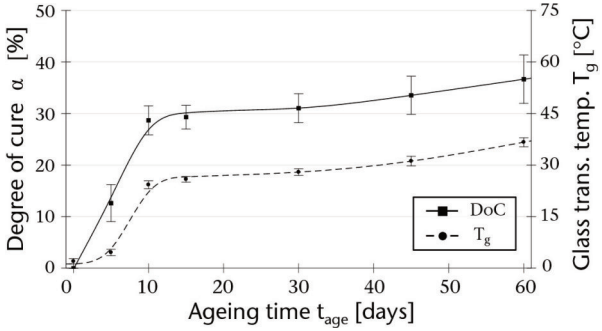

Figure 4-8. Effect of room temperature ageing on kinetic properties of carbon fiber/epoxy prepregs. Reprinted from [184] with permission from Elsevier, 2019.

DoC and T_g rise steeply within the first 10 days (tack life) with T_g reaching room temperature after this time span. Tack measured at room temperature for 10 days' old prepreg was completely lost, while an increased work of adhesion (up to 66 %) was measured at elevated temperatures. The bell-shaped curves described by Ahn et al. [224] were found to be shifting toward higher temperatures as prepreg resin viscosity increases in the wake of progressing cure reaction [184]. This assumption of ageing-affected molecular mobility can serve as an explanation for the somewhat contradictory results that are reported for the dependency of prepreg tack on ageing: While a decrease in tack was measured in refs. [186,209,212,227], a (temperature-related) increase is observed in refs. [184] and [214].

Several attempts have been made in literature to produce prepregs on laboratory-scale prepregging machines with tailored processing-relevant properties including tack. Tack properties were adjusted by the selective control of the level of resin cure (B-staging). The DoC of commercial prepregs in B-stage is known to be 25 % to 35 % [256]. Banks et al. [219], who developed a structural glass/epoxy prepreg for marine and civil infrastructure applications, report maximum fracture energy at 30 % DoC (**Figure 4-9**).

The value was also specified as the optimum level of resin cure in the tradeoff between handling, drape, and tack. Tack maxima as a function of DoC were also reported by Rajaei [217] and Shaghaghi [218] who investigated tack of phenolic/glass prepregs. However, tack maximum of phenolic prepregs formed at significantly lower conversion of 5.3 % pre-cure compared to epoxy-based systems [217]. Novolak and resole types of phenolic resins were shown to exhibit a varying

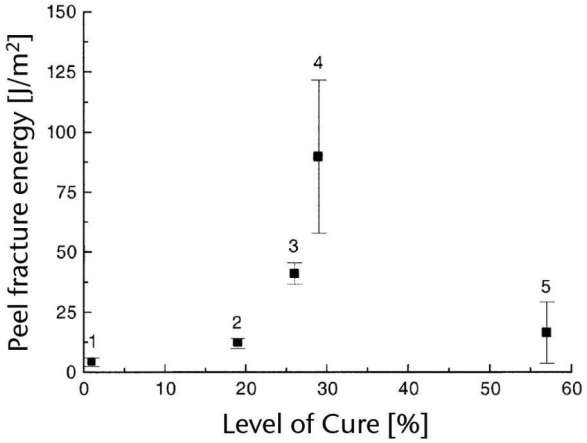

Figure 4-9. Prepreg tack as a function of cure level. Reprinted from [219] with permission from Elsevier, 2004.

tack level [218]. A direct comparison between epoxy and phenolic prepregs with different types of fiber reinforcements was drawn by Smith et al. [185]. Even carbon fiber prepregs with thermoplastic matrices that usually do not exhibit any tack at all near ambient temperature have been investigated for their levels of tack most recently: Shin et al. [257] performed tack tests on lab-scale produced prepregs using carbon fiber fabric and partially polymerized poly(methyl methacrylate). Tack decreased rapidly as a function of ageing-induced polymerization and was completely lost after 60 minutes of ambient exposure.

4.4.2.2 Moisture

Apart from tack implication, moisture absorption in uncured prepregs may result in void formation in out-of-autoclave laminates [258,259] and to a lesser degree even in autoclave-cured composite parts [260]. Water in the form of sorbed moisture is known to plasticize epoxy resins [261] affecting the processability of prepregs in the same manner as the mechanical performance of cured parts. Buehler and Seferis [220] studied water absorption and desorption of glass and carbon fiber prepregs and conducted tack measurement on these materials with low and high solvent contents (from impregnation process). While water uptake was found to peak at 11 % to 13 % after 1200 hours of absorption, moisture drops to 3 % after 450 hours of additional exposure in a desorption environment. No tack results are

presented for the moisture exposed specimens but the adhesive properties of glass prepreg are reported to have doubled after solvent removal. Wohl et al. [183] investigated the combined impact on tack which is entailed by changes in relative humidity conditioning in combination with other input parameters (contact time, contact force, and temperature). The surface plots from probe tack testing using a rheometer as a test apparatus are displayed in **Figure 4-10**.

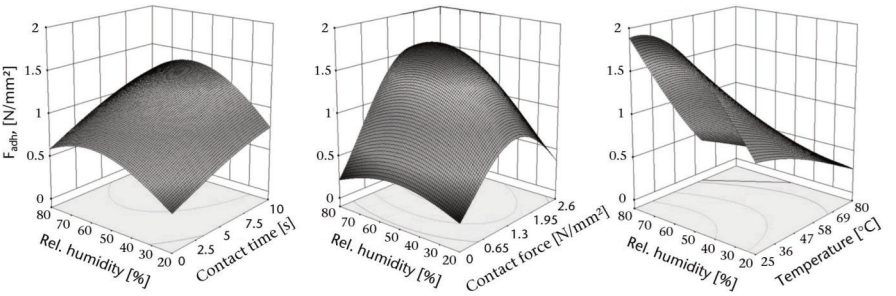

Figure 4-10. Response surfaces of tack (F_{adh}) measured as a function of relative humidity and second input variables (contact time, contact force, and temperature). Reprinted from [183] with permission from the Society for the Advancement of Material and Process Engineering (SAMPE), 2017. Figure labels were renewed for improved readability.

Together with the other displayed input variables, a parameter set could be determined by optimization analysis in order to achieve maximized F_{adh}. Desirability for maximum tack includes relatively low temperature, high contact time and a specific threshold of compaction force. For humidity, however, interdependencies with other input variables turn out to be more complex as moderate to high values should be favored [183].

The partly ambiguous dependence of tack on water uptake can be seen in the peel test results performed in [209]. Here, lower tack values in general are reported for humidity-exposed samples (33 %, 43 %, and 59 % RH) than for unconditioned prepregs on the one hand. This finding was also made by Dubois for 80 % and 20 % RH exposure [186]. On the other hand, a significant increase in tack from 34 % and 43 % to 59 % RH is observed in [209] which appears to be contradictory considering the generally lower tack of conditioned specimens compared to fresh prepreg. The authors consider plasticization effects to be responsible for this. In summary, the small number of studies on the topic has revealed that there is a

significant influence on humidity exposure and accompanied moisture uptake on prepreg tack. Still, causal relationships are not fully understood yet and require further studying.

4.4.3 Material properties

Prepregs for automated lay-up technology are commercially available in a wide range of material properties, for example, in terms of matrix formulation, fiber type, and reinforcement weight. As a result, composite manufacturers can opt for material systems meeting their demands for both the final part performance as well as the processing factors including tack.

4.4.3.1 Resin viscosity

Prepreg matrix resins and PSA traditionally differ in terms of polymer formulation. While epoxies, cyanate esters, and phenolic resins are mainly used for prepreg material, a large variety of both natural and synthetic polymers such as acrylics [262–264], natural rubbers [265], polyurethanes [266], polyvinyl ethers [267] and many more are processed for PSA. Despite the difference, both materials are based on polymers and, therefore, exhibit viscoelastic behavior which decisively affects their tack properties. Time, shear rate, and temperature dependence of prepreg resin viscosity has thus been analyzed in several studies and brought together with tack characterization as reviewed below.

In order to exhibit maximum tack, prepreg resin viscosity needs to fulfill contradictory requirements in agreement with the temperature discussion in Section 4.4.1.1: good viscous flow for substrate surface wetting and high viscosity for a certain shear resistance during debonding ([219,268]; also see Dahlquist's criterion in section 4.4.1.2). The first aspect was targeted by Rao et al. [216] who set up a full factorial DOE for lay-up load, speed, and temperature. Peel tack was recorded as a function of input parameters and additional DMA was conducted for viscoelastic characterization. **Figure 4-11** shows the complex viscosity and loss factor tan δ in a temperature range between room temperature and 300 °C.

The authors report a strong increase in peel force for both input parameters compaction load and speed when raising the temperature from 25 °C to 65 °C. Within the investigated temperature range, complex viscosity drops by almost a full magnitude from 1.25 to $0.2*10^9$ Pa s.

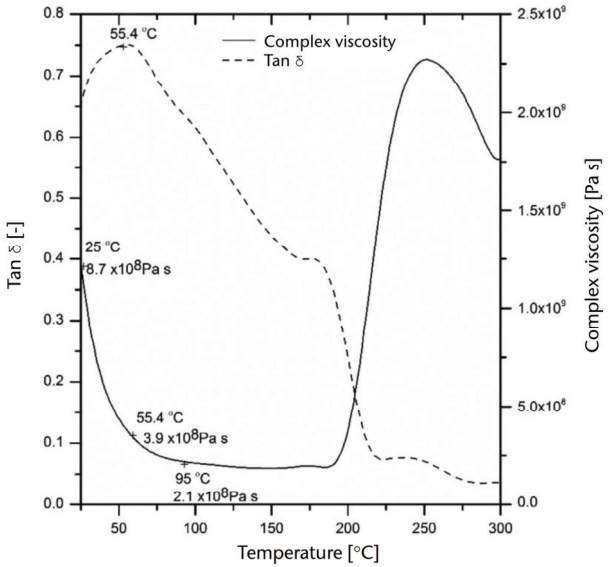

Figure 4-11. Loss factor tan δ and complex viscosity of epoxy towpreg resin as a function of temperature (1 Hz, 5 K min^{-1}). Reprinted from [216] with permission from SAGE, 2016.

Tan δ, which describes the ratio between loss modulus G" (viscous portion) and storage modulus G' (elastic portion), following accordingly from 0.4 to 0.1 indicating a strong shift toward a more viscous behavior of the matrix resin. The rheological findings were considered to be responsible for improved surface wetting and, consequently, a higher measured tack. However, the debonding process was not taken into consideration. Both viscosity and the cohesive debonding portion of tack were shown to follow Arrhenius-type, exponentially decreasing functions of temperature elsewhere [184].

Ahn et al. [225] used the resin viscosity as one of four intrinsic material parameters to describe prepreg tack as a bulk viscoelastic property and developed a model presented in section 4.5. The correlation between matrix viscosity and tack can also be represented by the TTS principle. With the help of the concept, polymer viscoelasticity is described over a wide range of deformation rate and temperature [269]. It allows master curves to be produced based on shift factors from models such as the William-Landel-Ferry equation [270] or Arrhenius plots [187,244]. For PSA, the applicability of the principle to tack was demonstrated early by Kaelble in

the 1960s [271] and frequently reproduced in PSA research [175,272]. Crossley [207] successfully transferred TTS to prepreg tack (and dynamic stiffness) with the help of the WLF equation and experimental data from oscillatory rheology and peel tack measurement. **Figure 4-12** shows the shifted tack curves of a glass/epoxy ATL tape as a function of feed rate V (debonding rate) and temperature.

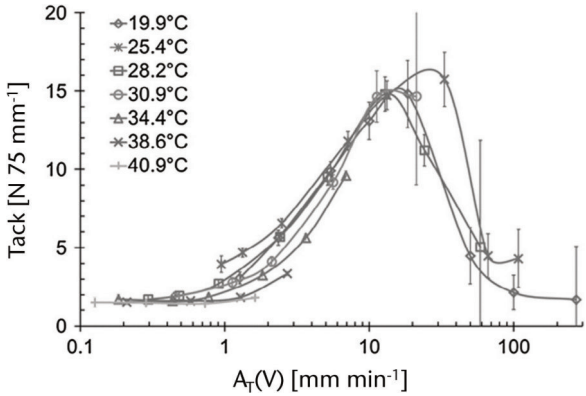

Figure 4-12. Tack curves shifted by time-temperature superposition. Reprinted from [207] with permission from Elsevier, 2013.

A high degree of overlapping shifted tack curves for different temperatures indicates the general applicability of the principle to prepreg tack. Surprisingly, it was found that the TTS relationship could be employed for both adhesive and cohesive prepreg fracture, in other words, the left and the right slopes of the bell-shaped curves. Usually for PSA, only cohesive failure within the adhesive follows the TTS principle (see PSA references above). A discussion on this topic for prepregs can be found at the end of [207] as well as in other studies by the authors [147,208,209], in which the TTS concept was repeatedly reapplied for further investigation.

In the context of viscosity and tack, Chang developed the Chang Window [273] which lassifies PSAs into different specialist applications (protective films, medical tapes, labels, etc.) as a function of complex rheological data, namely G' and G" measured at different frequencies. The window's deformation frequency range (≈ tack measurement range) was set to 0.01 to 100 s^{-1} by Chang. Direct transfer of prepreg tack data toward the Chang Window has not been performed yet despite its

active reception in PSA research [235]. However, a similar categorization for prepregs can be beneficial if viscoelastic classification is possible, for example, according to data sheet information (low, medium, high tack) or even its matter of use (AFP/ATL/hand lay-up).

4.4.3.2 Prepreg arcitecture and fiber volume fraction

The presence of reinforcement fibers in prepregs is the most apparent distinctive feature in comparison to the homogeneous, bulk-like appearance of PSA layers. Investigating the role reinforcement fibers on the adhesive performance of prepreg, therefore, is essential. Crucial aspects are the fiber volume fraction (FVF) as well as the local distribution of both prepreg components.

In [186], stress-strain curves obtained from probe testing pure epoxy "pancakes" and prepreg were compared and discussed. The authors attribute differences in the shape of single displacement phases (cavitation, fibrillation, etc.) to the presence of reinforcement fibers in the prepreg material. The structural aspects discussed are gradients of resin content in z-direction, prepreg roughness due to surface-near fibers and others. Endruweit et al. [208,209] investigated the tack of the inner (when on a roll; no protective paper: 'N-Face') and outer (with paper: 'P-Face') face of ATL tape. Experimental data revealed a 93 % higher peel tack of the P-Face toward steel than for the N-Face. The difference was attributed to different distributions and volume of resin on the surface. However very little discrepancy was found between P-P and N-N prepreg-prepreg combinations. It was generally deducted that prepreg architecture influences both adhesive and cohesive mechanisms of prepreg tack. In the same studies, a sharp rise in tack was measured for larger inter-ply angles between two prepreg layers. Peel tack increases by 67 % from 0° to 90° ply angle.

Hayes et al. [222] produced prepregs from UD carbon fibers and a model epoxy resin formulation in order to investigate the influence of hotmelt prepregging-related structural properties on prepreg tack. As a result, the impregnation parameters (pressure and temperature) were varied and prepregs were examined in terms of impregnation level and FVF. The results from probe tack testing are displayed in **Figure 4-13**. Increasing both impregnation parameters leads to a better impregnation level and a slightly raised FVF. Considering this anticipated relationship, it can be concluded from **Figure 4-13** that the higher the impregnation level of the prepreg is, the lower the measured tack will be.

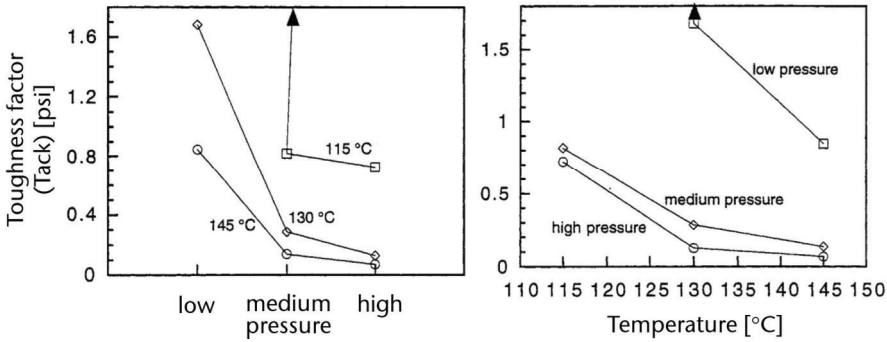

Figure 4-13. Tack (toughness factor) as a function of impregnation pressure and impregnation temperature. Reprinted from [222] with permission from Wiley, 2004.

The correlation was attributed to an insufficient amount of surface resin to fully wet the interface. In contrast, a thicker bulk resin layer will contribute to the viscoelastic debonding if the prepreg is poorly impregnated. This finding supports the industrial prepregging practice of impregnating reinforcement fibers or adding a second tack-enhancing layer [5].

4.5 Model approaches

Model approaches to tack of prepregs have rarely been presented in literature compared to the numerous and partially elaborate models developed for PSA [274–276]. Research on prepregs has focused on utilizing experimental methods for characterization instead, as presented in the previous section. In 2011, Lukaszewicz [241] stated that "tack is still a prepreg property that is not fully explored and cannot be accounted for in process models." Almost a decade later, the first claim of his statement has been alleviated by continuing research but in our opinion still holds in general. However, knowledge on prepreg tack has reached a state of basic model applicableness as recently demonstrated by Forghani et al. who have presented a modeling framework for the simulation of prepreg tack in AFP processes [277,278]. The proposed numerical tack model ([279]; **Figure 4-14**) is based on experimental calibration by probe tack testing in a rheometer as presented in [183].

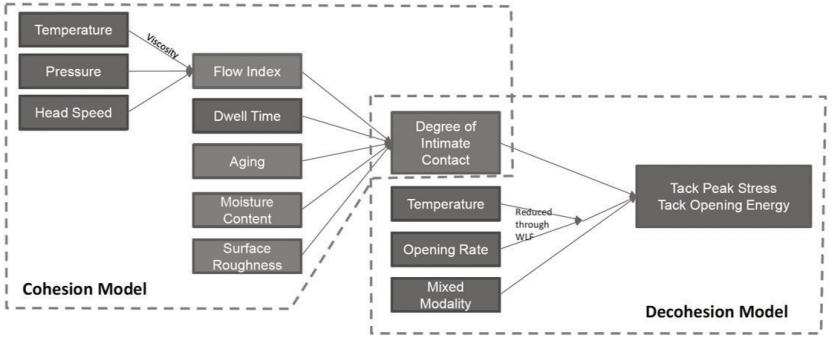

Figure 4-14. Flowchart presenting dependencies on tack response. Reprinted from [279] with permission from the Society for the Advancement of Material and Process Engineering (SAMPE), 2017.

Tack phenomena are split into two stages, namely, the cohesion and decohesion stages, which represent influencing factors of the bonding/compaction and the debonding/separation phases. Both stages are modeled separately with the so-called degree of intimate contact (DoIC, ratio of wetted contact area) acting as the linking intermediate state variable ($0 \leq DoIC \leq 1$). A validation study [280] in the model framework was eventually conducted that aimed at demonstrating the model's ability to predict defect formation in AFP steering for a simple curve arc.

Ahn et al. present an early attempt to describe prepreg tack as a bulk viscoelastic property of a laminate stack [225]. The authors used the standard linear solid model, which had been proven applicable for thermoset composite materials before [281,282], and modified it with regard to prepregs (void content, fiber areal weight, etc.). Four intrinsic material parameters from viscoelastic analysis were determined and represented in the model. Good agreement between model prediction and experimental data was found. Experimental data include the stress-strain curves from probe tack testing and the tack indicator called compression tack index (CTI*) which is defined as the ratio of output energy while debonding and the compressive input energy during bonding. Some authors of later experimental studies on prepreg tack reuse the CTI* as a tack indicator [184,221].

4.6 Conclusion/future perspective

This review article presents a summary and discussion of the current state of research on the adhesive behavior of prepreg material and its relevance for automated lay-up technology. The characterization of prepreg tack has been an active area of research for several decades and was shown to be primarily targeted by employing experimental methods of investigation in the past. The lack of a standardized measurement technique* has led to different methods of quantifying the tack of thermoset pre-impregnated fiber composite fibers. The variety of measurement techniques employed in combination with a large set of tack-determining influence parameters makes it difficult to describe the complex mechanisms of prepreg tack thoroughly. Consequently, misinterpretation of experimental results may occur easily when investigating single parameters within narrow variation intervals. Seemingly contradictory results, however, can be explained by the adhesion-cohesion balance as demonstrated repeatedly throughout this review article. It can be regarded as a prepreg tack fundamental representing the tack-governing mechanisms of intimate contact formation and viscoelastic deformation behavior. Generally, the instantaneous adhesion upon the light pressure application of prepregs resembles the behavior of PSA. The profound knowledge base of longtime research on PSA has been steering and will continue to steer prepreg tack characterization in the future by providing proven experimental, modeling and simulation approaches.

Although considerable knowledge on prepreg tack has been generated by experimental investigation and has yielded first process modeling approaches to this day, substantial shifts toward selective process adjustment have not yet been made. However, this will be the next step necessary to overcome the trial and error-based practice in AFP and ATL. Validation studies are necessary in order to prove that tack measurement and model results can be turned into successful operating points of composite manufacturing systems. This way, prospective process improvement can be achieved by increased robustness toward laminate defects and machine breakdown. Challenges will arise when conciliating measures of tack-relevant process adjustment and production efficiency, for example, in terms of lay-up speed or material storage.

*this claim is no longer valid since publication of ASTM D8336 in 2021 (see section 4.7.4)

Acknowledgments

The authors would like to acknowledge the financial support of the European Regional Development Fund (ERDF) and the federal state of Lower Saxony for the interdisciplinary research project 'FlexProCFK'.

ORCID

Dennis Budelmann: https://orcid.org/0000-0003-4465-5714

4.7 Research on prepreg tack after 2020

For completeness, the most recent scientific progress made in the field of prepreg tack after publication I (2020) is outlined in the following. Details on the results of individual studies that are directly related to the thesis investigations can be found in the introduction sections of the respective research papers (chapters 5.1-8.1). The overview is therefore limited to tabular compilations of research articles and theses which - in a classified manner - are meant to round out **Table 4-2**.

4.7.1 ASTM D8336

In midyear 2021, the American Society for Testing and Materials (ASTM) issued the standard ASTM D8336-21 'Standard Test Method for Characterizing Tack of Prepregs Using a Continuous Application-and-Peel Procedure' [283]. Its testing equipment is based on the 'Crossley Apparatus' which was first presented in 2009 [205], discussed in detail in 2012 [147] and repeatedly utilized for scientific studies at the University of Nottingham up to the present day (see publication I, section 4.2 for details). The scientific findings achieved by utilizing the apparatus were eventually merged with industry demands of both material suppliers and composite manufacturers who contributed to the elaboration of the standard. After its release, the University of Nottingham (Composite Research Group) initiated a round robin exercise as an inter-laboratory test with the main goal of determining

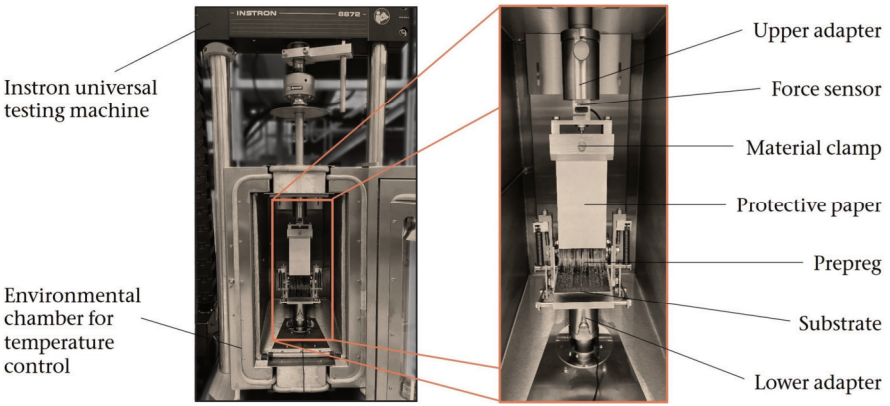

Figure 4-15. Setup for tack measurement according to ASTM D8336 in a universal testing machine.

the reproducibility of the standard's test procedure and equipment. The international consortium (USA, UK, GER, ESP) was composed of eight industry partners (aircraft and wind turbine manufacturers, material suppliers, aerospace component suppliers) and four research facilities including the participation of Clausthal University of Technology (Institute of Polymer Materials and Plastics Engineering). A version of the standard revised on the basis of the round robin results was eventually submitted to the ASTM committee in late 2023. An overview of the underlying research and a discussion of the process of successfully passing an ASTM ballot can be found in [284]. The fixture design (**Figure 4-15**), measurement cycle and experimental results from ASTM D8336 were benchmarked by Budelmann et al. (section 9.3 [285]) against other prepreg tack measurement techniques.

4.7.2 Studies focusing on the lay-up process

Table 4-3. Publications on the interrelation between lay-up process and prepreg tack since 2020.

Ref.	Year	1st author	Topic/description
[286]	2020	Smith	Process maps for AFP parameters considering prepreg ageing
[287]	2021	Belhaj	Finding optimal process parameter combination for high resultant tackiness in AFP by using the Taguchi method
[288]	2021	Netzel	Effect of humidity exposure of prepregs on defect generation
[289]	2022	Heller	Tack-related steering defects depending on different test and process parameters as a function of out-time
[290]		Heller	
[291]	2022	Pan	Response surface method to find optimal process parameter combination for high tack levels
[292]	2022	Pan	Model-based estimation of critical steering radii based on experimental tack data
[293]	2022	Wang	Implementation of a multi-factor tack model into an AFP modelling framework

4.7.3 Studies focusing on materials

Table 4-4. Publications with a focus on material properties in conjunction with tack since 2020.

Ref.	Year	1st author	Topic/description
[294]	2020	Poulavand	Tailored tack and drape for a dual-cure epoxy resin system
[69]	2021	Yousefi	Comparison of tack between solid and liquid epoxy resins
[295]	2021	Tonye	Influence of different reinforcements (fabric vs. UD)
[296]	2021	Hübner	DGEBA/DICY resin system for prepregs
[297]	2021	Kuliaei	Relationship between tack and degree of cure in DGEBA/DICY/ diuron epoxy resins
[298]	2021	Szpoganicz	Rheology and ageing influence on tack of phenolic prepregs
[299]	2021	Silva	Characterization and tack testing of sisal epoxy prepregs
[300]	2023	Malakhovskii	Commercial prepreg and binder characterization by probe and peel testing

4.7.4 Studies focusing on tack fundamentals

Table 4-*5*. Publications targeting the fundamental mechanisms involved in the stickiness of thermoset prepreg materials since 2020.

Ref.	Year	1st author	Topic/description
[301]	2020	Rajan	Traction-separation laws for cohesive separation of thermoset prepregs in the context of AFP
[302]	2021	Choong	Exploration of the correlation between contact area and tack
[303]	2022	Das	Friction and tack characterization with in-situ contact area inspection
[304]	2022	Zu	Relationship between viscosity and process parameters
[305]	2022	Xiao	Two-stage model for prepreg interface bonding
[306]	2022	del Rey	Time temperature superposition (William Landel Ferry eq.) applied to probe tack testing

Chapter 5

5. Process and environmental parameters – Publication II

Interaction of process parameters and material properties with regard to prepreg tack in automated lay-up and draping processes

D. Budelmann[a], H. Detampel[a], C. Schmidt[b], D. Meiners[c]

[a]Institute of Polymer Materials and Plastics Engineering, Clausthal University of Technology, Ottenbecker Damm 12, Stade, Germany

[b]Institute of Production Engineering and Machine Tools, Leibniz Universität Hannover, Ottenbecker Damm 12, Stade, Germany

[c]Institute of Polymer Materials and Plastics Engineering, Clausthal University of Technology, Agricolastr. 6, Clausthal-Zellerfeld, Germany

Composites Part A: Appl. Sci. and Manuf.* 117 (2019) 308-316.

*Journal metrics:

CiteScore: **15.2** (Scopus, 2023)
Rank 16/398; 96th Percentile (Engineering: Mechanics of Materials)

Impact factor: **8.1** (Clarivate, 2023)

Abstract

Selectively adjusting the tackiness of epoxy pre-impregnated carbon fibers is considered mandatory in terms of process stability of automated lay-up and draping. This experimental study investigates the influence of crucial process and material parameters such as temperature, compaction force, debonding rate and ageing on prepreg tack using a rheometer as a test apparatus. Accompanying material characterization is conducted in terms of cure kinetics and rheology to establish a profound understanding of tack-determining mechanisms and material behavior. Two evaluated tack indicators are found to be sensitive to temperature and steadily increased as a function of compaction stress. The maximum tack plateau of progressively aged prepreg shifts towards higher temperatures. Material is still processable after tack life with tack properties exceeding the adhesive performance of fresh prepreg when being processed at elevated temperatures. Tackiness of impregnated tape for automated draping and aerospace epoxy prepreg differs in both quantitative extent and pivotal mechanisms.

* Corresponding author.
E-mail address: dennis.budelmann@tu-clausthal.de (D. Budelmann).

https://doi.org/10.1016/j.compositesa.2018.12.001
Received 28 September 2018; Received in revised form 27 November 2018; Accepted 1 December 2018
Available online 03 December 2018
1359-835X/

5.1 Introduction

Within the last two decades, evolution of aeronautical and automotive structural design concepts like the Airbus A350 XWB, Boeing 787 or lightweight car body structures has boosted the demand for highly automated carbon fiber reinforced plastics (CFRP) manufacturing processes. Both Automated Fiber Placement (AFP) and Automated Tape Laying (ATL) are the dominant technologies for highest quality and cost-effective manufacturing of large composite structures when using epoxy-based pre-impregnated carbon fibers [167,307]. Steadily increasing numbers of scientific publications in the field of AFP and ATL since the upcoming of prepreg materials in the 1960s [4] underline the growing interest in automated lay-up technologies. In combination with autoclave curing, the major advantages of these processes are the producibility of large composite parts with low porosity, high fiber volume fractions and tailored laminate design [100] as well as a significant reduction of material waste and hand labor [40,308]. As automated robot-based CFRP production processes, they are predestined and - to a certain extent - reliant to achieving a high level of cross-linking between physical and digital domains. Implementation of digital tools like online-monitoring for defect detection [130] or the use of neural networks for lay-up machine learning [309] can contribute to the strong potential of AFP/ATL technology to tackle challenges of modern Industry 4.0 composite manufacturing.

Though being considered one of the crucial material properties for manufacturability and final laminate quality for automated lay-up [223], prepreg tack has not been addressed by extensive scientific research yet. Tack refers to the prepreg's ability to self-adhere to either other materials or to itself when processed [5,310]. When being regulated and handled adequately, it ensures the pre-impregnated fibers to be deposited at desired positions by a robot-based AFP/ATL machine and to remain in place throughout the manufacturing process. Although there is no generally acknowledged definition of prepreg tack in terms of a mutual scientific agreement on which mechanisms are characteristic or how to quantify them, parallels towards pressure sensitive adhesives (PSA) can be drawn easily. For both materials, PSA and thermoset prepreg, tack evolves as a resistance to separate two surfaces that have been brought together under low pressure and over a short period of time in absence of any solvent evaporation or chemical reactions [240,246].

Usually, manufacturers of structural materials provide very little information on tack properties of their commercially distributed prepreg. Data sheets are traditionally limited to imprecise ordinal data such as 'low', 'medium' or 'high' tack as well as an approximate period of time the prepreg can be stored at room temperature and still provide sufficient tack properties ('tack life'). From a practical viewpoint, processors mainly have to rely on experience while running the risk of using unprocessable material or disposing expensive functional prepreg after tack life has expired. As a result, common lay-up defects like buckling or bridging can be traced back to insufficient knowledge on tack properties and its interaction with the manufacturing process [248,311]. Hence, a general understanding on the interdependency between material ageing, lay-up process parameters and tack would vastly inure to the benefit of processors.

However, just like the lack of a definition of prepreg tack there is no standardized method of quantitative measurement. The most common approach in literature to quantify prepreg tack is to utilize the probe tack test (e.g., used in [143,186,223,225]) derived from the standard PSA probe tack test method [170]. For this test, the sample is brought between two parallel plates, compacted and debonded in a normal direction to the prepreg surface while recording the axial displacement and acting force. Experiments are generally performed in small universal testing machines that include a temperature chamber. Wohl et al. [183], however, use a rheometer to determine prepreg tack by probe tack testing. Several advantages like precise control of experimental parameters and high reproducibility have, among others, been demonstrated by the extensive work by Zosel [175] for PSA.

Crossley [147] developed a prototype peel test apparatus for compliance and prepreg tack determination by 90° peeling of glass fiber/epoxy prepreg. By peeling instead of normally separating the prepreg from the surface upright, the authors intend to approach a test setup that simulates the automated lay-up process of impregnated fibers as both normal and shear forces are investigated. The results raised by this kind of tack testing are found to be consistent with 16% standard deviation. However, the comparison between both tack measuring methods probe tack testing and peeling revealed major differences in the obtained results. Crossley's peel test apparatus was used for further studies of prepreg tack, e.g. by Endruweit et al. [209] who emphasize the necessity to examine a range of test

parameters in order to fully explore the complex tack behavior based on their findings.

Several authors conducted research on the effects of prepreg ageing on the final post-cure laminate quality indicated by mechanical performance like flexural, compressive, ILSS or impact properties [227,254,312,313]. As far as prepreg ageing is concerned, however, little scientific effort has been expended towards its influence on manufacturing properties such as tack. Ahn [224] investigated the influence of ageing at low storage temperatures (-18 °C) over a long period of time of up to 46 months. Cole [227] conducted qualitative tack tests using prepreg samples aged at room temperature for up to 66 days. In case of failing the tack test a cleaned steel plate, which is applied under a prepreg specimen with light pressure, simply drops off within a time span of 30 min. Although the crucial ageing time was found to be 25 days, no quantitative results can be obtained from this kind of tack testing procedure. The tack properties of two CRFP prepregs were investigated in the study of Blass [314] who determined the prepreg T-peel resistance after different time spans of room temperature ageing. Here, peel resistance is reported to decrease on a linear basis as a function of preaging with no measurable tack after 60 days for both materials. It has to be noted, still, that all measurements in this study are performed at room temperature while in modern AFP/ATL machines, temperature is usually adjusted within the lay-up head and/or the mold [5].

Ahn and Seferis [225] make an exclusive attempt of modeling the adhesive properties and dynamics of debonding by describing tack as a bulk viscoelastic property of a prepreg laminate stack. The authors developed a model that is characterized by four intrinsic material parameters, namely relaxed and unrelaxed modulus, relaxation time and initial void content which were raised from the measuring method itself, though. Still, the basic modeling methodology of separating intrinsic material parameters and extrinsic test parameters/operating conditions seems to be suitable to characterize the interdependency between prepreg tack and automated lay-up process.

The preceding considerations on to AFP/ATL of commercial prepreg are also applicable to automated draping processes [315] as the wet impregnated fabric or nonwoven makes direct contact towards different production-relevant surfaces, e.g. the draping device, steel toolings (first plie issues), autoclave-ready shaping foam for sandwich structures or previously draped plies.

From a manufacturing point of view, scientific research on tack of impregnated carbon fibers for composite parts is far from equaling a status in which it can be accounted for in automated lay-up or draping process models [241]. Thus, the aim of this study is to investigate the influence of manufacturing process parameters of AFP/ATL/draping technology and ageing on the tack properties of thermoset carbon fiber prepreg and draping material. Establishing a better understanding of the interdependency between intrinsic material properties and external process parameters is aspired. The results can be beneficial for both the purposeful development of prepreg resins at material suppliers and, secondly, processors who take interest in optimizing their automated lay-up processes.

5.2 Experimental

5.2.1 Materials

The prepreg material (A) used in this study was an aerospace-grade, unidirectional carbon reinforced fiber pre-impregnated by a toughened epoxy resin system for use in primary and secondary structures. Nominal fiber volume content is 60 % resulting in a prepreg mass of 294 g m^{-2}. The prepreg is suited for press or autoclave cure at 180 °C. Tack life expires after 10 days while the maximum accumulated period of time of the prepreg being stored outside the freezer ('out life') should be limited to less than 30 days according to data sheet.

With a view to examine the tack properties of a resin impregnated tape (B), which is to be processed by an automated draping machine [315], material samples are manually produced by hand laminating. For this purpose, a unidirectional carbon spread tow tape (200 g m^{-2}) is impregnated by Prism EP2400 resin by Cytec Industries Inc., Woodland Park, NJ at elevated temperatures (~100 °C). The resin is a one-part, toughened liquid epoxy system for injection processes. A curing cycle of two hours at 180 °C is recommended and results in a 179 °C T_g (dry). The resin's wide range of viscosity as a function of temperature facilitates the draping process control by purposive adjustment of resin temperature.

5.2.2 Test parameters raised from AFP/ATL and automated draping processes

In order to investigate the interdependency between manufacturing process parameters and prepreg tack, probe tack test parameters are derived from manufacturing process parameters. According to [17,316], the three most relevant manufacturing parameters (a, b and c) with regard to both laminate quality and process stability in automated lay-up processes are

a) Prepreg/tooling temperature at compaction point: Influencing the viscoelastic properties of the prepreg's matrix resin, temperature adjustment can be regarded as one of the most beneficial measures to control prepreg tack.
b) Compaction force applied by the compaction roller in order to deposit the prepreg onto the substrate surface: E.g. for ATL, compaction stress typically is below 0.1 MPa [4] but the necessary force can vary greatly depending on material width, amount of placed tows etc.
c) Lay-up speed: Adjustment of lay-up speed can be considered as a compromise between productivity (laid kg hour^{-1}) and process stability (avoiding production-induced defects). Most automated lay-up systems operate at maximum linear velocities up to 1 m s^{-1}.
d) Furthermore, the influence of prepreg ageing at room temperature is investigated in this study as the proceeding crosslinking of the matrix resin is expected to influence the prepreg's adhesive performance.

The tack properties of impregnated carbon tape for draping are examined in terms of the influence of temperature (e) and draping surface (f):

e) The tape/tooling temperature at the draping point generally effects the draping process in the same way (see above) it does for AFP/ATL processes.
f) The tack properties towards different surfaces are of note for the draping process as impregnated tape is draped over variable materials: The first ply of impregnated tape is usually applied on either a (heated) steel or aluminum mold, also known as hard toolings, or, alternatively, on structural foam for producing sandwich structures. After the first ply is laid down, the second ply of the laminate is to be placed on precedent uncured wet tape.

Consequently, the tackiness between three material combinations (tape - tape, steel, foam) are investigated. In addition to the tape presented in the previous section, stainless steel X10CrNi18-8 as well as Rohacell 71 HERO autoclave-ready structural foam are used as the other surface materials. For all tests including the conventional commercial prepreg, tackiness between two plies of prepreg is measured. **Table 5-1** recapitulates the experimental fractional factorial design of the study.

Table 5-1. Overview of the experimental tack survey.

Material	Lay-up or draping parameter	→	Input variable of experiment	Variation range
A: Prepreg	a) Temperature	→	Temperature T in oven	10 – 70 °C
	b) Compaction force	→	Compaction stress σ_c	0.66 – 13.33 N cm^{-2}
	c) Lay-up speed	→	Displacement rate v_d	0.02 – 2 mm s^{-1}
	d) Prepreg ageing	→	Storage/ageing time t_{age} at RT	Fresh (0 days) – 60 days
B: Impregnated tape for draping	e) Temperature	→	Temperature T in convection oven	20 – 120 °C
	f) Draping surface	→	Material combination	Tape – tape/steel/ structural foam

5.2.3 Tack measurement

Prepreg tack tests are conducted using a rheometer as test apparatus (**Figure 5-1**).

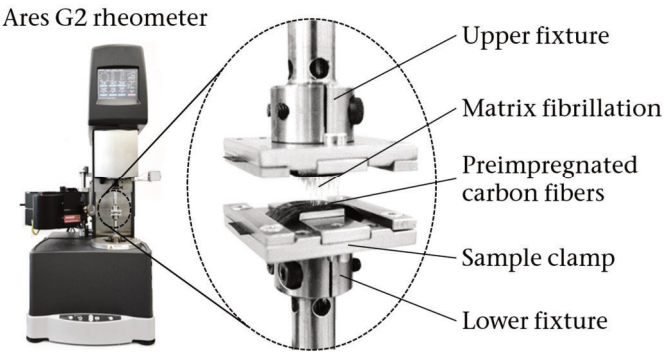

Figure 5-1. Ares G2 rotational rheometer and prepreg sample holder used for probe tack testing.

Being used in this study, the ARES G2 rotational rheometer by TA Instruments (New Castle, DE, USA) includes an axial servo control system enabling transient normal force measurements within an axial transducer range of 0.001-20 N at a fine resolution of 10^{-5} N. Hence, the tack measurement can be performed as a high precision probe tack test which is derived from adhesion characterization of pressure sensitive adhesives as to be found in [176,317–319]. Fixtures were designed and manufactured to pick up and hold down the strips of pre-impregnated carbon fiber throughout the measurement cycle displayed in **Figure 5-2**.

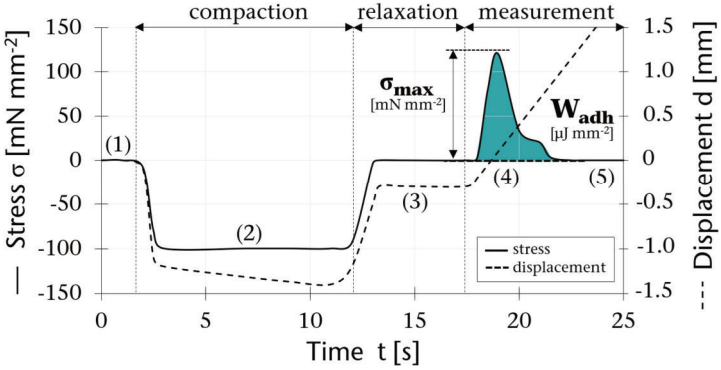

Figure 5-2. Measuring cycle of the probe tack test.

The fiber orientation is maintained parallel during measurement by locking the motor drive of the rotatable lower fixture subsequent to aligning. The method includes five consecutive steps that are programmed via the rheometer software interface. Initially, the prepreg sample is loaded by a constant compaction force of 1-20 N corresponding a compaction stress σ_c of 0.66-13.33 N cm^{-2} on a rectangular measuring area of 1.225·1.225 cm^{-2} (1). Compaction stress is being applied for 10 s (2) before relaxing the sample in a loadfree condition (3). Slight changes in displacement occur due to viscoelastic behavior of the matrix while compression stress remains unaltered in steps (2) and (3). During tensile phase (4) the sample is gradually separated at different constant traverse speeds (0.02-10 mm s^{-1}) until the measured stress drops to zero indicating full sample separation (5). Fiber orientation between upper and lower prepreg samples is kept parallel at all stages of the cycle. Maximum tack stress σ_{max} is determined at the local maximum force

during step (4) divided by 1.50 cm^2 of active measurement surface. The work of adhesion W_{adh} is defined as the energy needed to fully separate the sample interface. Let λ_5 be the displacement when separation starts and λ_5 when ending, respectively ($\sigma_{adh}(\lambda_4, \lambda_5) = 0$), the work of adhesion is given by

$$W_{adh} = \int_{\lambda 4}^{\lambda 5} \sigma_{adh}(\lambda) d\lambda. \qquad \textbf{Eq. (5-1)}$$

In order to evaluate the ratio between the stress being induced into the sample during compaction σ_c (see **Figure 5-2**: phase 2) and the tack stress σ_{max} needed to subsequently separate the sample (phase 4), the dimensionless compression tack index (CTI_σ) [225] is calculated as follows:

$$CTI_\sigma = \frac{\sigma_{max}}{\sigma_c} \qquad \textbf{Eq. (5-2)}$$

Temperature control during tack measurement is achieved by a forced convection oven surrounding both upper and lower sample fixtures mounted to the rheometer transducers. The feeding oven airstream is provided by a mechanical chiller system and heated by two resistive gun heaters guaranteeing constant temperature during measurements (range: -100 to 600 °C; deviation: ±0.2 K). A camera in the forced convection oven of the rheometer is used to record real-time sample images enabling optical distinction between different failure modes (e.g. adhesive vs. cohesive failure). Additionally, the fibrillation process can be analyzed with increasing axial displacement.

5.2.4 Differential scanning calorimetry

A Differential Scanning Calorimeter (DSC) Discovery DSC by TA Instruments (New Castle, DE, USA) is used to determine the glass transition temperature (T_g) and degree of cure α (DoC) of aged prepreg samples. DSC measurement is performed at a modulated heating rate of 1 K min^{-1} (amplitude: 0.159 K, period: 60 s) between -30 and 260 °C. Prior to DoC determination the prepreg samples are aged at room temperature (21 °C) in a humidity control glove box (RH <0.1 %) to avoid moisture pickup over a period of time. The degree of cure α is calculated by the enthalpy ratio

$$\alpha = \frac{H_f - H_a}{H_f} \qquad \textbf{Eq. (5-3)}$$

where H_f and H_a are the enthalpies of fresh and aged prepreg samples, respectively. Enthalpies are determined by integrating the normalized non-reversible heat flux dQ/dt which is provided by the measurement. It has to be noted that the 'fresh' prepreg material is supplied with its B-staged epoxy resin already being partially cured. As a result, the actual reference DoC of fresh prepreg is not 0 % as assumed for this study but usually amounts to 25-35 % for typical thermosetting prepreg matrices provided in B-stage [256].

5.2.5 Rheology

The temperature-dependent complex viscosity of neat Cytec EP 2400 toughened epoxy resin used for impregnation of the draping tape is measured using the Ares G2 rheometer presented in section 5.2.2. Measurements are performed as oscillation tests at 2 % strain and a shear rate of 10 rad s^{-1} between two parallel plate geometries at 0.5 mm gap. A temperature profile between 20 and 120 °C is applied. Running a steep temperature ramp of 5 K min^{-1} results in a short test time to avoid undesired temperature - and time-dependent cure during viscosity measurement.

5.3 Results and discussion

5.3.1 Prepreg (Material A)

The upper graph of **Figure 5-3** displays characteristic stress-strain curves obtained from probe tack testing fresh prepreg as a function of temperature (20-70 °C). The examined material does not show any distinctive tackiness until temperatures near room temperature are reached. Maximum tack strength σ_{max} at 10 °C is as low as 0.22 mN mm^{-2} (SD = 0.05 mN mm^{-2}) which is why a corresponding stress-strain curve cannot be depicted properly in the figure. For elevated temperatures, the stress-strain curves extend over an increasing elongation reaching its maximum at 40 °C where fibrillation is observed to be most pronounced. It is worth mentioning that the debonding mechanism generally takes place in a surface-near distance of up to 3 mm away from the compaction interface. For most temperatures the

debonding process is even completed within 1 mm of displacement. For medium temperatures ~40 °C, fibrillation can actually be observed for displacement values far beyond 3 mm although the resin matrix is not able to absorb any further appreciable debonding energy as tack stress drops to zero.

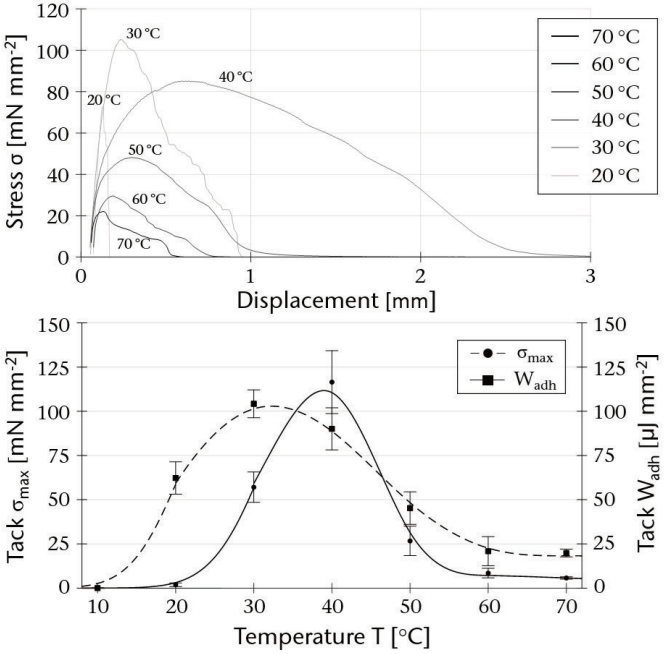

Figure 5-3. Stress-strain curves and tack parameters σ_{max} and W_{adh} of fresh prepreg (v_d = 0.2 mm s^{-1}, σ_c = 10 N cm^{-2}).

5.3.2 Temperature

When plotting σ_{max} and work of adhesion W_{adh} as functions of temperature (**Figure 5-3**, lower graph), both graphs show similar courses: Both tack indicators form local maxima at 30 and 40 °C, respectively, as tack values decrease rapidly towards lower and higher temperatures. While no tackiness can be measured for low temperatures <10 °C, a certain tack level still persists for elevated temperatures ≥60 °C. Our findings match the results of Crossley et al. [147] who also observed temperature-dependent peak formation, however, as a result of peel testing.

Relatively seen, the W_{adh} graph is shifted towards higher temperatures by 10 °C compared to σ_{max}. In general, the presence of this shift indicates that examining both tack indicators W_{adh} as well as σ_{max} is not redundant for the characterization of prepreg tack. The shift can phenomenologically be explained by having a closer look at the stress strain curves. For low temperatures, narrow stress peaks are formed within very limited displacement. This material behavior may be attributed to the domination of the elastic component when the storage modulus G' of the resin is high in comparison to the loss modulus G" at low temperatures. On the one hand, the matrix resin does not fully wet the interface region due to a lack of flow ability during compaction. On the other hand, the stored energy is quickly released elastically without considerable viscous flow.

With rising temperatures, the viscosity of the matrix resin decreases which is assumed to result in better wetting of the measurement surface. Improved wetting enlarges the actual surface area partaking in the debonding process and, therefore, is believed to favor the tack performance of the interface. For PSA, it is well known that a storage modulus $G' < 3 * 10^5$ Pa (Dahlquist criterion) marks the onset of high tack as result of sufficient wetting [246]. Crossley [147] showed for prepreg that passing the Dahlquist criterion can be associated with a transition from interfacial to cohesive failure when peeling. In our probe test study, exceeding a prepreg temperature of 40 °C where a maximum of adhesion energy is reached and fibrillation is strongest, leads to a significant decrease in both maximum displacement and stress. It is assumed that for high temperatures a large amount of separation energy is dissipated during debonding as a result of a dominating viscous portion represented by loss modulus G". In conclusion, the shape of the W_{adh} graph with its local maximum at 40 °C has to be formed by at least two contrariwise mechanisms with one of them steadily favoring and the other one hindering tackiness with increasing temperature. These are most likely an improvement of interface wetting due to lower resin viscosity and a lower resin's ability to resist shear stress as discussed above. The finding of temperature-dependent tack maxima for both indicators is contrary to the results of Dubois [186] who found the maximum debonding force to decrease in a monotonic way as a function of temperature. The authors asserted that a decreasing resin viscosity causes the matrix to migrate out of the debonding interface. Possibly, Dubois' testing parameters were chosen in a way so that their experiments were performed in a

temperature range which starts on the right side of the local tack maximum of σ_{max} (30 °C, see **Figure 5-3**).

In terms of processing the investigated fresh prepreg via an automated TL/FP, the performed tack measurement of our study unveils the importance of accurately adjusting the temperature during CFRP manufacturing. Both tack indicators W_{adh} and σ_{max} show very high dependence on temperature within narrow temperature ranges, e.g. W_{adh} is quartered when increasing temperature from 40 to 50 °C. Therefore, tack properties may be insufficient, especially for first ply lay-up as the adhesive strength is only brought up from one side of the formed interface if not using an additional tackifier layer.

Reproducibility of the developed tack measurement method using a rheometer is sufficiently high to determine a significant influence of temperature on the tack properties of fresh prepreg. The average standard deviation in the measured temperature range for W_{adh} is 15.2 % and 12.8 % for σ_{max}, respectively. Tack SD for the other investigated input variables (compaction force, displacement rate and ageing) are alike. Since the resolution of the rheometer's axial force and displacement is as fine as described previously (see section 5.2.3), the deviation is exclusively attributed to sample preparation and prepreg inhomogeneity. Factors, which influence the results from a material standpoint, might be variance in resin content or the topographic condition of the prepreg which are obviously no aspects that disqualify the tack measurement method itself. Furthermore, inequalities in sample width might occur during manual cutting of the prepreg as part of sample preparation. As a result, the active measurement surface slightly diverges from the envisaged 1.50 cm^{-2}.

5.3.3 Compaction force

In the following section, the results of tack measurement are presented which are obtained from varying the compressive stress σ_c during compaction phase (phase 2, see section 5.2.3). Again, fresh prepreg is used and compaction period as well as displacement rate are remained constant for 10 s of loading and 0.2 mm s^{-1}, respectively. In **Figure 5-4**, W_{adh} is plotted as a function of compaction force F and temperature T. The depicted surface plot is based on a 7 (10-70 °C) * 4 (1-20 N) experimental data matrix.

In response to low stress of 0.66 N cm^{-2} inflicted by 1 N compaction force, a marginal level of prepreg tackiness can be achieved, which is considered to be insufficient for a stable automated lay-up process. However, tack properties rise greatly as a result of increasing compaction force. Although the growth in maximum tack attenuates for F > 8 N at 40 °C, elevating the compaction force apparently leads to a continuous widening of high tack values towards both higher and, especially, lower temperatures around 40 °C. When compacting the 2-ply pre-

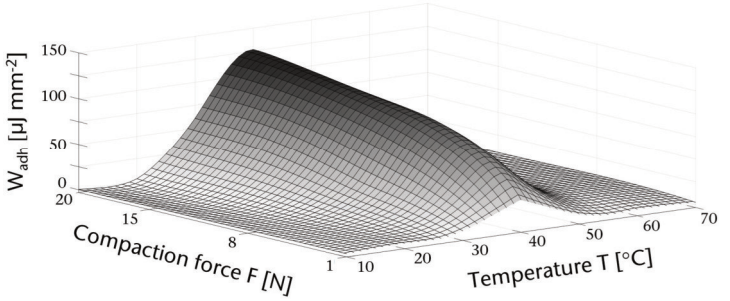

Figure 5-4. Work of adhesion as a function of compaction force and temperature of fresh prepreg.

preg stack by the maximum axial load of 20 N, considerable adhesive resistance has to be overcome for almost the entire investigated temperature range. It is assumed that the lack of resin flowability at low temperatures is compensated by increased resin pressure resulting in a better wetting of the interface. Furthermore, structural phenomenon might play a role as surface near fibers slide into one another as a result of high compression. During the debonding phase, an additional frictional force between reinforcement fibers has to be overcome as fibers have to pass along each other for full sample separation. These assumptions are strengthened by the pronounced difference in compaction displacement in z-direction: While the 2-ply prepreg stack is compressed by 0.053 mm under load of 1 N, compaction by 20 N result in a z-displacement of 0.086 mm (both values measured at 20 °C).

For all measurements including a variation of the compressive stress σ_c, the plateau of maximum adhesion energy W_{adh} remains constant at 40 °C. However, if σ_c was raised considerably higher than in this study, maximum tack values are expected to shift towards lower temperatures. From a manufacturing point of view, the stretching of high tack values towards higher and lower temperatures for high

pressure compaction can be utilized by prepreg processors: If precise temperature control of the prepreg and/or the mold is problematic due to e.g. lay-up machine restrictions, the lack of tackiness can be compensated by increasing the force which is applied by the compaction roller during lay-up. As argued above, this finding can be utilized most effectively at low temperatures near RT. Unfortunately, the phenomenon only comes into effect to its whole extent in consecutive prepreg layers whereas in first ply, which usually is the more challenging layer due to higher heat losses and more difficult temperature control of the tooling, there are no entangling fibers and the phenomenon is limited to better surface wetting at higher compaction forces. **Figure 5-5** depicts the maximum tack stress σ_{max} and compression tack index CTI_σ, which describes the dimensionless proportion between σ_{max} and σ_c (see **Eq. (5.2)**).

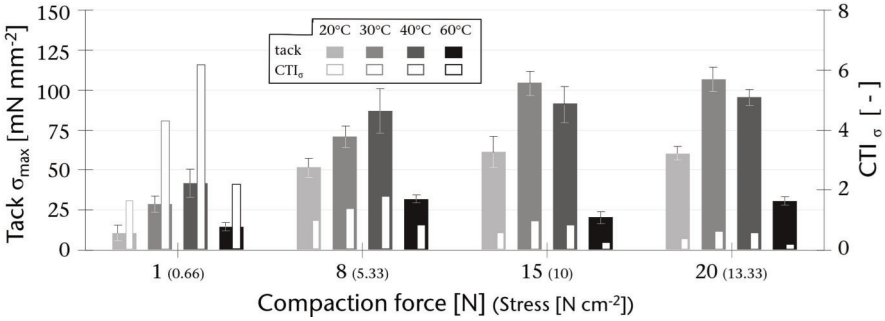

Figure 5-5. Tack (σ_{max}) and CTI_σ as a function of compaction force and prepreg temperature.

In accordance with W_{adh}, both parameters the measured σ_{max} as well as the corresponding CTI_σ form maxima at specific temperatures. The maximum, which is located at 40 °C for low compression stress of 1 and 8 N, shifts to 30 °C at higher loads (15 and 20 N). Again, compensation of the lack of resin flow ability can serve as an explanation. No significant difference of tack performance between 15 and 20 N is observed at all investigated temperatures. Surprisingly, CTI_σ is considerably higher than 1.0 under 1 N and 8 N compaction load. For 40 °C and 1 N compaction force, CTI reaches its maximum of >6. This finding was not expected as no chemical reactions occur within the short time of compaction which could enhance the adhesive performance by this extent.

5.3.4 Lay-up speed

The influence of different debonding speeds is investigated which is experimentally represented by variation of the displacement rate during measurement phase (phase 4, see section 5.2.3). Establishing a connection between the displacement rate as an experimental parameter and the actual debonding speed during lay-up is challenging as the actual debonding speed is highly dependent on the occurring defect: E.g., for bridging, the debonding speed will be several magnitudes lower than for the scenario in which the compaction roller peels of the prepreg directly after lay-up. In the latter case, the experimental displacement rate would have to be equal to the lay-up speed which cannot be realized due to machine restrictions of the rheometer. Instead, the experimental variation of displacement rate had to be limited to a maximum of 2 mm s^{-1} because the measured debonding force reaches the rheometer's maximum axial transducer limit of 20 N at higher rates.

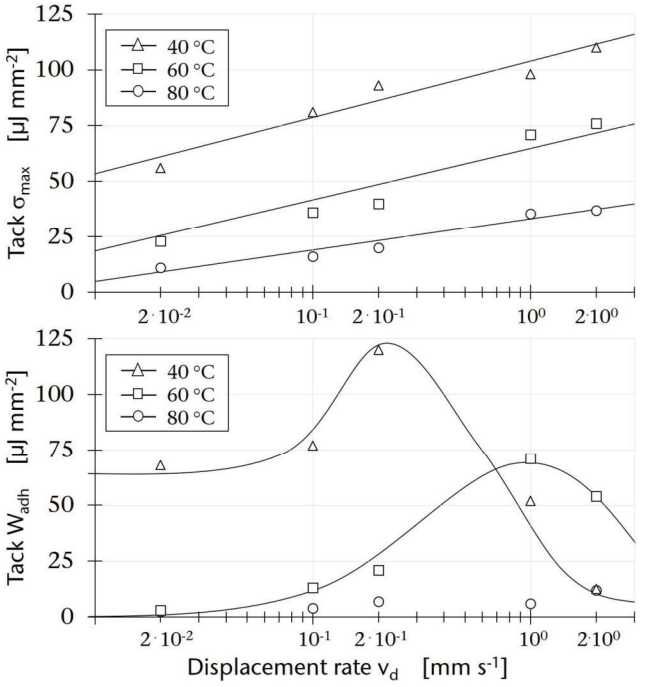

Figure 5-6. Prepreg tack σ_{max} and W_{adh} measured for different displacement rates and temperatures.

Standard test parameters (σ_c = 10 N cm^{-2} and fresh prepreg) are used while probe temperature and displacement rate are varied. **Figure 5-6** shows the tack indicators in dependence of debonding rate in a range between 0.02 and 2 mm s^{-1}.
Maximum tack stress σ_{max} (**Figure 5-6**, upper graph) is found to steadily increase as a function of displacement rate v_d. The strongest rise is observed for low separation velocities, which is why σ_{max} can be described logarithmically for all three investigated temperatures. Looking at the shape of stress strain curves behind it, the increase in v_d leads to higher, but more narrow stress peaks. It is assumed that when shear rates are high, there is no time available for the interface to relieve stresses by relaxation. Dubois [186], who utilized σ_{max} (normalized) as the only indicator of prepreg tack performance, also observed a steady increase as a function of displacement rate. However, no temperature influence was investigated by the authors.
According to our study, tack expectedly decreases when raising the test temperature from 40 to 60 and 80 °C as these measurements are performed at temperatures on the right hand side of the tack maximum displayed in **Figure 5-3**. The work of adhesion W_{adh} (**Figure 5-6**, lower graph) forms maxima for 40 and 60 °C. By raising the temperature, the maximum of W_{adh} is both lowered in extent as well as shifted towards higher temperatures. The maximum of 80 °C is, therefore, expected to exist beyond the investigated range of displacement rate. The two contrary mechanisms which may be responsible for the maximum formation, are both time-dependent: On the one hand, low displacement rate results in a long period of time for stress relaxation of the matrix resin. As a consequence, the stress, which is integrated over the displacement, is considerably lower throughout the whole debonding phase. On the other hand, the observed high stresses within very limited displacement, leads to lower W_{adh} values at high displacement rates.

5.3.5 Prepreg ageing

Cure kinetics and stages of room temperature-aged carbon fiber prepreg samples are characterized by differential scanning calorimetry. The results of DoC and T_g as a function of ageing time are shown in **Figure 5-7**.

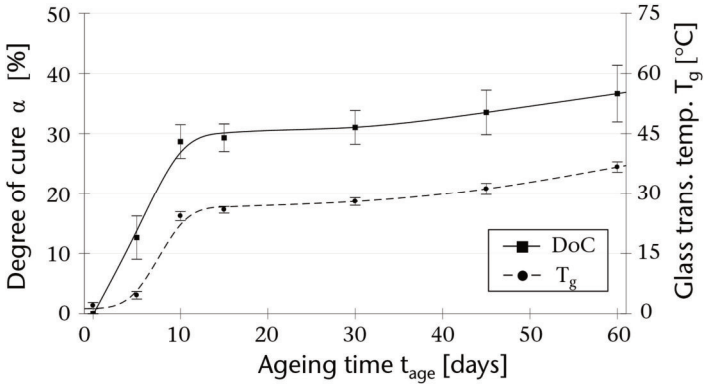

Figure 5-7. DoC and T_g of room temperature-aged prepreg samples measured by DSC.

According to DSC measurement, T_g exceeds room temperature after the epoxy prepreg has been aged for more than 10 days. The result could be confirmed by a subjective observation during sample preparation for probe tack testing: For prepreg aged >10 days, the preexistent bending compliance required for easily draping the material over the sample holder (see **Figure 5-1**) at RT was lost. This T_g-related stiffening was not witnessed for prepreg aged for less than 10 days accordingly. The critical 10 days time span regarding T_g trespassing RT conforms with the time span which is declared as the prepreg's tack life in the datasheet. After 10 days, the rate of conversion $d\alpha/dt$ decreases significantly. This finding does not surprise much as it is well known that for epoxy systems the reaction is kinetically controlled prior to vitrification ($T_g < T_{ageing}$) and becomes diffusion-controlled afterwards ($T_g > T_{ageing}$) [320]. Subsequent to the investigated maximum ageing time of 60 days, the prepreg reaches 37 % DoC and a T_g of 35 °C, respectively. 1.9 °C are measured as T_g of fresh prepreg material while DoC is set to 0 % by definition.
High standard deviation of the DoC is attributed to the prepreg's inhomogeneity in terms of resin content in combination with the small tested DSC sample size (~4 mg). However, DSC results are in very good agreement with the study of Grunenfelder and Nutt [321] who monitored the cure behavior of two prepreg materials (Cytec Cycom 5320-1 and ACG MTM44-1) over 56 days by modulated DSC: The uncured T_g increased from 0 to 20 and 40 °C while the estimated DoC was raised from 0 to between 10 and 30 % (in dependence of material).

Figure 5-8 presents the adhesive energy W_{adh} which is expended while separating fresh and aged prepreg samples at a displacement rate of 0.2 mm s^{-1}. Here, both temperature T (10-70 °C) and ageing time t_{age} (fresh-60 days) are varied. The data used as nodes for surface plotting is depicted as black dots in the figure.
It becomes obvious that room temperature aged prepreg does not fully lose its fundamental tackiness within the investigated time span. Instead, the longer the prepreg material is stored outside the freezer the further the 'high tack plateau' is shifted towards higher temperatures. Bringing together the cure kinetics shown in **Figure 5-7** and the temperature-dependent tack of **Figure 5-8**, this finding does not surprise too much as the prepreg is far from being fully cured even after 60 days of RT exposure. The plateau of maximum tack values stretches strongest within the 15 days ageing time span in which the rate of conversion $d\alpha/dt$ is highest according to DSC measurement.

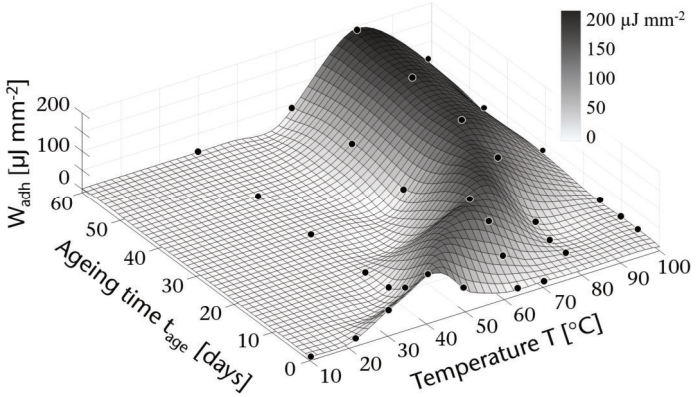

Figure 5-8. Plateau of temperature-dependent tack properties measured for different prepreg out-times.

Throughout the whole investigated range of temperature and ageing time no tack is measured as long as the prepreg temperature stays below its corresponding T_g. Considerable levels of tackiness (W_{adh} = 20 % $W_{adh,max}$) cannot be achieved until raising the prepreg processing temperature T_{proc} by at least 17 °C above T_g (fresh prepreg). Detailed information on temperature differences between T_g and T_{max} (temperature at $W_{adh,max}$) as well as T_g and T_{proc} as a function of ageing time is given in **Table 5-2**. Temperature differences are obtained from the surface plot data.

Table 5-2. Shifts between different characteristic temperatures of RT aged prepreg.

Ageing [days]	T_g [°C]	$T_{proc} - T_g$ [°C]	$T_{max} - T_g$ [°C]
fresh	2	17	38
5	6	24	42
10	26	18	38
15	27	28	45
30	29	39	45
45	31	37	46
60	36	34	44

Although no significant influence of ageing on both temperature differences can be determined, a slight tendency towards higher temperature differences is observed as the prepreg becomes older. In order to achieve maximum tackiness of aged prepreg, the material should be processed at about 40 °C above T_g.

Ahn [224], who also used work of adhesion as the tack indicator, found that by raising temperature the tackiness of aged prepreg can partly be restored compared to fresh material. However, the experimental data of our study show that tack levels can not only be restored but even be excelled by an increase of processing temperature during automated lay-up. E.g., W_{adh} of 60 days aged samples at 80 °C (193.6 µJ mm^{-2}) is 66.2 % higher than for prepreg which was freshly taken out of the freezer (116.5 µJ mm^{-2}) and tested at 40 °C. Apparently, a high DoC as a result of advanced ageing involves the formation of a cross-linked macromolecular structure. The molecular weight distribution is shifted towards higher molecular weights - a state in which larger and more highly cross-linked polymer chains are most likely able to resist greater shear stress and surpass the tack performance of fresh B-staged material. However, tackiness will be lost after DoC has exceeded a certain level of cross-linking which is when the prepreg will behave like a solid even at elevated temperatures. This reversal point was not reached within the investigated ageing time span of 60 days.

Analogous to the results gained for the variation of compaction stress, a widening of the 'high tack plateau' is found for long prepreg out times. (see **Figure 5-8**). Apparently, the aged prepreg's level of tackiness is not as sensitive to temperature deviation as the one of prepreg which was freshly taken out of the freezer. Reason might be a broader molecular weight distribution due to advanced conversion of the resin. Irrespectively of the reason, prepreg processors can tolerate occurrent

temperature deviation to still run stable CFRP manufacturing processes - provided that, firstly, lay-up can be performed at elevated temperatures (~80 °C) and, secondly, that the material feed of the lay-up machine can be heated as the handling of old prepreg becomes problematic when T_g exceeds RT.

5.3.6 Impregnated carbon tape for draping (Material B)

In order to investigate the influence of temperature of resin impregnated carbon tape on its adhesive draping behavior, tack and rheological properties have been determined experimentally. **Figure 5-9** shows the maximum tack stress σ_{max} of impregnated tape and the complex viscosity η^* of neat Prism EP2400 resin as a function of temperature. Tack tests are performed for three different material combinations, namely tape-tape, tape-steel and tape-foam.

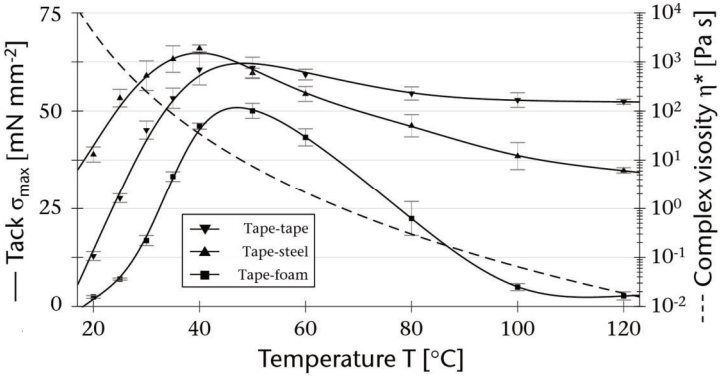

Figure 5-9. Resin viscosity and tack (σ_{max}) of mat. B towards different surface materials (v_d = 0.2 mm s^{-1}, σ_c = 10 N cm^{-2}).

Within the measured temperature range η^* exponentially drops by more than five magnitudes, which is characteristic for infusion resins. Tack strengths σ_{max} of the impregnated tape, however, show absolute maxima at specific temperatures which is comparable to the results obtained for prepreg (material A). The maxima of different material combinations are slightly shifted between 40 and 50 °C while differing in extent. Differences between the investigated material combinations strongly suggest that the surfaces show diverse wetting behavior. The surface topography is considered the main source of influence on prepreg tack, the reason

being the absence of chemical reactions during measurement which might occur due to different resin reactivity with the surface material. For structural foam, which stands out in terms of surface roughness, low resin viscosity is needed to wet the surface and, therefore, to create a larger contact area actually partaking in the debonding mechanism. Consequently, the local tack maximum of structural foam is shifted towards higher temperatures where viscosity is lower. The smooth surface of the steel probe necessitates lowest temperatures in order to form a fully wetted interface as a result of compaction. In general, the finding that tack performance of material B is dependent on the contact surface is in accordance with the observation of Endruweit et al. [209]. The authors provided evidence that commercial prepreg's tack significantly differs towards fluorinated ethylene propylene, steel or prepreg as well.

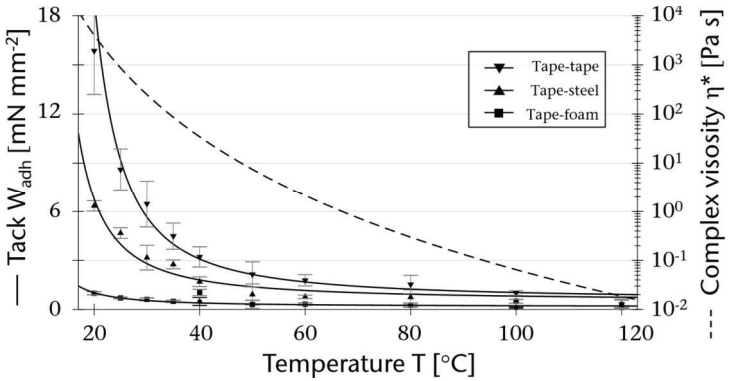

Figure 5-10. Resin viscosity and tack (W_{adh}) of mat. B towards different surface materials (v_d = 0.2 mm s^{-1}, σ_c = 10 N cm^{-2}.

When plotting the work of adhesion W_{adh} vs. temperature (**Figure 5-10**), two major differentials become evident compared to commercial aerospace prepreg (mat. A). Firstly, the measured energies, which are necessary to fully separate the interface, are more than one magnitude lower than for prepreg throughout the entire investigated temperature range. This finding quantitatively underlines the importance of procuring epoxy resin (B-staging) if high tack levels are required for processing.

The second difference applies to the general shape of the W_{adh} graph: In contrast to the prepreg investigation, no local maximum is recorded as tack values and viscosity steadily decrease in like manner. Hence, it is concluded that the influence of an improved wetting at elevated temperatures is negligible compared to the tremendous decrease in resin's shear resistance. The latter is represented by the steep drop in the resin's complex viscosity η^* as a function of temperature. Still, wetting issues for material A are generally present for W_{adh}, too, as the graphs differ up to a temperature of 80 °C. Analogous with σ_{max}, W_{adh} tack values are highest for tape-tape material combination followed by tape-steel and, lastly, autoclave-ready structural foam which resin impregnated tape shows marginal tackiness to. From 80 °C onwards, no significant difference between the investigated surface materials is measured which indicates a fully wetted interface for all tested materials.
As W_{adh} and η^* are found to decrease exponentially in like manner, modeling both parameters by an Arrhenius-type model (**Eq. (5-4)**) strongly suggests itself:

$$W_{adh}, \eta^* = a * \exp\left(\frac{b}{T}\right) \qquad \textbf{Eq. (5-4)}$$

Applied to the work of adhesion, the model parameter *a* represents a minimum tack level that is reached for high temperatures while *b* determines the rate at which the tack level decreases (**Table 5-3**).

Table 5-3. Coefficient of determination of the model fit (**Eq. (5.5)**).

Material combination	a	b	R^2
W_{adh} tape - tape	0.5	72.8	0.9608
W_{adh} tape - steel	0.48	52.97	0.9511
W_{adh} tape - foam	0.15	38.11	0.9329
Viscosity	0.36	197.7	0.9996

As both material parameters show a linear correlation between their logarithmic values W_{adh}; η^* and the reciprocal of temperature T, a linear relationship can be found for tack W_{adh} and viscosity η^*:

$$W_{adh} = e^k * \eta^* \qquad \textbf{Eq. (5-5)}$$

The following **Figure 5-11** displays the linear correlation between logarithmic values of W_{adh} and η^* (model and experimental data) for the investigated material combinations. Apparently, there is large deviation between model and measurement for high temperature and low viscosity, respectively (100/120 °C, left of dotted line), which can be explained by the inaccuracy of the Arrhenius viscosity model at the corresponding temperatures: Although the model's coefficient of determination R^2 is very high (0.9996, see **Table 5-3**) the model does not reflect low viscosities at high temperatures accurately.

If the modelled W_{adh} is plotted as a function of experimental viscosity data, good agreement is found for high temperature/low viscosity as well. In general, the model validity of these assumptions indicates that both tack parameters W_{adh} and σ_{max} represent different tack debonding mechanisms of epoxy-impregnated carbon fibers for draping. For material A, tackiness described by the tack parameter W_{adh} is a linear function of resin viscosity and, therefore, an exclusively resin-driven debonding phenomenon. It is expected that similar results would have been gained if tack measurements were performed with neat resin in the absence of carbon reinforcement fibers.

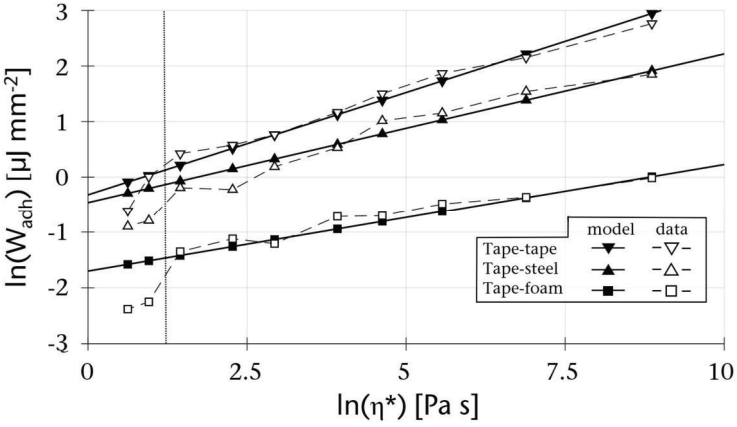

Figure 5-11. Correlation between tack and complex viscosity for model and experimental data.

5.4 Conclusion

Experimental determination of tack properties of epoxy impregnated carbon fibers has been performed using a rheometer as a measuring device for probe tack testing. The choice of the two investigated pre-impregnated carbon fiber reinforcements complies with composite manufacturing via automated lay-up technologies AFP/ATL and draping.

Due to the high accuracy of the rheometer, e.g. in terms of temperature/ displacement control, normal stress measurement and data sampling, tack measurements using the developed method have revealed significant correlations between controlled and measured variables. Tack performance is found to be influenced by both process- (temperature, compaction force, lay-up speed) and material-related (age, matrix resin, lay-up/draping surface) issues. In respect thereof, the prepreg supplier's tack classification of 'high', 'medium' or 'low' seems far from being capable of characterizing the complexity of tack properties adequately. Systematically adjusting the tackiness of prepreg in order to ensure stable automated lay-up processes requires a deeper understanding of interdependencies between material and process. The key findings of the study can be summarized as follows:

- Carbon fiber epoxy prepreg tack is found to be very sensitive to temperature variation within the investigated experimental range. Both tack indicators σ_{max} and W_{adh} are not redundant in terms of tack characterization and form local maxima at different temperatures.
- Tack steadily increases as a function of compaction stress σ_c. However, only little influence is observed as soon as σ_c surpasses a critical level of compression.
- Debonding rate is found to influence both tack parameters unequally. While σ_{max} logarithmically increases within the investigated range, W_{adh} forms a maximum. The maximum decreases in extent and moves towards higher debonding rates.
- The plateau of maximum tack performance generally shifts towards higher temperatures as the ageing process of prepreg progresses outside the freezer. Material, which has exceeded tack life according to data sheet, was found to still be processable with tack properties even exceeding the adhesive

performance of fresh material by more than 65 % when being processed at elevated temperatures.
- Manually injection resin-impregnated tape for automated draping shows tack performances of more than one magnitude lower than commercial aerospace epoxy prepreg. W_{adh} of this material can be modelled by an Arrhenius type equation and is a linear function of viscosity.

Based on the experimental results presented in this study, further work should be progressed towards an experimental validation in an automated lay-up process like AFP or ATL. Therefore, the influence of purposeful prepreg tack adjustment on production-related aspects (defect formation, material feed issues, lay-up speed, etc.) should be studied that eventually are decisive in terms of final laminate quality. In doing so, the entirety of automated composite manufacturing via lay-up or draping (material, process, and composite part) is covered in terms of prepreg tack.

Declarations of interest

None.

Funding

This work was supported by the European Regional Development Fund (ERDF), the federal state of Lower Saxony, Germany and the Federal Ministry for Economic Affairs and Energy, Germany.

Acknowledgements

The authors would like to acknowledge the financial support by the European Regional Development Fund (ERDF) and the federal state of Lower Saxony granted for the interdisciplinary research project ‘FlexProCFK’. Further gratitude is expressed to the Federal Ministry for Economic Affairs and Energy for financially supporting the research project ROBUFIL.

Chapter 6

6. Adhesive mechanisms – Publication III

Adhesion-cohesion balance of prepreg tack in thermoset automated fiber placement. Part 1: Adhesion and surface wetting

D. Budelmann[a], C. Schmidt[b], D. Meiners[c]

[a]Institute of Polymer Materials and Plastics Engineering, Clausthal University of Technology, Ottenbecker Damm 12, Stade, Germany

[b]Institute of Production Engineering and Machine Tools, Leibniz Universität Hannover, Ottenbecker Damm 12, Stade, Germany

[c]Institute of Polymer Materials and Plastics Engineering, Clausthal University of Technology, Agricolastr. 6, Clausthal-Zellerfeld, Germany

Composites Part C: Open Access* 6 (2021) 100204.

*Journal metrics:

CiteScore: **8.6** (Scopus, 2023)
Rank 78/672; 88th Percentile (Engineering: Mechanical Engineering)

Impact factor: **5.3** (Clarivate, 2023)

Abstract

The constitution of prepreg tack in automated fiber placement (AFP) is affected by a sensitive balance between adhesive interfacial bond strength and cohesive strength of the prepreg resin. In an effort to explore the role of interfacial liquid-solid interaction on the tack of commercial aerospace-grade epoxy prepreg, a surface wetting analysis was performed on AFP-related substrates. The standard test liquid combination water/diiodmethane and extracted neat epoxy resin were used for contact angle measurement employing the sessile drop method and the OWRK model. Additional rheological and topographical analyses were carried out to account for viscous resin flow on surfaces of different roughness. The results from the material characterization are discussed against the background of tack measurement by probe tack testing utilizing a rheometer. Significant differences between the investigated surfaces in terms of both the maximum tack level and the onset temperatures of adhesion were found as a function of test parameters relevant for contact formation. General agreement with the experimental tack results was observed employing a topographically extended version of the Dahlquist criterion. For each substrate, a temperature-dependent critical storage modulus could be determined that conforms to the onset temperature of tackiness. Contact angle measurements revealed a correlation between the thermodynamic work of adhesion and maximum tack and, moreover, the tack onset in the adhesive regime when additionally incorporating surface topography. Matching ratios of polar and dispersive surface free energy and surface tension components were found to favor the molecular interaction at the interface between prepreg resin and substrate.

* Corresponding author.
E-mail address: dennis.budelmann@tu-clausthal.de (D. Budelmann).

https://doi.org/10.1016/j.jcomc.2021.100204
Received 7 September 2021; Received in revised form 29 October 2021; Accepted 2 November 2021
Available online 5 November 2021

6.1 Introduction

Automated fiber placement (AFP) and automated tape laying (ATL) are highly productive processes for advanced manufacturing of large composite parts in the aerospace industry. In these processes, thin stripes or sheets of pre-impregnated carbon fibers (prepregs) are laid in a mold by placement heads attached to industrial robots or gantry systems. Subsequent autoclave cure of the laid laminates at 180 °C results in high-performance structural components with excellent strength-to-weight ratios [228]. Despite its high productivity and level of automation, the lay-up process is subject to causing different types of defects in the laminate [46]. Although effort has been put towards the development of automated defect detection systems [130,322], substantial research on the causes of defect occurrence can still contribute to more stable manufacturing processes. The formation of defects in AFP is often linked to inadequate levels of material stickiness (tack) and lack of knowledge on how to precisely control it by process adjustment, respectively [52]. This in particular applies to bonding defects such as wrinkling and bridging. Here, prepreg tack counteracts detaching forces that occur during defect formation and is therefore necessary to ensure proper positioning of the prepreg tows.

Prepreg epoxy resins are not primarily tailored towards tack but rather undergo development to meet the thermo-mechanical requirements of cured parts such as high damage tolerance, strength and glass transition temperature T_g. Thus, tack adjustment is not a matter of resin formulation but needs to be performed by b-staging and especially by process adaption during processing. For this purpose, Smith et al. [286] recently presented tack process maps which can help composite manufacturers to account for out time effects of prepreg tack by lay-up parameter adaption. The most practical approach to control tack throughout the lay-up process is to control the material and mold temperature, e.g., by infrared heaters attached to the AFP machine. Since the very beginning of experimental research on prepreg tack in the 1980s [143], its dependence on the temperature has been a point of focus. Several studies [184,205,225] have revealed bell-shaped curves independent from the actual test method when plotting experimentally determined prepreg tack as a function of temperature. Evidence was found that the shape of these curves is the result of two major mechanisms which determine the nature of the prepreg's adherence. Similar to the functionality of pressure sensitive adhesives (PSA), maximum stickiness is exhibited when the prepreg matrix on the

one hand entirely wets the substrate and on the other hand is able to resist high application loads [323]. The requirements of rapid surface wetting for bond formation and high fracture toughness upon bond separation are partly contradictory as both are highly dependent on the matrix viscosity. An increased flowability constituted by low viscosity will result in enhanced wetting while simultaneously lowering the bearable load. Providing high levels of tack is therefore a matter of sensitive tradeoff which has been described as the adhesion-cohesion balance (**Figure 6-1**) in PSA research [235,246,324].

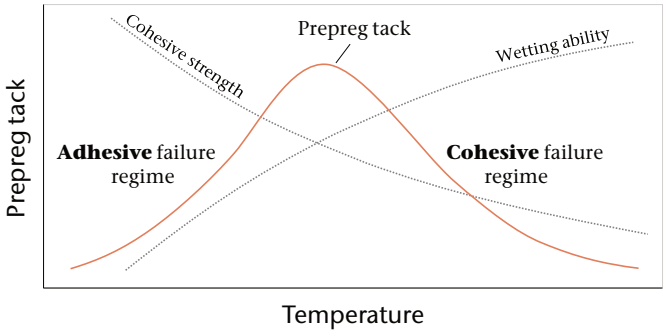

Figure 6-1. The temperature-dependent adhesion-cohesion balance of prepreg tack.

While most structural adhesives undergo a phase transition from liquid to solid, e.g., by chemical reaction, solvent evaporation or cooling, PSA and prepregs (during lay-up) remain in a viscoelastic state throughout application and removal. As a consequence, adhesion at the interface cannot be achieved by covalent bonds but has to rely on intermolecular forces (IMF) at the interface which hold the resin/adhesive and the adherend together. IMF with the most common representatives being van der Waals forces and H-bonding, range roughly two magnitudes below covalent bonds in terms of bond energies [325] which makes up for the low separation energies of prepreg tack compared to physically or chemically curing adhesives. A requirement for these forces to be effective is to establish intimate contact between adhesive/resin and the substrate as IMF come into effect in the range of nanometers. With regard to establishing this kind of intimate contact in the AFP process, the driving force provided by the compaction roller is assisted by both interfacial attractiveness and viscous flowability in order

to effectively spread resin on the adherend surface. The contact formation of prepregs on different surfaces was recently studied by Choong et al. [302] who investigated contact evolution between prepreg and a glass substrate by optical microscopy as demonstrated before for PSA [243]. After exploring the relationship between the degree of intimate contact (DoIC) and tack, the authors concluded that the DoIC plays an important role, but its simple maximization turns out insufficient for process optimization. Instead, utilizing the superordinate tack curves is more appropriate and represents both the adhesive and cohesive phenomena governing prepreg tack.

This is the first research paper of a two-part series dealing with the adhesion-cohesion balance of prepreg tack and its relevance for automated fiber placement processes. For the present paper, the adhesive portion of the balance is covered by examining the fundamentals of bond formation between prepreg and different AFP-related contact materials. Therefore, a wetting analysis for prepregs is presented for the first time in literature allowing insight into the interfacial interaction governing adhesion. The wetting analysis is based on contact angle measurements between standard test liquids as well as extracted neat prepreg resin and solid substrate, namely stainless steel of different surface roughness, siliconized backing paper, polyurethane and the prepreg itself. Complementary optical characterization of the surface topographies is performed by laser scanning microscopy. Viscoelastic behavior of prepreg resin is examined by oscillatory rheology and results are used to test the validity of selected contact formation criteria for prepregs that have originally been developed for PSA. All findings from material analysis are discussed against the background of tack measured on a commercial carbon fiber-epoxy prepreg system in a probe tack test carried out in a rheometer. The two-phase design of the test procedure (compression to tension) enables to exclusively vary test parameters, which influence contact formation and therefore adhesion, while cohesion-relevant deformation parameters are kept constant. Strict separation of adhesive and cohesive contribution can thus be achieved and both portions investigated individually. The novel approach of this study aims at gaining fundamental insight into to the connectivity between interfacial resin-substrates interaction and macroscopic aspects involved in practical prepreg tack measurement.

6.2 Materials

6.2.1 Prepreg

The commercially available prepreg system HexPly 8552 [326] by Hexcel Corporation was used for all investigations and material characterization presented. The unidirectional aerospace-grade prepreg system is made up of AS4 carbon fiber and amine-cured epoxy resin featuring a nominal fiber volume fraction of 57.42 vol% and a nominal laminate density (cured) of 1.58 g cm^{-3}, respectively. The prepregs contain a thermoplastic toughener (~20 wt.% PES), which is initially miscible in uncured resin and forms a second phase upon curing for the toughening effect [327]. The recommended cure cycle is performed in an autoclave at 180 °C maximum temperature. 10 days tack life, 30 days out life and 12 months shelf life are guaranteed by the supplier according to data sheet.

6.2.2 Neat resin

Since formulation details and commercial availability of resin used for prepregs are strictly limited by material suppliers, neat resin had to be extracted from prepreg sheets by solvent extraction. Tetrahydrofuran (THF, >99.9%, BHT-inhibited) was used as a solvent for the extraction procedure shown in **Figure 6-2**. THF is known to be an excellent solvent for epoxy resins and is thus commonly used as eluent for molecular weight analysis by gel permeation chromatography (GPC). After dissolving the prepreg matrix in THF at room temperature and removing the carbon fibers manually, the THF/resin solution was conditioned at 80 °C and 100 mbar over a period of 4 h to guarantee total solvent evaporation. The resin/toughener morphology and potential changes due to the presence of THF remain unknown. However, the solved state of the toughener is unlikely to change as all subsequent

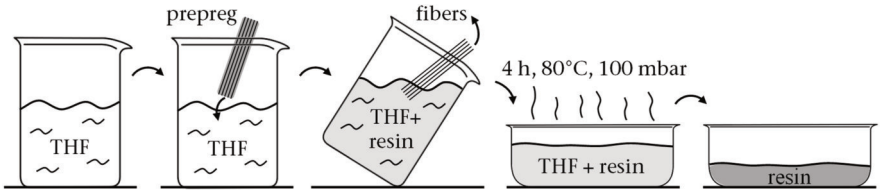

Figure 6-2. Prepreg resin extraction procedure in tetrahydrofuran.

investigation and preparation take place prior to cure. THF evaporation was eventually assumed complete after 4 h of conditioning as the viscosity values of extracted neat resin matched the data sheet (~500 Pa s at 60 °C and 1 Hz [18]). Untreated resin specimens as well as specimens that were comparatively treated for only 2 h showed significantly lower viscosity indicating residual solvent. In case of the 4 h samples, the risk of undesired cure reaction could be eased by DSC measurement, which showed no significant difference between cure peak enthalpies of fresh (486.3 J g^{-1}) and 4 h-conditioned (489.2 J g^{-1}) prepreg specimens (Appendix: **Table 6-5**). Hence, all results gained from material analysis are assumed to be representative for the resin within the prepreg as delivered.

6.2.3 Contact materials

Prepreg tack and surface wetting is investigated on different substrates that are in contact towards prepreg material during fiber placement. Apart from using the commercial prepreg/backing paper substrates (Section 6.2.1) as delivered, a standard X5CrNi18-10 stainless steel is ground using SiC 80 grit grinding paper (ground specimens). The same steel is sequentially ground with 80, 120, 220, 500, 800, 1200 and 2000 grit SiC paper with a subsequent 3 and 1 µm diamond suspension polishing procedure to produce polished specimens. Polyurethane samples are fabricated by casting Sika Biresin U1404, a two-component, amine-crosslinked elastomeric casting resin, on a flat mold. The mold-facing sides of the samples are used for investigation due to higher planarity compared to the air-facing sides. Table 6-1 provides an overview of the examined substrates and their relevance in AFP.

Table 6-1. Investigated contact materials and their role in automated fiber placement processes.

Substrate		Occurrence in AFP	Abbreviation
Prepreg		Previously laid plies	PP
Backing paper		Protective film on prepreg	BP
Polyurethane		Compaction roller material	PU
Steel	ground	Mold material	ST
	polished	Mold material	ST_{pol}

6.3 Experimental methods and data analysis

6.3.1 Tack measurement

Tack measurement was performed as a probe tack test (compression to tension test) using a TA Instruments ARES G2 rheometer (**Figure 6-3**).

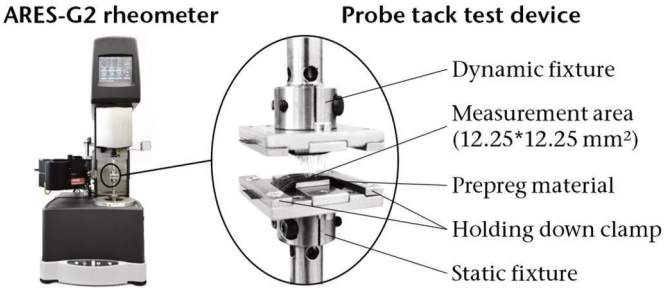

Figure 6-3. Utilized equipment for prepreg tack measurement by probe tack testing.

Prepreg material is clamped on a lower, static fixture which prevents the material from undesired detaching or bending. The upper fixture is attached to the axial servo control system of the rheometer enabling transient normal force measurements within an axial transducer range of 0.001–20 N. The dynamic upper fixture holding the probe is normally brought into contact with the prepreg until a distinctive pressure is built up, held (pressure-controlled) for a set dwell time and is eventually removed in an upwards direction at a controlled rate. The separation work W_{tack} defined as the energy needed to fully separate the sample interface during the tension phase is employed as an indicator for tack and calculated by integration of the stress strain curves. Throughout the whole procedure, precise temperature control (deviation ≤ 0.2 K) in the tack-relevant temperature range between 20 °C and 70 °C is guaranteed by a forced convection surrounding the specimen holders. The two-phase measurement cycle is presented in detail in [10] and allows to separately control the compression and tension phases. Therefore, testing parameters that influence adhesive bond formation/wetting process (compaction time and pressure) and those which determine cohesion upon debonding (debonding rate) can be investigated independently of each other. For this study, the latter is remained constant at 0.1 mm s^{-1} for all experiments.

Compaction time and pressure are varied at increments of 5/10/15 N cm^{-2} and 0.5/5/50 s, respectively. 10 N cm^{-2} and 5 s of compaction are used as standard test parameters for all experiments without compaction variation. Three fresh prepreg samples were prepared and tested for each testing parameter to evaluate reproducibility as performed in our previous experimental study [184]. The variation range of the experimental compaction parameters does not fully represent actual process parameters of AFP (due to restrictions of the measurement device) as compaction pressure is usually higher and compaction time significantly shorter depending on the lay-up velocity and roller geometry. However, the large investigation range of the study is considered beneficial for getting an understanding of the fundamentals of prepreg resin surface wetting.

6.3.2 Wetting analysis

Liquid-solid interaction of neat epoxy resin and standard test fluids with different contact materials is carried out by three-phase contact angle measurement using a Kruess DSA25 Drop Shape Analyzer. The analytical apparatus includes the optional accessories of a temperature-controlled measurement chamber and syringe dosing unit to perform wetting experiments in the tack-relevant temperature range between 20 and 70 °C. The contact angle (CA) θ is estimated using the sessile drop technique and is related to the solid surface free energy σ_{SG}, solid/liquid interfacial free energy σ_{SL} and (liquid) surface tension σ_{LG} via Young's equation [328]:

$$\sigma_{SG} = \sigma_{SL} + \sigma_{LG} * \cos\theta \qquad \textbf{Eq. (6-1)}$$

The surface free energies (SFE) as a quantitative measure of the intermolecular forces at the surfaces of the investigated contact materials are determined employing the method by Owens, Wendt, Rabel and Kaelble (OWRK, [329]). Here, the underlying interactions are divided into dispersive and polar portions represented by $\sigma_{SG}^{d}/\sigma_{LG}^{d}$ (dispersive) and $\sigma_{SG}^{p}/\sigma_{LG}^{p}$ (polar), respectively:

$$\sigma_{SL} = \sigma_{SG} + \sigma_{LG} - 2\sqrt{\sigma_{SG}^{d}\sigma_{LG}^{d}} - 2\sqrt{\sigma_{SG}^{p}\sigma_{LG}^{p}} \qquad \textbf{Eq. (6-2)}$$

Substituting for σ_{SL} from **Eq. (6-1)** gives **Eq. (6-3)** in a linear form:

$$\underbrace{\frac{\sigma_{LG}(1+\cos\theta)}{2\sqrt{\sigma_{LG}^{d}}}}_{y} = \underbrace{\sqrt{\sigma_{SG}^{p}}}_{m} * \underbrace{\sqrt{\frac{\sigma_{LG}^{p}}{\sigma_{LG}^{d}}}}_{x} + \underbrace{\sqrt{\sigma_{SG}^{d}}}_{c} \qquad \textbf{Eq. (6-3)}$$

A graphical representation of **Eq. (6-3)** can now be established by adding polar and dispersive surface tension (SFT) values of standard test liquids. For this study, analytical grade water and diiodmethane were used. SFT literature values for both standard liquids were verified by employing the pendant drop method at room temperature in an air atmosphere. The high viscosity of b-staged neat prepreg resin at room temperature prevented reproducible drop formation so that the measurement temperature needed to be increased. A temperature of 70 °C within the measurement chamber was found to be high enough for forming stable drops hanging from a needle (1.5 mm inner diameter) with a corresponding viscosity of 200 Pa s. The sessile drop experiments, including the extracted epoxy resin, were carried out at 70 °C as well. It was ensured that all wetting experiments were carried out within ~60 minutes after placing the resin syringes in the heated measurement device to avoid undesired resin cure.

6.3.3 Rheology

Viscoelastic characterization of neat prepreg resin won by the extraction procedure presented in Section 6.2.2 was performed as oscillatory rheometry utilizing the TA Instruments ARES G2 rheometer. Running a plate-plate configuration of 25 mm diameter, the complex viscosity η^*, viscoelastic storage modulus G" and loss modulus G' as well as the equivalent loss factor tan δ were determined at 1 mm gap. Temperature, frequency and amplitude sweeps were carried out according to the testing parameters displayed in **Table 6-2**.

The temperature increments for frequency and amplitude sweeps were reduced to 5 K min^{-1} within the highly-sensitive temperature range of prepreg tack between 30 and 50 °C.

Table 6-2. Parameters for the rheological analysis of neat prepreg resin.

Sweep	Temperature	Frequency	Strain
Temperature	**20 - 70 °C, linear: 5 K min^{-1}**	1 s^{-1}	1 %
Frequency	20 - 70 °C, 10 K increments	**10^{-2} – 10^{2} s^{-1} log: 20 pts dec^{-1}**	1 %
Amplitude	20 - 70 °C, 10 K increments	1 s^{-1}	**10^{-2} – 10^{2} % log: 20 pts dec^{-1}**

6.3.4 Surface topography

The substrate topography is investigated optically using a Keyence 3D Laser Scanning Confocal Microscope VK-X. Root mean square roughness R_q of the ordinate value z(x) is determined within a sampling length l_r of 2.5 mm according to **Eq. (6-4)**. Cutoff wavelengths in order to distinguish between roughness and waviness profiles are set according to the recommendations of ASME B46.1 [330]. Additionally, the maximum wavelength of each roughness profile λ_0 is determined for the experimental verification of a stickiness criterion. Five different locations on each substrate are measured in order to quantify standard deviation of the roughness parameters.

$$R_q = \sqrt{\frac{1}{l_r}\int_0^{l_r} z(x)^2\,dx} \qquad \textbf{Eq. (6-4)}$$

6.4 Results and discussion

6.4.1 Surface tension (SFT)

Pendant drop experiments were carried out to determine the surface tension of the test liquids water, diiodmethane and prepreg resin. The SFT values serve as the foundation for further interfacial wetting analysis. [228] **Figure 6-4** shows representative drop shapes and sizes. With the help of a Young-Laplace fit of the optically determined drop geometries and the known test liquid densities, the total surface tensions σ_{LG} were calculated and summarized in **Table 6-3**.

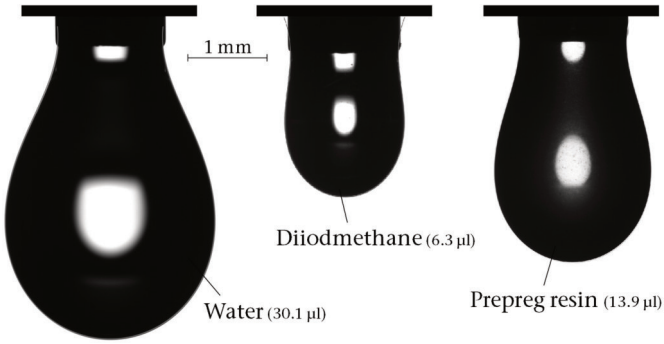

Figure 6-4. Representative pendant drops of water, diiodmethane (room temperature) and prepreg resin (70 °C) hanging from a 1.5 mm blunt cannula for SFT determination.

Polar and dispersive portions could be obtained from the liquid-solid interaction of the test liquids with the fully dispersive backing paper (section 6.4.2). The SFT including its polar and dispersive component of both standard test liquids are in overall good agreement with the values presented in literature. The slight but significant deviation between SFT values from literature and own measurements (**Table 6-3**) is likely attributed to contamination during storage and test preparation. Especially for the total SFT of water, the difference between literature and own measurement (0.49 mN m^{-1}) is notable considering the low standard deviation of 0.06 mN m^{-1}. The surface tension of prepreg resin at 70 °C amounts to 39.74 mN m^{-1} with a polar portion of 20.73 % equaling $\sigma^{p}_{LG} = 8.24$ and $\sigma^{d}_{LG} = 31.50$ mN m^{-1}, respectively. In contrast to the standard test liquids, the drop formation of the prepreg resin was highly influenced by viscoelastic behavior. However, dimensionally stable drops that ceased from deformation after a time span of approximately 60 s could be produced when dosing 14 µl resin from the

Table 6-3. Total surface tension σ_{LG} as the sum of the polar σ^{p}_{LG} and dispersive σ^{d}_{LG} components of standard test liquids and extracted resin from HexPly 8552 prepreg. Literature values [228] and own data are given in mN m^{-1}.

	Literature values			Pendant drop experiments		
Test liquid	σ_{LG}	σ^{p}_{LG}	σ^{d}_{LG}	σ_{LG}	σ^{p}_{LG}	σ^{d}_{LG}
Water (20 °C)	72.8	51.0	21.8	72.31 ± 0.06	50.90 ± 0.55	21.41 ± 0.55
Diiodmethane (20 °C)	50.8	0.0	50.8	50.27 ± 0.36	0.47 ± 1.50	49.80 ± 1.46
Epoxy 8552 (70 °C)	-	-	-	39.74 ± 0.64	8.24 ± 1.26	31,50 ± 1.12

syringe. The resin drops remained a Laplacean shape so that SFT could be calculated with the resin density of 1.2 g cm^{-3}. Overall, the findings for the resin SFT match the results presented Synytska et al. [331] who measured SFT by pendant drop experiments on two epoxy resins and amine hardeners. The SFT of the mixed systems were not measured directly but assumed to amount between both components (resins: 44.1 and 36.3 mN m^{-1}; hardeners: 35.7 and 33.3 mN m^{-1}). Wilhelmy experiments on bisphenol A diglycidyl ether (DGEBA) and tetraglycidyl methylene dianiline (TGMDA) performed by Page et al. [332] revealed SFT between 35 and 40 mN m^{-1}. No subdivision of SFT into polar and dispersive components were made in these studies.

Although the exact formulation of the commercial prepreg resin is unknown, a substantial share of polarity can be contributed to the presence of polar epoxide groups (**Figure 6-5**, left) within the B-staged, partly cured resin. Here, the highly electronegative oxygen atom leads to separation of charge and to an electric dipole moment. As the resin is amine-cured according to data sheet, a similar effect can be expected to result from the presence of amine groups (**Figure 6-5**, right).

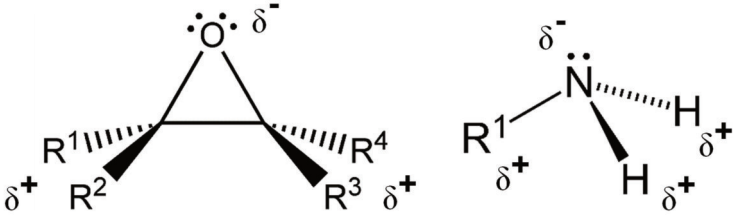

Figure 6-5. Polarity of epoxide (left) and primary amine (right) groups due to high electronegativity of oxygen and nitrogen.

Epoxy resin systems used for aerospace primary structures usually contain the 4,4'-diaminodiphenyl sulfone (DDS) as the hardener component in order to achieve a high glass transition temperature T_g (>160 °C) after autoclave cure [333]. The diamine-based hardener has a central sulfonyl group (O=S=O) which is highly polar measuring 4.5 Debye [334] and will most likely account for to the resin polarity as well. A more detailed insight into functional groups and their role for molecular polarity can be achieved by spectroscopic measurement techniques such as Fourier-transform infrared spectroscopy.

6.4.2 Substrate wetting analysis of standard test liquids

The substrate wetting analysis is based on three-phase contact angle measurement between the gaseous (air), solid (investigated substrates) and the liquid (water, diiodmethane, resin) phases with the SFT as presented in the previous section. Significant differences between the contact angles (CA) of the standard test liquids water and diiodmethane on the investigated substrates were observed as pictured in **Figure 6-6**.

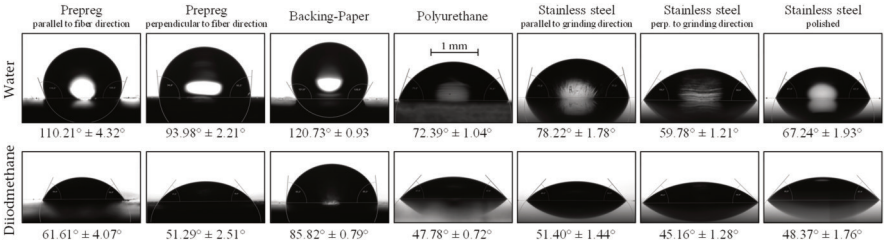

Figure 6-6. Sessile drops (~2 µl) and their contact angles of water and diiodmethane on different AFP-related substrates. Seven drops were measured for each liquid/solid combination immediately after drop placement.

Strong deviation from radial drop symmetry arose on surfaces with high directional surface topography as drops formed ellipsoidal shapes. As a consequence, divergent CA were measured on the same surfaces for different sample orientations. The phenomenon was most pronounced on the roughly ground stainless steel surface and on unidirectional prepreg which is why sessile drop formation was investigated parallelly and perpendicularly to the grinding/fiber direction on these surfaces. Detailed information on the direction-related differences in surface topography are provided in section 6.4.6.

The wetting ability of water decreases in the order of increasing measured CA as follows: backing paper (BP), prepreg (parallel, PP∥), prepreg (perpendicular, PP⊥), ground stainless steel (parallel, ST∥), polyurethane (PU), polished stainless steel (ST_{pol}), ground stainless steel (perpendicular, ST⊥). As expected, water generally forms greater CA due to its higher SFT and specifically its notable polar component. Diiodmethane turned out to be a suitable fully dispersive test liquid as CA > 0° formed on all surfaces. The wetting order of diiodmethane slightly differs from the order observed for water, however, these differences are within standard deviation.

The overall measured CA of the standard liquids range from the most likely silicone-coated backing paper (CA > 120° for water) to the perpendicularly ground stainless steel surface (CA ≈ 45° for diiodmethane). Applying the OWRK model to the CA measurement results, the linear regressions displayed in **Figure 6-7** can be calculated using **Eq. (6-3)**.

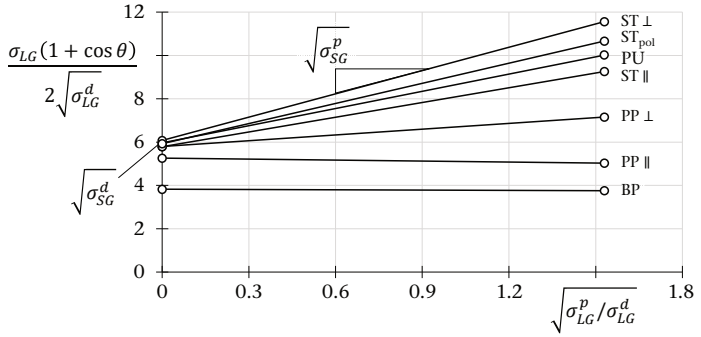

Figure 6-7. Linear regressions for SFE determination according to the OWRK model.

By utilizing the model, the interfacial interactions are divided into dispersive and polar SFE components. As the graph slopes represent the square root of the polar SFE components, a horizontal line signals a fully dispersive surface with evanescent polar contribution. The dispersive component can be read directly from the ordinate measuring the square root of the dispersive component. The SFE compositions of the investigated substrates are displayed in **Figure 6-8**.

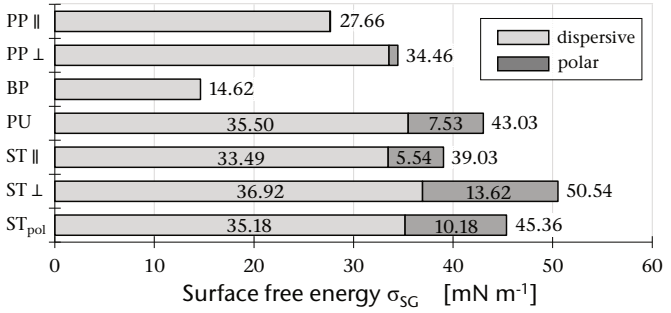

Figure 6-8. Surface free energies σ_{SG} with their polar σ_{SG}^p and dispersive σ_{SG}^d components.

The polished and perpendicularly ground stainless steel substrates show the highest total SFE values followed by PU and ST‖. For these substrates, polar portions between 14.19 % and 26.95 % were measured. The siliconized backing paper exhibits an extremely low, fully dispersive SFE of 14.62 mN m^{-1}. Despite its strongly polarized -(Si-O)- backbone, outside methyl groups shield polarity which results in a fully dispersive surface with excellent release properties. The polar portion of the prepreg SFE were also found to be near zero and therefore, lower than the SFT polar portion of neat resin. Reasons for this discrepancy may be exposed non-polar carbon fibers on the prepreg surface or small amounts of solvent residue in the resin from the extraction process. SFE on the roughest surfaces (PP and ST, see section 6.4.6) were generally lower if measured in a parallel orientation to the fiber/grinding direction. This observation is most likely caused by enhanced flowability of the test liquids along grooves due to capillarity. The drop spreads elliptically in fiber/grinding direction and, for this test setup, leads to higher contact angles and lower SFE, respectively.

Wetting envelopes are a useful type of exemplification whenever liquids are to be modified in order to achieve desired wetting properties on surfaces with known SFE. For prepreg resins, they can reveal possibilities of resin modification in the material development phase in terms of the polar-to-dispersive SFT ratio. **Figure 6-9** shows the wetting envelopes of the investigated surface materials for full drop spreading (CA = 0°). Liquids with $\sigma_{LG}/\sigma_{LG}^{p}$ pairs of values, that are located within the envelopes, will fully wet the corresponding surface. Sizes of the wetting envelopes

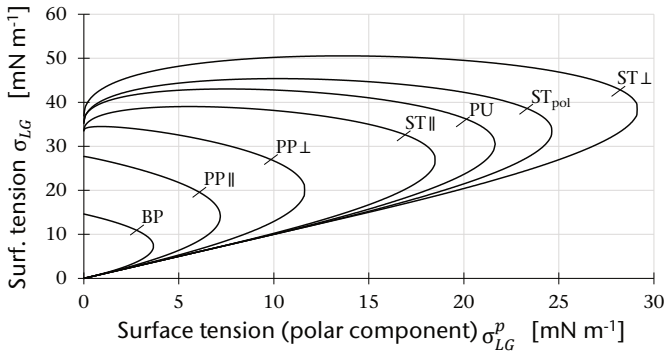

Figure 6-9. Wetting envelopes for fully spreading liquids (θ = 0°) based on the OWRK model.

unsurprisingly follow the same order as the wetting ability of the standard test liquids presented **Figure 6-6**. Complete spreading of liquids on backing-paper will exclusively be observable for liquids with extremely low SFT such as perfluorohexane (~12 mN m^{-1}).

6.4.3 Surface wetting of viscous prepreg resin

While characterizing the wetting behavior of the low-viscosity standard test liquids diiodmethane and water turned out unconditionally, restrictions had to made concerning the contact angle measurements of the extracted prepreg resin. On the one hand, the resin was not dosable from the syringe below temperatures of 70 °C due to high viscosity (>200 Pa s). On the other hand, pronounced viscoelastic behavior led to strong time-dependent deformation of the sessile resin drops after drop placement. The dynamics of viscous liquids on rigid surfaces in general and its quantification by contact angle measurement in particular are a special matter of liquid/solid interaction. The issue has been attended to by advancing and receding contact angle measurement in literature [335–337]. **Figure 6-10** shows the evolution of contact angles on the investigated substrates as a function of time.
The resin drop CA exponentially decreases on all substrates until finally reaching a threshold. The threshold value is reached after 180 sc for all substrates excluding the prepreg surfaces in both directions. Viscoelastic relaxation of stresses induced during drop placement influences the three-phase equilibrium state of the drops and is therefore considered the driving force of time-dependent CA evolution. Also, time-dependent mechanisms, in which polymer chains are rearranged and polar

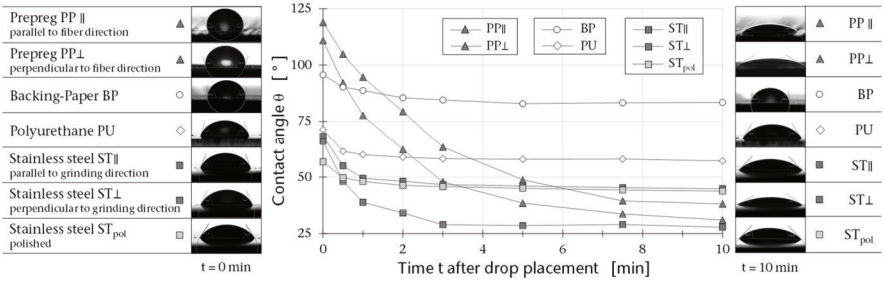

Figure 6-10. Evolution of prepreg resin drops on different substrates over a time span of 10 min (right) after drop placement (left).

groups exposed at the interface have been reported in literature [338] and most likely contribute to the observations as well. On prepreg, the resin continuously spreads and reaches close to complete spreading within the investigated time range. It is assumed that a drop of prepreg resin on a prepreg surface at elevated temperatures cannot be treated as a model system of three ideally separated phases. The prepreg surface (excluding the contribution of the carbon fibers) is in a viscous state and creates a semi-solid interface which is most likely dominated by autohesion/self-diffusion mechanisms.

For all following calculations involving the contact angles of resin drops, the CA values in the equilibrium stage after 180 s are utilized. The spreading coefficient (SC) can be expressed as the difference between surface tension/energy σ_{SG}/σ_{LG} and the interfacial tension σ_{SL}:

$$SC = \sigma_{SG} - (\sigma_{LG} + \sigma_{SL}) \qquad \textbf{Eq. (6-5)}$$

In **Figure 6-11**, spreading coefficient isolines are drawn for prepreg resin as a function of both dispersive and polar SFE components. Grey dots indicate the measured SFE value pairs for the investigated substrates. According to the simple relationship of **Eq. (6-5)**, it appears that wetting is favored by a low interfacial free energy, a high solid surface energy and a low liquid surface tension. Negative spreading coefficients will give a measurable CA > 0°. The OWRK model using standard test liquids predicts complete drop spreading (SC < 0; CA = 0°) for prepreg

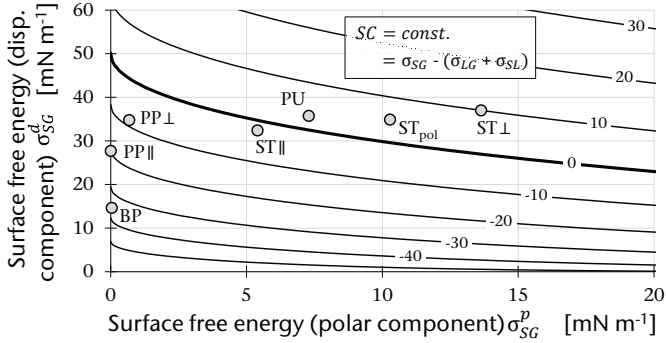

Figure 6-11. Spreading coefficient SC [mN m^{-1}] isolines for prepreg resin (70 °C) as a function of polar and dispersive SFE components.

resin on polyurethane and stainless steel. These predictions were not fully supported by the measured CA presented in **Figure 6-10** as threshold CA > 0° were observed on all surfaces. However, CA were significantly smaller and matched the model-predicted order - with the exception of the prepreg surfaces due to diffusion being the dominant contact mechanism. In terms of topographical anisotropy, the significant differences between PP∥ and PP⊥ as well as ST∥, ST⊥ and ST_{pol} cannot be explained by chemical factors as these surfaces are obviously identical in terms of chemical composition. The different wetting behavior is therefore rather a matter of flowabilty and surface topography which is why an additional analysis of both factors was performed (sections 6.4.5 and 6.4.6).

6.4.4 Role of adhesive attraction for prepreg tack

In an effort to test the hypothesis that the thermodynamic work of adhesion determines the adhesive attraction and, eventually correlates with the tack of prepregs in the adhesive regime, tack measurements were performed for the contact materials utilizing the probe tack test in a rheometer. The measured data was fitted by Gaussian curves as done by Choong [302], Smith [286] and Endruweit [209] pointed out by the authors, the Gaussian fit is a purely phenomenological fit and lacks physical representation. However, the model fit enables the calculation of curve characteristics such as maximum tack and tack onset as a function of temperature as the independent variable. The Gaussian fit of temperature-dependent tack between two prepreg plies are plotted in **Figure 6-12**.

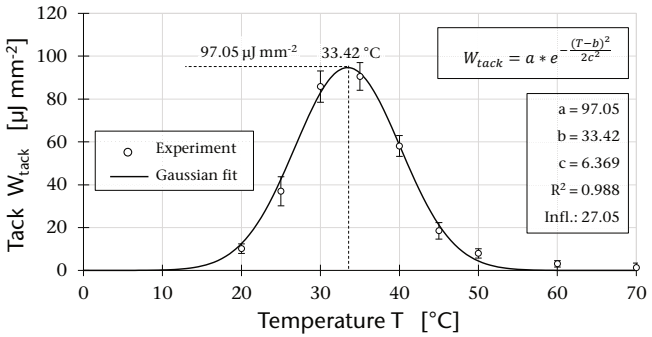

Figure 6-12. Experimental data and Gaussian model fit of tack between two prepreg plies as a function of temperature. The data is obtained for standard parameters of 10 N mm^{-2} compaction pressure and 5 s compaction time.

Here, the fit parameter *a* represents the maximum tack at the temperature *b*, while *c* determines the slope shape and therefore the sensitivity of prepreg tack to temperature deviation. The temperature of 27.05 °C marks the first inflection of the Gaussian fit where dW_{tack}/dT is maximum in the adhesive regime (left side of the bell-shaped curve). For this study, it will be regarded as the onset temperature of tackiness T_{onset} at which bonding is controlled by interfacial adhesion between resin and substrate. The corresponding failure mechanism is adhesive failure and is indicated by the absence of resin residue on the contact material. In this context, the thermodynamic work of adhesion W_{SL} is a measure of the strength of the contact between two phases [339]. W_{SL} is defined as the reversible thermodynamic work required to separate the interface from the equilibrium state of two phases to a separation distance of infinity [141]. It amounts to the difference between the released energies due to the respective surface tensions of σ_{LG}/σ_{SG} and the depleted interfacial tension σ_{SL} when forming a new liquid-solid interface. It is closely related to the spreading coefficient (**Eq. (6-5)**) and is calculated as follows:

$$W_{SL} = \sigma_{LG} + \sigma_{SG} - \sigma_{SL} \qquad \textbf{Eq. (6-6)}$$

Figure 6-13 shows the investigated surface materials as a function of SFE and their classification between W_{SL} isolines. Based on the surface wetting analysis and the herein determined model-based work of adhesion alone, prepreg tack - at least in the low temperature, adhesive fracture regime - is expected to increase in the order:

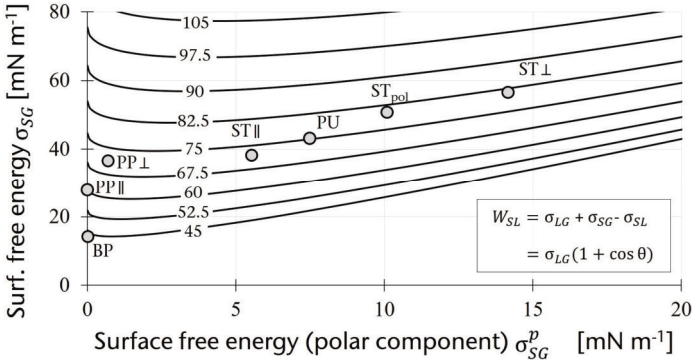

Figure 6-13. Thermodynamic work of adhesion W_{SL} [mN m^{-1}] isolines as a function of polar and dispersive SFE components.

BP, parallel, PP∥), prepreg (perpendicular, PP⊥), ground stainless steel (parallel, ST∥), polyurethane (PU), polished stainless steel (ST_{pol}), ground stainless steel (perpendicular, ST⊥). Tack between prepreg-prepreg specimens is expected to be highest due to intermolecular entanglement as a result of self-diffusion during the compression phase (see discussion in section 6.4.3). **Figure 6-14** shows the probe tack curves of prepreg for different surfaces as a function of temperatures.

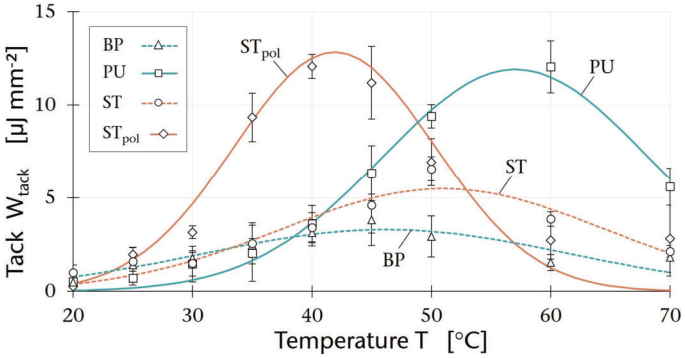

Figure 6-14. Temperature-dependent tack for different surface combinations utilizing the probe test.

Again, experimental data and fitted Gaussian curves are presented. Generally, prepreg tack towards the investigated solid substrates is found to be significantly lower (roughly one magnitude) than between two prepreg sheets. Similar results were reported by Endruweit et al. [209] and Crossley et. al [206]. A significant difference in tack of prepregs towards different contact materials was also observed by Choong et al. [16] who measured maximum tack force of 42.41 ± 1.66 N for prepreg-prepreg and 5.07 ± 0.53 N for prepreg-steel. All aforementioned authors used a continuous application-and-peel procedure which has recently been standardized in ASTM D8336-21 [283].

Comparing the model with the experimental probe tack curves of different substrates reveals that the aforementioned model-predicted order is not fully supported as the thermodynamic work of adhesion W_{SL} apparently does not exclusively determine the adhesive portion of prepreg tack. This becomes most evident for the steel substrates that differ greatly in both maximum tack and the corresponding temperature despite the similar W_{SL} of 78.47 and 84.90 N m^{-1}: Also, polyurethane is located in the same range in terms of W_{SL} and adheres significantly

better than ground steel. The lowest measured tack towards backing paper was anticipated in view of the facts that the absolute W_{SL} is lowest (42.96 mN m^{-1}) and its polar/dispersive SFE component ratio (fully dispersive) matches the ratio of prepreg resin (20.73 %) least. Comparing the ratios between the polar and the dispersive portion of the SFT of liquids and the SFE of solids generally enables an assessment of adhesion: The better the ratios coincide, the more interaction can be expected possible between the involved phases. The low, fully dispersive interaction of the prepreg resin towards backing paper is exclusively dominated by van der Waals forces which result from temporary fluctuations of the charge distribution (London dispersion forces). The interactions of the other surfaces include a polar portion that increases the thermodynamic work of adhesion and presumably leads to the formation of intermolecular hydrogen bonds between resin and substrate. Although higher W_{SL} at the interface appears to lead to higher absolute tack, the wetting analysis based on contact angle measurement cannot fully clarify all substrate-related differences in prepreg tack including the temperature-shifts and the exact order of increasing tack. Thus, additional rheological analysis was performed to investigate its role in the wetting process.

6.4.5 Rheological implication in resin surface wetting

Characteristic viscoelastic parameters of neat prepreg resin, namely complex viscosity η*, storage modulus G', loss modulus G" and its ratio the loss factor tan δ, are given in **Figure 6-15** as a function of temperature for a frequency of 1 Hz.

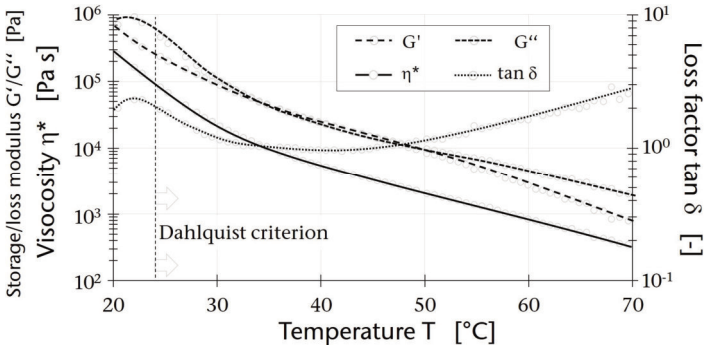

Figure 6-15. Viscoelastic parameters of extracted prepreg resin within the tack-relevant temperature range.

The decrease in viscosity extends to three magnitudes within the examined temperature range. Questions arise as to when the viscosity is low enough for the prepreg resin to sufficiently wet a substrate which would mark the onset of measurable tackiness. The presumably most prominent criterion to estimate the adhesive reliability of soft polymers on rigid substrates, that means to determine whether a viscoelastic material is contact efficient or deficient, is the Dahlquist criterion [245]. Although this criterion is limited to the single characteristic viscoelastic value of G' < 0.3 MPa, it has shown remarkable universality across different kinds of PSA and substrates. Crossley et al. [147] tested the Dahlquist criterion's applicability for epoxy prepregs using a single-stage peel test for different hand lay-up prepregs.

Although the general criterion principle was found valid, it was assumed by the authors that the criterion is rather a function of prepreg and mold surface conditions. Examining the viscoelastic analysis in this paper, the G' curve of extracted prepreg resin crosses the 0.3 MPa Dahlquist line at 23.8 °C (**Figure 6-15**).

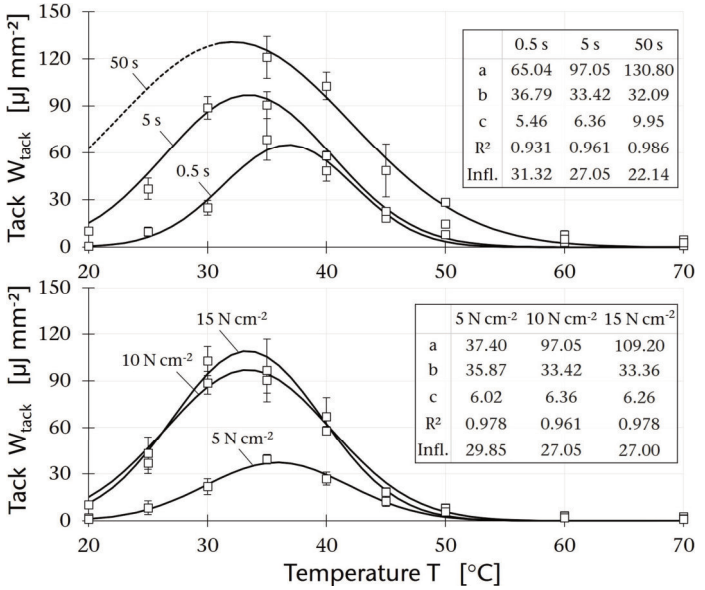

Figure 6-16. Tack between two prepreg plies as function of compaction time (upper graph), compaction pressure (lower graph) and temperature. The dashed line for 50 s compaction was extrapolated due to reaching the load restriction of the test apparatus.

Meanwhile, T_{onset} for the prepreg-prepreg surface combination amounts to 27.05 °C (**Figure 6-12**) with a corresponding G' of 0.16 MPa. This finding is considered a decent agreement with the Dahlquist criterion for this particular material combination. However, the limitations of the Dahlquist criterion for prepreg tack become apparent when consulting the tack results as a function of the contact relevant test parameters compaction time and compaction pressure displayed in **Figure 6-16**.

The dependence of T_{onset} on the compaction parameters indicates that the Dahlquist criterion can only be regarded as a rule of thumb rather than as a clear-cut value independent from further factors. As expected, an increase in both compression parameters leads to a shift of the maximum tack (fit parameter *b*) and tack onset (Infl.) towards lower temperatures. Furthermore, higher absolute tack is measured likewise which has repeatedly been reported in literature for different measuring techniques [52].

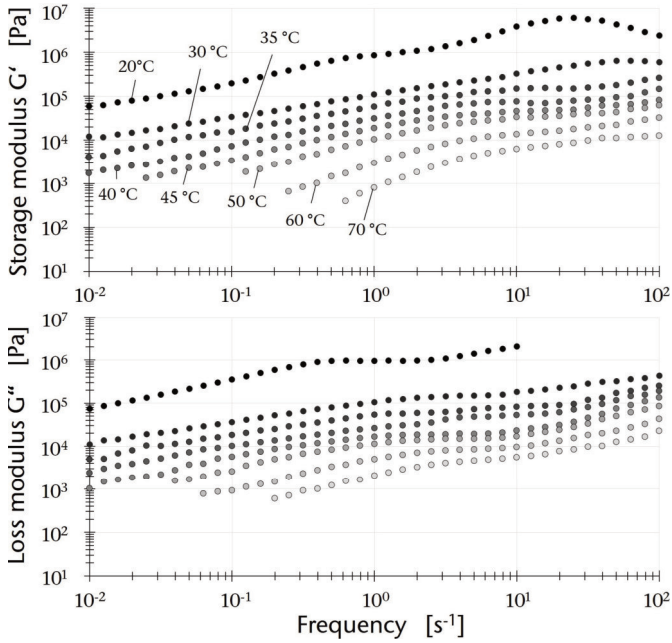

Figure 6-17. Frequency-dependent viscoelastic moduli G' and G''. Data for low frequencies and high temperatures is not shown due to high fluctuation in this region. Here, curve smoothing was performed by average determination of five adjacent data points.

A more sophisticated evaluation of the role of viscoelasticity for tack performance of PSA was made by Chang [273]. According to Chang's proposal, tack-relevant application takes place within the frequency range of 10^{-2} Hz (creep) to 10^{2} Hz (peel). The corresponding viscoelastic moduli in this frequency range are shown in **Figure 6-17** for different temperatures. Consulting Chang windows for tack characterization of adhesives and resins does not exclusively focus on the wetting process but includes the debonding behavior as well [340]. This way, a categorization of tack performance (e.g., removable, high shear etc.) can be realized resting upon viscoelastic behavior. The windows are spanned within four corner points that are defined by the frequency-dependent G'/G" pairs of values at $10^{-2}/10^{-2}$, $10^{-2}/10^{2}$, $10^{2}/10^{-2}$ and $10^{2}/10^{2}$ s^{-1}. Based on the data shown in **Figure 6-17**, Chang windows were constructed by this procedure for selected temperature levels in **Figure 6-18**.

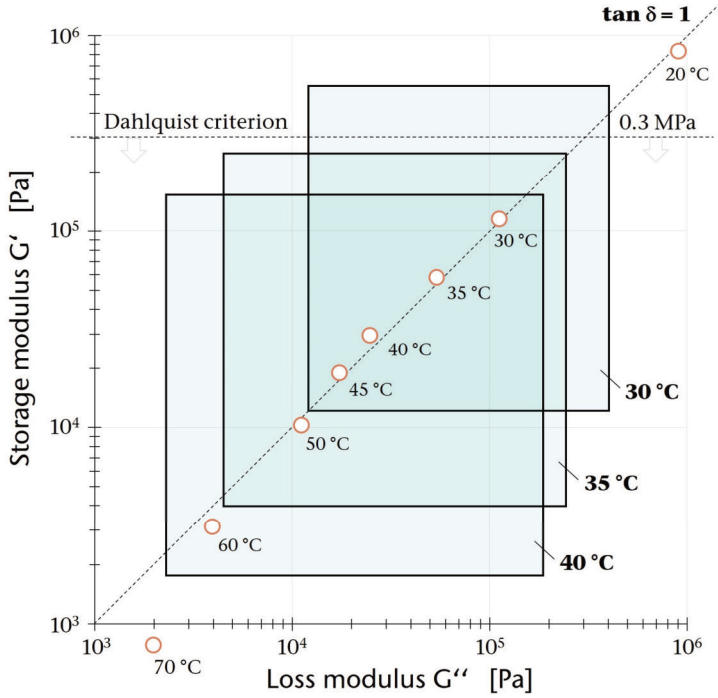

Figure 6-18. Chang windows of neat prepreg resin for different temperatures.

1 Hz results (white dots) for all temperature levels are located near the G'/G" cross-over line (tan δ = 1) that separates the two regions of elastically and viscously dominated behavior. The closer a dot or a constructed viscoelastic window is located towards the top-left hand corner of the plot, the better removable the adhesive will be with an adhesive failure mechanism. Conversely, a location near the lower right hand corner of the plot will result in a more viscous, cohesively breaking material. The displayed Chang windows of 30, 35 and 40 °C are actually the only investigated temperature levels whose windows can fully be constructed within the storage and loss modulus range between 10^3 and 10^6 Pa.

Remarkably, these are the medium temperature levels exhibiting maximum tack between two prepreg plies (see **Figure 6-12**). Higher temperatures push the windows towards lower moduli while the low temperature window of 20 °C exceeds the graph towards higher moduli. According to our measurement at ~1 Hz, the highest tack levels for the prepreg-prepreg combination can be achieved when the Chang window of prepreg resin is located in the range of a 'general purpose PSA' (G' and G" roughly between 10^4 and 10^5 Pa) with a slight tendency towards higher moduli which corresponds to moderately lower temperatures. Based on this finding, adjusting a resin storage modulus G' of 10^4 Pa (at material deposition temperature) in the b-staging process is recommended if maximum tackiness is required in AFP.

In general, the Chang windows for prepreg resin appear significantly wider than the majority of Chang windows reported in PSA research [340–342]. Following the construction process of these viscoelastic windows, this is evidently observable due to a stronger frequency dependence of the viscoelastic parameters for epoxy prepreg resin than for most PSA formulations. Reasons are most likely that PSA design is performed to meet specific application requirements (clean removable, high resistance etc.) [343]. Meanwhile, rather the mechanical properties in combination with the reinforcement fibers are deciding for prepreg resin formulation. Considering the implication for practical use in advanced composite manufacturing, the results substantiate the challenging aspects of process adjustment: On the one hand, the high temperature- and frequency-dependence, and therefore large Chang windows, give processors the possibility of adjusting the lay-up process in a wide spectrum. This is beneficial if different tack levels are needed at different stages in the process, e.g., during material feeding/cutting and deposition. On the other hand, precise temperature control of the laid prepreg is

mandatory and practically challenging, especially under special process conditions such as variable lay-up speed, complex geometries etc. [233].

No amplitude sweeps are presented here as no significant influence of the oscillatory deformation stress could be determined within the investigated measurement range for temperatures ≥35 °C. Hence, the limit of the linear viscoelastic region (LVE region) was not reached for these temperatures and plateau values could be determined. For lower temperatures near room temperature, repeated downturns of the moduli curves were observed indicating brittle fracturing behavior of the prepreg resin sample for high stresses outside the LVE region.

6.4.6 Roughness-extended Dahlquist criterion

Both criteria shown in the previous section are exclusively based on the viscoelastic behavior of the prepreg resin and therefore independent from contact material properties such as surface free energy and topography despite their apparent implication in prepreg tack. **Figure 6-19** shows topographic images of the contact materials taken by a 3D laser scanning confocal microscope. Non-contact optical measurement turned out to be the only suitable way to analyze the surface of uncured epoxy prepregs topographically. With the scale being normalized for comparison reasons, it becomes evident that the investigated surfaces differ greatly in terms of roughness. The order of round mean square roughness R_q (**Eq. (6-4)**) is determined as PP > PU > ST > BP > ST_{pol}. In contrast to structural adhesives, rougher surfaces are known decrease the adhesive performance of PSA [344]. For this type of bonding, deviations from an ideally smooth surface result in an increased potential

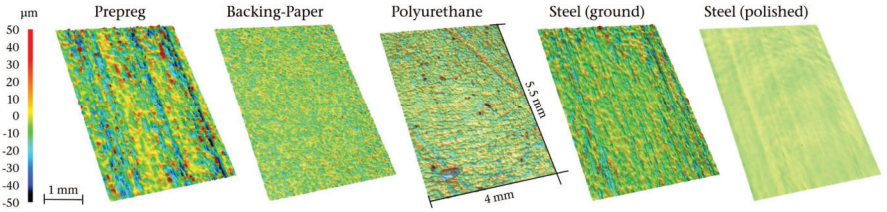

Figure 6-19. Surface topographies of the investigated contact materials. Pictures were taken by 3D laser scanning microscopy (2.5x) and scale was normalized.

contact area but will at the same time hinder the wetting process of viscous liquids [201]. The observation that surface conditions play an important role in PSA adhesion has eventually led to repeated refinement of the Dahlquist criterion in literature. In this context, Ciavarella and Papangelo [345] proposed an extended criterion incorporating surface topography based on a generalized Johnson parameter. Topographical surface characteristics are represented by the root mean square roughness R_q and the maximum wavelength in the roughness profile λ_0 which are then combined with the thermodynamic work of adhesion W_{SL} as per:

$$G'_c = \frac{W_{SL}\,\lambda_0}{4\,{R_q}^2} \qquad \textbf{Eq. (6-7)}$$

The simple relationship postulates that high adhesive attraction (represented by W_{SL}) and high wavelength will result in high critical moduli G'_c while rougher surfaces need low modulus liquids in order to achieve proper surface wetting. Utilizing the rheological data of **Figure 6-17**, a corresponding critical temperature T_c can be determined for G'_c. At this specific temperature, the prepreg resin will fill the surface cavities (equaling a high degree of intimate contact) which should in theory result in a considerable increase in tack. Dahlquist and other authors did not specify in detail, when a PSA is to be considered contact efficient, e.g., as defined by a specific measurable tack level or degree of intimate contact. Hence, we define the first inflection point of the bell-shaped tack curves as the onset temperature of a considerable level of tackiness T_{onset}. (section 6.4.4). It can be calculated from the Gaussian fits of the temperature-dependent tack curves presented in **Figure 6-14**. **Table 6-4** sums up the experimental topographical results and the calculated criterion-relevant contact parameters. As probe tack experiments are carried out perpendicularly towards the sample surfaces, different fiber/grinding directions cannot be respected. The G'_c values for PP and ground ST are therefore calculated by using the arithmetic mean values of R_q, λ_0 and W_{SL} for both directions.

Table 6-4. Gaussian model fit parameters and characteristic value. Arithmetic mean values of R_q, λ_0 and W_{SL} are used for surfaces with significant influence of grinding/fiber direction (prepreg and ground steel). The OWRK-based surface polarities are given for comparison reasons with the resin polarity (20.73 %).

Surface material	R_q [µm]	λ_0 [µm]	W_{SL} [mN m^{-1}]	G'_c [MPa]	T_c [°C]	T_{onset} [°C]	T_{max} [°C]	Polarity [%]
Prepreg	11.62 ± 2.16	39.7 ± 0.41	59.61 ± 3.42	0.005	53.9	27.05	33.42	0
Backing-paper	2.47 ± 0.38	17.9. ± 0.27	42.96 ± 0.61	0.031	38.2	30.79	46.22	0
Polyurethane	7.41 ± 0.53	50.10 ± 1.33	82.63 ± 0.64	0.019	42.1	45.97	57.05	17.49
Steel (ground)	2.04 ± 0.26	25.3 ± 0.65	78.47 ± 1.22	0.128	28.0	37.49	50.99	20.57
Steel (polished)	0.51 ± 0.06	31.3 ± 0.49	84.90 ± 1.33	2.554	11.2	33.51	41.91	22.44

Comparing the experimentally determined T_{onset} to the criterion-based T_c reveals basic applicability of the criterion to prepreg tack: The smooth surface of the polished steel specimens combined with high W_{SL} at the interface, e.g., leads to the highest modulus and therefore requires only low temperatures in order to guarantee sufficient surface wetting. The rougher ground steel surface with similar W_{SL} and λ_0 starts adhering at higher temperatures as predicted by the criterion. The medium roughness in conjunction with low W_{SL} of the backing paper leads to a medium modulus. However, the T_c of ST and BP appears less meaningful due to the less pronounced dependence of tack on the temperature (**Figure 6-14**).
In summary, the criterion is able to serialize the investigated surface materials in terms of a prepreg resin temperature that is necessary for surface wetting. The theoretical succession was generally supported by tack measurement except for the prepreg-prepreg combination (see section 6.4.3 for discussion). However, the absolute values of T_c and T_{onset} differ significantly. There are several aspects that may be causing the difference:

- A potential temperature-dependency of the resin wetting process, which may influence W_{SL}, could not be accounted for in the wetting analysis because the viscous prepreg resin did not form stable drops for temperatures <70 °C.
- The resin surface of the prepreg, which serves as the adhesive in the tack tests, is comparatively rough by itself (R_q = 11.2 µm) while only the roughness of the adherend was considered for the criterion.
- The anisotropy of the surfaces could not be respected for tack measurement, which is why calculation of T_{onset} is based on arithmetic mean values.

- Prepreg tack is subject to a variety of influencing factors [5]. The displayed results are only representative of a single set of testing parameters. The results presented in **Figure 6-16** illustrate that test parameter variation can cause shifts in the temperature spectrum.
- Compaction pressure and time are not considered by the criterion.
- In general, the validation procedure of the topographically extended Dahlquist criterion as performed in this study is very sensitive to deviation and measurement uncertainty. A slight difference in the estimated critical modulus G_c will, for example, result in a relatively large temperature shift due to the pronounced G' dependency on resin temperature.

6.5 Conclusion

In this paper, unidirectional carbon fiber prepreg was investigated in terms of probe tack and the interfacial interaction towards different AFP-related contact materials. Emphasis was placed on the bonding process by examination of the influence of surface wetting, rheology and topography. The results elucidate the fundamental mechanisms for contact formation and its role for measurable prepreg tack in the adhesive regime of the temperature-sensitive adhesion-cohesion balance. The key findings can be summarized as follows:

- Contact angle measurement in combination with the OWRK model proved to be a suitable approach to reveal significant differences in surface wetting of prepreg resin as well as standard test liquids on solid surface materials that are present in AFP.
- Contact formation between two prepreg plies cannot be treated as model system of three ideally separated phases and is therefore not approachable through CA measurement. For this material combination, adhesion is rather provided by autohesion mechanisms which eventually entail higher measurable tack than prepregs show towards solid substrates.
- High adhesive attraction between prepreg resin and a solid surface (represented by thermodynamic work of adhesion W_{SL}) favors higher tack values. However, the relation is found not to be straightforward as, e.g.

differences in tack are found between steel surfaces of different surface roughness despite similar W_{SL}.

- Higher tack can be achieved on substrates with matching polar and dispersive SFT/SFE ratios. This way, both dispersive (van der Waals forces) and polar (h-bonding, dipole-dipole-interaction) can come to fruition at the interface.
- Rheological approaches to surface wetting and tack performance developed for pressure sensitive adhesives (PSA) proved to be basically applicable for thermoset prepregs but could not explain surface-related wetting phenomena in its entity. Variation of contact-relevant test parameters and contact materials could exemplify the limitations of these criteria.
- A topographically extended version of the Dahlquist criterion was successfully applied to investigate the implication of W_{SL}, surface topography and rheology in the temperature-dependent onset of tack in the adhesive failure regime via an estimated critical storage modulus G'_c. Although, absolute temperatures determined by tack measurement did not exactly match the criterion-predicted temperatures, the basic dependencies could be verified: While high W_{SL} and large wavelengths in the roughness profile promote low temperature wetting, higher resin temperatures/lower storage moduli are required to thoroughly wet rough surfaces and, eventually, promote adhesion.

CRediT authorship contribution statement

D. Budelmann: Conceptualization, Methodology, Validation, Formal analysis, Investigation, Writing - original draft, Writing – review & editing. **C. Schmidt**: Conceptualization, Resources, Writing – review & editing, Supervision, Funding acquisition. **D. Meiners**: Conceptualization, Resources, Writing – review & editing, Supervision, Project administration, Funding acquisition.

Declaration of Competing Interest

The authors declare that they have no competing financial interests or personal relationships associated with this publication.

Acknowledgements

The authors would like to acknowledge the financial support by Deutsche Forschungsgemeinschaft (DFG – German Research Foundation) granted for the research project 'TackTIC – Tack of Thermoset Impregnated Carbon Fibers' (project number 458900231).

Appendix

Table 6-5. DSC and rheological data of the extracted THF/resin mixture after different times of conditioning at 80 °C and 100 mbar.

	DSC		Viscosity at 60 °C/1Hz [Pa s]	
Conditioning time [h]	T_{onset} [°C]	Cure enthalpy [J g^{-1}]	Pure resin (datasheet [18])	Measurement
0	124.3	486.3	500	131
2	123.6	488.9	-	384
4	125.6	489.2	-	493

Chapter 7

7. Prepreg resin formulation – Publication IV

Tack of epoxy resin films for aerospace-grade prepregs: Influence of resin formulation, B-staging and toughening

D. Budelmann[a], C. Schmidt[b], D. Meiners[c]

[a]Institute of Polymer Materials and Plastics Engineering, Clausthal University of Technology, Ottenbecker Damm 12, Stade, Germany

[b]Institute of Production Engineering and Machine Tools, Leibniz Universität Hannover, Ottenbecker Damm 12, Stade, Germany

[c]Institute of Polymer Materials and Plastics Engineering, Clausthal University of Technology, Agricolastr. 6, Clausthal-Zellerfeld, Germany

Polymer Testing* 114 (2022) 107709.

*Journal metrics:

CiteScore: **10.7** (Scopus, 2023)
Rank 13/211; 94th Percentile (Chemistry: Organic Chemistry)

Impact factor: **5.0** (Clarivate, 2023)

Abstract

Aerospace-grade prepreg resin films based on multifunctional tetraglycidyl-4,4'-methylenedianiline (TGMDA), triglycidyl p-aminophenol (TGAP), Bisphenol A diglycidyl ether (DGEBA) and curing agent 4,4'diaminodiphenyl sulfone (DDS) are investigated in terms of tackiness by probe testing. The model epoxy systems are modified regarding the thermoplastic toughener content (polyethersulfone, PES) and the B-stage level, which is adjusted by cure prediction based on a model-free isoconversional method (Flynn-Wall-Ozawa). Additional DSC and rheological analysis are performed to study the thermal and viscoelastic material behavior in conjunction to its impact on temperature-dependent tack. Maximum achievable tack is found to decrease as a function of both degree of conversion and toughener content. Meanwhile, both influencing factors shift the tack maximum towards higher temperatures corresponding to increased flow characteristics attributed to evolving network formation and the incorporation of high molecular weight PES. In terms of absolute tack level and corresponding temperature, probe tack values similar to commercial prepreg systems (~100 µJ mm^{-2}) are recorded for TGMDA-based formulations containing 10 wt% PES at 20 % pre-cure. Model formulations, which have neither been exposed to B-staging nor toughened, show exceptionally high tack below room temperature for all investigated epoxy prepolymers and are therefore not considered processable by automated fiber placement.

* Corresponding author.
E-mail address: dennis.budelmann@tu-clausthal.de (D. Budelmann).

https://doi.org/10.1016/j.polymertesting.2022.107709
Received 3 May 2022; Received in revised form 22 June 2022; Accepted 14 July 2022
Available online 19 July 2022

7.1 Introduction

Composites structures for aerospace applications such as fuselage sections or wings have to meet strict requirements in terms of thermomechanical performance in service [346]. High strength and modulus must be guaranteed at elevated temperatures [347], which limits the number of suitable polymeric matrices. Aerospace-grade prepregs based on epoxy matrix systems in combination with carbon fiber reinforcements have proved to capitalize on highest strength-to-weight ratios, advantageous automated processability and thermal resistance which has made them the predominant material combination for structural aerospace composite parts [348]. In order to ensure a desired high glass transition temperature T_g of >160 °C after cure, multifunctional epoxy prepolymers are widely used in aerospace-grade matrices [105,333]. Prominent representatives of this material group are the tetrafunctional tetraglycidyl-4,4'-methylenedianiline (TGMDA) and trifunctional triglycidyl p-aminophenol (TGAP). Moreover, the aromatic amine diaminodiphenyl sulfone (DDS) is a commonly applied curing agent for aerospace prepregs [349]. 4,4'-DDS features a para-substitution in contrast to the meta-substitution of the isomer 3,3'-DDS which have been reported to result in both different processing and after cure properties [350]. In order to improve fracture toughness, e.g., high molecular weight polyethersulfone (PES [351–353]) or polyimide (PEI [354–356]) are added to resin systems. The addition of these high performance thermoplastics typically amounts to ~20 wt% of the matrix system [357,358]. With the toughening agent being soluble in the uncured epoxy resin, a two-phase morphology is generated during the curing process which reduces crack propagation and, therefore, leads to an increased fracture toughness [92]. Local shear yielding of the toughening agent around the crack tip is considered the most influential toughening mechanism at this juncture [93].

The aforementioned material considerations are related to the composites application in load-bearing components after cure (C-stage). However, processing prepregs in automated lay-up processes such as automated fiber placement (AFP) and automated tape laying (ATL) requires specific pre-cure material properties. Together with drape and resin flow, the stickiness (tack) of the thermoset prepregs is of major importance [52]. Tack is needed to ensure reliable positioning and prevent sliding of the prepreg material during lay-up of a laminate [303], which is subsequently cured in an autoclave at ~180 °C over several hours. Experimental

characterization of tack has mainly been focused in literature using commercially available prepregs. Following this pragmatic approach, experimental results can directly be translated to the manufacturing process, e.g., as demonstrated by Smith et al. for the dependence of prepreg tack on ageing [286]. However, as formulations of commercial prepreg resin systems are kept secret by material suppliers, no correlation between chemical composition and tack can be established.

Few studies have investigated the influence of formulation-relevant variation on tack: Pouladvand et al. [294] introduced and characterized a dual-curable epoxy-amine formulation based on Bisphenol A diglycidyl ether (DGEBA), diethylenetriamine (DETA) and dicyandiamide (DICY) for prepregs. The B-staged system was found to achieve maximum tack at a degree of cure (DoC) of 20–25 % depending on test temperature. Similar results were reported in a subsequent paper by the authors including a study of the resin cure kinetics [297]. Asaro et al. [359] attributed a rise in tack of nanoclay-filled phenolic prepregs to an increase in conversion and bentonite content. The influence of the prepreg impregnation process parameters of a model epoxy system (including TGMDA, DGEBA, DDS and DICY) on tack was studied by Hayes et al. [222]. The studies presented here were predominantly conducted to explore properties of model resins with tack being an ancillary processing aspect among several others. They therefore lack a systematic approach to study tack as the complex phenomenon it has been shown to be in studies incorporating commercial prepreg systems [52].

This paper hence aims at exploring the relationship between epoxy resin formulation and prepreg tack. For this purpose, epoxy-based model resins were varied with respect to three formulation- and processing relevant aspects, namely the utilized epoxy prepolymers, the PES toughener content and the B-staging level. Three epoxy monomers (TGMDA, TGAP and DGEBA) were used to formulate resin systems with DDS acting as the curing agent for all formulations. The toughener content of the TGMDA system was varied at 0, 10, 20 and 30 wt% PES while the B-stage level was set to nominal 10, 20 and 30 % cure in addition to the initial A-stage. B-staging was achieved by exposing the resin to a defined isothermal heat treatment which was proposed based on the model-free isoconversional method of Flynn-Wall-Ozawa (FWO). For all resin variations, tack was measured utilizing a probe tack test in a rheometer as function of material and probe temperature. Complementary material analysis was carried out to reveal differences in thermal and rheological behavior affecting tack.

7.2 Materials

7.2.1 Model resin formulation

The components for resin formulation in this study were chosen to yield properties of typical aerospace-grade epoxy matrices in carbon fiber prepregs for automated lay-up technologies. Commercially used resins, especially 180 °C cure systems, are complex in terms of their multifaceted and in large part unknown composition. For this study, simplified model resins based on three different polyfunctional epoxy prepolymers, an aromatic amine hardener and a thermoplastic toughening agent were used as shown in **Figure 7-1**.

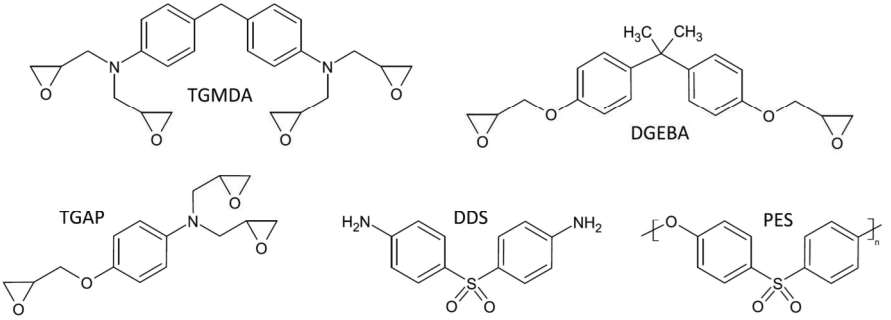

Figure 7-1. Epoxy prepolymers (TGMDA, TGAP, DGEBA), curing agent (4,4'DDS) and thermoplastic toughener (PES) used for prepreg resin formulation and tack characterization.

The epoxy resins comprised a tetrafunctional tetraglycidyl-4,4'–methylenedianiline (TGMDA, epoxy equivalent weight (EEW) ~113 g mol^{-1}), a trifunctional triglycidyl p-aminophenol (TGAP, EEW ~100 g mol^{-1}) and a bifunctional Bisphenol A diglycidyl ether (DGEBA, EEW ~174 g mol^{-1}). The aromatic amine 4,4'diaminodiphenyl sulfone (DDS, amine hydrogen equivalent weight (AHEW) ~62 g mol^{-1}) was used as the curing agent in a stoichiometric ratio of a/e = 0.9. All aforementioned chemicals were supplied by Merck KGaA, Germany. The functionalized polyethersulfone Sumikaexcel PES 5003 MP, which is supplied by Sumitomo Co. as a finely ground powder with an average grain size of 45 µm, is added as a thermoplastic toughening agent. Sumikaexcel PES 5003 MP

contains 1.1 –OH groups per 100 polymer relating units while its average molar mass was reported to amount 42 kg mol^{-1} [360].
Resin variations were formulated by using TGMDA, TGAP and DGEBA as sole epoxy prepolymers as well as by preparing a blend of TGMDA and TGAP at a 1/1 wt ratio. Furthermore, the toughener content was varied for the TGMDA-based resins at 10, 20 and 30 wt%. Formulation-relevant data and the prepared PES epoxy amine systems are summarized in **Table 7-1**. EEW, AHEW and molar masses were adopted from the technical data sheets of the supplier.

7.2.2 Sample preparation

Resin batches of 100-150 g were produced in a nitrogen-flooded glove box according to the weight ratios presented in **Table 7-1** following the undermentioned procedure. First, the epoxy prepolymers were heated up to 150 °C on a heating plate before adding PES toughening powder. The mixtures were homogenized until complete dissolution of PES in the epoxy component was achieved under 60 min of mechanical stirring. The mixing time of TGAP-based formulations was extended to 180 min as the toughener showed significantly slower dissolubility in TGAP. Before adding the curing agent DDS at an a/e-ratio of 0.9, the epoxy-toughener mixtures were cooled down to 80 °C to avoid undesired premature cure. Incorporation of the hardener was performed for by mechanical stirring for 15 min. The resin formulations were cooled to room temperature and were transitioned to the freezer, where they were kept at -18 °C before analysis.

Table 7-1. Reaction-relevant data and components weight proportion for resin formulation.

	Epoxy prepolymers			Hardener	Toughener
	TGMDA	TGAP	DGEBA	DDS	PES
EEW/AHEW [g mol^{-1}]	113	100	174	62	-
mol. mass [g mol^{-1}]	422.5	277.2	340.4	248.3	42,000
TGMDA (10)	60.25 %	-	-	29.75 %	10 %
TGMDA 20	53.55 %	-	-	26.45 %	20 %
TGMDA 30	46.86 %	-	-	23.14 %	30 %
TGMDA/TGAP	29.49 %	29.49 %	-	31.02 %	10 %
TGAP	-	57.77 %	-	32.23 %	10 %
DGEBA	-	-	68.15 %	21.85 %	10 %

7.3 Experimental methods

7.3.1 Differential scanning calorimetry

Thermal analysis for both establishing a dynamic kinetics model (section 7.4.1), subsequent cure monitoring and measuring glass transition temperatures T_g was conducted by modulated differential scanning calorimetry (DSC) using a TA Instruments Discovery DSC. Determination of the kinetics model parameters for each investigated epoxy formulation was based on temperature profiles between 50 and 330 °C at heating rates β of 1, 2, 5 and 10 K min^{-1}. The degree of cure α is the amount of partial heat converted H_p divided by the total reaction enthalpy H_R or can be expressed as **Eq. (7-1)** if the residual heat of reaction H_{res} is measured. Values of T_g were drawn from the inflections of the reversible heat flow in DSC curves recorded between -50 and 50 °C.

$$\alpha = 1 - \frac{H_{res}}{H_R} \qquad \textbf{Eq. (7-1)}$$

7.3.2 Cure kinetics

The model-free FWO kinetic approach developed independently by Flynn/Wall [361,362] and Ozawa [363] was applied for the kinetic analysis. With the FWO method being an isoconversional method, both activation energy E_a and pre-exponential factor A are functions of the degree of cure α. Just like most other kinetic models for describing the cure behavior of thermosets, the method is based on the general rate equation

$$\frac{d\alpha}{dt} = k(T)\, f(\alpha) \qquad \textbf{Eq. (7-2)}$$

which consists of a specific rate constant at a certain temperature k(T) and a conversion-dependent function f(α) representing the reaction mechanism. The FWO approach assumes the reaction rate to be only a function of temperature at constant degrees of conversion. Using Doyle's approximation of the temperature integral, the model's fundamental **Eq. (7-3)** can be expressed as per

$$\ln \beta = \ln\left(\frac{AE_a}{R}\right) - \ln F(\alpha) - 5.3305 - 1.052\left(\frac{E_a}{RT}\right) \quad \textbf{Eq. (7-3)}$$

with the integral conversion function

$$F(\alpha) = \int_0^{\alpha} \frac{d\alpha}{f(\alpha)}) \quad \textbf{Eq. (7-4)}$$

By using data from dynamic DSC measurements, temperatures could be determined at which a specific degree of conversion α is reached for each heating rate β. Plotting ln β vs. T^{-1} renders straight lines where E_a is represented by the slope of the linear regressions for each α and could be calculated according to **Eq. (7-3)**.

7.3.3 Rheology

Flow and deformation characterization of the formulated resin samples was performed by oscillatory shear rheometry in a TA Instruments ARES G2 rheometer. The tests were carried out using a standard 25 mm diameter parallel plate-plate geometry at 1 mm gap. The samples were exposed to temperature sweeps between 0 and 100 °C at a rate of 2 K min^{-1}. Test frequency and shear deformation were kept constant for all rheological experiments at 1 Hz and 2 % strain, respectively. The complex viscosity η^*, storage modulus G' and loss modulus G" were recorded as the rheological parameters of interest throughout the set temperature range.

7.3.4 Tack testing

A probe tack testing procedure in an ARES G2 rheometer (compression to tension test), which has successfully been applied to commercial prepreg systems before [184,364] was adapted to tack characterization of neat resin samples. Therefore, modifications of the test fixtures were made by removing the sample clamps in the favor of a circular probe with a diameter of 7 mm. The tests are carried out within the rheometer convection oven ensuring precise temperature control in the tack-relevant temperature range. The test setup is shown in **Figure 7-2**.

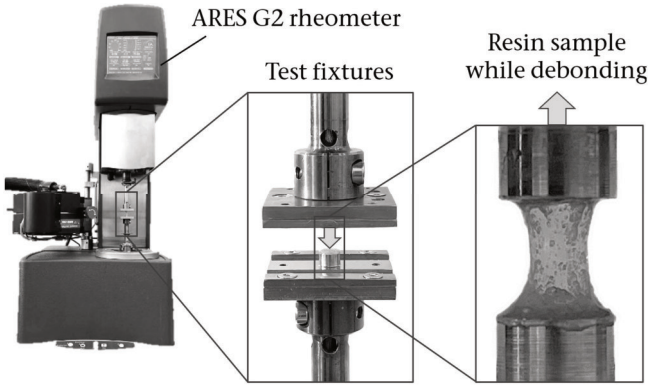

Figure 7-2. Probe tack test setup for neat resin samples attached to an ARES G2 rheometer.

Samples for tack testing were produced from the investigated formulations by hot pressing thin resin films (0.4 mm) in a small manual press at elevated temperatures (80 °C). The final desired sample geometry for tack testing was achieved by piercing circular 7 mm samples with a hollow punch. Employing the probe tack testing procedure, the produced resin samples were laid on specimen holder and brought into contact with a stainless steel probe both equaling in size (7 mm diameter). A compaction force of 3.8 N corresponding to a pressure of 1 bar was applied for 5 s. Subsequent debonding was performed at a constant rate of 0.1 mm s^{-1}. Integration of the stress strain curves gives the work of separation W_t which served as a measure of tackiness in this study. All test parameters other than material temperature were held constant throughout the experiments to ensure comparability between all formulations, B-stage levels and toughening contents.

7.4 Results and discussion

7.4.1 Cure kinetics

In the first instance, a series of non-isothermal DSC experiments was conducted in order to characterize the cure behavior of the prepreg resins and to derive kinetic parameters for B-staging. **Table 7-2** summarizes the basic DSC data, namely total cure enthalpy and glass transition temperatures. The mean values and standard

Table 7-2. Cure enthalpy and glass transition temperatures of A-stage resin formulations.

Epoxy resin formulation	Total cure enthalpy [J g^{-1}]	Glass transition temperature [°C]
TGMDA[a)]	550.8 ± 5.5	-6.02 ± 0.65
TGMDA (20 wt% PES)	497.1 ± 6.6	2.53 ± 0.49
TGMDA (30 wt% PES)	428.1 ± 13.1	14.53 ± 1.06
TGMDA/TGAP[a)]	574.6 ± 9.5	-7.38 ± 1.23
TGAP[a)]	584.3 ± 15.8	-14.73 ± 1.10
DGEBA[a)]	272.5 ± 20.21	-10.11 ± 0.70

[a)] Including 10 wt% PES toughening

deviations for both values were calculated from 1, 2, 5 and 10 K min^{-1} dynamic measurement cycles. Both the highest cure enthalpy and lowest glass transition temperature were measured for the TGAP-based formulation. TGMDA with the same amount of toughener content exhibited slightly less enthalpy upon cure while a higher toughening content led to weaker exothermic reactions. As expected, the relative decrease in cure enthalpy was in the range of the increased portion of toughening agent (~10 wt%) indicating a minor influence of PES on the reaction mechanism. The TGMDA/TGAP blend placed between pure TGMDA and TGAP in terms of reaction heat. The same trends in a reversed order were observed for T_g. The bifunctional DGEBA system fully cured releasing a significantly lower energy of 272.5 J g^{-1} and had an initial T_g of -10.11 °C.

The evolution of the cure reactions for the formulated resins, which were varied in terms of toughener content and utilized epoxy prepolymers, were studied using dynamic DSC experiments (Appendix: **Figure 7-9**). Despite being functionalized with reactive –OH groups, the PES-based toughener showed a negligible influence of its content on cure behavior for the TGMDA-based formulations in the investigated range (<30 wt%). The finding is in accordance with the study conducted by Rosetti et al. [352] who used similar components for epoxy formulation and found no difference between PES toughened (13 wt%) and untoughened systems in terms of cure behavior. Despite using the same curing agent DDS, the apparent reactivity increased when using TGAP as epoxy component with the TGMDA/TGAP blend ranging between pure TGMDA and TGAP. The low-functionality DGEBA-based resin cured comparably at low conversion but tended to require more time to complete network formation at high

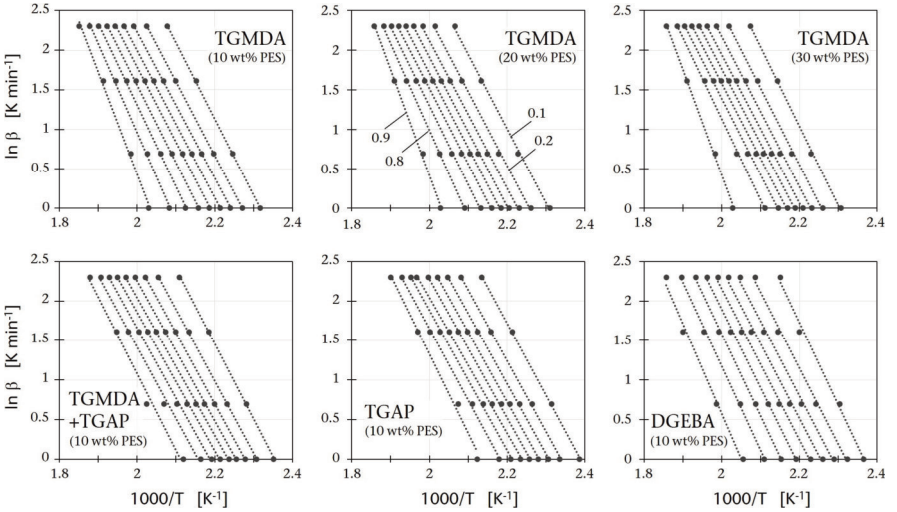

Figure 7-3. Flynn-Wall-Ozawa plots of epoxy resin formulations for determining the activation energy E_a and pre-exponential factor A. The linear regression lines for different degrees of conversion (0.1 to 0.9) are shown in an increasing order (left to right).

DoC. Plotting the logarithmic heating rate ln β against the inverse temperature at fixed degree of conversions (α = 0.1, 0.2, ..., 0.9) yields the Flynn-Wall-Ozawa plots shown in **Figure 7-3**.

The kinetics parameter, namely activation energies E_a could be determined from the graph's slopes. The experimental data could be fitted accurately by linear regression using **Eq. (7-3)** as coefficients of determination R^2 range between 0.997 and 0.931. Parallelism of the linear regression curves generally indicates a constant energy barrier throughout the whole curing process as the curve slopes represent the activation energy. However, lack of parallelism was observed especially at high and low levels of cure for all tested resin formulations. This manifests in the evolution of E_a as a function of cure progress as shown in **Figure 7-10** (Appendix). The dependence of E_a on conversion indicated a multi-step reaction with autocatalytic behavior which has been reported repeatedly in literature for epoxy cure reactions [365]. The curing process passed multiple steps namely, primary amine reaction with epoxy, secondary amine reaction with epoxy, etherification and homopolymerization [366]. The general course of the determined curves was in accordance with studies, which also explored the dependence of E_a on α of

multifunctional epoxies, e.g. by Pramanik et al. [367] for DGEBA and 3,3'-DDS or by Ignatenko et al. [103] for using 4,4'-DDS.

Utilizing the derived kinetic parameters, isothermal heat treatments for specific B-staging levels could now be designed and eventually used to prepare B-staged resin samples for tack testing as presented in section 7.3.4. Despite epoxy resins being known to yield autocatalytic behavior and due to the low desired degrees of cure (≤ 30 %), a first order reaction ($G(a) = 1-\alpha$) was assumed to calculate the pre-exponential factor A and eventually be able to predict the B-staging parameters. Isothermal time-conversion plots (not shown here) were constructed and a B-staging temperature of 140 °C was chosen. The B-staging temperature of 140 °C was selected as a tradeoff between shortened process duration at higher temperatures and enhanced accuracy due to higher practicability at lower temperatures. The model-predicted necessary time spans for B-staging at this temperature amounted to 34 min (10 %), 55 min (20 %) and 76 min (30 % cure), respectively.

7.4.2 Influence of epoxy prepolymer on tack

In an effort to characterize tack behavior of the investigated epoxy prepolymers TGMDA, TGAP, a blend of both and DGEBA, its dependence on temperature was plotted in **Figure 7-4**.

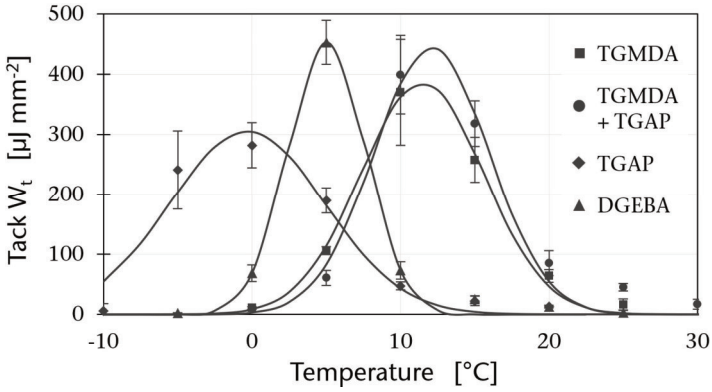

Figure 7-4. Evolution of tack W_t of the investigated epoxy resins (10 wt% PES) as a function of temperature.

The experimental data was fitted by Gaussian curves. The procedure has proven beneficial for fitting data generated by peel testing [209,286,302] according to the new tack testing standard for prepregs (ASTM D8336-21 [283]) as well as probe testing [364]. In terms of maximum tack at peak temperatures, all A-stage resin formulations studied here outperformed commercial prepreg systems, which were characterized with the same testing equipment and parameters in our earlier studies, by factor 3 to 4 [184,364]. The comparably thick resin layer of 0.4 mm in conjunction to the absence of reinforcement fiber in our study may be assumed to cause the differences especially in the cohesive failure regime prima facie. Here, excessive fibrillation in the debonding process was observed which finally resulted in bulk fracture as well as the same amount of resin residue between probe and the substrate. Very high tack was yet measured for adhesive fracture (on the left-hand side of the bell-curve) which is dominated by resin-solid interaction near the interface. Moreover, increased toughening content and pre-cure quickly lowered the resin tack to values in the same magnitude as commercial systems of about 100 μJ mm^{-2} (see sections 7.4.3-7.4.5 for a detailed discussion).

Even though similar maximum tack was achieved by all A-stage formulations, the positioning of the maxima differed significantly within the investigated temperature spectrum. Following the scientifically acknowledged assumption that the shape and the location of tack bell curves in the temperature spectrum is caused by a sensitive balance between interfacial adhesion and cohesive strength [235], oscillatory rheological analysis was performed to reveal differences in the causative viscoelastic behavior. The results of the temperature sweeps are summarized in **Figure 7-5** displaying temperature-dependent complex viscosity η^* (a) and storage modulus G' (b).

The viscosity of all resins decreased by 4–5 orders of magnitude while the sequence of increasing flow resistance (DGEBA < TGAP < TGMDA+TGAP < TGMDA) was maintained throughout the entire investigated temperature range. The storage modulus, which is attributed major importance for tack behavior of pressure sensitive adhesives [368], was reduced accordingly at higher temperatures. A comparison between the occurrences of maximum tack for all A-stage resins to the corresponding viscoelastic data was drawn in **Table 7-3**.

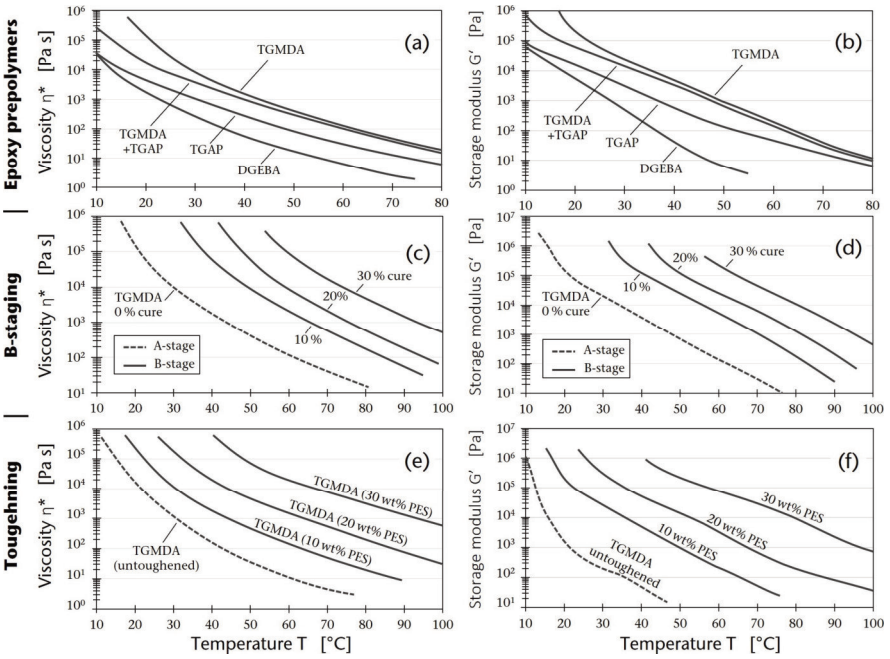

Figure 7-5. Temperature-dependent rheological data (complex viscosity η* and storage modulus G') acquired for different epoxy prepolymers (a, b), B-staging levels (c, d) and toughening contents (e, f) by oscillatory rheometry.

Table 7-3. Temperature at maximum tack T_{max}, maximum tack $W_{t,max}$ and corresponding rheological data.

Resin formulation	T_{max} [°C]	$W_{t,max}$ [μJ mm^{-2}]	η* (T_{max}) [Pa s]	G' (T_{max}) [Pa]
TGMDA[a)]	11.46	386.0	>10^6	>10^7
TGMDA (20 wt% PES)	22.25	232.9	>10^6	>10^7
TGMDA (30 wt% PES)	51.40	68.2	4*10^4	2*10^5
TGMDA/TGAP[a)]	12.08	444.3	3*10^5	7*10^5
TGAP[a)]	-0.38	305.1	5*10^5	3*10^5
DGEBA[a)]	5.04	452.9	7*10^5	2*10^5
TGMDA (10 % cure)[a)]	34.89	410.6	3*10^5	5*10^5
TGMDA (20 % cure)[a)]	45.99	94.9	2*10^5	5*10^5
TGMDA (30 % cure)[a)]	63.83	55.7	4*10^4	1*10^5

[a)] Including 10 wt% PES toughening

Remarkably, the tack curves of all formulations with the exception of modestly toughened TGMDA formed maxima at temperatures at which G′ is in the range of 10^5 Pa. Values of η^* at the same time leveled off between ~$5*10^4$ and ~$5*10^5$ Pa s – the range of optimal balance between adhesive wetting performance and cohesive deformation resistance. The observation is in general agreement with the findings of Szpoganicz et al. who obtained a constant range of viscosity and G' within the maximum tack plateau by balancing the resin DoC and testing temperature of phenolic prepregs and resins [298].

The order of increasing flow resistance mentioned above could not exactly be reproduced by the tack experiments in terms of Tmax (TGAP < DGEBA < TGMDA < TGMDA + TGAP). While most differences could be ascribed to the rheological data, the discrepancy between TGMDA and TGMDA + TGAP could not be explained in this way. Addition of 50 wt% TGAP (in relation to the epoxy prepolymer component) did not change T_{max} significantly (11.46 vs. 12.08 °C) notwithstanding the fact that both η^* and G' were considerably higher for pure TGMDA in this temperature region. For temperatures well above this region, both curves started to converge (**Figure 7-5**, a and b).

7.4.3 Influence of B-staging on tack

After B-staging the TGMDA-based formulation (10 wt% PES) by utilizing the isothermal B-staging treatment developed in section 7.4.1, DSC measurements yielded the experimental data presented in **Table 7-4**. In an effort to evaluate the success of the B-staging process, the actual achieved degrees of cure were compared to nominal values. The actual B-stage level was calculated according to **Eq. (7-1)** by dividing the residual cure enthalpy by the total reaction heat of TGMDA (0 % cure).

Table 7-4. Residual cure enthalpies, degrees of cure and glass transition temperatures of TGMDA (10 wt.-% PES) resin formulations measured by DSC after B-staging.

Resin formulation	(Residual) cure enthalpy [J g^{-1}]	Actual B-stage level [%]	Glass transition temperature [°C]
TGMDA (0 % cure)	550.8 ± 5.5	-	-6.02 ± 0.65
TGMDA (10 % cure)	501.8 ± 8.9	7.32	15.83 ± 0.49
TGMDA (20 % cure)	455.8 ± 13.1	17.25	25.45 ± 1.25
TGMDA (30 % cure)	407.0 ± 8.4	26.11	39.14 ± 0.81

A slight discrepancy was observed between both values as the actual DoC remain lower than desired for all B-stage levels. Reasons may be inaccuracies caused by the choice of conversion-dependent function (1st order). However, the resin samples featured the targeted cure increment of ~10 % cure and were therefore considered practical for further investigation of tack properties. The glass transition temperature was steadily increased in the course of the B-staging process from -6.02 (A-stage) to 39.14 °C (30 % cure). At the same time, the tack bell curves were shifted towards higher temperatures as shown in **Figure 7-6**.

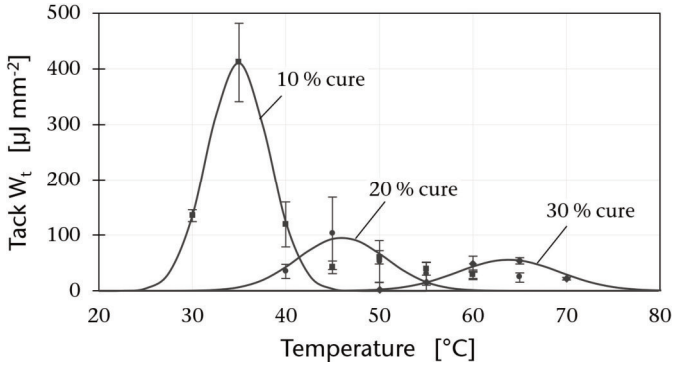

Figure 7-6. Temperature-dependent tack W_t of TGMDA resin samples (10 wt% PES) as a function of pre-cure.

Comparing the data of B-staged resins to A-stage TGMDA (**Figure 7-4**), an initial pre-cure of 10 % led to a shift in T_{max} of more than 20 K with the absolute tack being maintained. Additional pre-cure of 10 % shifted T_{max} further but was concomitant with a significant decrease in tack by more than 75 % which resulted from notable suppression of fibrillation. The goodness of fit of the Gaussian models was lowered to $R^2 = 0.6836$ for $\alpha = 20\,\%$ and $R^2 = 0.8789$ for $\alpha = 30\,\%$, respectively. The temperature shifts due to increased DoC and concomitant network formation were in very good agreement to the rheological discussion of the epoxy prepolymer influence of section 7.4.2 (see **Table 7-3** and **Figure 7-5**, c and d). Storage modulus settled in the magnitude of 10^5 Pa, which satisfies the Dahlquist criterion ($G' \leq 3*10^5$ Pa) of efficient contact formation to the substrate [245]. Remarkably, storage moduli at maximum tack remain in the same order of magnitude considering the B-staging process shifts the tack minimums by ~30 K. The

observation of decreased tackiness, however, was to some degree unanticipated considering our previous study using the same probe test setup [364]. Here, a slight increase or at least a close to constant level of tack as a function of room temperature out-time and the accompanied progress in cure for commercial epoxy prepreg was observed when processing the prepregs at higher temperatures. Similar results were recently reported by Hübner et al. [296] for DGEBA/ dicyandiamide, by Szpoganicz et al. [298] for commercial phenolic prepregs and by Smith et al. [286] who conducted additional gel permeation chromatography and found no significant effect of room temperature ageing on the molar mass distribution and hence, on the length of resin polymer chains. The B-staging at elevated temperatures as performed in this study was therefore considered to advance macromolecular network formation to an extent that considerably reduced maximum tackiness in contrast to room temperature ageing.

7.4.4 Influence of toughening on tack

Successive incorporation of high-molecular polyethersulfone (42 kg mol^{-1}) led to a rise in viscosity (**Figure 7-5**, e and f) as well as a linear increase in T_g from -6.02 °C (10 wt%) to 14.53 °C (30 wt%, **Table 7-2**). Complete solubility of the toughener in the prepared A-stage epoxy resins was assumed as only one glass transition region was present in the DSC graph. DSC analysis of our formulations in C-stage (after 3 h at 180 °C) revealed two separate glass transition temperatures indicating phase separation into epoxy rich regions and thermoplastic toughening particles. The first glass transition was found at ~175 °C with a slight tendency to higher temperatures with increasing PES content. The second T_g, which was assigned to the polyethersulfone, was detected at 225.5 °C and constant for all toughening levels. The dependence of probe tack W_t of A-stage resins on temperature and polyethersulfone toughener content is displayed in **Figure 7-7**.

Temperature shifts towards higher temperatures and a reduction in absolute tack similar to the observations made for B-staging (section 7.4.3) followed from an increase in PES toughening content. The Gaussian model fits got wider the more PES was incorporated in the epoxy resin indicating a less pronounced dependence on temperature. An increase in PES content by 10 wt% approximately involved a halving of maximum achievable tack while the overall reduction in tack and shift distance due to toughening is still observed to be slightly lower than by B-staging.

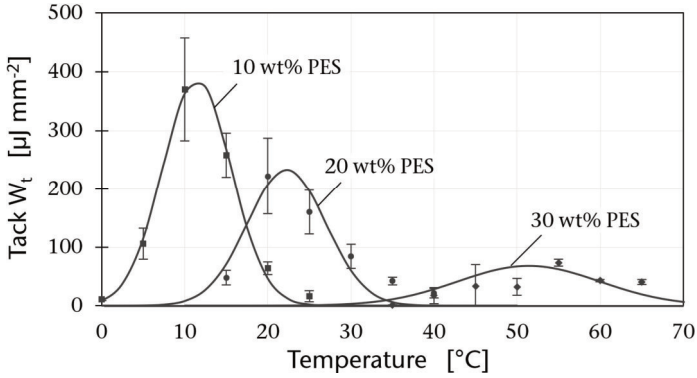

Figure 7-7. Tack W_t of A-stage TGMDA-based epoxy resin as a function of temperature for different PES toughener contents.

Failure of all resin samples took place at optimum conditions of adhesive and cohesive properties contributing to the debonding mechanism During the debonding process, cohesive failure however occurred at higher forces over a shorter deformation distance of <1 mm indicating increased shear resistance.

7.4.5 Manufacturing implication

The preceding results display the experimental basis to tailor the pre-cure properties of aerospace-grad prepreg resins based on epoxy in terms of tackiness. From an industrial manufacturing point of view, lay-up temperatures between room temperature and a maximum of 70 °C are common for commercial prepreg systems with unknown resin composition [38]. Higher temperatures will lead to the initiation of laminate cure and should therefore be avoided [71]. Comparing the AFP-related implication of temperature control to our experimental results it becomes apparent that processing all A-stage resins will be challenging due to their extraordinary high tack level below or near room temperature: Despite the incorporation of 10 wt% PES, all investigated A-stage formulations held a tack maximum below 13 °C (**Table 7-2**). In practice, this will most likely cause material jamming in the placement head and therefore require additional cooling in the material feed prior to lay-up. Our results indicate that both B-staging and toughening (or a combination of both) can push maximum tack above room temperature to avoid this challenge. A B-stage level of 20 % and a toughener

content of 10 wt% reduced tack to ~100 µJ mm^{-2} (**Figure 7-6**) - a value that we also measured for Hexcel's HexPly 8552 commercial epoxy aero-space prepreg at identical test parameters [364]. If a higher toughening content of 30 % is required in favor of the mechanical performance in C-stage, B-staging can be reduced or waived in order to yield similar tackiness (**Figure 7-6**). For both cases, lay-up with medium tack levels can be performed at medium temperatures of ~50 °C which equals 15–25 K above glass transition ($\Delta T = T_{max} - T_g$). The same general phenomenon of constant values for ΔT was also observed by other authors who investigated the out-time effects on tack, e.g. by Ahn et al. [224] for carbon fiber prepregs, by Szpoganicz et al. [298] for phenolic systems and in our previous work on epoxy-based systems [184]. A summary of characteristic temperatures for maximum tack and its connection to the glass transition temperature for all investigated epoxy resin formulations is given in **Figure 7-8**.

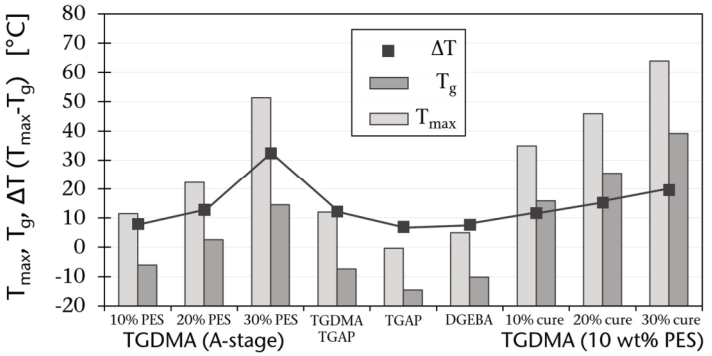

Figure 7-8. Characteristic temperatures at maximum tack (T_{max} based on Gaussian model fit) and glass transition (T_g) and their spread ΔT for all investigated prepreg resin formulations.

A slight tendency of increasing ΔT as a function of raised B-staging level and toughening content was observed. However, values remained in the narrow above-mentioned temperature window even if different epoxy prepolymers are used for resin formulation.

In general, restrictions have to be made on the preceding findings as the study is limited to exploring tack of resin films instead of prepregs. Differences in terms of measurable tack are expected as a consequence of both the diverse structure of prepregs (thinner resin layer, reinforcement fibers [295], etc.) as well as the

prepregging process. The latter was examined by Hayes et al. [222] revealing differences in tack as a function of prepregging process parameters, namely impregnation pressure and temperature.

7.5 Conclusion

High-performance model epoxy resins for aerospace-grade prepregs were formulated with varying the used multifunctional epoxy prepolymers, B-stage level and content of thermoplastic polyethersulfone toughening agent. The resin samples were characterized in terms of temperature-dependent tack behavior by probe tack testing. Tack levels of all A-stage resins were found to exceed commercial prepreg systems by the factor of 3–4 at low temperatures while both increased pre-curing (based on the Flynn-Wall-Ozawa kinetics model) and toughening caused a drastic loss of tackiness. Quantitatively, 30 % of pre-curing the model resins led to a decrease in tackiness from 386.0 to 55.7 µJ mm^{-2} while the incorporation of 30 wt% PES in A-stage resin lowered tack to 68.2 µJ mm^{-2}. At the same time, the tack curves were shifted towards higher temperatures up to a point of similar storage moduli G' (10^5-10^6 Pa). A B-stage level of 20 % and a polyethersulfone toughener content of 10 wt% yields medium tack in the range of commercially available prepreg systems which have been characterized in an analogous manner. The tack maxima of all formulations with the exception of highly toughened TGMDA were found to be of 15–25 K above T_g. The findings give insight in efficient ways of resin formulation to tailor pre-cure properties for processing epoxy-based prepregs via automated fiber placement.

CRediT authorship contribution statement

D. Budelmann: Conceptualization, Methodology, Validation, Formal analysis, Investigation, Writing - original draft, Writing – review & editing. **C. Schmidt**: Conceptualization, Resources, Writing – review & editing, Supervision, Funding acquisition. **D. Meiners**: Conceptualization, Resources, Writing – review & editing, Supervision, Project administration, Funding acquisition.

Declaration of competing interest

The authors declare that they have no competing financial interests or personal relationships associated with this publication.

Acknowledgements

The authors would like to acknowledge the financial support by Deutsche Forschungsgemeinschaft (DFG – German Research Foundation) granted for the research project 'TackTIC – Tack of Thermoset Impregnated Carbon Fibers' (project number 458900231).

Appendix

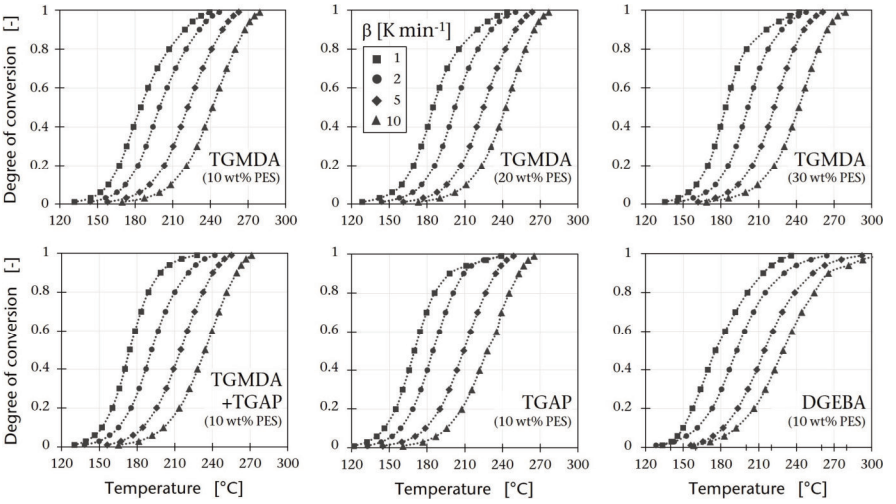

Figure 7-9. Fractional conversion α of the investigated epoxy systems for different heating rates β measured by DSC.

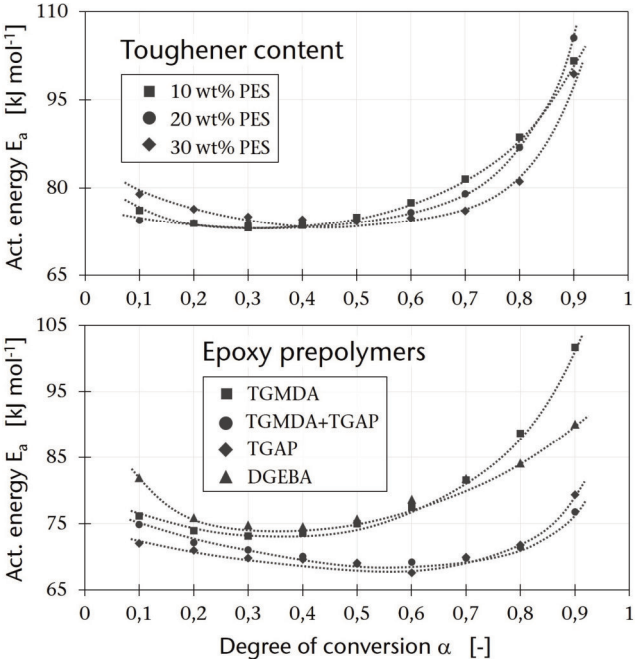

Figure 7-10. Apparent activation energies E_a as a function of cure progress.

Chapter 8

8. Contact formation and autohesion – Publication V

Adhesion-cohesion balance of prepreg tack in thermoset automated fiber placement. Part 2: Ply-ply cohesion through contact formation and autohesion

D. Budelmann[a], C. Schmidt[b], L. Steuernagel[c], D. Meiners[c]

[a]Institute of Polymer Materials and Plastics Engineering, Clausthal University of Technology, Ottenbecker Damm 12, Stade, Germany

[b]Institute of Production Engineering and Machine Tools, Leibniz Universität Hannover, Ottenbecker Damm 12, Stade, Germany

[c]Institute of Polymer Materials and Plastics Engineering, Clausthal University of Technology, Agricolastr. 6, Clausthal-Zellerfeld, Germany

Composites Part C: Open Access* 12 (2023) 100396.

*Journal metrics:

CiteScore: **8.6** (Scopus, 2023)
Rank 78/672; 88th Percentile (Engineering: Mechanical Engineering)

Impact factor: **5.3** (Clarivate, 2023)

Abstract

Contact formation and autohesion with respect to their role as the major mechanisms governing the tack between thermoset prepregs in automated fiber placement were explored. Therefore, a novel 90° peel test with strictly separated and individually controllable compaction and debonding phases was employed for experimental tack characterization in a rheometer. Variation of compaction pressure, dwell time and temperature enabled the experimental isolation of contact formation and autohesion influences. The experimentally determined tack, ply-ply contact area and resin viscoelastic characteristics were used to parametrize simplified semi-empirical bond strength sub-models that have originally been developed for thermoplastic composite manufacturing techniques. The model prediction was validated successfully within the experimentally reproducible parameter range. Eventually, manufacturing scenarios for thermoset automated fiber placement (AFP) respecting different lay-up velocities (up to 1 m s^{-1}), compaction pressures (up to 10 N mm^{-2}) and both lay-up and mold temperatures (20–60 °C) were assessed in terms of estimated prepreg tack. The implication of both mechanisms, contact formation and autohesion, in the evolution of prepreg tackiness was found to be able to replicate the bell-shaped tack curves proposed by the adhesion-cohesion balance.

* Corresponding author.
E-mail address: dennis.budelmann@tu-clausthal.de (D. Budelmann).

https://doi.org/10.1016/j.jcomc.2023.100396

Available online 6 September 2023

8.1 Introduction

Automated fiber placement (AFP) of unidirectional carbon fiber prepregs is recognized as the predominant production process for large aerospace primary structures while spearheading advanced composite manufacturing techniques in terms of both the level of automation and attainable mechanical part performance. The remarkable technological progress in this field since the 1980s is driven by an increased necessity for automation to meet the growing global demand for airplanes and the competitiveness to low-wage countries [369]. From a scientific perspective, the technological evolution of AFP was recapitulated by multiple research groups who authored review articles featuring the most crucial topics such as general process considerations [4,38–40,370], process modelling [371,372], materials [41–43], component properties [44,45], path planning [51] and laminate defects [47,48,50] including their detection techniques [46,49,373]. However, the continuous increase in AFP-related publication output in recent years implicates that the potential of automated lay-up technologies is yet to be fully exploited.

A central challenge of process control originates from the dynamic nature of AFP and its complex interaction between prepreg material, machinery and the built laminate, which are constantly kept in relative motion throughout the material deposition process. For thermoplastic AFP, the aim of process control is to reduce the laminate void content by promoting intimate interlaminar bonding and at the same time enabling high matrix crystallinity to achieve high thermo-mechanical properties by rapid out-of-autoclave manufacturing [374]. For the matured and industrially established thermoset AFP, however, the focus of process refinement is rather on establishing higher productivity (e.g. by higher lay-up speed, more simultaneously placed tows or exchangeable/modular heads) while avoiding macroscopic defects to occur in the laminate. AFP-induced defects have been studied in detail in terms of both their effect on mechanical properties of cured composite parts [6,375,376] and their cause of formation [150,160,292]. The latter was shown to be closely related to the prepreg's ability to adhere to mold surfaces and to itself upon the application of light pressure by the compaction roller – a property commonly related to as tack.

In order to control prepreg tack in thermoset AFP, material and mold temperatures are adjusted by different types of heat sources, e.g. traditional infrared heaters [230,377] or more energy-efficient LED arrays [233] and pulsed xenon light heaters

[378]. For optimum temperature control in terms of tack, a conflict of goals originates between sufficient contact formation between prepreg plies at higher temperatures/low resin viscosity and reasonable cohesive strength of the bulk resin at lower temperatures/higher viscosity, respectively. High temperature prepreg deposition will lead to excellent consolidation but the interface will thereupon be broken with ease. Maximum tack is found at a medium 'sweet spot' temperature at which an optimal tradeoff between these two mechanisms is on hand. This relationship was originally described in the context of pressure sensitive adhesives (PSA) as the adhesion-cohesion balance [236] but evidence in the form of bell-shaped tack curves [147,222,379] was found that thermoset prepregs show similar behavior (**Figure 8-1**).

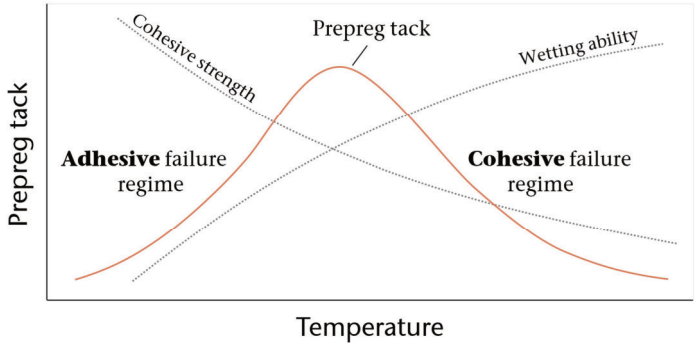

Figure 8-1. The temperature-dependent adhesion-cohesion balance of prepreg tack.

For maximum tack to be obtained, two prepreg plies have to be consolidated in a way that the interface disappears and reaches a state of the bulk material. This status is achieved as macromolecular chains are free to move across the interface in a process called autohesion. Autohesion, also known as self-bonding, (inter)diffusion or healing, describes the formation of bonds between two surfaces of an identical polymer at elevated temperatures, usually just above the glass transition temperature T_g and has been studied extensively for polymer welding as reviewed in [380]. This process, however, can only take place at locations, where the consolidated prepreg plies are in direct contact. The ratio between the area in contact and the total area of interest traditionally serves as a quantitative measure for consolidation quality and is defined as the degree of intimate contact (DoIC).

In the context of AFP, the involved mechanisms have almost exclusively been examined for thermoplastic AFP for obvious reasons: The formation of intimate contact and subsequent polymer chain interdiffusion between thermoplastic prepreg tapes is vital for consolidation quality and the ensuing mechanical performance of the composite part [45]. Modelling the sequential stages and especially their coupling is a multi-physics problem of mechanical, thermal and physical processes [371]. Both sequences, namely establishing a high DoIC between prepreg plies [381–383] and autohesion [384,385] have been studied in-depth for thermoplastic AFP. For thermoset AFP however, the mechanisms are only relevant in the built-up phase of the pre-cured laminate as the final mechanical part properties are not obtained until autoclave cure. Studies on the tack-related issues of DoIC and autohesion for thermoset prepregs were rarely carried out accordingly. Choong et al. [302] experimentally studied the relationship between DoIC and tack, both measured as a function of temperature and lay-up speed/compaction. Despite achieving high DoIC, tack was reported to decrease with decreasing feed rate as soon as the cohesive failure regime was entered. Based on this observation, it was reasoned that maximizing DoIC may be an insufficient criterion for optimizing AFP processes as prepreg tack is affected by both the DoIC-influencing compaction phase and the subsequent measuring/debonding phase. Isolating the influences of compaction time and debonding rate as well as the temperatures of both stages, however, was not possible due to the continuous nature of the utilized tack measurement device (ASTM D8336-21 [283]). Wang et al. [293] recently modelled the evolution of DoIC (based on the work of [386]) to estimate tack of epoxy-based prepregs within a comprehensive AFP modelling framework. The only research paper known to the authors on thermoset autohesion of prepregs was presented by Xiao et al. [305] who proposed a two-stage model comprising diffusion and viscous stages. The diffusion stage was modelled using the highly recognized theory of polymer crack healing by Wool and O'Connor [387] which is based on the reptation model of macromolecular chains in a tube. For the viscous stage, contact formation was estimated consulting creep curves of stacked prepreg plies. The effect of the highly influential temperature deviation on contact formation, however, was not directly measured but rather estimated based on the principle of time temperature superposition.

Here, the second research paper of a two-part series attributed to the adhesion-cohesion balance of prepreg tack and its relevance for automated fiber placement

processes is presented. It is a follow-up to our first study [364] which covered the adhesive portion of the balance by examination of contact formation and wetting behavior between epoxy prepregs and multiple AFP-related solid contact materials. One of the major observations shown therein was that – in contrast to solid contact materials like, e.g., the compaction roller or mold – the interface of two prepreg plies cannot be treated as a model system of three ideally separated phases (solid, liquid, gaseous) and was therefore not approachable through surface wetting analysis by contact angle measurement. On this account, the role of contact formation and autohesion in developing cohesive strength at the ply-ply interface was explored in this study. Prepreg tack was measured using in-house designed test fixtures to carry out a highly flexible 90° peel testing procedure with the help of a rheometer. The experimental latitude of the test design was used to study the peel fracture energy of partly and fully contacted interfaces as a function of compaction pressure, dwell time and temperature while monitoring the progression of DoIC. The time- and temperature-dependent mechanism of autohesion was analyzed based on rheological data to estimate the resin relaxation time with the help of the Carreau-Yasuda approach. Both mechanisms were eventually merged in a semi-empirical bond strength model which was derived from thermoplastic composite manufacturing literature and adjusted to thermoset AFP. Coupling the contact formation and adhesion models allows for assessing the tack between two thermoset prepreg plies which have been consolidated in an arbitrary manner with regard to lay-up speed, compaction pressure and temperatures during both the roller consolidation phase as well as the unpressurized phase after deposition.

8.2 Materials

A commercial Hexcel carbon fiber epoxy prepreg for primary and secondary aircraft structures (HexPly 8552) was characterized in terms of tack and related properties. The same prepreg was used for the first study [364] of the two-part series. The unidirectional prepreg system is made from AS4 carbon fiber (1.79 g cm^{-3}) embedded in a PES-toughened amine-cured epoxy resin (1.30 g cm^{-3}) which results in a nominal laminate density (cured) of 1.58 g cm^{-3} at a fiber volume fraction of 57.42 vol%. A two-step autoclave cure cycle (120/180 °C) is recommended according to data sheet. The prepreg material was defrosted in vacuum-sealed bags

prior to testing and processed within 8 hours of out-time exposure. For tack testing, the outer faces of the prepreg (opposite side of the protective backing paper) were brought into contact as this is normally the face to be applied in AFP. Neat epoxy resin for viscosity measurement was extracted from the prepregs by using the same solvent-based (tetrahydrofuran, THF) procedure as presented in [364].

8.3 Experimental methods and data analysis

8.3.1 Tack measurement cycles

Tack between two unidirectional prepreg plies was characterized by peel testing based on an in-house designed and manufactured fixture to be used in conjunction with a TA Instruments ARES G2 oscillatory rheometer. The rheometer was equipped with a forced convection oven (~50·50·70 mm³) enabling temperature control in the tack-relevant temperature range between 20 and 60 °C. It is capable of normal force and torque measurement while performing step-wise programmable rotational and axial motions which were converted into the desired prepreg manipulation. Other than the new standard for peel testing ASTM D8336 [43] which features a continuous application-and-peel procedure, the presented method separated the compaction from the separation phase. In this way, the dwell time could be adjusted while independently choosing the peel rate. In an effort to isolate and explore the influences of contact formation and autohesion on prepreg tack, three test cycles were designed as summarized in **Table 8-1**. Differences between the cycles applied to the initial compaction stage. The concluding peel stage was remained unchanged at a vertical peel velocity of 1 mm s^{-1} and the desired measurement temperature between 20 and 60 °C, respectively. Details on the test cycles are provided in the beginning of the corresponding result sections.

Table 8-1. Employed peel tack measurement cycles.

Test cycle	Target tack value	Special feature
Standard	Tack G_{std} [J m^{-2}]	Isothermal application and debonding (20-60 °C)
Full contact	Tack G_{fc} [J m^{-2}]	High pressure, dwell time and temperature application
Autohesion	Tack G_{auto} [J m^{-2}]	Unpressurized autohesion stage between application and debonding

The measurement cycles and their representation in the mechanisms of bond strength development between two plies in AFP can be assessed in **Figure 8-2**:

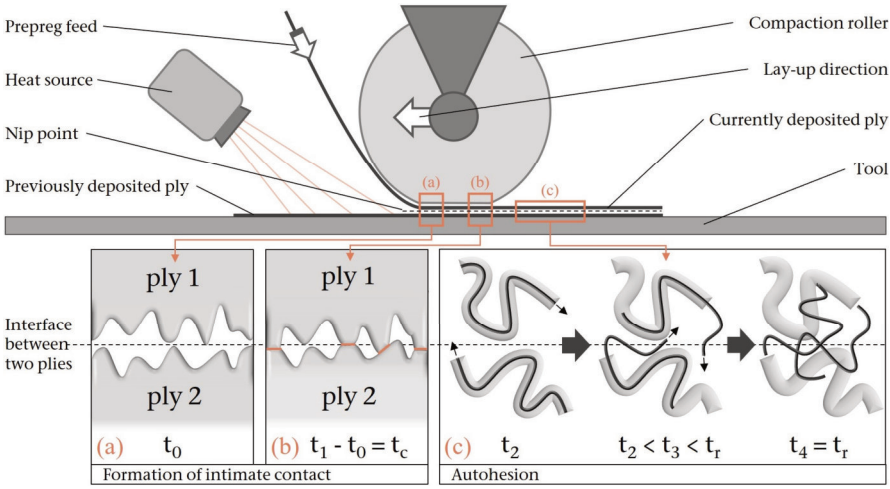

Figure 8-2. Schematic representation of the automated fiber placement process. The tack-relevant mechanisms, namely formation of intimate contact (a-b) and autohesion (c) between two prepreg plies are highlighted in orange and schematically specified in the subjacent detail boxes.

The fed prepreg tow approaches the already deposited laminate with no initial contact at t_0 (a) in front of the compaction roller. During compaction at t_c, (b) the roller applies pressure to the stack and establishes a contact area between the plies (red) which can be quantified by the degree of intimate contact. After surpassing the compaction roller (c), the absence of pressure will cause the DoIC to remain mostly unaltered but the macromolecules will start to diffuse across the interface at t_2. Each molecule will either partly (t_3) or fully (t_4) diffuse across the interface depending on time and temperature the stack has remained behind the compaction roller. According to the reptation theory of de Gennes, the polymer chain will eventually have fully escaped its tube at the temperature-dependent reptation time t_r and relaxation time λ, respectively. At this point, the interface is fully healed so that bulk material and interface cannot be distinguished between in matters of material properties.

8.3.2 Peel testing procedure

Peeling under a fixed angle of 90° is a dynamic process and requires compensatory relative motion of the specimen or the substrate to maintain a constant peel angle and/or static peel point as the peel front translates orthogonal to vertical. The testing device shown in **Figure 8-3** was designed to enable the prepreg manipulation necessary in order to perform a 90° peel test in the limited available space of the rheometer convection oven. The device consisted of two fixtures attached to the rheometer. The upper one executed a downwards (compaction) and upwards (debonding) motion while the lower fixture remained static. The relative

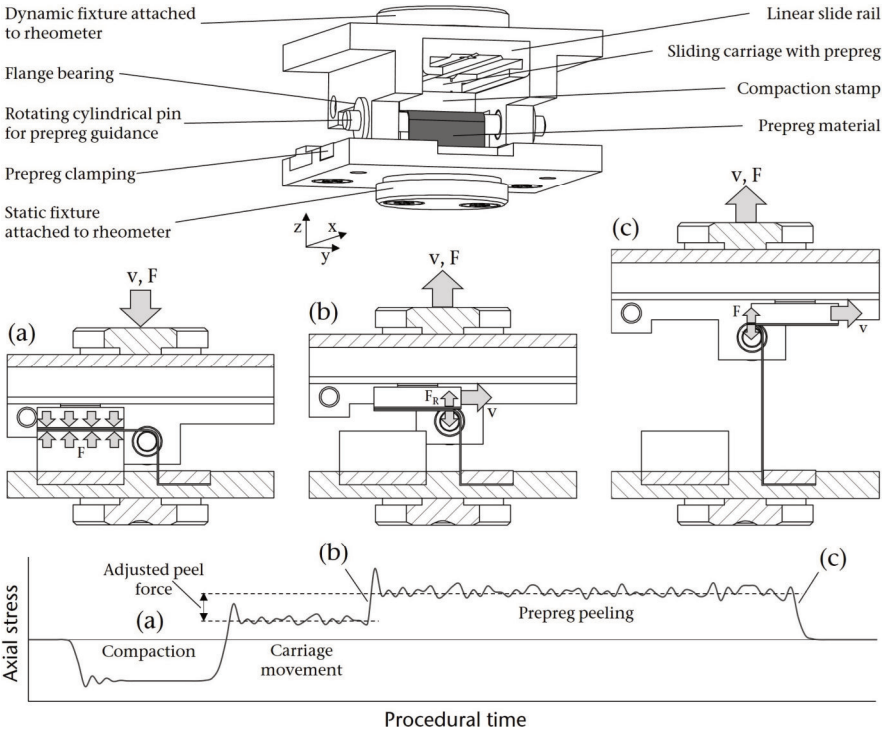

Figure 8-3. Schematic representation of the 90° peel test setup (upper figure) to be mounted to the rheometer. The lower sequence of figures displays the test procedure with its characteristic steps of compaction (a), the beginning (b) and ending (c) of the debonding/test phase. The axial stress/procedural time graph is for illustration purposes and not true to scale.

motion was facilitated by a sliding carriage which held the substrate and moved horizontally in an overhead linear sliding rail. The test procedure can be retraced consulting the lower schematic drawings of **Figure 8-3** which show cross sections (x-z-plane). First, a prepreg strip of nominal 12.2 mm width and 60 mm length was clamped on the lower fixture, guided around a rotatable cylindrical pin (∅ 3 mm) and eventually placed between a compaction stamp and the sliding carriage. The stamp was equipped with a release tape to avoid adherence. Prepreg material was pasted on the carriage using double-sided adhesive tape. Adherence between the tape and prepreg material was found to prevail throughout all experiments, so that the tack between two prepreg plies could be measured. The test procedure was initiated with the upper fixture applying a set pressure to the prepreg plies on the carriage and stamp to form a contact area of 150 mm² at aligned fiber directions (**Figure 8-3**, **a**). By integrating the compaction phases into the rheometer test cycles, undesired sample affection was avoided which likely occurs when transferring samples after prepreg application in a secondary process. As the upper dynamic fixture was then moved upwards after compaction (z-orientation), a tensile force initiated the carriage to slide to the right (x-orientation) due to the guidance provided by the cylindrical pin being placed directly under the material clamping of the lower fixture. As soon as the carriage reached the cylindrical pin (**Figure 8-3, b**), peeling set in which marks the beginning of the debonding phase. The prepreg strip was gradually peeled from the sliding carriage at a velocity of 1 mm s^{-1} and a constant peel angle of 90° until the carriage fully passed the pin (**Figure 8-3, c**). The peel adhesion was measured between phases (b) and (c) by recording the separation force as a function of displacement. It was determined in the steady-state peeling region between 3 and 9 mm of displacement (total peel length: 12.2 mm) in order to avoid perturbation at the beginning and ending of the peel process. Peel testing is usually accompanied by friction between substrate and guidance elements. Therefore, the average force signal recorded between phases (a) and (b) was determined for all testing temperatures and subtracted from the results of the subsequent measurement phase yielding the adjusted (steady-state) peel force F. This way, non-tack related influences like friction of the sliding carriage and in the flange bearing, the interaction between prepreg and the pin as well as the prepreg bending stiffness were accounted for.

In terms of the tack indicator obtained from this measurement technique, the well-established equation to determine the fracture energy for PSA on flexible substrates (**Eq. (8-1)** [169]) could be utilized. Here, fracture energy G_a is defined by:

$$G_a = \frac{F}{w}(1 + \varepsilon_a - \cos\theta) - h\int_0^{\varepsilon_a} \sigma d\varepsilon - G_p \qquad \textbf{Eq. (8-1)}$$

where F is the adjusted peel force, w is the prepreg width and θ is the peeling angle. The backmost terms are the energy G_p involved to plastically deform the bending arm and a term for the arm's elastic energy given as a function of the peel arm thickness h, actual stress σ and strain ε_a. In opposition to PSA peeling on flexible substrates, it was assumed for the characterization of prepreg tack that the peeling arm is not deformed elastically as a result of tensile forces due to the high stiffness of the incorporated carbon fiber. Also the plastic work done in bending of the peel arm G_p was already respected as the adjusted peel force was used for calculation. With the assumptions to prepreg materials made, **Eq. (8-1)** is reduced to:

$$G_a = G = \frac{F}{w} \qquad \textbf{Eq. (8-2)}$$

which gives the fracture energy in the form of work per unit area J m^{-2} (equaling N m^{-1}) for a constant peeling angle of 90° and is equivalent to the total energy G which could directly be measured with our peel test setup. The simple equation matches the results from the work of Kendall [388] who demonstrated that the elastic terms are essentially negligible for high peeling angles of lower than ~0.1 rad anyway – the point at which the peel test rather resembles a lap shear test.

8.3.3 Rheology

Frequency sweeps were performed in a shear rate range between 10^{-2} and 10^{2} s^{-1} to measure the complex viscosity of neat prepreg resin at constant temperatures (10 K increments) between 20 and 100 °C. The rheometric experiments were carried out in the above-mentioned TA Instruments ARES G2 oscillatory rheometer at a 0.5 mm gap and 1 % strain between two parallel plates of 40 mm diameter. The Carreau-Yasuda viscosity model (**Eq. (8-3)**) was applied to determine the temperature-dependent relaxation times λ as input parameters for the autohesion model (sections 8.4.4 and 8.4.5).

$$\eta(\dot{\gamma}) = \eta_\infty + \frac{(\eta_0 - \eta_\infty)}{[1 + (\lambda * \dot{\gamma})^a]^{\frac{(1-n)}{a}}} \quad \textbf{Eq. (8-3)}$$

Here, the rate-dependent viscosity $\eta(\dot{\gamma})$ is a function of the fit parameters zero shear viscosity η_0 and infinite shear viscosity η_∞, respectively, which marks the horizontal rate-independent asymptotes of the viscosity spectrum. The remaining fit parameters, namely transition parameter a and power law exponent n dictate the course of the shear-thinning region at medium shear rates. Carreau-Yassuda curve fitting was performed with the help of Origin Lab's OriginPro.

Furthermore, rheological shift factors a_T as demonstrated for prepreg tack by Crossley et al. [207] were determined by utilizing the rheological data of neat prepreg resin and applying time temperature superposition (TTS) according to **Eq. (8-4)** (William-Landel-Ferry, WLF):

$$\log(a_T) = \frac{-C_1(T - T_{ref})}{C_2 + (T - T_{ref})} \quad \textbf{Eq. (8-4)}$$

8.3.4 Degree of intimate contact (DoIC)

The DoIC represents the true contact area between prepreg plies which is established by pressurization of the interface in relation to the initial nominal area of interest. Here, the DoIC was determined experimentally by employing the two-sheet type Fujifilm Prescale pressure measurement film. The lowest available film system (ultra extreme low pressure: 0.006–0.05 N mm^{-2}, type 5LW) was chosen in order to guarantee the visualization of the entire area where contact was established. These regions on the film will turn red when being pressurized above the pressure threshold. For testing, the film was positioned between two prepreg plies which are ultimately pressurized by a cylindrical probe (12 mm diameter) attached to the rheometer. The rheometer axial force of compression was adjusted in a way that compaction pressures of 0.02, 0.1 and 0.2 N mm^{-2} were applied while additionally varying compaction time (0.2, 0.5 and 2 s) and temperature (20–60 °C). Three specimens were produced for each varied parameter set.

Hereby obtained film specimens were immediately scanned at a resolution of 600 dpi to create TIF images, which were subjected to image processing before analysis. The image processing routine included cropping to circular shape,

despeckling and smoothing, adjusting brightness and contrast, converting to 8 bit greyscale and thresholding. At this stage, the DoIC could be extracted from the binarized images by referring the black area to the total region of interest (ROI, black + white areas).

8.4 Results and discussion

8.4.1 Contact formation – experiment

Within the context of composite manufacturing, the importance of true contact area between deposited prepreg plies was initially introduced by Lee and Springer [389] who gave distinction to the DoIC concept in the late 1980s. Here, its knowledge is also mandatory to study the role of autohesion on thermoset prepreg tack as the DoIC represents the interfacial area where autohesion can take place and bond strength can develop. This area is represented by the dark specimen regions in **Figure 8-4** showing characteristic images of scanned pressures sensitive films obtained from the compaction and processing procedure presented in section 3.4. Apparently, large parts of the DoIC spectrum between no (zero) and full interfacial contact (unity) between prepreg plies are covered by the compaction experiments. For all specimens, a distinctive influence of the ply orientation is visible. The prepreg plies have been aligned parallel prior to testing.

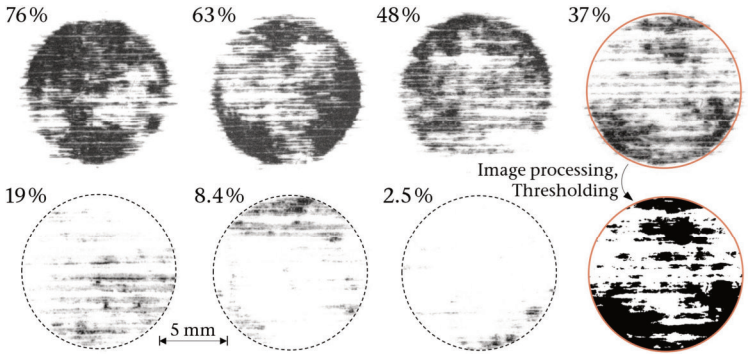

Figure 8-4. Characteristic contact area images with corresponding DoIC. An exemplarily processed and binarized image is circled in orange.

The corresponding quantitative data showcasing the dependence of the DoIC on dwell time and pressure is displayed in **Figure 8-5**.

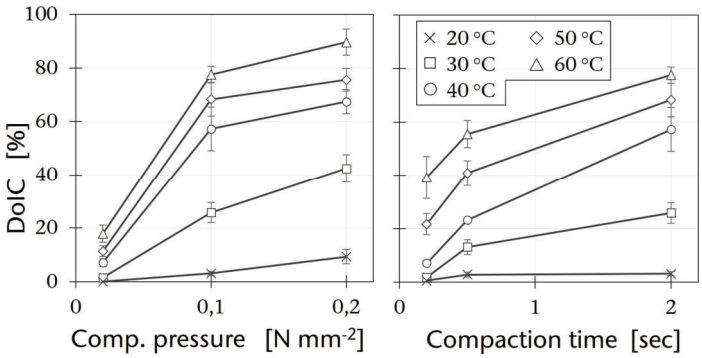

Figure 8-5. DoIC as a function of compaction pressure (left graph for 2 s), compaction time (right graph for 0.1 N mm^{-2}) and test temperature.

As expected, the general relationship was found to be straight-forward with the DoIC monotonically increasing as a function of both variables. Meanwhile, higher temperatures lead to higher achievable DoIC within our investigated ranges due to enhanced resin flowability. Full surface wetting (100 % DoIC) was not achieved for our test parameters as a maximum DoIC of 86 % was recorded for 0.2 N mm^{-2}, 2 s and 60 °C. However, complete contact seems attainable when further increasing the investigated test parameters in order to flatten the remaining asperities. The results are generally consistent with the findings of Choong et al. [302], who found the DoIC to vary between 0 and 100 % and demonstrated the applicability of time temperature superposition to estimate the DoIC at arbitrary reference temperatures for their test setup. Here, the contact evolution between prepreg and a glass surface was explored by quantifying the true contact area from optical micrographs using image analysis. Divergence in absolute DoIC values between both studies may be caused by differences in the compaction setup (stiff roller vs. probe), the investigated interface (smooth rigid glass-ply vs. ply-ply) and test parameters. Another study to compare our findings to was recently presented by Wang et al. [293], who estimated the DoIC between prepreg plies based on an adapted squeeze flow model as part of a comprehensive AFP modelling framework. Within the investigated parameter set, an average DoIC of 5 % was reported and used for

further calculation which appears to be underestimated considering the results by Choong et al. [302] and our experimental findings.
It has to be noted that our test parameters do not reflect AFP process parameters to the full extent: Assuming a state of the art lay-up speed of up to 60 m min^{-1} [390] and a typical compaction length by the roller of 50 mm [72], compaction times will be ~50 ms and, therefore, about 5 times shorter than the shortest compaction time which could be realized by peel testing. At the same time, a maximum compaction pressure of 0.2 N mm^{-2} could not be exceeded due to limitations of the test setup, resulting in a lower pressure than usually applied in thermoset AFP. Still, a wide set of parameters was investigated in terms of contact formation which can be used to parametrize the bonding model in the following.

8.4.2 Contact formation – model

Several models have been proposed in literature to determine the evolution of the DoIC between two prepreg plies for thermoplastic prepreg processing by hot pressing, filament winding, AFP and others. A highly recognized model originally developed by Lee and Springer [389] and successively elaborated (i.a. by Mantell and Springer [391]) is based on the squeeze flow deformation of rectangular elements representing surface resin asperities. These asperities are proposed to flatten as a result of bringing the two surfaces together under pressure. Instead of determining the involved geometric surface parameters by surface topography analysis, a roughness parameter a can alternatively be determined empirically according to **Eq. (8-5)** [392] if the degree of intimate contact D_{ic} is known for a set of compaction scenarios.

$$D_{ic} = a\left[\int_0^{t_c} \frac{P_{app}}{\eta(T)}\,dt\right]^{\frac{1}{5}} \qquad \textbf{Eq. (8-5)}$$

Here, t_c is the overall time of compaction, P_{app} is the applied pressure and $\eta(T)$ is the temperature-dependent resin viscosity. Plotting the experimental data from **Figure 8-5** as a function of the right term of **Eq. (8-5)** gives the linear relationship shown in **Figure 8-6** where the slope of the graph is equal to the roughness parameter a. With the linear fit featuring a negative y-intercept, the model predicts a threshold value (function of P_{app}, η and dwell time) that has to be overcome in

order to provide initial contact between the thermoset prepreg plies. This observation is contrary to, e.g. the findings of Butler et al. [392] who gained a positive y-intercept which indicates a certain amount of initial contact (D_{ic0}) even before pressure is applied to the interface. The discrepancy may be attributed to the threshold pressure of the used pressure sensitive film. The negative y-intercept may lead to negative DoIC which obviously contradicts its definition. This however, will only occur at very low temperatures (high resin viscosity) and compaction pressures that are not representative of the AFP process.

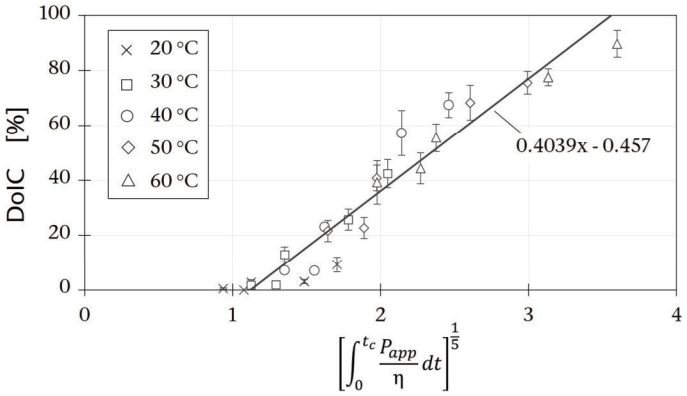

Figure 8-6. Fitted experimental DoIC data to determine the empirical roughness parameter a.

8.4.3 Tack measured by standard isothermal peel test

In an effort to correlate the established DoIC to experimental tack data, the standard test procedure shown in **Figure 8-7** was employed to study tack between two prepreg plies by the newly developed peel test method. The measurement cycle comprises a short compaction phase at a specific temperature (20–60 °C, 5 K increments) followed by the debonding phase at the same temperature. This isothermal approach is considered standard as it is the most common way to experimentally determine prepreg tack whenever universal testing machines or rheometers in combination with environmental chambers were used in literature. Plotting the hereby determined experimental results as a function of compaction/peel temperature generates the tack data points shown

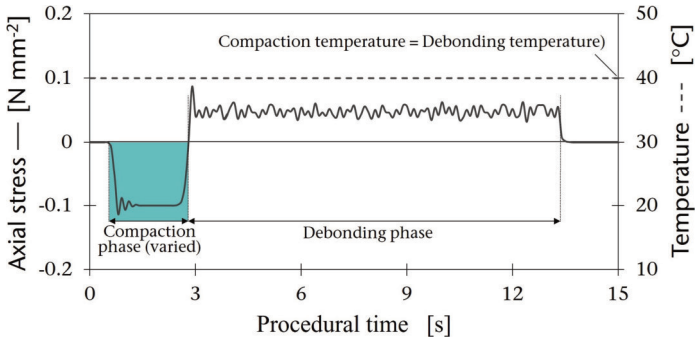

Figure 8-7. Axial stress evolution (idealized) during the isothermal standard test procedure. The dwell time and pressure during the compaction phase as well as temperatures are exemplary and were varied.

in **Figure 8-8** which were subsequently fitted using Gaussian curves (dark line, see [364] for details of the fitting procedure). Model fitted data will be used for any further calculation from this point on in the paper.

The reproducibility of the new peel test procedure is 12.8 % which is slightly higher than the reported 11 % for ASTM D8336-21 [283]. Reasons are most probably the higher influence of sample preparation to the significantly smaller specimen size and the pronounced force fluctuation as a result of the prepreg's higher bending stiffness. This would also explain the observation that the standard deviation of data points for low temperatures (high bending stiffness) are significantly greater than for high temperatures. The large error bars are indicative of pronounced stick-

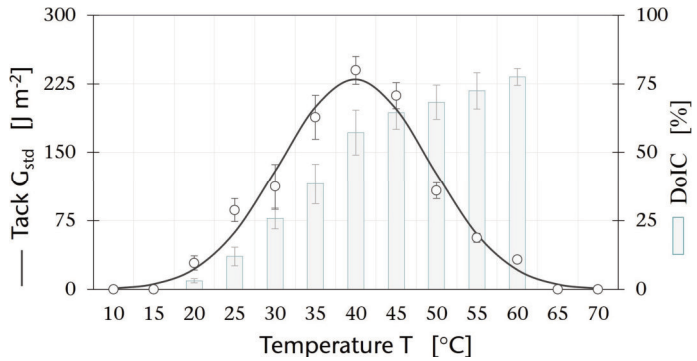

Figure 8-8. Peel tack obtained from the standard test procedure and corresponding measured DoIC as a function of temperature.

-slip behavior at low temperatures. As the same parameters for the compaction phase were used for tack measurement and the determination of DoIC (0.1 N mm^{-2}, 2 s), it is possible to directly link the DoIC of section 8.4.1. to the tack results. The DoIC is additionally plotted on the secondary axis of **Figure 8-8**. Both, tack and DoIC show very similar trends up to medium temperatures ~40 °C where maximum tack is recorded. From this point on, tack drops drastically while the DoIC proceeds to increase monotonically approaching its boundary value by definition of 100 %. The experimentally determined progressive increase of DoIC as a function of temperature is in accordance with the model prediction by **Eq. (8-5**) as the resin viscosity decreases for higher temperatures. The drop of tackiness at higher temperatures in defiance of a rising DoIC leads to the assumption that the loss of bulk fracture toughness overweighs the improved contact formation at temperatures >40 °C. Cohesive failure is indicative at this point as well. In an effort to characterize this interrelation in detail and to describe the involve mechanisms qualitatively, preliminary exploration of the tack of fully contacted interfaces is mandatory.

8.4.4 Tack of fully contacted ply interfaces

The standard isothermal tack test shown in Fig. 7 was modified with the objective of reaching 100 % DoIC prior to recording the tack of the interface at different temperatures of interest. During compaction, the plies are brought into contact at very high temperature of 70 °C for 60 s (**Figure 8-9**: highlight in blue color).

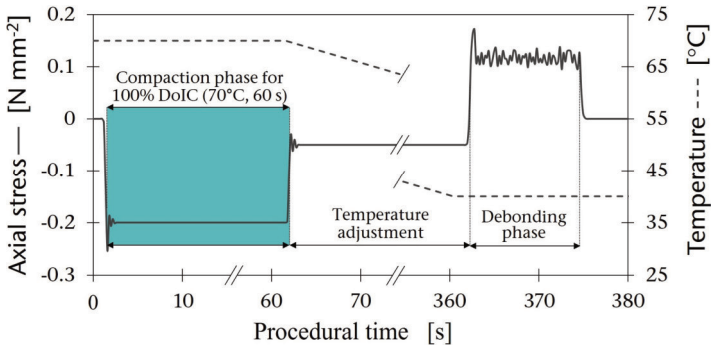

Figure 8-9. Test procedure (idealized) to study the influence of debonding temperature on the tackiness of fully contacted prepreg interfaces (100 % DoIC).

Assuming 100 % appears reasonable based on the fact that 2 s of compaction at 0.2 N mm^{-2} and 60 °C yet lead to 89.6 % DoIC. In fact, secondary analysis of the hereby created interface (not shown here) revealed a DoIC of 97.3 %. The compaction phase is followed by a cooling phase in which the temperature is adjusted to match the desired debonding temperature. A residual interface pressure of 0.5 N mm^{-2} is kept up during cooling to maintain the built bonding area up to the point of peeling onset. A potential influence by the temperature adjustment phase, which varies in length depending on the target peel temperature, is assumed negligible. Applying the test procedure of **Figure 8-9** to the investigated prepreg system, gives the tack curve plotted in **Figure 8-10** (black data points). For comparison reasons, the results from the standard test cycle are included as well. Tack after full contact G_{fc} is found to decrease monotonically in a way that the

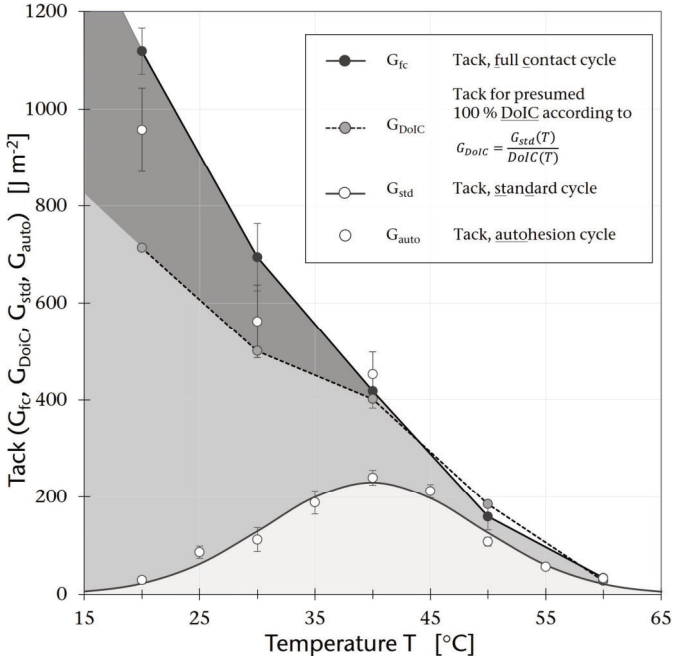

Figure 8-10. Comparison of tack between fully contacted prepreg ply interfaces (G_{fc}, dark grey), estimated tack for 100 % DoIC (G_{DoiC}, medium grey), tack obtained from the standard (isothermal compaction and debonding) peel test cycle (G_{std}, light grey) and tack after an additional autohesion phase and projected to 100 % DoIC (G_{auto}, white data points, discussed in section 8.4.6).

curve converges the experimental data of G_{std}. The pictured results show that the fracture energy of a fully contacted ply-ply interface at room temperature is ~10 times higher than for commercial office tape (129 J m^{-2}) and ~4 times higher than for duct tape (306 J m^{-2}) bonded to a glass substrate [393] at virtually identical test parameters. The gap in tack for temperatures >50 °C shown in **Figure 8-10** becomes negligible indicating that for high temperatures, contact formation is no longer the limiting factor to achieve high tack. Multiplying G_{std} with the reciprocal value of the measured DoIC at the same temperature gives G_{DoIC} – a theoretical tack value representing a peel force to be overcome to separate an interface with a projected DoIC of 100 %. It becomes evident that G_{DoIC} shows the same curve progression as G_{fc} (monotonic decrease) as opposed to G_{std} (bell curve) but remains lower in extent for temperatures <40 °C (adhesive failure regime). It can be concluded that simple projection does not allow for estimating G_{fc} and, therefore, does not accommodate for all mechanisms involved in prepreg tack. In fact, the difference between G_{fc} and G_{DoIC} becomes larger with decreasing peel temperatures. The growing gap between both values may be a result of the temperature-driven mechanism of autohesion, which will be investigated based on the rheological behavior of neat prepreg resin in the following.

8.4.5 Autohesion: Determination of relaxation time

The relaxation time λ is a well-accepted viscoelastic measure that determines the rate of autohesion as a function of temperature as pointed out in section 8.3.1, **Figure 8-2**. It was determined as the inverse critical shear rate $\dot{\gamma}_c$ which marks the onset of shear thinning in the frequency-dependent viscosity spectrum. This part of the spectrum is shown in **Figure 8-11**, comprising both experimental data of the resin's complex viscosity and its model fit by Carreau-Yasuda regression. Good agreement between the conducted rheological experiments and the Carreau-Yasuda model was found in the zero shear viscosity/transition regimes being the relevant range for calculating λ. Here, the horizontal asymptote of the zero shear viscosity graphically intersects the shear thinning slope at the critical shear rate $\dot{\gamma}_c$ (**Figure 8-11**: exemplary orange dotted lines for 60 °C). The x-coordinate where

$$\dot{\gamma} = \dot{\gamma}_c = \lambda^{-1} \qquad \textbf{Eq. (8-6)}$$

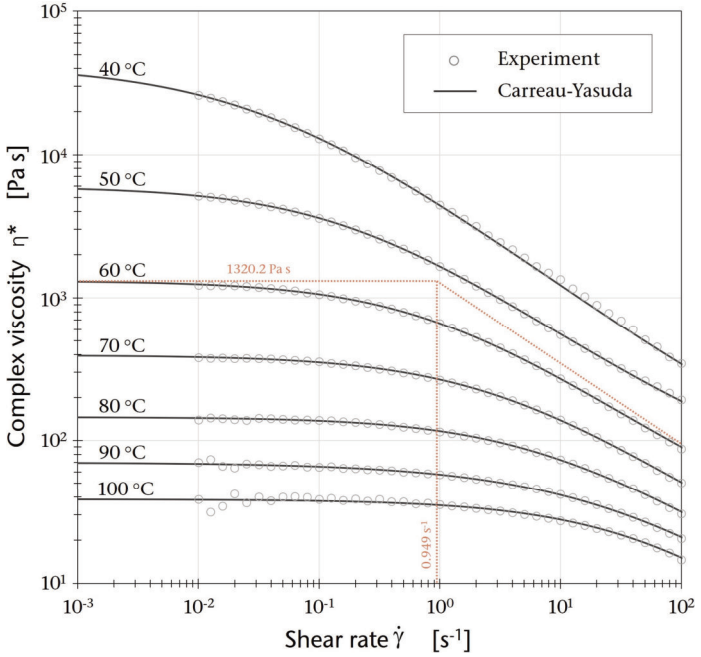

Figure 8-11. Complex viscosity of neat prepreg resin as a function of shear rate and temperature determined by rheometry (dots) and Carreau-Yasuda model fits (continuous lines).

is valid, is also accessible analytically through the Carreau-Yasuda equation (Eq. 3). The thus calculated relaxation times between 40 °C and 100 °C as well as the corresponding fit parameters are summarized in the appendix (**Table 8-2**, Appendix of chapter 8). Plotting the relaxation times as a function of resin temperature yields the logarithmic graph shown in **Figure 8-12**.

In an effort not to overrate high relaxation time values for the exponential curve fitting, a percentage least square regression was carried out. This way, data for λ can be extrapolated beyond the experimentally founded range, especially towards lower temperatures near room temperature which was identified as a potential tack-determining region for autohesion before. An exponential relationship between relaxation time and temperature is found for the pre-cured, epoxy-based prepreg resin system as shown in **Figure 8-12**. The finding is generally consistent with a multitude of other studies in which cured epoxy resins were modeled based on Arrhenius plots, e.g. in [394,395]. Relaxation times in the tack-relevant spectrum

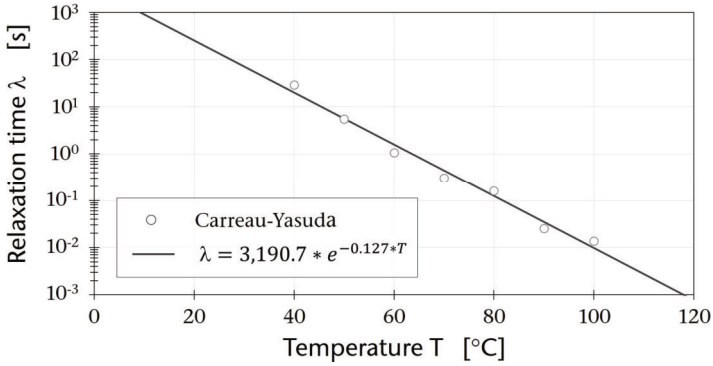

Figure 8-12. Relaxation times determined by application of the Carreau-Yasuda rheology model (dots) and exponential regression (line) for data interpolation and extrapolation within the tack-relevant temperature range.

range between 250 s (20 °C) and 1 s (60 °C). For relaxation times which have been determined for thermoplastic AFP modelling, narrower ranges have been reported, e.g. by Khan et al. [396] who measured ~$5 \cdot 10^{-2}$–10^{-1} s for polyether ether ketone (PEEK). Based on the fact that the two and a half orders of magnitude lie in between the prepreg resin relaxation times at room temperature and at 60 °C, a substantial influence of autohesion on tack is estimated.

8.4.6 Autohesion – model

The degree of autohesion D_a can be defined as the ratio between the fracture energy G of a partly healed polymer interface and the necessary fracture energy G_∞ needed to separate a fully healed interface. According to Wool and O'Connor [387], the dimensionless value follows the square root of the time t available for self-diffusion in relation to the relaxation time λ at a temperature T:

$$D_a = \frac{G}{G_\infty} = \left(\frac{t}{\lambda(T)}\right)^{\frac{1}{2}} \qquad \textbf{Eq. (8-7)}$$

Using the temperature-dependent relaxation times λ(T) determined by Carreau-Yasuda model in section 8.4.5, Da can be estimated as a function of temperature as shown in **Figure 8-13** (numerical data in the appendix of chapter 8: **Table 8-3**).

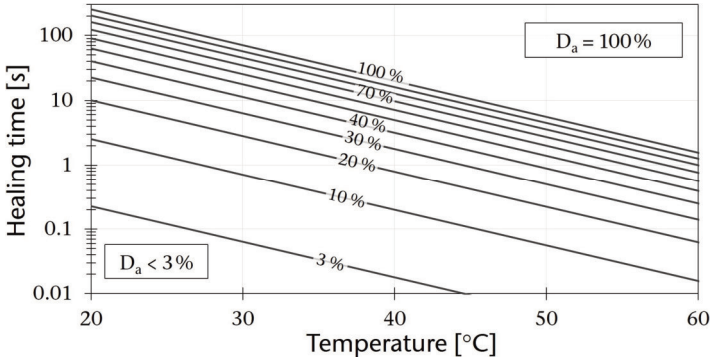

Figure 8-13. Isolines of the estimated degree of autohesion D_a as a function of temperature and healing time.

The healing times necessary to achieve the corresponding degree of autohesion can directly be read from the individual isolines. The strong dependence of λ on the temperature directly affects the healing times so that the epoxy-epoxy interface in contact is predicted to fully heal within 1.56 s for 60 °C while a time span of more than four minutes is needed at 20 °C.

Particularly with regard to the AFP process, any area in contact at the beginning of roller compaction will only be healed for ~5 % at the end of a 40 ms isothermal compaction phase (point t_c in **Figure 8-2**) at 40 °C. The same area of interest will reach full randomization and thus, full bond strength after 20 s at medium temperatures of 40 °C at which maximum tack was measured with the standard test cycle (section 8.4.3). This corresponds to a reduction in healing time by a factor of 12 compared to room temperature lay-up. A summary of the isothermal is given in the appendix. As stated before, the data presented in **Figure 8-10** revealed significant differences between tack of fully contacted interfaces G_{fc} and the calculated value of G_{DoIC} which represents the estimated tack value if tack was only a matter of contact formation. For low temperatures of 20, 30 and 40 °C, an additional autohesion phase (250, 70 and 19 s) was added after the compaction phase subject to the procedure presented in **Figure 8-14**.

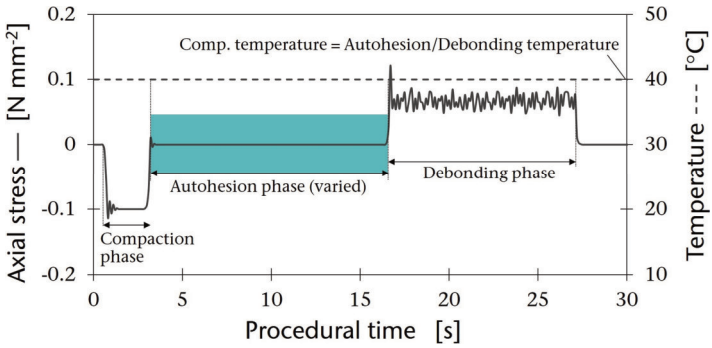

Figure 8-14. Peel test procedure (idealized) to study the influence of unpressurized, post-compaction autohesion on prepreg tack. The duration of the autohesion phase and temperatures are exemplary and were varied.

The hereby determined experimental data points were also projected to 100 % DoIC (analogously to G_{DoIC}) and added to **Figure 8-10** as G_{auto}. As proposed, the additional autohesion stage increases the projected tack significantly up to values similar to the fracture energies of fully contacted prepreg interfaces. The results give proof of the necessity to respect the slow autohesion mechanism for low temperature in terms of bond strength development between two prepreg plies.

8.4.7 Transfer to AFP scenarios

Coupling the contact formation and adhesion models allows for the estimation of the tack between two thermoset prepreg plies which have been consolidated in an arbitrary manner with regard to lay-up speed, compaction pressure and temperatures during both the roller consolidation phase as well as the subsequent unpressurized phase after material deposition (see **Figure 8-2**). For the compaction phase, constant temperature and pressure application is assumed over a specific dwell time which directly scales with the compaction roller size (area in contact) and is inversely proportional to the lay-up velocity. The estimation of DoIC as a function of lay-up velocity and compaction pressure as shown in **Figure 8-15** is based on an idealized compaction roller that maintains a constant contact of 50 mm in lay-up direction throughout the whole explored parameter range. Therefore, the lay-up velocity range represents compaction times between infinity (0 m s^{-1}) and 50 ms (1 m s^{-1}). The data shows that for a medium parameter set (40 °C,

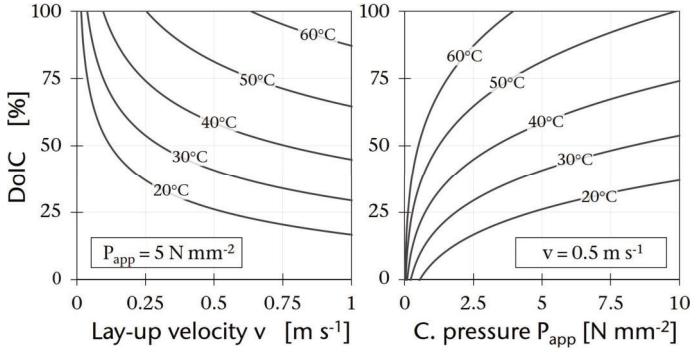

Figure 8-15. Model-based prediction of the ply-ply contact after consolidation at different temperatures, lay-up velocities and compaction pressures in an AFP process.

5 N mm^{-2}, 0.5 m s^{-1}) a contact area of ~50 %can be expected. Room temperature compaction leads to low DoIC with the exception of very low deposition rates which entail dwell times in the magnitude of seconds. It can also be concluded that full contact between plies will not be reached in most scenarios common for composite production by AFP. For this purpose, high lay-up temperatures >50 °C in combination with high pressures/low velocities are necessary. Compaction pressure may yet be limited by robot capacity or tool resilience while low velocities are not compliant with high manufacturing productivity.

The experimental results shown in **Figure 8-8** and **Figure 8-10** proof that a large area in contact does not inevitably yield high tack. In an effort to estimate the tack between two prepreg plies, the preceding relationships of contact formation (**Eq. (8-5)**) and autohesion (**Eq. (8-7)**) can be combined to calculate the degree of bonding D_b according to:

$$D_b = \frac{G}{G_{fc}} = D_{ic} * D_a \qquad \textbf{Eq. (8-8)}$$

When being applied to different lay-up scenarios, the experimental tack data for a fully contacted and healed interface G_{fc} can satisfy **Eq. (8-8)** resulting in the tack process maps shown in **Figure 8-16**. It has to be noted that autohesion throughout the compaction phase is neglected mainly due to two reasons: First, the compaction times are rather short (usually <100 ms) compared to the relaxation times at the temperatures of interest. Second, the temperature at the ply interface after

consolidation in thermoset AFP does not drop below temperatures where autohesion ceases. This is a main difference compared to thermoplastic AFP where the interface temperature rapidly falls below the glass transition temperature and causes autohesion to fade. For this reason, models have been developed for thermoplastic AFP which couple contact formation and autohesion during the compaction phase, e.g. by a convolution integral presented by Butler et al. [392].

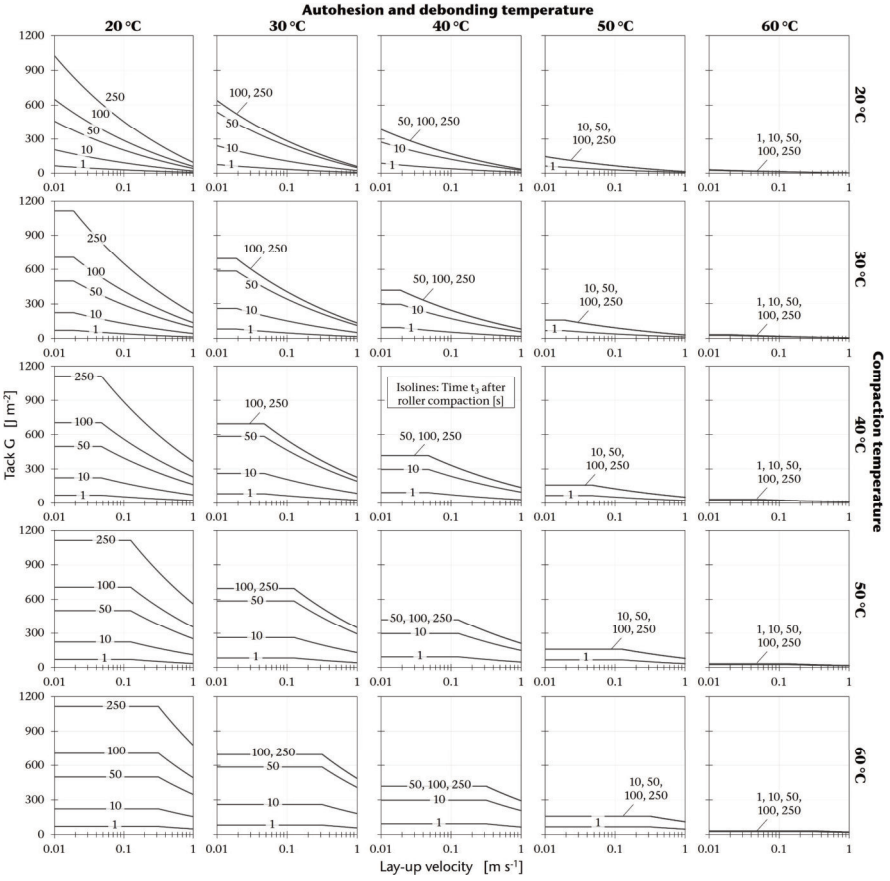

Figure 8-16. Process maps showing the estimated tack as a function of lay-up velocity, compaction temperature (rows) and adhesion/debonding temperature (columns) for different time spans after ply-ply consolidation by the compaction roller. Data was generated for constant 5 N mm^{-2} compaction pressure applied over a roller contact length of 50 mm and a debonding rate of 1 mm s^{-1}.

In general, the variation of lay-up velocity and compaction pressure yield similar curves in terms of estimated tack as both parameters directly influence the DoIC term of **Eq. (8-5)**. Therefore, the constructed process maps shown in **Figure 8-16** are limited to the variation of lay-up velocity at this point. Reducing the lay-up velocity leads to an increase of the model-estimated tack up to critical velocity which corresponds to a dwell time sufficiently long to create full contact between prepreg plies. From this point on, tack is no longer a function of lay-up velocity as the DoIC has reached unity for the investigated compaction pressure. However, the critical lay-up velocity is shifted to higher values when increasing the compaction temperature (follow the columns downwards in the process map matrix) due to the reduced temperature-dependent viscosity governing the DoIC term at constant pressure. In terms of autohesion, a significant influence of the considered time span after deposition (1, 10, 50, 100 and 250 s isolines) on tack can be observed: While low autohesion/debonding temperatures entail high tack if the interface is given enough time to heal, high temperatures result in low tack. The transition region between these two extremes is characterized by a progressive convergence of the long-term autohesion isolines: E.g. for the very middle graph (40 °C/40 °C), the 50, 100 and 250 s isolines are identical indicating a shift from autohesion-governed to contact formation-governed bonding mechanism for the corresponding parameter set. For the highest investigated temperatures, healing can be considered instantaneous after consolidation due to relaxation times in millisecond range (**Table 8-4**, appendix of chapter 8). It has to be noted that the model's relative error caused by neglecting autohesion throughout the compaction phase will be higher as dwell times and relaxation times are similar for temperatures ≥60 °C and very low lay-up velocities.

Despite full contact and complete healing at the ply-ply interface, the estimated tack for high temperatures is still very low at the debonding rate of 1 mm s^{-1}. The curve of tack between two fully contacted plies G_{fc} plotted in **Figure 8-10** showed logarithmic temperature dependence in a similar way as the complex viscosity of the prepreg resin. Crossley et al. [207] have already demonstrated for thermoset prepregs that shifting tack data in the time domain is valid when utilizing the time temperature superposition (TTS) principle based on the Williams-Landel-Ferry equation (**Eq. (8-4)**). The empirical constants C_1 and C_2 are adjusted by horizontally shifting G' and G" data to reference temperatures T_{ref} between 20 °C

and 60 °C within the shear rate spectrum. The resulting rheological master curves are shown in **Figure 8-17** for different T_{ref}.

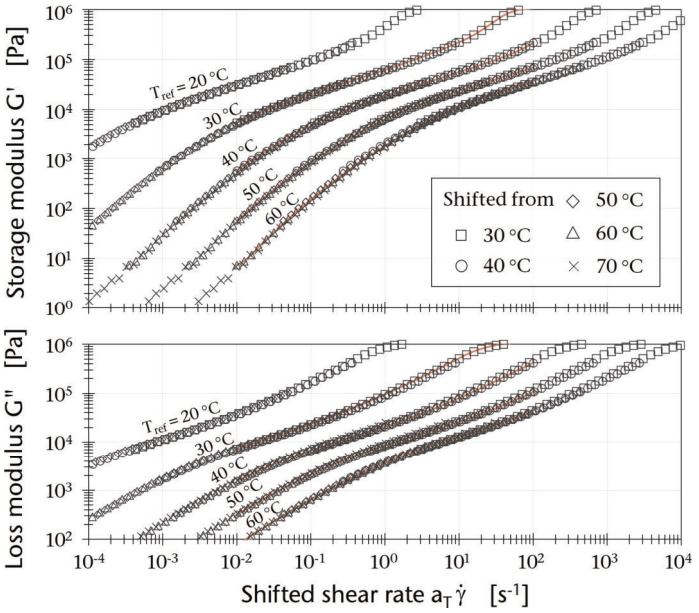

Figure 8-17. Storage modulus G‘ and loss modulus G” shifted to different reference temperatures.

Smooth overlapping of the curves for each T_{ref} indicates general compliance of TTS with the rheological behavior of the prepreg resin within the investigated temperature and shear rate range. The used empirical data for TTS is summarized in the appendix (**Table 8-4**). Shifting the tack data of G_{fc} with the rheological shift factors a_T allows for the construction of tack master curves at different reference temperatures as shown in **Figure 8-18**.

Other than the bell-shaped tack curves reported when using the test fixture of ASTM D8336-21 [147,207,302], our rate-dependent tack is found to increase monotonically. E.g., a considerably high tack of ~1 kJ m^{-2} can be expected at a debonding rate of 1 m s^{-1} and a temperature of 50 °C The reason for the observed monotonicity is that the data is limited to the debonding process and is not influenced by the application. If the TTS-based shifting procedure is connected to the modelled contact formation and autohesion mechanisms, tack can now be esti-

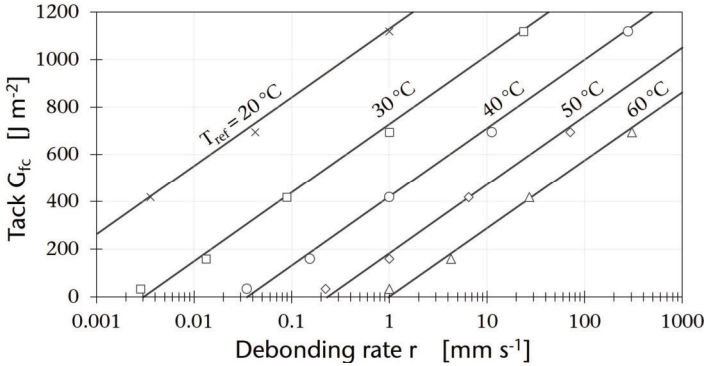

Figure 8-18. Tack data shifted to different reference temperatures by TTS to predict the fracture energies of fully contacted ply-ply interfaces G_{fc} at different reference temperatures and debonding rates.

mated for AFP-related defect scenarios (e.g. bridging, tow pull-off etc.) in which different debonding rates prevail.

8.4.8 Adhesion-cohesion balance of prepreg tack

The concept of the adhesion cohesion balance known from PSA characterization proposes that tack is found to peak at a medium 'sweet spot' temperature at which an optimal tradeoff between contact formation/autohesion and shear resistance is on hand. As a result, plotting tack as a function of temperature will give a bell shape curve for processes with isothermal application and debonding. In an effort to ascertain that the tack model can reproduce the bell shaped tack curves which have repeatedly been reported in experimental studies [147,222,379], ply-ply tack is calculated for four AFP scenarios which differ in lay-up velocity v and compaction pressure P_{app}. The corresponding isolines for the time span after compaction for each scenario are shown in **Figure 8-19**.

The model data is found to be able to replicate the bell-shaped curves proposed by the adhesion-cohesion balance. For the shown scenarios (isothermal application, autohesion and debonding; debonding rate of 1 mm s^{-1}), the following dependencies can be described:

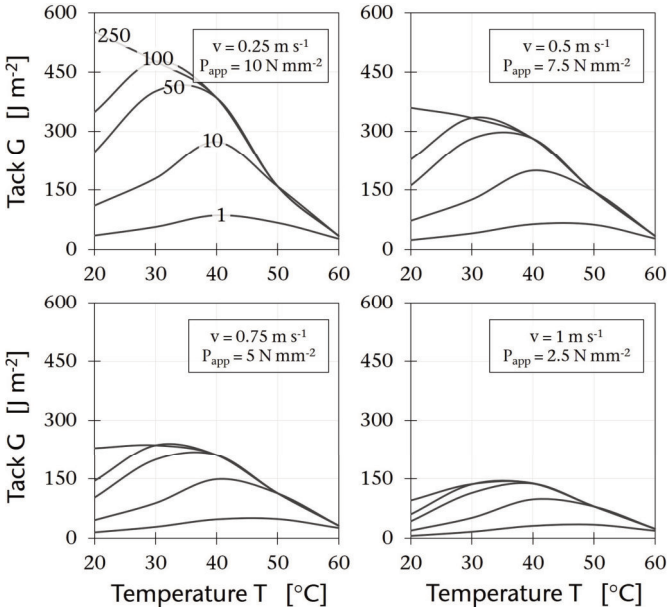

Figure 8-19. Temperature-dependent bell-shaped curve progression indicative of the validity of the adhesion-cohesion balance for prepreg tackiness.

- Increasing compaction pressure and decreasing lay-up velocity leads to higher absolute tack.
- Increasing lay-up velocity and decreasing pressure shifts the tack maximum to higher temperatures.
- The 'time after compaction' isolines converge at high temperatures and long autohesion times.
- Tack values for all scenarios remain significantly lower than the maximum bond strength of 1,150 J m^{-2}.

The reasons behind the dependencies have been discussed in detail earlier in the paper. Concludingly, experimental tack data of the standard test cycle (**Figure 8-7**) were used for model validation purpose. Therefore, the experimental data is plotted in **Figure 8-20** together with the model-estimated tack for equivalent test parameters (P_{app} =0.1 N mm^{-2}, v = 0.025 m s^{-1} equaling a dwell time of 2 s, r = 1 mm s^{-1}). For the time after compaction (autohesion time), 10 s are used for the

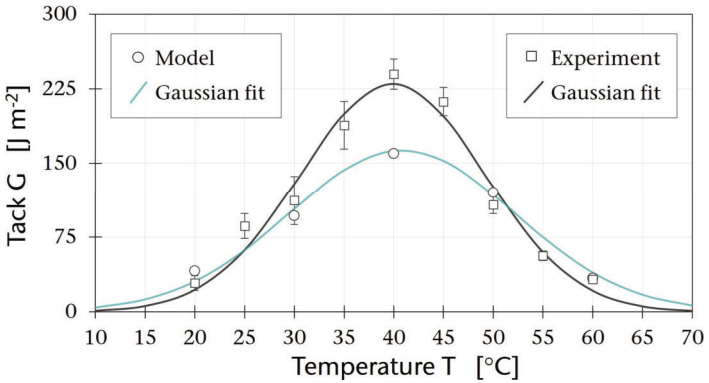

Figure 8-20. Comparison of experimental tack data obtained from the standard isothermal test cycle with tack predicted by the model for equivalent test parameters.

calculation as this time conforms to the duration between compaction and the onset of debonding in the standard test cycle.

Good general agreement between the model and experimental Gaussian fits is found. For the investigated set of parameters, the model underestimates the tackiness between the prepreg plies at medium temperatures of 40 °C by up to 30 %. The reason can most likely be found in the autohesion stage: The calculation here is based on a relaxation time $\lambda(40\,°C)$ of ~20 s which is in the same order of magnitude as the time span available for autohesion (10 s). Therefore, even slight measurement inaccuracy will translate into relatively large tack deviation for this set of test parameters according to **Eq. (8-7)**. Furthermore, several seconds pass between the beginning and the ending of the evaluated peel length which in theory will lead to different D_a and, hence, could influence tack. Excellent agreement is yet observed in terms of the prediction of the temperature at maximum tack, absolute tack at low and high temperatures as well as the general temperature-dependency.

8.5 Conclusion

A 90° peel test was employed to experimentally study the tackiness of two consolidated unidirectional carbon fiber/epoxy prepreg tapes. Specific variation of the compaction phase (compaction pressure, dwell time and temperature) as well as the implementation of an unpressurized autohesion stage within the testing

procedure enabled the exploration of the individual contribution of contact formation and autohesion to the bond strength development. In terms of contact formation, the degree of intimate contact – monitored with the help of pressure-sensitive films – was found to be influenced by all compaction variables in a way that virtually the full DoIC range between 0 and 1 was covered in the experiments. The experimental data was used to parametrize a contact formation model from thermoplastic composite literature. Despite the DoIC increasing as a function of compaction pressure, dwell time and temperature, tack measured by standard isothermal peel test cycle G_{std} followed Gaussian curves at equivalent test parameters. As opposed to the employed standard cycle, the fracture energy G_{fc} was, however, found to decrease monotonically as a function of debonding temperature if full contact (DoIC = 1) had been established between the prepreg plies. At room temperature and a debonding rate of 1 mm s^{-1}, a maximum ply-ply tack of >1kJ m^{-2} was recorded which exceeds the adhesive performance of commercial duct tape on glass substrates by the factor of 4. These values could not be reached by proposing an estimated tack value G_{DoIC} that exclusively considers the influence of contact formation on tack. Hence, the influence of autohesion was studied by employing a reptation bond strength model based on the determination of the relaxation time using the Carreau-Yasuda approach. The relaxation time of the b-staged resin was found to range between several minutes at RT and 9 ms at 100 °C, adverting to a substantial influence of time and temperature for interface healing in thermoset AFP. The rheological data was also used to shift the debonding rate in the time domain with the help of TTS.

Linking the submodels allowed for the estimation of prepreg tackiness for different simplified AFP scenarios by respecting the lay-up velocity, compaction pressure, debonding rate and temperatures throughout compaction, after compaction and during debonding. The interaction between the temperature-dependent, tack-governing mechanisms of contact formation, autohesion and debonding (adhesion-cohesion balance), which results in bell-shaped tack curves, could successfully be replicated by the bond strength model. From a practical point of view, AFP parameters can be adjusted in an informed manner to meet the process demands in terms of prepreg tackiness and, therefore reduce the risk of lay-up defects. The approach can also potentially be expanded, e.g. by the incorporation of ageing-related changes in resin viscosity.

CRediT authorship contribution statement

D. Budelmann: Conceptualization, Methodology, Validation, Formal analysis, Investigation, Writing – original draft, Visualization, Writing – review & editing. **C. Schmidt**: Conceptualization, Resources, Writing – review & editing, Supervision. **L. Steuernagel**: Resources, Project administration, Writing – review & editing. **D. Meiners**: Conceptualization, Resources, Supervision, Funding acquisition, Writing – review & editing.

Declaration of Competing Interest

The authors declare that they have no competing financial interests or personal relationships associated with this publication.

Acknowledgements

The authors are grateful for the financial support by Deutsche Forschungsgemeinschaft (DFG – German Research Foundation) granted for the research project 'TackTIC – Tack of Thermoset Impregnated Carbon Fibers' (project number 458900231). The authors also acknowledge the financial support by the Open Access Publishing Fund of Clausthal University of Technology.

Appendix

Table 8-2. Carreau-Yasuda regression parameters for neat prepreg resin at different temperatures. The last column includes data points of the fitted curve shown in Fig. 8-12.

Temp.	Zero-shear viscosity	Infinite-shear viscosity	Relaxation time/time constant	Critical shear rate	Transition parameter	Power law exponent	Coeff. of determination	Relaxation time (exp. fit)
T	η_0	η_∞	λ	$\dot{\gamma}_c$	a	n	R^2	λ
[°C]	[Pa s]	[Pa s]	[s]	$[s]^{-1}$	[-]	[-]	[-]	[s]
20	-	-	-	-	-	-	-	251.639
30	-	-	-	-	-	-	-	70.668
40	42,192.2	54.8447	28.9078	0.0345	0.5403	0.3766	0.99990	19.845
50	5,967.5	51.1451	5.4898	0.1821	0.6111	0.4067	0.99998	5.573
60	1,320.2	17.5589	1.0529	0.9497	0.6152	0.3912	0.99976	1.565
70	395.6	5.6513	0.3069	3.2575	0.5967	0.4055	0.99969	0.439
80	145.5	1.5123	0.1595	6.2660	0.6248	0.4818	0.99886	0.123
90	70.1	0.3457	0.0252	39.603	0.4879	0.3727	0.99354	0.034
100	38.6	0.2125	0.0136	73.313	0.5823	0.3021	0.94915	0.009

Table 8-3. Estimated time span to reach a specific degree of autohesion D_a at a specific temperature based on Eq. 8-7.

D_a	20 °C	30 °C	40 °C	50 °C	60 °C	70 °C	80 °C	90 °C	100 °C
0 %	0	0	0	0	0	0	0	0	0
1 %	0.025	0.007	0.0019	0.0005	0.0001	4.395 E-05	1.234 E-05	3.466 E-06	9.73 E-07
3 %	0.226	0.063	0.0178	0.0050	0.0014	0.0003	0.0001	3.119 E-05	8.767 E-06
10 %	2.516	0.706	0.1984	0.0557	0.0156	0.0043	0.0012	0.0003	9.73 E-05
20 %	10.06	2.826	0.7938	0.2229	0.0626	0.0175	0.0049	0.0013	0.0003
30 %	22.64	6.360	1.7861	0.5016	0.1408	0.0395	0.0111	0.0031	0.0008
40 %	40.26	11.30	3.1753	0.8917	0.2504	0.0703	0.0197	0.0055	0.0015
50 %	62.90	17.66	4.9614	1.3933	0.3912	0.1098	0.0308	0.0086	0.0024
60 %	90.59	25.44	7.1445	2.0064	0.5634	0.1582	0.0444	0.0124	0.0035
70 %	123.3	34.62	9.7244	2.7309	0.7669	0.2153	0.0604	0.0169	0.0047
80 %	161.0	45.22	12.701	3.5669	1.0017	0.2813	0.0790	0.0221	0.0062
90 %	203.8	57.24	16.075	4.5144	1.2677	0.3560	0.0999	0.0280	0.0078
100 %	251.6	70.66	19.845	5.5733	1.5651	0.4395	0.1234	0.0346	0.0097

Table 8-4. Fitted empirical constants C_1 and C_2 for TTS and the corresponding superposition parameters $\log(a_T)$.

T_{ref}	C_1	C_2	$\log(a_T)$				
			T = 30 °C	T = 40 °C	T = 50 °C	T = 60 °C	T = 70 °C
20 °C	11.2	71.6	-1.373	-2.445	-3.307	-4.014	-4.605
30 °C	8.9	74.8	-	-1.049	-1.877	-2.547	-3.101
40 °C	7.2	78.6	1.049	-	-0.813	-1.460	-1.988
50 °C	6.6	91.2	1.854	0.813	-	-0.652	-1.187
60 °C	5.4	95.2	2.484	1.436	0.633	-	-0.513

Chapter 9

9. Implications for industrial practice

The aim of this thesis is to contribute to building a fundamental knowledge basis on the complex material-process interaction and underlying adhesive/cohesive mechanisms involved the tack of thermoset prepreg materials. Despite the fundamental character of both the general approach to the topic and the research presented in the papers for this cumulative thesis, the results comprise valuable pragmatic implications for advanced composite manufacturing as well as prepreg handling and production. In the following section 9.1, these implications are exemplified by bringing together the basic findings of chapters 5-8 and a study showcasing the manufacturing of a large-scale aircraft composite part by AFP. Furthermore, concise recommendations to tailor the tack of epoxy-based prepreg resins for prepregs are in section 9.2 and insights into the challenge of informed prepreg tack measurement are shared in section 9.3.

9.1 Case study: Lay-up of an aircraft part using AFP

The aforementioned case study was conducted in an effort to demonstrate the effect of adjusting AFP process parameters to account for prepreg tack in a practice-related manufacturing scenario. Therefore, process times required for material lay-up were assessed as indicators for productivity and economic feasibility. Knowledge of process times is crucial to guarantee efficient cycle time management in the aerospace industry [397]. The case study procedure can be summarized as follows:

– First, the part geometry and stacking sequence of the laminate were defined and implemented into the lay-up simulation software.
– All remaining production-relevant parameters were set for simulation (tow width and height, number of tows placed simultaneously, etc.)
– Process cycle times were predicted for different lay-up velocities.
– Finally, the simulated cycle times were correlated with the tack levels which have been estimated on the basis of the model presented in chapter 8.

9.1.1 Part geometry & stacking sequence

A large-scale composite part from the empennage of a civil aircraft was used for the case study. Using the CAD solid modeler SolidWorks by Dassault Systèmes, FR, a model of the part was created which was based on the dimensions and the general design of modern wide-body airplanes, measuring 9.7 m in height and 6.5 m in width. Digitally forming the part gave a positive mold, in which a laminate was eventually meant to be built up from ¼" UD thermoset carbon fiber prepregs – the same material as used in the previous chapters. As original laminate stacking sequences for AFP composite parts of aircrafts are well-kept industrial secrets of airplane manufacturers and, therefore, are not freely available, a simplified laminate was modelled featuring six full stacks of the following symmetric, quasi-isotropic laminate:

$$[0° / \pm 45° / 90°]_S$$

This type of laminate is considered balanced and features isotropic in-plane properties while at the same time reducing the risk of undesired coupling effects. The chosen stacking sequence[2] resulted in a total amount of 48 plies (0.13 mm nominal cured ply thickness) adding up to a total part thickness of 6.24 mm which was constant throughout the whole laminate due to the lack of patches.

[2] Noteworthily, genuine AFP-manufactured laminates contain very few full plies but rather rely on the incorporation of fiber patches to locally reinforce the laminate to meet specific load cases.

9.1.2 Lay-up simulation

The lay-up simulation was carried out using the robot programming software for AFP processes AddPath (v.1.6.3) by Addcomposites, FI. An in house-built experimental AFP head (Institute of Production Engineering and Machine Tools, Leibniz Universität Hannover) attached to an industrial robot was implemented in the software to create a digital workshop environment (**Figure 9-1**). In practice, the placement head has to be moved by a gantry system due to a part size of almost 10 m in height. 24 tows (¼" ≙ 6.35 mm), which added up to a total placement width of 152.4 mm if nonexistence of gaps is assumed, were set to be placed simultaneously by the AFP head per pass.

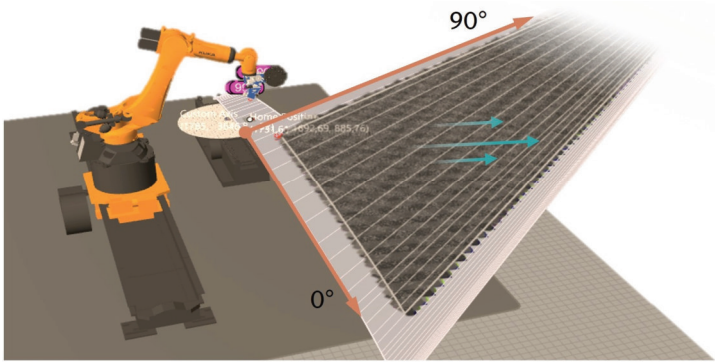

Figure 9-1. Digital workshop environment for the prepreg lay-up simulation of the CFRP aircraft part. The lay-up direction of the currently deposited 45° ply is highlighted in blue.

A reference lay-up time was initially determined for a deposition speed of 0.5 m s^{-1}. Here, the lay-up time t_l was defined as the sum of the actual time of lamination t_{lam} and the non-productive lay-up time t_{off} spent by the head for approaching, retracting and turning. Other auxiliary process times consumed, e.g., for machine setup, spool changes or defect detection/correction measures were not considered. It was assumed that t_{off} is constant for the chosen parameter set (**Table 9-1**) while t_{lam} is a function of the varied lay-up velocity.

Table 9-1. Robot speeds, retract/approach settings and ply parameters used for lay-up simulation.

Robot setting	Value	Retract & Approach	Value	Ply design parameter	Value
Runway speed	50 mm s^{-1}	Retract height	25 mm	Gap	0.0 mm
Approach speed	100 mm s^{-1}	Retract angle	70°	Overtravel	10 mm
Lay-up speed	variable	Approach height	25 mm	Staggering	0 %
Homing speed	20 %	Approach angle	-70°	Covering edges	100 %
Acceleration	100 %			Tool tilt	0 %
Travel speed	500 mm s^{-1}				

The estimated pass, weight and time parameters for each ply as well as for the full laminate of 48 plies are summarized in **Table 9-2**. The simulation predicted a total non-productive time t_{off} of 552 min ≙ 9 h, 12 min. For the reference lay-up velocity of 0.5 m s^{-1}, the time of lamination t_{lam} amounted to 386 min ≙ 6 h, 26 min and the total lay-up time t_l to 938 min ≙ 15 h, 38 min. The untrimmed CFRP part was expected to weigh 362.61 kg at a total of 278 km of ¼“ laid prepreg slit tape.

Table 9-2. Simulation results of the AFP manufacturing case study at a lay-up speed of 0.5 m s^{-1}. Full laminate values are calculated for a $[0°/\pm45°/90°]_6$ stacking sequence.

Simulation result	Unit	Ply				Full laminate (48 plies)
		0°	45°	-45°	90°	
Number of passes	[-]	66	26	100	77	3,228
Pass length	[m]	241.7	241.9	237.5	244.1	11,582
Material length	[m]	5,802	5,808	5,699	5,859	278,009
Material weight	[kg]	7.57	7.57	7.43	7.64	362.61
Non-productive time t_{off}	[min]	11.6	9.1	13.0	12.4	552.0
Lamination time t_{lam}	[min]	8.1	8.1	7.9	8.1	386.0
Total lay-up time t_l	[min]	19.6	17.1	20.9	20.5	938.0

9.1.3 Effect of tack control on lay-up time

Figure 9-2 and **Figure 9-3** display the results from merging the manufacturing simulation data with the model-predicted tack data of chapter 8. From these graphs, the estimated process time needed to manufacture the composite aircraft part by a 24 tow AFP system (¼“) can directly be read as a function of a desired tack level at specific process parameters. The graphs differ in terms of whether the mold is heated or not.

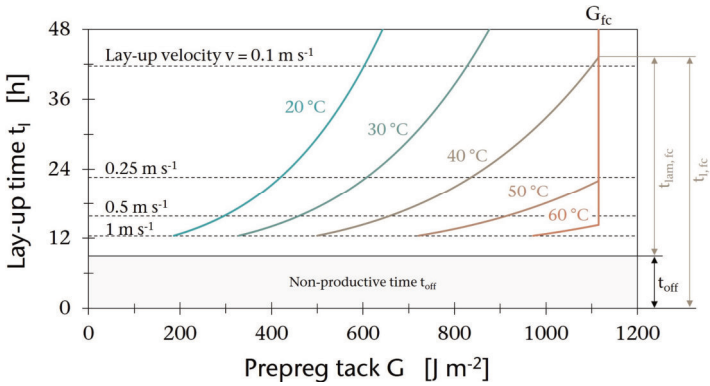

Figure 9-2. Simulated lay-up time t_l as a function of desired tack level and compaction temperature for **unheated** molds (compaction pressure: 5 N mm^{-2}, mold temperature after compaction: 20 °C, time after compaction: >250 s)

The data of **Figure 9-2** represents a manufacturing scenario featuring prepreg lay-up at a specific temperature (20-60 °C) by an applied compaction pressure of 5 N mm^{-2}. Here, the mold was considered unheated (20 °C) and tack was assessed >250 s after compaction at 20 °C so that $D_a = 1$ according to **Eq. (8-7)** which corresponds to a fully healed interface in terms of autohesion. The results showed that the higher the lay-up temperature was chosen, the less time was required to reach the maximum tack of a fully contacted ply-ply interface G_{fc} of ~1,100 J m^{-2}. At 60 °C, this state was achieved within 14 h, 17 min of total lay-up time $t_{l,fc}$ of which 9 h, 12 min were spent on non-productive time t_{off}. The corresponding lay-up velocity was recorded 0.63 m s^{-1}. A reduction in lay-up temperature to 40 °C increased the necessary lay-up time for equivalent tack to 43 h, 26 min – an increase by more than 200 % as a result of the low required lay-up speed of 0.095 m s^{-1} at 40 °C. In order to manufacture the full laminate with maximum ply-ply tack G_{fc} at the low lay-up temperature levels of 20 and 30 °C, highly uneconomical lay-up times of 223 h (20 °C) and 96 h (30 °C) were predicted. However, G_{fc} marks the maximum achievable tack at RT and will most likely not be necessary to restrict defect formation in practice. For comparison, duct tape adhered to a glass substrate develops a peel fracture toughness of ~300 J m^{-2}. The actual desired tack level is suggested to be estimated through one of the numerous proposed defect models in literature. By linking defect models to the results from this thesis, tack-related process boundaries of defect-free AFP can effectively be disclosed.

For the preparation of **Figure 9-3**, the interdependence between tack and manufacturing times were calculated for heated molds, i.e. for different compaction temperatures being held throughout the whole lay-up process all over the laminate.

In this case, the best trade-off between process efficiency (low lay-up times) and tack was observed for sets of process parameters relying on medium temperatures. At best-performing 40 °C, autohesion could be marked complete and contact formation at a respectable level while the interface was still able to withstand considerable peel forces (adhesion-cohesion balance). Within the economically attractive region between 0.5 and 1 m s^{-1} lay-up velocity, which resulted in lay-up times of ~15.5 and ~12.5 h, respectively, relatively high tack levels of 150 ± 20 J m^{-2} could be estimated at this temperature. Another positive aspect with practical implication is that prepreg tack appeared to be less sensitive to process parameter deviations in the region of interest due to the flat course of the 40 °C graph. For high temperatures of 50 and 60 °C, losses in favor of productivity (equaling longer lay-up times) were found to no longer be compensated for by enhanced tack performance as the graphs very quickly converged vertically. Fiber placement at room temperature on the other hand would consume a lot of lamination time to reach sufficient tack levels. E.g., lay-up at 0.1 m s^{-1} (estimated tack: 120 J m^{-2}) was predicted to take the AFP head 41 h, 22 min (t_{lam} = 32 h, 10 min) to manufacture the aircraft part.

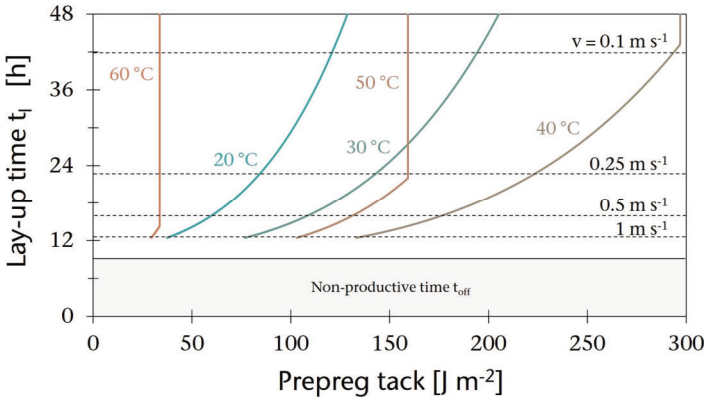

Figure 9-3. Simulated lay-up time t_l as a function of desired tack level and compaction temperature for **heated** molds (compaction pressure: 5 N mm^{-2}, isothermal mold and material, time after compaction: 10 s)

9.2 AFP-oriented tack control of prepreg resins

In an effort to tailor the tackiness of TGMDA/DDS model prepreg resins in accordance with a given set of AFP process parameters, a resin formulation map (**Figure 9-4**) based on the findings of chapters 7 and 8 was compiled. For this purpose, the viscosity data from **Figure 7-5** was merged with tack data predicted with the help of the tack model of chapter 8. In practice, both investigated measures, namely B-staging and toughening will take place at different stages of prepreg manufacturing: While the toughener component is incorporated during resin production, prepregs are mostly B-staged after impregnation [398].

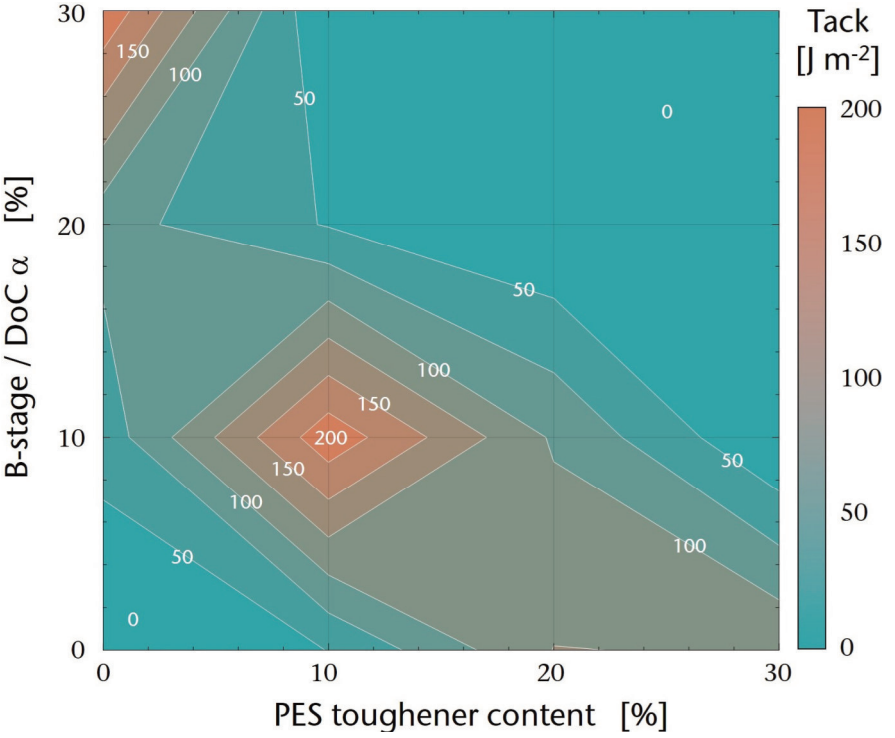

Figure 9-4. Prepreg resin formulation map for tack adjustment of TGMDA/DDS systems. Tack values were estimated at 40 °C, 5 N mm^{-2} compaction pressure applied over a roller contact length of 50 mm, 10 s after compaction and 1 mm s^{-1} debonding rate.

In order to achieve high-tack resins for prepreg production, the resin formulation map of **Figure 9-4** proposed medium target values for DoC and toughening content at 10 % each. Deviation from 10 % was found to have similar impact in terms of tackiness. However, a slightly higher sensitivity to B-staging was observed. Both scenarios, that is no as well as excessive B-staging/toughening in combination led to insignificant stickiness as a result of very low and high resin viscosity, respectively. This finding highlights the necessity to carefully balance both influencing factors to gain the desired tack properties for automated prepreg lay-up technology.

Untoughened resins needed considerable pre-curing of >20 % in order to increase the resin viscosity and, therefore, exhibit high tack at 40 °C. On the other hand, resins lacking pre-cure were predicted to exhibit medium tack for toughening contents >10 %. If high toughening contents are mandatory on grounds of mechanical performance of cured CFRP parts, low B-stage levels are recommended to maintain tack. Another way to achieve the desired tack from a process perspective is to raise the lay-up temperature. In general, an increase in lay-up temperature will shift the rhombic high-tack area of **Figure 9-4** towards the top right side of the diagram. Decreasing the lay-up velocity and/or increasing the compaction pressure will enforce the same outcome while absolute tack values can be expected to rise concomitantly.

9.3 Recommendations for tack testing in practice

Throughout the preparation of this thesis, fixtures and measurement cycles to perform probe tack testing (section 5.2.3) and peel testing (section 8.3.2) were developed, implemented and evaluated to quantify the stickiness of thermoset prepreg materials. Another study was conducted in an effort to compare tack data gained from the implementation of different measuring methods (probe, peel, shear, loop and ASTM D8336). The corresponding measurement results (on the same material as used in this study) and a detailed discussion can be found elsewhere [285] while the most general deductions drawn from the study are summarized in the following **Table 9-3**.

Table 9-3. Benefits, drawbacks and suitability of different prepreg tack measurement techniques.

Test	Benefits	Drawbacks	Suitability
Probe	– Strict separation and control of bonding/ debonding phase – Easy process control and setup – Simple fixtures due to one-dimensional motion of probe	– Test parameter and debonding mechanism differ significantly from AFP process	– Studying fundamental adhesive mechanisms
Peel	– Strict separation and control of bonding/ debonding phase – Accounts for bending stiffness	– Challenging sample preparation due to small sample size – Relatively complicated fixture	– Studying fundamental adhesive mechanisms – Adjusting AFP process
Shear	– Simple fixture design	– Lowest reproducibility – Test parameter differ significantly from AFP process	– Determination of material parameters for defect modeling
Loop	– Minimal fixture design – Very quick and easy to perform	– Temperature-related differences in compaction pressure – Very low compaction pressures – Dependence on prepreg bending stiffness	– Quality control – Basic exploration of tackiness
ASTM D8336	– Standardized for prepregs – Mimics prepreg lay-up in AFP – Uses universal testing machine – Accounts for bending stiffness	– Unable to separately control compaction and debonding velocity – Relatively complicated fixture	– Comparing materials at standard test parameters – Adjusting AFP process

Chapter 10

10.Conclusion & Outlook

Concludingly, aim and methodology of the thesis are recapitulated in the following section 10.1 while key findings are presented in section 10.2 by addressing the research questions initially raised throughout the outline section 2.1. Section 10.3 provides a short critical discussion on the thesis' general achievements and restrictions, from which the need for future research approaches is derived.

10.1 Recapitulation

The aim of this thesis was to characterize, understand and describe the adhesive behavior of thermoset carbon fiber prepregs used for the production of large-scale composite parts via automated lay-up technologies. Four consecutive research papers were prepared to address the main research desiderata which have been identified prior in the course of a literature review (Publication I). The first research article (Publication II) investigated the dependence of tack on AFP-derived test parameters and material ageing using commercially available aerospace-grade prepreg system. The tack adhesion-cohesion balance detected in this context was further elaborated by publishing a two-part series (Publication III+V) which addressed the contributions of surface wetting (III) and contact formation/ autohesion (V). The tack of model resin formulations was assessed in publication IV while varying epoxy prepolymers, B-stage levels and toughening contents. A semi-empirical approach to model prepreg tack was proposed and transferred to AFP

manufacturing scenarios. Finally, the implications of prepreg tack for laminate lay-up of a large-scale composite part were demonstrated in a case study.

10.2 Key findings

Chapter 4: **State of research** (Publication I)

– *Which are the most relevant but unaccounted influencing factors of prepreg tack in literature?*

Based on the literature review, a large variety of influencing factors was identified, which appear to effect prepreg tack. The factors can be categorized according to the classification of prepreg production and processing stages shown in **Figure 10-1**.

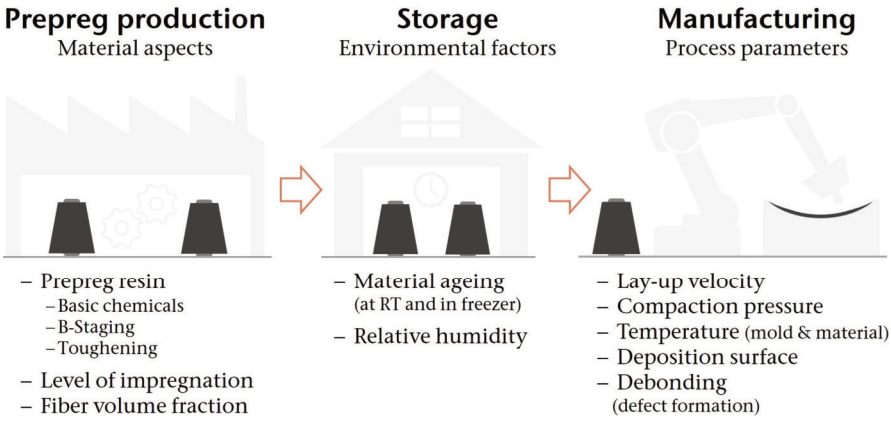

Figure 10-1. Tack-relevant stages of composite manufacturing from prepregs and corresponding influencing factors.

– *Are there any methodical lackings in prepreg tack characterization?*

Until 2021, the absence of a standardized measurement method spurred the composites society to devise or modify various approaches for assessing the tack of thermoset pre-impregnated fiber. The assortment of measurement techniques coupled with an array of factors influencing tack, complicates the comprehensive understanding of prepreg tack. Consequently, there is a risk of misinterpreting experimental findings or even choosing and developing unsuitable modeling approaches - especially when focusing on individual parameters within narrow ranges of variation.

Chapter 5: **Process and environmental factors** (Publication II)

– *How does a variation of temperature influence prepreg tack?*

The tack of carbon fiber epoxy prepreg was found to exhibit significant sensitivity to temperature fluctuations within the explored experimental domain when measuring tack isothermally: E.g., tack decreases by >75 % when increasing the test temperature from 40 °C to 50 °C. Meanwhile, both assessed tack metrics, σ_{max} and W_{adh}, demonstrate non-redundancy in assessing tack properties and exhibit distinct local maxima at varying temperature levels. The bell-shaped form of temperature-dependency was assigned to a balance between adhesive and cohesive mechanisms which were investigated in detail further along the line.

– *Is there a influence of room temperature ageing on tack and how can it be accounted for in AFP processes? How does the prepreg material change in terms of cure progression?*

The influence of ageing on tack was found to be highest within the first ten days of RT exposure at which the material reaches a DoC of ~28 % and a T_g of 17 °C (15 °C increase). Contrary to popular belief, it was observed that material surpassing its designated tack lifespan, as indicated by the datasheet, retained processability with tack properties surpassing those of fresh material by more than 65 % when subjected to elevated temperatures during processing. At the investigated test parameters, highest tack values were measured at 35-40 °C above T_g.

– *In which way do the process/test parameters compaction force and debonding rate generally affect the measured stickiness?*

Tack steadily increases as a function of compaction stress σ_c. However, only little influence is observed as soon as σ_c surpasses a critical level of compression. Generally, the correlation between compaction force and tack is found to be the only straight-forward one among all investigated test parameters. In other words, higher compaction pressures will always result in higher tack values independent from other applied test parameters. The highly viscoelastically-governed debonding rate is noted to differentially impact both tack parameters. While σ_{max} logarithmically increases within the examined spectrum, W_{adh} reaches a peak. This peak diminishes in magnitude and shifts towards higher debonding rates if tested at higher temperatures.

Chapter 6: **Adhesive mechanisms** (Publication III)

– *Is there a difference in prepreg adhesion between variable AFP-related surface materials such as polyurethane (compaction roller), backing paper and mold materials (steel)?*

The expected difference between the investigated solid surfaces could be verified but was found to be low in terms of absolute deviation compared to ply-ply tack. The positions of peak tack in the temperature spectrum differ significantly while absolute maximum tack values are in the order ST_{pol} > PU > ST (ground) > BP.

– *Is prepreg tack on solid surfaces a matter of surface wetting and can it be approached through a wetting analysis based on contact angle measurement?*

Employing contact angle measurement in conjunction with the OWRK model has emerged as a viable approach for elucidating notable variances in surface wetting characteristics between prepreg resin and standard test liquids on solid surface materials prevalent in AFP applications. However, contact formation between two prepreg plies cannot be treated as model system of three ideally separated phases and is therefore not approachable through CA measurement. For this material combination, adhesion is rather governed by the mechanisms of ply-ply contact formation with subsequent autohesion which were examined in Publication V.

– *Can differences in adhesion be related to various types of intermolecular forces such as van der Waals forces, dipole-dipole interaction or h-bonding?*

Higher tack were observed on substrates with resin-matching polar and dispersive SFT/SFE ratios. In this case, dispersive (van der Waals forces) and polar (h-bonding, dipole-dipole-interaction) are expected to be present at the interface.

– *How does surface topography influence tack?*

A modified version of the Dahlquist criterion, expanded to incorporate topographical considerations, was effectively employed to explore the influence of the thermodynamic work of adhesion W_{SL} , surface topography, and rheological properties on the temperature-dependent initiation of tack. Although the absolute temperatures obtained from tack measurements did not precisely align with those predicted by the criterion, the fundamental relationships were confirmed: Enhanced W_{SL} and longer wavelengths in surface roughness profiles facilitate wetting at lower temperatures, whereas higher resin temperatures or lower storage moduli are necessary to achieve thorough wetting of rough surfaces.

Chapter 7: **Prepreg resin formulation** (Publication IV)

– *Does the use of different epoxy-prepolymers (TGMDA, TGAP and DGEBA) result in diverse levels of initial stickiness?*

Despite achieving similar maximum tack levels, the A-stage formulations exhibited significant variation in the positioning of their peak tack within the temperature range under investigation. While absolute tack followed the descending order of DGEBA < TGMDA + TGAP < TGMDA < TGAP, the stickiness of all A-stage resins was found to exceed commercial prepregs by the factor of 3-4. The variations could primarily be ascribed to differences in the initial viscosity of the used prepolymers.

– *Can the prepreg B-staging be tailored to reach desired tack levels based on the correlation between modeled cure stage (OWRK) and tack data?*

The OWRK cure kinetics model was demonstrated to be applicable to adjust the B-stage level of epoxy (TGMDA)-based prepreg resins. Increasing pre-cure led to a considerable loss in tackiness while T_g was steadily raised from -6.02 (A-stage) to 39.14 °C (30 % cure). The pre-cured storage moduli G'at maximum tack remained in the same order of magnitude ($G' \approx 3*10^5$ Pa, Dahlquist criterion) which is remarkable considering that B-staging process shifts the tack minimums by ~30 K.

– *Which thermoplastic toughener content is considered favorable for the use in epoxy-based prepregs in terms of tack?*

In general, progressive incorporation of the thermoplastic toughener PES showed a similar impact on tack as B-staging. At a B-stage level of 20 % in combination with a toughener content of 10 wt%, tack was lowered to approximately 100 µJ mm^{-2}, a value consistent with the measurement of Hexcel's HexPly 8552 commercial epoxy aerospace prepreg under the same testing conditions. Whenever enhanced mechanical performance in the C-stage necessitates a higher toughening content, B-staging can be minimized or omitted altogether to achieve comparable tackiness.

Chapter 8: **Contact formation and autohesion** (Publication V)

– *How does experimentally determined intimate ply-ply contact develop as a function of temperature, compaction force and dwell time?*

The degree of intimate contact (DoIC), assessed by using pressure-sensitive films, was observed to be influenced by all investigated compaction variables, resulting in

the experimental coverage of nearly the entire DoIC range between 0 and 1. Despite an increase in DoIC with compaction pressure, dwell time, and temperature, tack measured by the standard isothermal peel test cycle G_{std} followed Gaussian distributions under equivalent test conditions. At the same time, measurement values could not be reached by proposing an estimated tack value G_{DoIC} that exclusively takes contact formation into account. Hence, the influence of autohesion was studied by employing a reptation bond strength model based on the determination of the relaxation time using the Carreau-Yasuda approach.

– *Is it possible to transfer the autohesion concept known from thermoplastic polymer healing to thermoset prepregs to predict ply-ply bond strength?*

The (thermoplastic) autohesion concept was proven valid for thermoset prepregs: It was shown that the fracture toughness of ply-ply interfaces will increase after compaction as a function of time to fully heal the interfaces at a specific degree of intimate contact. The time spans needed for healing were highly temperature-dependent and ranged from miliseconds (80°C) to few minutes (RT).

– *Can contact formation and autohesion submodels be combined and applied to estimate tack as a function of multiple process and material parameters?*

By integrating the submodels, prediction of prepreg tackiness across various simplified AFP scenarios was made possible while considering factors such as lay-up velocity, compaction pressure, debonding rate, and temperatures during compaction, post-compaction, and debonding. The bond strength model effectively reproduced the interaction among temperature-dependent mechanisms governing tack, including contact formation, autohesion, and debonding which in combination are decicive for bell-shaped tack curves.

Chapter 9: **Implication for industrial practice**

– *How big is the economic impact with regard to process times when accounting for prepreg tack during the manufacturing of a close to reality aerospace composite part?*

The case study of the manufacturing of a CFRP aircraft part showcased that the economic impact of adjusting process parameters can be tremendous: On an unheated mold, lay-up at a temperature of 60 °C was simulated to be completed within 14 h, 17 min with 9 h, 12 min being spent on non-productive time. The corresponding lay-up velocity was recorded 0.63 m s^{-1}. In order to gain equivalent

ply-ply tack, a reduction in lay-up temperature to 40 °C increased the necessary lay-up time to 43 h, 26 min – an increase by more than 200 % as a result of the low required lay-up speed of 0.095 m s^{-1} at 40 °C.

– *In which way and to which extent should the prepreg's resin be modified in terms of pre-cure and toughening to meet stickiness requirements in industrial practice?*

A resin formulation map was compiled to enable tailoring the tackiness of TGMDA/DDS model prepreg resins in account with a given set of AFP process parameters. Generally, purposive resin adjustment was found to be inevitable as both excessive and no B-staging/toughening will result in insignificant tack levels. The map rather suggests medium target values for pre-curing and toughening content at 10 % each in order to achieve high-tack resins for prepreg production. If high toughening contents are mandatory to meet requirements of mechanical performance (cured), low B-stage levels should be aimed at to preserve tackiness.

– *What is the preferential test method to quantify the tackiness of prepregs?*

This question cannot be answered conclusively as the suitability of the test method is highly dependent on the exploratory objective. The choice of method should be made based on the study goal in combination with requirements regarding i.a. fracture mode, reproducibility, experience and instrumental/testing effort. A table comparing benefits, drawbacks and suitability of different test methods was assorted to provide guidance.

10.3 Future work

From a practical point of view, the findings of this thesis provide an informative basis for the adjustment of AFP processes in order to conform to requirements in terms of prepreg tackiness. The recommendations can be translated to a broader set of prepreg-processing manufacturing techniques such as filament winding (FW) or fiber patch placement (FPP) in which material stickiness is of the essence. Here, the similarities between quality-determining mechanisms and influencing factors are on hand so that a direct transfer can be made. The results may also create incentives to reduce the machine complexity for automated prepreg lay-up technologies due to a more informed knowledge on prepreg handling. Eventually, low-cost solutions

such as low-scale placement heads for towpregs, are prospects to serve more cost-sensitive industrial sectors such as the automotive in the medium term.

Building on this thesis, subsequent studies are encouraged to validate the lab-scale findings within a production environment: A model-estimated variation of process parameters such as lay-up velocity, compaction pressure and temperature should be conducted in the course of manufacturing trials of large composite parts using AFP. The occurrence of laying defects may meanwhile be recorded in dependence of the process parameter variation, e.g. with the aid of one the many proposed approaches in literature (thermography, profilometry, etc.). Following this approach, the overarching aim may be to verify that an informed adjustment of process parameters in terms of tack can lead to reduced risk of defect formation while taking minimal loss of economic efficiency.

Nevertheless, the results suggest that the complexity of the adhesive phenomenon 'prepreg tack' pushes physics-based models (PBM) to their limits. It was shown that isolated influencing factors or a limited number of interdependencies can be modelled adequately and that countermeasures can be taken accordingly to ensure process stability, e.g. compromised by progressing material ageing. A virtually holistic physical representation, however, is intricate and requires a considerable amount of characterization effort (rheology, cure kinetics, topography, etc.). This effort may easily go beyond companies' R&D capacities and/or competences every time a change in the processed prepreg system is due. With the ongoing rapid evolution of big data, artificial intelligence (AI) and machine learning (ML) in production environments, these key technologies not only bear great potential for advanced composites manufacturing in general but also for dealing with tack in AFP in particular. Statistical ML algorithms therefore need to be trained by linking process data with the occurrence of defects. Accurate live monitoring of the process in terms of temperature, compaction pressure, lay-up speed in combination with keeping track of workshop and prepreg conditions are mandatory. The black-box nature of DDM may not contribute to the phenomenological understanding of prepreg tack in the same way as the investigations carried out in the course of this thesis but may deliver a pragmatic approach for the advanced composite manufacturing of the future.

Figures, Tables, References

Further publications

- Blows R, Budelmann D, Call D, Chan C, Choong GYH, Collins J, De Focatiis DSA, Endruweit A, Fishpool D, Garber J, Ghose S, Giannis S, Golding J, Good S, Joesbury A, Jones BR, Meiners D, Nitsoo O, Palmer C, Qian C, Rivas A, Santacruz Rodriguez G, Stillwell RE, Vincent JD, Westwood J, Yuan H. Repeatability and reproducibility of the measurement of prepreg tack following ASTM D8336-21: Results of a round-robin study. Composites Part A: Applied Science and Manufacturing (2024) - under review -

- Budelmann D, Schmidt C, Meiners D. Measuring techniques for prepreg tackiness: A comparative study. SAMPE Europe Conference. Madrid (Spain), 2023.

- Meiners D, Budelmann D. Materialcharakterisierung von Prepregs für automatisierte Legeprozesse. WAK Jahresmagazin Kunststofftechnik (2019) 48-52.

- Budelmann D, Meiners D. Haftungseingeschaften duromerer Kohlenstofffaser-Prepregs im Automated Fiber Placement. Tagungsband 4. Symposium Materialtechnik (2021) 641-658.

- Budelmann D, Reichert L, Schmidt C, Meiners D. Design und Herstellung unkonventionell versteifter Flugzeugstrukturen. Sonderprojekte ATZ/MTZ 24 (2019) 46.

Figures

Figure 1-1. Composite laminate manufactured from ¼" carbon fiber/epoxy prepreg slit tapes by automated fiber placement (1) and tack-related laminate defects (2-5).....2

Figure 2-1. Overview of the thesis structure: Chapter sequence and relatedness. 8

Figure 3-1. Development of the structural weight portion of fiber reinforced plastics in civil and military airplanes. Data adapted from [16]. 20

Figure 3-2. Material composition of a modern civil aircraft (Airbus A350XWB). Data and aircraft scheme adapted from [20].....21

Figure 3-3. Evolution of the scientific interest in Automated Fiber Placement and Automated Tape Laying technology based on publication count. 24

Figure 3-4. Simplified workflow of composite part manufacturing via Automated Fiber Placement in the aerospace industry. 26

Figure 3-5. Manufacturing of a CFRP fuselage section by a gantry-attached Automated Fiber Placement head processing thermoset prepregs [Premium AEROTEC]. 27

Figure 3-6. Simplified representation of AFP course placement steps and machine hardware used in placement heads.....28

Figure 3-7. Airbus specification [83] for favorable temperature and humidity ranges (workshop conditions) in thermoset prepreg processing. ...30

Figure 3-8. Generational evolution of carbon fiber/epoxy prepreg composition and architecture used for aerospace applications. Microscopic images taken from [5]. 32

Figure 3-9. Classes and representatives of polymers used as matrix material in commercial prepregs.....34

Figure 3-10. Network formation as a result of epoxy cure reaction shown for TGMDA and DDS.....36

Figure 3-11. Reaction mechanism of epoxy-amine cure.....37

Figure 3-12. View out of an industrial autoclave used for curing large-scale aircraft composite parts made from carbon fiber reinforced plastics [Premium AEROTEC].....39

Figure 3-13. Temperature and qualitative viscosity progression during a typical autoclave cure process for thermoset aerospace-grade epoxy prepregs. 40

Figure 3-14. Types and categorization of defects in prepreg laminates produced during automated fiber placement. Figure adapted and extended from [130]. 41

Figure 4-1. Schematic representation of prepreg tack in automated tape laying (ATL) processes. Adapted from [147] with permission from Elsevier, 2012, and extended by authors. 47

Figure 4-2. Tack-related defect formation in automated lay-up processes. 48

Figure 4-3. Upper figure: Compression (A) and tension/measurement (B) phases in probe tack test; lower figure: 90° (D) and floating roller (E) peel test setups; right figure: Characteristic force/displacement curves (C) and (F). 52

Figure 4-4. Crossley's peel tack and dynamic stiffness measuring equipment. Reprinted from [207] with permission from Elsevier, 2013. 54

Figure 4-5. Bell-shaped curves of prepreg tack as a function of temperature. Left: reprinted from [225] with permission from Wiley, 1992. Center/right: Reprinted from refs. [147] and [184] with permission from Elsevier, 2012 and 2019. 57

Figure 4-6. Tack as a function of compaction force and compaction time at 30 °C probe temperature. Reprinted from [186] with permission from Springer Nature, 2009. Labels were renewed for improved readability. 59

Figure 4-7. Peel tack of automated tape laying (ATL) prepreg tape toward different contact materials. Reprinted from [206] with permission from Taylor & Francis, 2011. Figure labels were renewed for improved readability. 62

Figure 4-8. Effect of room temperature ageing on kinetic properties of carbon fiber/epoxy prepregs. Reprinted from [184] with permission from Elsevier, 2019. 65

Figure 4-9. Prepreg tack as a function of cure level. Reprinted from [219] with permission from Elsevier, 2004. 66

Figure 4-10. Response surfaces of tack (F_{adh}) measured as a function of relative humidity and second input variables (contact time, contact force, and temperature). Reprinted from [183] with permission from the Society for the Advancement of Material and Process Engineering (SAMPE), 2017. Figure labels were renewed for improved readability. 67

Figure 4-11. Loss factor tan δ and complex viscosity of epoxy towpreg resin as a function of temperature (1 Hz, 5 K min^{-1}). Reprinted from [216] with permission from SAGE, 2016. 69

Figure 4-12. Tack curves shifted by time-temperature superposition. Reprinted from [207] with permission from Elsevier, 2013. 70

Figure 4-13. Tack (toughness factor) as a function of impregnation pressure and impregnation temperature. Reprinted from [222] with permission from Wiley, 2004. 72

Figure 4-14. Flowchart presenting dependencies on tack response. Reprinted from [279] with permission from the Society for the Advancement of Material and Process Engineering (SAMPE), 2017. 73

Figure 4-15. Setup for tack measurement according to ASTM D8336 in a universal testing machine. 76

Figure 5-1. Ares G2 rotational rheometer and prepreg sample holder used for probe tack testing. 86

Figure 5-2. Measuring cycle of the probe tack test. 87

Figure 5-3. Stress-strain curves and tack parameters σ_{max} and W_{adh} of fresh prepreg (v_d = 0.2 mm s^{-1}, σ_c = 10 N cm^{-2}). 90

Figure 5-4. Work of adhesion as a function of compaction force and temperature of fresh prepreg. 93

Figure 5-5. Tack (σ_{max}) and CTI_σ as a function of compaction force and prepreg temperature 94

Figure 5-6. Prepreg tack σ_{max} and W_{adh} measured for different displacement rates and temperatures. 95

Figure 5-7. DoC and T_g of room temperature-aged prepreg samples measured by DSC. 97

Figure 5-8. Plateau of temperature-dependent tack properties measured for different prepreg out-times. 98

Figure 5-9. Resin viscosity and tack (σ_{max}) of mat. B towards different surface materials (v_d = 0.2 mm s^{-1}, σ_c = 10 N cm^{-2}). 100

Figure 5-10. Resin viscosity and tack (W_{adh}) of mat. B towards different surface materials (v_d = 0.2 mm s^{-1}, σ_c = 10 N cm^{-2}. 101

Figure 5-11. Correlation between tack and complex viscosity for model and experimental data. 103

Figure 6-1. The temperature-dependent adhesion-cohesion balance of prepreg tack. 110

Figure 6-2. Prepreg resin extraction procedure in tetrahydrofuran. 112

Figure 6-3. Utilized equipment for prepreg tack measurement by probe tack testing. 114

Figure 6-4. Representative pendant drops of water, diiodmethane (room temperature) and prepreg resin (70 °C) hanging from a 1.5 mm blunt cannula for SFT determination. 118

Figure 6-5. Polarity of epoxide (left) and primary amine (right) groups due to high electronegativity of oxygen and nitrogen. 119

Figure 6-6. Sessile drops (~2 µl) and their contact angles of water and diiodmethane on different AFP-related substrates. Seven drops were measured for each liquid/solid combination immediately after drop placement. 120

Figure 6-7. Linear regressions for SFE determination according to the OWRK model. 121

Figure 6-8. Surface free energies σSG with their polar σSGp and dispersive σSGd components. 121

Figure 6-9. Wetting envelopes for fully spreading liquids ($\theta = 0°$) based on the OWRK model. 122

Figure 6-10. Evolution of prepreg resin drops on different substrates over a time span of 10 min (right) after drop placement (left). 123

Figure 6-11. Spreading coefficient SC [mN m^{-1}] isolines for prepreg resin (70 °C) as a function of polar and dispersive SFE components. 124

Figure 6-12. Experimental data and Gaussian model fit of tack between two prepreg plies as a function of temperature. The data is obtained for standard parameters of 10 N mm^{-2} compaction pressure and 5 s compaction time. 125

Figure 6-13. Thermodynamic work of adhesion W_{SL} [mN m^{-1}] isolines as a function of polar and dispersive SFE components. 126

Figure 6-14. Temperature-dependent tack for different surface combinations utilizing the probe test. 127

Figure 6-15. Viscoelastic parameters of extracted prepreg resin within the tack-relevant temperature range. 128

Figure 6-16. Tack between two prepreg plies as function of compaction time (upper graph), compaction pressure (lower graph) and temperature. The dashed line for 50 s compaction was extrapolated due to reaching the load restriction of the test apparatus. 129

Figure 6-17. Frequency-dependent viscoelastic moduli G‘ and G“. Data for low frequencies and high temperatures is not shown due to high fluctuation in this region. Here, curve smoothing was performed by average determination of five adjacent data points. 130

Figure 6-18. Chang windows of neat prepreg resin for different temperatures. 131

Figure 6-19. Surface topographies of the investigated contact materials. Pictures were taken by 3D laser scanning microscopy (2.5x) and scale was normalized. 133

Figure 7-1. Epoxy prepolymers (TGMDA, TGAP, DGEBA), curing agent (4,4’DDS) and thermoplastic toughener (PES) used for prepreg resin formulation and tack characterization. 143

Figure 7-2. Probe tack test setup for neat resin samples attached to an ARES G2 rheometer. 147

Figure 7-3. Flynn-Wall-Ozawa plots of epoxy resin formulations for determining the activation energy E_a and pre-exponential factor A. The linear regression lines for different degrees of conversion (0.1 to 0.9) are shown in an increasing order (left to right). 149

Figure 7-4. Evolution of tack W_t of the investigated epoxy resins (10 wt% PES) as a function of temperature. 150

Figure 7-5. Temperature-dependent rheological data (complex viscosity η^* and storage modulus G’) acquired for different epoxy prepolymers (a, b), B-staging levels (c, d) and toughening contents (e, f) by oscillatory rheometry. 152

Figure 7-6. Temperature-dependent tack W_t of TGMDA resin samples (10 wt% PES) as a function of pre-cure. 154

Figure 7-7. Tack W_t of A-stage TGMDA-based epoxy resin as a function of temperature for different PES toughener contents. 156

Figure 7-8. Characteristic temperatures at maximum tack (T_{max} based on Gaussian model fit) and glass transition (T_g) and their spread ΔT for all investigated prepreg resin formulations.....157

Figure 7-9. Fractional conversion α of the investigated epoxy systems for different heating rates β measured by DSC. 159

Figure 7-10. Apparent activation energies E_a as a function of cure progress. 160

Figure 8-1. The temperature-dependent adhesion-cohesion balance of prepreg tack. 164

Figure 8-2. Schematic representation of the automated fiber placement process. The tack-relevant mechanisms, namely formation of intimate contact (a-b) and autohesion (c) between two prepreg plies are highlighted in orange and schematically specified in the subjacent detail boxes.....168

Figure 8-3. Schematic representation of the 90° peel test setup (upper figure) to be mounted to the rheometer. The lower sequence of figures displays the test procedure with its characteristic steps of compaction (a), the beginning (b) and ending (c) of the debonding/test phase. The axial stress/procedural time graph is for illustration purposes and not true to scale. 169

Figure 8-4. Characteristic contact area images with corresponding DoIC. An exemplarily processed and binarized image is circled in orange. .173

Figure 8-5. DoIC as a function of compaction pressure (left graph for 2 s), compaction time (right graph for 0.1 N mm^{-2}) and test temperature. 174

Figure 8-6. Fitted experimental DoIC data to determine the empirical roughness parameter a.....176

Figure 8-7. Axial stress evolution (idealized) during the isothermal standard test procedure. The dwell time and pressure during the compaction phase as well as temperatures are exemplary and were varied. 177

Figure 8-8. Peel tack obtained from the standard test procedure and corresponding measured DoIC as a function of temperature. 177

Figure 8-9. Test procedure (idealized) to study the influence of debonding temperature on the tackiness of fully contacted prepreg interfaces (100 % DoIC). 178

Figure 8-10. Comparison of tack between fully contacted prepreg ply interfaces (G_{fc}, dark grey), estimated tack for 100 % DoIC (G_{DoiC}, medium grey), tack obtained from the standard (isothermal compaction and debonding) peel test cycle (G_{std}, light grey) and tack after an additional autohesion phase and projected to 100 % DoIC (G_{auto}, white data points, discussed in section 8.4.6). 179

Figure 8-11. Complex viscosity of neat prepreg resin as a function of shear rate and temperature determined by rheometry (dots) and Carreau-Yasuda model fits (continuous lines). 181

Figure 8-12. Relaxation times determined by application of the Carreau-Yasuda rheology model (dots) and exponential regression (line) for data interpolation and extrapolation within the tack-relevant temperature range. 182

Figure 8-13. Isolines of the estimated degree of autohesion D_a as a function of temperature and healing time. 183

Figure 8-14. Peel test procedure (idealized) to study the influence of unpressurized, post-compaction autohesion on prepreg tack. The duration of the autohesion phase and temperatures are exemplary and were varied. 184

Figure 8-15. Model-based prediction of the ply-ply contact after consolidation at different temperatures, lay-up velocities and compaction pressures in an AFP process. 185

Figure 8-16. Process maps showing the estimated tack as a function of lay-up velocity, compaction temperature (rows) and adhesion/debonding temperature (columns) for different time spans after ply-ply consolidation by the compaction roller. Data was generated for constant 5 N mm^{-2} compaction pressure applied over a roller contact length of 50 mm and a debonding rate of 1 mm s^{-1}. 186

Figure 8-17. Storage modulus G‘ and loss modulus G” shifted to different reference temperatures. 188

Figure 8-18. Tack data shifted to different reference temperatures by TTS to predict the fracture energies of fully contacted ply-ply interfaces G_{fc} at different reference temperatures and debonding rates. 189

Figure 8-19. Temperature-dependent bell-shaped curve progression indicative of the validity of the adhesion-cohesion balance for prepreg tackiness. 190

Figure 8-20. Comparison of experimental tack data obtained from the standard isothermal test cycle with tack predicted by the model for equivalent test parameters. 191

Figure 9-1. Digital workshop environment for the prepreg lay-up simulation of the CFRP aircraft part. The lay-up direction of the currently deposited 45° ply is highlighted in blue. 199

Figure 9-2. Simulated lay-up time t_l as a function of desired tack level and compaction temperature for **unheated** molds (compaction pressure: 5 N mm^{-2}, mold temperature after compaction: 20 °C, time after compaction: >250 s) 201

Figure 9-3. Simulated lay-up time t_l as a function of desired tack level and compaction temperature for **heated** molds (compaction pressure: 5 N mm^{-2}, isothermal mold and material, time after compaction: 10 s) 202

Figure 9-4. Prepreg resin formulation map for tack adjustment of TGMDA/DDS systems. Tack values were estimated at 40 °C, 5 N mm^{-2} compaction pressure applied over a roller contact length of 50 mm, 10 s after compaction and 1 mm s^{-1} debonding rate. 203

Figure 10-1. Tack-relevant stages of composite manufacturing from prepregs and corresponding influencing factors. 208

Tables

Table 1-1. Published journal articles of the cumulative thesis.....4

Table 2-1. CRediT – contributor role taxonomy [9] used for this thesis' research articles. 13

Table 2-2. Individual authorship contribution to publication I (chapter 4)....14

Table 2-3. Individual authorship contribution to publication II (chapter 5). .15

Table 2-4. Individual authorship contribution to publication III (chapter 6). 16

Table 2-5. Individual authorship contribution to publication IV (chapter 7). 17

Table 2-6. Individual authorship contribution to publication V (chapter 8). .18

Table 3-1. Comparison of thermosets and thermoplastics used for prepregs. .33

Table 3-2. Characteristic properties of thermoset resins systems used for prepreg production [100]. 35

Table 3-3. Comparison of properties of reinforcing fibers for prepregs production [100]. 38

Table 4-1. AFP/ATL-related influences on prepreg tack. 49

Table 4-2. Overview of experimental studies of ATL/AFP-related influencing factors on prepreg tack. 55

Table 4-3. Publications on the interrelation between lay-up process and prepreg tack since 2020. 77

Table 4-4. Publications with a focus on material properties in conjunction with tack since 2020. 78

Table 4-5. Publications targeting the fundamental mechanisms involved in the stickiness of thermoset prepreg materials since 2020. 78

Table 5-1. Overview of the experimental tack survey. 86

Table 5-2. Shifts between different characteristic temperatures of RT aged prepreg. 99

Table 5-3. Coefficient of determination of the model fit (**Eq. (5.5)**). 102

Table 6-1. Investigated contact materials and their role in automated fiber placement processes. 113

Table 6-2. Parameters for the rheological analysis of neat prepreg resin. 117

Table 6-3. Total surface tension σLG as the sum of the polar σLGp and dispersive σLGd components of standard test liquids and extracted resin from HexPly 8552 prepreg. Literature values [228] and own data are given in mN m^{-1}. 118

Table 6-4. Gaussian model fit parameters and characteristic value. Arithmetic mean values of R_q, λ_0 and W_{SL} are used for surfaces with significant influence of grinding/fiber direction (prepreg and ground steel). The OWRK-based surface polarities are given for comparison reasons with the resin polarity (20.73 %). 135

Table 6-5. DSC and rheological data of the extracted THF/resin mixture after different times of conditioning at 80 °C and 100 mbar. 138

Table 7-1. Reaction-relevant data and components weight proportion for resin formulation..... 144

Table 7-2. Cure enthalpy and glass transition temperatures of A-stage resin formulations. 148

Table 7-3. Temperature at maximum tack T_{max}, maximum tack $W_{t,max}$ and corresponding rheological data. 152

Table 7-4. Residual cure enthalpies, degrees of cure and glass transition temperatures of TGMDA (10 wt.-% PES) resin formulations measured by DSC after B-staging. 153

Table 8-1. Employed peel tack measurement cycles..... 167

Table 8-2. Carreau-Yasuda regression parameters for neat prepreg resin at different temperatures. The last column includes data points of the fitted curve shown in Fig. 8-12..... 194

Table 8-3. Estimated time span to reach a specific degree of autohesion D_a at a specific temperature based on Eq. 8-7..... 194

Table 8-4. Fitted empirical constants C_1 and C_2 for TTS and the corresponding superposition parameters $\log(a_T)$. 195

Table 9-1. Robot speeds, retract/approach settings and ply parameters used for lay-up simulation..... 200

Table 9-2. Simulation results of the AFP manufacturing case study at a lay-up speed of 0.5 m s^{-1}. Full laminate values are calculated for a $[0°/\pm45°/90°]_6$ stacking sequence. 200

Table 9-3. Benefits, drawbacks and suitability of different prepreg tack measurement techniques..... 205

References

[1] Kallas S, Georghegan-Quinn M. Flightpath 2050: Europe's Vision for Aviation. Brussels: European Commission, 2011.
[2] Zepf H-P. Faserverbundwerkstoffe mit thermoplastischer Matrix: Hochleistungswerkstoffe für rationelle Verarbeitung. Renningen-Malmsheim: expert-Verlag, 1997.
[3] Schürmann H. Konstruieren mit Faser-Kunststoff-Verbunden. Berlin, Heidelberg: Springer, 2006.
[4] Lukaszewicz DH-J, Ward C, Potter KD. The engineering aspects of automated prepreg layup: History, present and future. Compos. Part B: Eng. 43 (2012) 997-1009.
[5] Lengsfeld H, Wolff-Fabris F, Krämer J, Lacalle J, Altstädt V. Composite Technology: Prepregs and Monolithic Part Fabrication Technologies. Munich: Carl Hanser, 2015.
[6] Croft K, Lessard L, Pasini D, Hojjati M, Chen J, Yousefpour A. Experimental study of the effect of automated fiber placement induced defects on performance of composite laminates. Compos. Part A: Appl. Sci. Manuf. 42 (2011) 484-491.
[7] Belhaj M, Hojjati M. Wrinkle formation during steering in automated fiber placement: Modeling and experimental verification. J. Reinf. Plast. Compos. 37 (2018) 396-409.
[8] Raos G, Zappone B. Polymer Adhesion: Seeking New Solutions for an Old Problem. Macromolecules 54 (2021) 10617-10644.
[9] Brand A, Allen L, Altman M, Hlava M, Scott J. Beyond authorship: attribution, contribution, collaboration, and credit. Learn. Pub. 28 (2015) 151-155.
[10] Soutis C. Aerospace engineering requirements in building with composites, in: Irving P, Soutis C (Eds.) Polymer Composites in the Aerospace Industry. Cambridge: Woodhead Publishing, 2020.
[11] Akovali G. Handbook of composite fabrication. Shawbury: Rapra Technology Ltd, 2001.
[12] Hsissou R, Seghiri R, Benzekri Z, Hilali M, Rafik M, Elharfi A. Polymer composite materials: A comprehensive review. Compos. Struct. 262 (2021) 113640.
[13] Rajak DK, Pagar DD, Kumar R, Pruncu CI. Recent progress of reinforcement materials: a comprehensive overview of composite materials. J. Mater. Res. Technol. 8 (2019) 6354-6374.
[14] Pleşa I, Noţingher PV, Schlögl S, Sumereder C, Muhr M. Properties of Polymer Composites Used in High-Voltage Applications. Polymers (Basel) 8 (2016).
[15] Rizwee M, Sudhakar Rao P, Khan MY. Recent advancement in electric discharge machining of metal matrix composite materials. Mater. Today Proc. 37 (2021) 2829-2836.
[16] Hiken A. The Evolution of the Composite Fuselage: A Manufacturing Perspective, in: Dekoulis G (Ed.) Aerospace Engineering. London: IntechOpen, 2019.
[17] Mouritz AP. Introduction to aerospace materials. Cambridge: Woodhead Publishing, 2012.
[18] Roeseler WG, Sarh B, Kismarton MA. Composite structures: The first 100 years. International Conference on Composite Materials. Kyoto (Japan), 2007.
[19] Fisher M, Hampe H. Interview with Hinrich Hampe, Toho Tenax. Reinf. Plast. 61 (2017) 330-331.
[20] Piquet B, Blumenfeld L, Birchall D. A350XWB. Airbus FAST Techn. Mag. 9 (2013) 1-25.
[21] Morse L, Mallardo V. Bottom-up manufacturing cost optimisation of composite aircraft structures: Manual layup vs. automated layup. AIP Conf. Proc. 2848 (2023) 20027.
[22] Maass D. Progress in automated ply inspection of AFP layups. Reinf. Plast. 59 (2015) 242-245.
[23] Hale J. Boeing 787: From the ground up. AERO Quarterly 24 (2006) 17-23.
[24] Valorosi F, Meo E de, Blanco-Varela T, Martorana B, Veca A, Pugno N, Kinloch IA, Anagnostopoulos G, Galiotis C, Bertocchi F, Gomez J, Treossi E, Young RJ, Palermo V. Graphene and related materials in hierarchical fiber composites: Production techniques and key industrial benefits. Compos. Sci. Technol. 185 (2020) 107848.
[25] Scelsi L, Bonner M, Hodzic A, Soutis C, Wilson C, Scaife R, Ridgway K. Potential emissions savings of lightweight composite aircraft components evaluated through life cycle assessment. Express Polym. Lett. 5 (2011) 209-217.

[26] Wu M, Sadhukhan J, Murphy R, Bharadwaj U, Cui X. A novel life cycle assessment and life cycle costing framework for carbon fibre-reinforced composite materials in the aviation industry. Int. J. Life Cycle Assess. 28 (2023) 566-589.
[27] Timmis AJ, Hodzic A, Koh L, Bonner M, Soutis C, Schäfer AW, Dray L. Environmental impact assessment of aviation emission reduction through the implementation of composite materials. Int. J. Life Cycle Assess. 20 (2015) 233-243.
[28] van Grootel A, Chang J, Wardle BL, Olivetti E. Manufacturing variability drives significant environmental and economic impact: The case of carbon fiber reinforced polymer composites in the aerospace industry. J. Cleaner Prod. 261 (2020) 121087.
[29] Meng F, Cui Y, Pickering S, McKechnie J. From aviation to aviation: Environmental and financial viability of closed-loop recycling of carbon fibre composite. Compos. Part B: Eng. 200 (2020) 108362.
[30] Rodrigues Dias VM, Jugend D, Camargo Fiorini P de, Razzino CdA, Paula Pinheiro MA. Possibilities for applying the circular economy in the aerospace industry: Practices, opportunities and challenges. J. Air Transp. Manag. 102 (2022) 102227.
[31] Naqvi SR, Prabhakara HM, Bramer EA, Dierkes W, Akkerman R, Brem G. A critical review on recycling of end-of-life carbon fibre/glass fibre reinforced composites waste using pyrolysis towards a circular economy. Resour. Conserv. Recycl. 136 (2018) 118-129.
[32] Borjan D, Knez Ž, Knez M. Recycling of Carbon Fiber-Reinforced Composites-Difficulties and Future Perspectives. Materials (Basel) 14 (2021).
[33] Yazdanbakhsh A, Bank L. A Critical Review of Research on Reuse of Mechanically Recycled FRP Production and End-of-Life Waste for Construction. Polymers (Basel) 6 (2014) 1810-1826.
[34] Witik RA, Teuscher R, Michaud V, Ludwig C, Månson J-AE. Carbon fibre reinforced composite waste: An environmental assessment of recycling, energy recovery and landfilling. Compos. Part A: Appl. Sci. Manuf. 49 (2013) 89-99.
[35] Stieven Montagna L, Ferreira de Melo Morgado G, Lemes AP, Roberto Passador F, Cerqueira Rezende M. Recycling of carbon fiber-reinforced thermoplastic and thermoset composites: A review. J. Thermoplast. Compos. Mater. 36 (2023) 3455-3480.
[36] Benzakein MJ. What does the future bring? A look at technologies for commercial aircraft in the years 2035–2050. Propuls. Power Res. 3 (2014) 165-174.
[37] Grimshaw MN, Grant CG, Diaz JML. Advanced Technology Tape Laying for Affordable Manufacturing of Large Composite Structures. SAMPE North America Conference. Long Beach (USA), 2001.
[38] Brasington A, Sacco C, Halbritter J, Wehbe R, Harik R. Automated fiber placement: A review of history, current technologies, and future paths forward. Compos. Part C: Open Access 6 (2021) 100182.
[39] Grant C. Automated processes for composite aircraft structure. Ind. Robot 33 (2006) 117-121.
[40] Frketic J, Dickens T, Ramakrishnan S. Automated manufacturing and processing of fiber-reinforced polymer (FRP) composites: An additive review of contemporary and modern techniques for advanced materials manufacturing. Addit. Manuf. 14 (2017) 69-86.
[41] Dhinakaran V, Surendar KV, Hasunfur Riyaz MS, Ravichandran M. Review on study of thermosetting and thermoplastic materials in the automated fiber placement process. Mater. Today Proc. 27 (2020) 812-815.
[42] Kostopoulos V, Masouras A, Baltopoulos A, Vavouliotis A, Sotiriadis G, Pambaguian L. A critical review of nanotechnologies for composite aerospace structures. CEAS Space J. 9 (2017) 35-57.
[43] Greenhalgh E, Hiley M. The assessment of novel materials and processes for the impact tolerant design of stiffened composite aerospace structures. Compos. Part A: Appl. Sci. Manuf. 34 (2003) 151-161.
[44] Yassin K, Hojjati M. Processing of thermoplastic matrix composites through automated fiber placement and tape laying methods. J. Thermoplast. Compos. Mater. 31 (2018) 1676-1725.
[45] Di Boon Y, Joshi SC, Bhudolia SK. Review: Filament Winding and Automated Fiber Placement with In Situ Consolidation for Fiber Reinforced Thermoplastic Polymer Composites. Polymers (Basel) 13 (2021).

[46] Sun S, Han Z, Fu H, Jin H, Dhupia JS, Wang Y. Defect Characteristics and Online Detection Techniques During Manufacturing of FRPs Using Automated Fiber Placement: A Review. Polymers (Basel) 12 (2020).
[47] Heinecke F, Willberg C. Manufacturing-Induced Imperfections in Composite Parts Manufactured via Automated Fiber Placement. J. Compos. Sci. 3 (2019) 56.
[48] Chevalier PL, Kassapoglou C, Gürdal Z. Fatigue behavior of composite laminates with automated fiber placement induced defects- a review. Int. J. Fatigue 140 (2020) 105775.
[49] Meister S, Wermes MAM, Stüve J, Groves RM. Review of image segmentation techniques for layup defect detection in the Automated Fiber Placement process. J. Intell. Manuf. 32 (2021) 2099-2119.
[50] Oromiehie E, Prusty BG, Compston P, Rajan G. Automated fibre placement based composite structures: Review on the defects, impacts and inspections techniques. Compos. Struct. 224 (2019) 110987.
[51] Rousseau G, Wehbe R, Halbritter J, Harik R. Automated Fiber Placement Path Planning: A state-of-the-art review. CAD&A 16 (2018) 172-203.
[52] Budelmann D, Schmidt C, Meiners D. Prepreg tack: A review of mechanisms, measurement, and manufacturing implication. Polym. Compos. 41 (2020) 3440-3458.
[53] Pora J. Composite Materials in the Airbus A380 - From History to Future. International Conference on Composite Materials. Beijing (China), 2001.
[54] Soutis C. Fibre reinforced composites in aircraft construction. Prog. Aerosp. Sci. 41 (2005) 143-151.
[55] Cantor B, Assender H, Grant P. Aerospace Materials. Boca Raton: CRC Press, 2015.
[56] Johnson AF, Thomson RS, David M, Joosten MW. Design and testing of crashworthy aerospace composite components, in: Irving P, Soutis C (Eds.) Polymer Composites in the Aerospace Industry. Cambridge: Woodhead Publishing, 2020.
[57] Katnam KB, da Silva L, Young TM. Bonded repair of composite aircraft structures: A review of scientific challenges and opportunities. Prog. Aerosp. Sci. 61 (2013) 26-42.
[58] Halbritter J, Harik R, Saidy C, Noevere A, Grimsley BW. Automation of AFP Process Planning Functions: Importance and Ranking. SAMPE North America Conference. Charlotte (USA), 2019.
[59] Qu W, He R, Cheng L, Di Yang, Gao J, Wang H, Yang Q, Ke Y. Placement suitability analysis of automated fiber placement on curved surfaces considering the influence of prepreg tow, roller and AFP machine. Compos. Struct. 262 (2021) 113608.
[60] Huang G, Wang H, Li G. An efficient reanalysis assisted optimization for variable-stiffness composite design by using path functions. Compos. Struct. 153 (2016) 409-420.
[61] Honda S, Igarashi T, Narita Y. Multi-objective optimization of curvilinear fiber shapes for laminated composite plates by using NSGA-II. Compos. Part B: Eng. 45 (2013) 1071-1078.
[62] Blom AW, Abdalla MM, Gürdal Z. Optimization of course locations in fiber-placed panels for general fiber angle distributions. Compos. Sci. Technol. 70 (2010) 564-570.
[63] Blom AW, Stickler PB, Gürdal Z. Optimization of a composite cylinder under bending by tailoring stiffness properties in circumferential direction. Compos. Part B: Eng. 41 (2010) 157-165.
[64] Shirinzadeh B, Cassidy G, Oetomo D, Alici G, Ang Jr MH. Trajectory generation for open-contoured structures in robotic fibre placement. Rob. Comput. Integr. Manuf. 23 (2007) 380-394.
[65] Yan L, Chen ZC, Shi Y, Mo R. An accurate approach to roller path generation for robotic fibre placement of free-form surface composites. Rob. Comput. Integr. Manuf. 30 (2014) 277-286.
[66] Zamani Z, Haddadpour H, Ghazavi MR. Curvilinear fiber optimization tools for design thin walled beams. Thin-Walled Struct. 49 (2011) 448-454.
[67] Haddadpour H, Zamani Z. Curvilinear fiber optimization tools for aeroelastic design of composite wings. J. Fluids Struct. 33 (2012) 180-190.
[68] Jeffries KA. Enhanced Robotic Automated Fiber Placement with Accurate Robot Technology and Modular Fiber Placement Head. SAE Int. J. Aerosp. 6 (2013) 774-779.

[69] Yousefi N, Evans AD, Harper LT, Maples HA, James T, Bismarck A. Solid epoxy resin systems for automated composite manufacturing. Compos. Part A: Appl. Sci. Manuf. 142 (2021) 106205.
[70] Denkena B, Schmidt C, Weber P. Automated Fiber Placement Head for Manufacturing of Innovative Aerospace Stiffening Structures. Procedia Manuf. 6 (2016) 96-104.
[71] Bakhshi N, Hojjati M. Effect of compaction roller on layup quality and defects formation in automated fiber placement. J. Reinf. Plast. Compos. 39 (2020) 3-20.
[72] Lichtinger R, Lacalle J, Hinterhölzl R, Beier U, Drechsler K. Simulation and experimental validation of gaps and bridging in the automated fiber placement process. Sci. Eng. Compos. Mater. 22 (2015).
[73] Jiang J, He Y, Wang H, Ke Y. Modeling and experimental validation of compaction pressure distribution for automated fiber placement. Compos. Struct. 256 (2021) 113101.
[74] Bahar M, Sinapius M. Adaptive Feeding Roller with An Integrated Cutting System for Automated Fiber Placement (AFP). J. Compos. Sci. 4 (2020) 92.
[75] Alhajahmad A, Abdalla MM, Gürdal Z. Optimal Design of Tow-Placed Fuselage Panels for Maximum Strength with Buckling Considerations. J. Aircraft 47 (2010) 775-782.
[76] Mejlej VG, Falkenberg P, Türck E, Vietor T. Optimization of Variable Stiffness Composites in Automated Fiber Placement Process using Evolutionary Algorithms. Procedia CIRP 66 (2017) 79-84.
[77] Oromiehie E, Prusty BG, Rajan G, Wanigasekara C, Swain A. Machine learning based process monitoring and characterisation of automated composites. SAMPE North America Conference. Seattle (USA), 2017.
[78] Measom R, Sewell K. Fiber placement low cost production for complex composite structures. American Helicopter Society's Annual Forum. Washington (USA), 1996.
[79] Raspall F, Velu R, Vaheed NM. Fabrication of complex 3D composites by fusing automated fiber placement (AFP) and additive manufacturing (AM) technologies. Adv. Manuf. Polym. Compos. Sci. 5 (2019) 6-16.
[80] Rakhshbahar M, Sinapius M. A Novel Approach: Combination of Automated Fiber Placement (AFP) and Additive Layer Manufacturing (ALM). J. Compos. Sci. 2 (2018) 42.
[81] Zhao C, Wang X, Liu X, Ma C, Chu Q, Xiao J. Study of integral hat-stiffened composite structures manufactured by automated fiber placement and co-curing process. Compos. Struct. 246 (2020) 112427.
[82] Pansart S. Prepreg processing of advanced fibre-reinforced polymer (FRP) composites, in: Bai J (Ed.) Advanced Fibre-Reinforced Polymer (FRP) Composites for Structural Applications. Cambridge: Woodhead Publishing, 2013.
[83] Airbus Process Instruction AIPI 03-02-018. Manufacture of Structural Sandwich Parts with Thermosetting Fiber Reinforced Skins. Blagnac (France): Airbus S.A.S., 2007.
[84] Cuntze R. Technical Terms for Composite Parts: Glossary for Civil- and Mechanical Engineering. Wiesbaden: Springer, 2019.
[85] Mallick PK. Materials, design and manufacturing for lightweight vehicles. Oxford: Woodhead Publishing, 2021.
[86] Ratna D, Banthia AK. Rubber toughened epoxy. Macromol. Res. 12 (2004) 11-21.
[87] Mousavi SR, Estaji S, Raouf Javidi M, Paydayesh A, Khonakdar HA, Arjmand M, Rostami E, Jafari SH. Toughening of epoxy resin systems using core–shell rubber particles: a literature review. J. Mater. Sci. 56 (2021) 18345-18367.
[88] Bagheri R, Marouf BT, Pearson RA. Rubber-Toughened Epoxies: A Critical Review. Polym. Rev. 49 (2009) 201-225.
[89] Hodgkin JH, Simon GP, Varley RJ. Thermoplastic toughening of epoxy resins: a critical review. Polym. Adv. Technol. 9 (1998) 3-10.
[90] Farooq U, Teuwen J, Dransfeld C. Toughening of Epoxy Systems with Interpenetrating Polymer Network (IPN): A Review. Polymers (Basel) 12 (2020).
[91] Unnikrishnan KP, Thachil ET. Toughening of epoxy resins. Des. Monomers Polym. 9 (2006) 129-152.

[92] Moosburger-Will J, Jäger J, Horn S, Wellhausen C. Investigation of phase morphology of polyetherimide-toughened epoxy resin by scanning probe microscopy. Polym. Test. 31 (2012) 1008-1018.
[93] Zhang H, Bharti A, Li Z, Du S, Bilotti E, Peijs T. Localized toughening of carbon/epoxy laminates using dissolvable thermoplastic interleaves and electrospun fibres. Compos. Part A: Appl. Sci. Manuf. 79 (2015) 116-126.
[94] Wetzel B, Rosso P, Haupert F, Friedrich K. Epoxy nanocomposites – fracture and toughening mechanisms. Eng. Fract. Mech. 73 (2006) 2375-2398.
[95] Shivakumar KN, Panduranga R, Sharpe M. Interleaved Polymer Matrix Composites - A Review. 54th AIAA/ASME/ASCE/AHS/ASC Structures, Structural Dynamics, and Materials Conference. Boston (USA), 2013.
[96] Shakil UA, Hassan SBA, Yahya MY, Nauman S. Mechanical properties of electrospun nanofiber reinforced/interleaved epoxy matrix composites - A review. Polym. Compos. 41 (2020) 2288-2315.
[97] Chen H, Li S, Wang J, Ding A. A focused review on the thermo-stamping process and simulation progresses of continuous fibre reinforced thermoplastic composites. Compos. Part B: Eng. 224 (2021) 109196.
[98] Parameswaranpillai J, Pulikkalparambil H, Rangappa SM, Siengchin S. Epoxy Composites: Fabrication, Characterization and Applications. Weinheim: Wiley, 2021.
[99] Strong AB. Fundamentals of composites manufacturing: Materials, methods and applications. Dearborn: Society of Manufacturing Engineers, 2008.
[100] Yi X, Du S, Zhang L. Composite Materials Engineering, Volume 2. Singapore: Springer, 2018.
[101] Jin F-L, Li X, Park S-J. Synthesis and application of epoxy resins: A review. J. Ind. Eng. Chem. 29 (2015) 1-11.
[102] Fache M, Montérémal C, Boutevin B, Caillol S. Amine hardeners and epoxy cross-linker from aromatic renewable resources. Eur. Polym. J. 73 (2015) 344-362.
[103] Ignatenko VY, Ilyin SO, Kostyuk AV, Bondarenko GN, Antonov SV. Acceleration of epoxy resin curing by using a combination of aliphatic and aromatic amines. Polym. Bull. 77 (2020) 1519-1540.
[104] Darroman E, Bonnot L, Auvergne R, Boutevin B, Caillol S. New aromatic amine based on cardanol giving new biobased epoxy networks with cardanol. Eur. J. Lipid Sci. Technol. 117 (2015) 178-189.
[105] Liu T, Zhang L, Chen R, Wang L, Han B, Meng Y, Li X. Nitrogen-Free Tetrafunctional Epoxy and Its DDS-Cured High-Performance Matrix for Aerospace Applications. Ind. Eng. Chem. Res. 56 (2017) 7708-7719.
[106] Guadagno L, Raimondo M, Vittoria V, Vertuccio L, Naddeo C, Russo S, Vivo B de, Lamberti P, Spinelli G, Tucci V. Development of epoxy mixtures for application in aeronautics and aerospace. RSC Adv. 4 (2014) 15474-15488.
[107] Yi J-W, Um M-K, Byun J-H, Lee S-B, Lee S-K. Development of high Tg epoxy resin and mechanical properties of its fiber-reinforced composites. J. Appl. Polym. Sci. 127 (2013) 4328-4333.
[108] Hill DJT, George GA, Rogers DG. A systematic study of the microwave and thermal cure kinetics of the DGEBA/DDS and DGEBA/DDM epoxy-amine resin systems. Polym. Adv. Technol. 13 (2002) 353-362.
[109] Cai H, Li P, Sui G, Yu Y, Li G, Yang X, Ryu S. Curing kinetics study of epoxy resin/flexible amine toughness systems by dynamic and isothermal DSC. Thermochim. Acta 473 (2008) 101-105.
[110] Sbirrazzuoli N, Vyazovkin S, Mititelu A, Sladic C, Vincent L. A Study of Epoxy-Amine Cure Kinetics by Combining Isoconversional Analysis with Temperature Modulated DSC and Dynamic Rheometry. Macromol. Chem. Phys. 204 (2003) 1815-1821.
[111] Garschke C, Parlevliet PP, Weimer C, Fox BL. Cure kinetics and viscosity modelling of a high-performance epoxy resin film. Polym. Test. 32 (2013) 150-157.
[112] Pramanik M, Fowler EW, Rawlins JW. Cure kinetics of several epoxy–amine systems at ambient and high temperatures. J. Coat. Technol. Res. 11 (2014) 143-157.

[113] Opalicki M, Kenny JM, Nicolais L. Cure kinetics of neat and carbon-fiber-reinforced TGDDM/DDS epoxy systems. J. Appl. Polym. Sci. 61 (1996) 1025-1037.
[114] Cole KC, Hechler JJ, Noel D. A new approach to modeling the cure kinetics of epoxy/amine thermosetting resins. 2. Application to a typical system based on bis[4-(diglycidylamino) phenyl]methane and bis(4-aminophenyl) sulfone. Macromolecules 24 (1991) 3098-3110.
[115] Wu F, Zhou X, Yu X. Reaction mechanism, cure behavior and properties of a multifunctional epoxy resin, TGDDM, with latent curing agent dicyandiamide. RSC Adv. 8 (2018) 8248-8258.
[116] Bledzki AK, Seidlitz H, Goracy K, Urbaniak M, Rösch JJ. Recycling of Carbon Fiber Reinforced Composite Polymers-Review-Part 1: Volume of Production, Recycling Technologies, Legislative Aspects. Polymers (Basel) 13 (2021).
[117] Witten E, Mathes V. The European Market for Fibre Reinforced Plastics/ Composites in 2021: Market developments, trends, challenges and outlook. AVK Market Reports (2022).
[118] Krauklis AE, Karl CW, Gagani AI, Jørgensen JK. Composite Material Recycling Technology - State-of-the-Art and Sustainable Development for the 2020s. J. Compos. Sci. 5 (2021) 28.
[119] Tane M, Okuda H, Tanaka F. Nanocomposite microstructures dominating anisotropic elastic modulus in carbon fibers. Acta Mater. 166 (2019) 75-84.
[120] Deng K, Zhang C, Dong X, Fu KK. Rapid and energy-efficient manufacturing of thermoset prepreg via localized in-plane thermal assist (LITA) technique. Compos. Part A: Appl. Sci. Manuf. 161 (2022) 107121.
[121] Çelik M, Noble T, Jorge F, Jian R, Ó Brádaigh CM, Robert C. Influence of Line Processing Parameters on Properties of Carbon Fibre Epoxy Towpreg. J. Compos. Sci. 6 (2022) 75.
[122] Gilbert EN, Hayes BS, Seferis JC. Interlayer toughened unidirectional carbon prepreg systems: effect of preformed particle morphology. Compos. Part A: Appl. Sci. Manuf. 34 (2003) 245-252.
[123] Liu L, Zhang B-M, Wang D-F, Wu Z-J. Effects of cure cycles on void content and mechanical properties of composite laminates. Compos. Struct. 73 (2006) 303-309.
[124] Upadhya AR, Dayananda GN, Kamalakannan GM, Ramaswamy Setty J, Christopher Daniel J. Autoclaves for Aerospace Applications: Issues and Challenges. Int. J. Aerosp. Eng. 2011 (2011) 1-11.
[125] Mallow AR, Campbell FC. Autoclave Processing, in: Davé R, Loos A (Eds.) Processing of Composites. München: Carl Hanser, 2000.
[126] Centea T, Grunenfelder LK, Nutt SR. A review of out-of-autoclave prepregs – Material properties, process phenomena, and manufacturing considerations. Compos. Part A: Appl. Sci. Manuf. 70 (2015) 132-154.
[127] Nele L, Caggiano A, Teti R. Autoclave Cycle Optimization for High Performance Composite Parts Manufacturing. Procedia CIRP 57 (2016) 241-246.
[128] Wang L, Zhu W, Wang Q, Xu Q, Ke Y. A heat-balance method for autoclave process of composite manufacturing. J. Compos. Mater. 53 (2019) 641-652.
[129] Aymonier A, Papon E, Castelein G, Brogly M, Tordjeman P. Influence of surface and bulk structures of acrylic PSA films onto their tack properties. J. Colloid Interface Sci. 268 (2003) 341-347.
[130] Denkena B, Schmidt C, Völtzer K, Hocke T. Thermographic online monitoring system for Automated Fiber Placement processes. Compos. Part B: Eng. 97 (2016) 239-243.
[131] Wang Y, Mahapatra S, P.-H. Belnoue J, Ivanov DS, Hallett SR. Modelling the effect of process conditions on steering-induced defects in automated fibre placement (AFP). Compos. Part A: Appl. Sci. Manuf. 173 (2023) 107702.
[132] Nelson ES, Reddy DR. Green Aviation: Reduction of Environmental Impact Through Aircraft Technology and Alternative Fuels. Boca Raton: CRC Press, 2018.
[133] Siddiqui T. Aircraft materials and analysis. New York: McGraw-Hill Education, 2015.
[134] Bajpai PK, Singh I. Reinforced Polymer Composites: Processing, Characterization and Post Life Cycle Assessment. Weinheim: Wiley, 2019.
[135] Jawaid M, Thariq M. Sustainable Composites for Aerospace Applications. Amsterdam: Elsevier Science, 2018.

[136] Campbell FC. Manufacturing Technology for Aerospace Structural Materials. Amsterdam: Elsevier Science, 2011.
[137] Liu Y-N, Yuan C, Liu C, Pan J, Dong Q. Study on the resin infusion process based on automated fiber placement fabricated dry fiber preform. Sci. Rep. 9 (2019) 7440.
[138] Smith RP, Qureshi Z, Scaife RJ, El-Dessouky HM. Limitations of processing carbon fibre reinforced plastic/polymer material using automated fibre placement technology. J. Reinf. Plast. Compos. 35 (2016) 1527-1542.
[139] Marsh G. Automating aerospace composites production with fibre placement. Reinf. Plast. 55 (2011) 32-37.
[140] Benedek I. Developments In Pressure-Sensitive Products. Boca Raton: CRC Press, 2005.
[141] Ebnesajjad S, Landrock AH. Adhesives Technology Handbook. Amsterdam: Elsevier Science, 2014.
[142] Brockmann W, Geiß PL, Klingenberg J, Schröder B. Adhesive bonding: Materials, applications and technology. Weinheim: Wiley, 2009.
[143] Gillanders AM, Kerr S, Martin TJ. Determination of prepreg tack. Int. J. Adhes. Adhes. 1 (1981) 125-134.
[144] Stone KL. Automation in composite processing. SAMPE North America Conference. Reno (USA), 1984.
[145] Eaton HL. Cost effective tape laying. SAMPE North America Conference. Reno (USA), 1984.
[146] Meier RA. An advanced control system for composite material placement. SAMPE North America Conference. Covina (USA), 1986.
[147] Crossley RJ, Schubel PJ, Warrior NA. The experimental determination of prepreg tack and dynamic stiffness. Compos. Part A: Appl. Sci. Manuf. 43 (2012) 423-434.
[148] Brooks TR, Martins JR. On manufacturing constraints for tow-steered composite design optimization. Compos. Struct. 204 (2018) 548-559.
[149] Shadmehri F, Ioachim O, Pahud O, Brunel JE, Landry A, Hoa SV, Hojjati M. Laser-vision inspection system for automated fiber placement (AFP) process. International Conference on Composite Materials. Copenhagen (DK), 2015.
[150] Belnoue JP-H, Mesogitis T, Nixon-Pearson OJ, Kratz J, Ivanov DS, Partridge IK, Potter KD, Hallett SR. Understanding and predicting defect formation in automated fibre placement pre-preg laminates. Compos. Part A: Appl. Sci. Manuf. 102 (2017) 196-206.
[151] Li X, Hallett SR, Wisnom MR. Modelling the effect of gaps and overlaps in automated fibre placement (AFP)-manufactured laminates. Sci. Eng. Compos. Mater. 22 (2015).
[152] Dodwell TJ, Butler R, Hunt GW. Out-of-plane ply wrinkling defects during consolidation over an external radius. Compos. Sci. Technol. 105 (2014) 151-159.
[153] Brüning J, Denkena B, Dittrich M-A, Hocke T. Machine Learning Approach for Optimization of Automated Fiber Placement Processes. Procedia CIRP 66 (2017) 74-78.
[154] Nguyen MH, Vijayachandran AA, Davidson P, Call D, Lee D, Waas AM. Effect of Automated Fiber Placement (AFP) Manufacturing Signature on Mechanical Performance. AIAA Scitech 2019 Forum. San Diego (USA), 2019.
[155] Falcó O, Mayugo JA, Lopes CS, Gascons N, Costa J. Variable-stiffness composite panels: Defect tolerance under in-plane tensile loading. Compos. Part A: Appl. Sci. Manuf. 63 (2014) 21-31.
[156] Woigk W, Hallett SR, Jones MI, Kuhtz M, Hornig A, Gude M. Experimental investigation of the effect of defects in Automated Fibre Placement produced composite laminates. Compos. Struct. 201 (2018) 1004-1017.
[157] Sawicki A, Minguett P. The effect of intraply overlaps and gaps upon the compression strength of composite laminates. 39th AIAA/ASME/ASCE/AHS/ASC Structures, Structural Dynamics, and Materials Conference and Exhibit. Long Beach (USA), 1998.
[158] Matveev MY, Schubel PJ, Long AC, Jones IA. Understanding the buckling behaviour of steered tows in Automated Dry Fibre Placement (ADFP). Compos. Part A: Appl. Sci. Manuf. 90 (2016) 451-456.
[159] Bakhshi N, Hojjati M. Time-dependent wrinkle formation during tow steering in automated fiber placement. Compos. Part B: Eng. 165 (2019) 586-593.

[160] Bakhshi N, Hojjati M. An experimental and simulative study on the defects appeared during tow steering in automated fiber placement. Compos. Part A: Appl. Sci. Manuf. 113 (2018) 122-131.
[161] Chen J, Chen-Keat T, Hojjati M, Vallee AJ, Octeau M-A, Yousefpour A. Impact of layup rate on the quality of fiber steering/cut-restart in automated fiber placement processes. Sci. Eng. Compos. Mater. 22 (2015).
[162] Zhao C, Xiao J, Huang W, Huang X, Gu S. Layup quality evaluation of fiber trajectory based on prepreg tow deformability for automated fiber placement. J. Reinf. Plast. Compos. 35 (2016) 1576-1585.
[163] Lichtinger R, Tang T, Drechsler K. Peel tack simulation with applied cohesive fracture in reference to feed rate and compaction force. European Conference on Composite Materials. Vienna (Austria), 2012.
[164] Nilakantan G, Nutt S. Reuse and upcycling of thermoset prepreg scrap: Case study with out-of-autoclave carbon fiber/epoxy prepreg. J. Compos. Mater. 52 (2018) 341-360.
[165] Oldani T. Increasing productivity in fiber placement processes. SAE Aerospace Manufacturing and Automated Fastening Conference & Exhibition. North Charleston (USA), 2008.
[166] Hagnell MK, Åkermo M. A composite cost model for the aeronautical industry: Methodology and case study. Compos. Part B: Eng. 79 (2015) 254-261.
[167] Schubel PJ. Cost modelling in polymer composite applications: Case study – Analysis of existing and automated manufacturing processes for a large wind turbine blade. Compos. Part B: Eng. 43 (2012) 953-960.
[168] Mills A. Automation of carbon fibre preform manufacture for affordable aerospace applications. Compos. Part A: Appl. Sci. Manuf. 32 (2001) 955-962.
[169] Mohammed IK, Charalambides MN, Kinloch AJ. Modelling the interfacial peeling of pressure-sensitive adhesives. J. Non-Newtonian Fluid Mech. 222 (2015) 141-150.
[170] ASTM D2979-16. Test Method for Pressure-Sensitive Tack of Adhesives Using an Inverted Probe Machine. West Conshohocken: ASTM International, 2016.
[171] Kajtna J, Krajnc M. UV crosslinkable microsphere pressure sensitive adhesives—influence on adhesive properties. Int. J. Adhes. Adhes. 31 (2011) 29-35.
[172] Fujita M, Kajiyama M, Takemura A, Ono H, Mizumachi H, Hayashi S. Effects of miscibility on probe tack of natural-rubber-based pressure-sensitive adhesives. J. Appl. Polym. Sci. 70 (1998) 771-776.
[173] Kim B-J, Kim S-E, Do H-S, Kim S, Kim H-J. Probe tack of tackified acrylic emulsion PSAs. Int. J. Adhes. Adhes. 27 (2007) 102-107.
[174] Drzal PL, Shull KR. Adhesive Failure of Model Acrylic Pressure Sensitive Adhesives. J. Adhes. 81 (2005) 397-415.
[175] Zosel A. Adhesion and tack of polymers: Influence of mechanical properties and surface tensions. Colloid. Polym. Sci. 263 (1985) 541-553.
[176] Lakrout H, Sergot P, Creton C. Direct Observation of Cavitation and Fibrillation in a Probe Tack Experiment on Model Acrylic Pressure-Sensitive-Adhesives. J. Adhes. 69 (1999) 307-359.
[177] Yamaguchi T, Doi M. Debonding dynamics of pressure-sensitive adhesives: 3D block model. Eur. Phys. J. E 21 (2006) 331-339.
[178] Nakamura Y, Imamura K, Yamamura K, Fujii S, Urahama Y. Influence of crosslinking and peeling rate on tack properties of polyacrylic pressure-sensitive adhesives. J. Adhes. Sci. Technol. 27 (2013) 1951-1965.
[179] Hammond FH. Polyken Probe Tack Tester. Adhesion (ASTM International). West Conshohocken (USA), 1964.
[180] Creton C, Hooker J, Shull KR. Bulk and Interfacial Contributions to the Debonding Mechanisms of Soft Adhesives: Extension to Large Strains. Langmuir 17 (2001) 4948-4954.
[181] Kim H-J, Hayashi S, Mizumachi H. Miscibility and fracture energy of probe tack for acrylic pressure-sensitive adhesives: acrylic copolymer/tackifier resin systems. J. Appl. Polym. Sci. 69 (1998) 581-587.
[182] Dillard DA, Pocius AV. The Mechanics of Adhesion. Amsterdam: Elsevier Science, 2002.

[183] Wohl C, Palmieri F, Forghani A, Hickmott CW, Bedayat H, Coxon B, Poursartip A, Grimsley BW. Tack measurements of prepreg tape at variable temperature and humidity. Composites and Advanced Materials Expo. Orlando (USA), 2017.
[184] Budelmann D, Detampel H, Schmidt C, Meiners D. Interaction of process parameters and material properties with regard to prepreg tack in automated lay-up and draping processes. Compos. Part A: Appl. Sci. Manuf. 117 (2019) 308-316.
[185] Smith EJ, Grubb C, Misasi J, Larson N. Developing a Procedure for Prepreg Tack Characterization. Composites and Advanced Materials Expo. Anaheim (USA), 2019.
[186] Dubois O, Le Cam J-B, Béakou A. Experimental Analysis of Prepreg Tack. Exp. Mech. 50 (2010) 599-606.
[187] Peykova Y, Lebedeva OV, Diethert A, Müller-Buschbaum P, Willenbacher N. Adhesive properties of acrylate copolymers: Effect of the nature of the substrate and copolymer functionality. Int. J. Adhes. Adhes. 34 (2012) 107-116.
[188] da Silva L, Dillard DA, Blackman B, Adams RD. Testing Adhesive Joints: Best Practices. Weinheim: Wiley, 2012.
[189] ASTM D6862-11. Test Method for 90 Degree Peel Resistance of Adhesives. West Conshohocken: ASTM International, 2016.
[190] ASTM D903-98. Test Method for Peel or Stripping Strength of Adhesive Bonds. West Conshohocken: ASTM International, 2017.
[191] ASTM D1876-08. Test Method for Peel Resistance of Adhesives (T-Peel Test). West Conshohocken: ASTM International, 2015.
[192] ASTM D3167-10. Test Method for Floating Roller Peel Resistance of Adhesives. West Conshohocken: ASTM International, 2017.
[193] ASTM D1781-98. Test Method for Climbing Drum Peel for Adhesives. West Conshohocken: ASTM International, 2012.
[194] ASTM D3330/D3330M-04. Test Method for Peel Adhesion of Pressure-Sensitive Tape. West Conshohocken: ASTM International, 2018.
[195] Aubrey DW, Welding GN, Wong T. Failure mechanisms in peeling of pressure-sensitive adhesive tape. J. Appl. Polym. Sci. 13 (1969) 2193-2207.
[196] Sherriff M, Knibbs RW, Langley PG. Mechanism for the action of tackifying resins in pressure-sensitive adhesives. J. Appl. Polym. Sci. 17 (1973) 3423-3438.
[197] Nakajima N, Babrowicz R, Harrell ER. Rheology, composition, and peel-mechanism of block copolymer–tackifier-based pressure sensitive adhesives. J. Appl. Polym. Sci. 44 (1992) 1437-1456.
[198] Benyahia L, Verdier C, Piau J-M. The Mechanisms of Peeling of Uncross-Linked Pressure Sensitive Adhesives. J. Adhes. 62 (1997) 45-73.
[199] ASTM D6195-03. Test Methods for Loop Tack. West Conshohocken: ASTM International, 2019.
[200] ASTM D3121-17. Test Method for Tack of Pressure-Sensitive Adhesives by Rolling Ball. West Conshohocken: ASTM International, 2017.
[201] Kowalski A, Czech Z. The effects of substrate surface properties on tack performance of acrylic Pressure-Sensitive Adhesives (PSAs). Int. J. Adhes. Adhes. 60 (2015) 9-15.
[202] Woo Y, Plaut RH, Dillard DA, Coulthard SL. Experiments and inelastic analysis of the loop tack test for pressure-sensitive adhesives. J. Adhes. 80 (2004) 203-221.
[203] Petersen, Link RE, Miyagi Z, Yamada N, Urahama N, Yamamoto K. Analysis of Plowing and Adhesive Effects in the Rolling Ball Tack Method for Pressure Sensitive Adhesives. J. Test. Eval. 25 (1997) 23.
[204] Mizumachi H, Saito T. Rolling Motion of a Ball on Pressure Sensitive Adhesives. J. Adhes. 20 (1986) 83-97.
[205] Crossley RJ, Schubel PJ, Warrior NA. The experimental characterisation of prepreg tack. International Conference on Composite Materials. Edingbourgh (UK), 2009.
[206] Crossley RJ, Schubel PJ, Warrior NA. Experimental determination and control of prepreg tack for automated manufacture. Plast. Rubber Compos. 40 (2011) 363-368.

[207] Crossley RJ, Schubel PJ, Focatiis D de. Time–temperature equivalence in the tack and dynamic stiffness of polymer prepreg and its application to automated composites manufacturing. Compos. Part A: Appl. Sci. Manuf. 52 (2013) 126-133.
[208] Endruweit A, Focatiis DSA de, Warrior NA, Ghose S, Johnson BA, Younkin DR. Characterization of Prepreg Tack to Aid Automated Material Placement. SAMPE North America Conference. Long Beach (USA), 2016.
[209] Endruweit A, Choong GY, Ghose S, Johnson BA, Younkin DR, Warrior NA, Focatiis DS de. Characterisation of tack for uni-directional prepreg tape employing a continuous application-and-peel test method. Compos. Part A: Appl. Sci. Manuf. 114 (2018) 295-306.
[210] Crossley RJ. Characterisation of tack for automated tape laying. Doctoral Thesis. Nottingham: University of Nottingham, 2011.
[211] Böckl B, Jetten C, Heller K, Ebel C, Drechsler K. Assessment of the tack of prepreg slit tapes during the Automated Fiber Placement process. SICOMP Conference on Manufacturing and Design of Composites. Lulea (Sweden), 2018.
[212] Böckl B, Jetten C, Heller K, Ebel C, Drechsler K. Online Monitoring System for the Tack of Prepreg Slit Tapes Used in Automated Fiber Placement. EuropeanConference on Composite Materials. Athens (Greece), 2018.
[213] ASTM D1002-10. Test Method for Apparent Shear Strength of Single-Lap-Joint Adhesively Bonded Metal Specimens by Tension Loading (Metal-to-Metal). West Conshohocken: ASTM International, 2019.
[214] Nguyen DC, Krombholz C. Influence of process parameters and material ageing on the adhesion of prepreg in AFP processes. European Conference on Composite Materials. Munich (Germany), 2016.
[215] Nguyen DC, Delisle D. First ply tack of an automated fiber placement process - Influence of heatable mould surface, release films and process parameters. SAMPE Europe Conference. Stuttgart, 2017.
[216] Rao S, Umer R, Thomas J, Cantwell WJ. Investigation of peel resistance during the fibre placement process. J. Reinf. Plast. Compos. 35 (2016) 275-286.
[217] Rajaei M, Beheshty MH, Hayaty M. Preparation and Processing Characterization of Glass/Phenolic Prepregs. Polym. Polym. Compos. 19 (2011) 789-796.
[218] Shaghaghi S, Beheshty MH, Rahimi H. Preparation and Rheological Characterization of Phenolic/Glass Prepregs. Iran. Polym. J. 20 (2011) 969-977.
[219] Banks R, Mouritz AP, John S, Coman F, Paton R. Development of a new structural prepreg: characterisation of handling, drape and tack properties. Compos. Struct. 66 (2004) 169-174.
[220] Buehler F, Seferis J. Effect of reinforcement and solvent content on moisture absorption in epoxy composite materials. Compos. Part A: Appl. Sci. Manuf. 31 (2000) 741-748.
[221] Popp A, Klostermann D, Chartoff R. Correlation of Prepreg Tack with Process Performance in Laminated Object Manufacturing. SAMPE North America Conference. Long Beach (USA), 2000.
[222] Hayes BS, Seferis JC, Chen JS. Development and hot-melt impregnation of a model controlled flow prepreg system. Polym. Compos. 17 (1996) 730-742.
[223] Putnam JW, Seferis JC, Pelton T, Wilhelm M. Perceptions of Prepreg Tack for Manufacturability in Relation to Experimental Measures. Sci. Eng. Compos. Mater. 4 (1995) 55.
[224] Ahn KJ, Peterson L, Seferis JC, Nowacki D, Zachmann HG. Prepreg aging in relation to tack. J. Appl. Polym. Sci. 45 (1992) 399-406.
[225] Ahn KJ, Seferis JC, Pelton T, Wilhelm M. Analysis and characterization of prepreg tack. Polym. Compos. 13 (1992) 197-206.
[226] Ahn KJ, Seferis JC, Pelton T, Wilhelm M. Deformation parameters influencing prepreg tack. SAMPE Quaterly 23 (1992) 54-64.
[227] Cole KC, Noël D, Hechler J-J, Cielo P, Krapez J-C, Chouliotis A, Overbury KC. Room-temperature aging of Narmco 5208 carbon-epoxy prepreg. Part II: Physical, mechanical, and nondestructive characterization. Polym. Compos. 12 (1991) 203-212.

[228] McIlhagger A, Archer E, McIlhagger R. Manufacturing processes for composite materials and components for aerospace applications, in: Irving P, Soutis C (Eds.) Polymer Composites in the Aerospace Industry. Amsterdam: Elsevier, 2020.
[229] Astrom BT. Manufacturing of Polymer Composites. Boca Raton: CRC Press, 2018.
[230] Lichtinger R, Hörmann P, Stelzl D, Hinterhölzl R. The effects of heat input on adjacent paths during Automated Fibre Placement. Compos. Part A: Appl. Sci. Manuf. 68 (2015) 387-397.
[231] Hörmann P, Stelzl D, Lichtinger R, van Nieuwenhove S, Mazón Carro G, Drechsler K. On the numerical prediction of radiative heat transfer for thermoset automated fiber placement. Compos. Part A: Appl. Sci. Manuf. 67 (2014) 282-288.
[232] Hassan N, Thompson JE, Batra RC, Hulcher AB, Song X, Loos AC. A Heat Transfer Analysis of the Fiber Placement Composite Manufacturing Process. J. Reinf. Plast. Compos. 24 (2005) 869-888.
[233] Orth T, Krahl M, Parlevliet P, Modler N. Optical thermal model for LED heating in thermoset-automated fiber placement. Adv. Manuf. Polym. Compos. Sci. 4 (2018) 73-82.
[234] Sarrazin H, Springer GS. Thermochemical and Mechanical Aspects of Composite Tape Laying. J. Compos. Mater. 29 (1995) 1908-1943.
[235] Benedek I. Pressure-Sensitive Adhesives and Applications. Boca Raton: CRC Press, 2004.
[236] Benedek I, Feldstein MM. Fundamentals of pressure sensitivity. Boca Raton: CRC Press, 2009.
[237] Czech Z, Kowalczyk A. Pressure-Sensitive Adhesives for Medical Applications, in: Akyar I (Ed.) Wide Spectra of Quality Control. London: InTech, 2011.
[238] Paul CW. Pressure-Sensitive Adhesives (PSAs), in: Da Silva LFM, Öchsner A, Adams RD (Eds.) Handbook of Adhesion Technology. Berlin, Heidelberg: Springer, 2011.
[239] Sun S, Li M, Liu A. A review on mechanical properties of pressure sensitive adhesives. Int. J. Adhes. Adhes. 41 (2013) 98-106.
[240] Satas D. Handbook of pressure sensitive adhesive technology. Boston: Springer US, 1989.
[241] Lukaszewicz DH-J. Optimisation of high-speed automated layup of thermoset carbon-fibre preimpregnates. Doctoral Thesis. Bristol (UK): University of Bristol, 2011.
[242] Cheng J, Zhao D, Liu K, Wang Y, Chen H. Modeling and impact analysis on contact characteristic of the compaction roller for composite automated placement. J. Reinf. Plast. Compos. 37 (2018) 1418-1432.
[243] Creton C, Leibler L. How does tack depend on time of contact and contact pressure? J. Polym. Sci. B Polym. Phys. 34 (1996) 545-554.
[244] Tsukatani T, Hatano Y, Mizumachi H. Bonding and Debonding Processes in Tack of Pressure-Sensitive Adhesives. J. Adhes. 31 (1989) 59-71.
[245] Dahlquist CA. Pressure-Sensitive adhesives, in: Patrick RL (Ed.) Treatise on adhesion and adhesives. Volume I: Theory. New York: Dekker Publishing, 1969.
[246] Pocius AV. Adhesion and Adhesives Technology. Munich: Hanser, 2012.
[247] Abbott S. Adhesion Science: Principles and Practice. Lancaster: DEStech Publications, 2015.
[248] Lopes CS, Gürdal Z, Camanho PP. Variable-stiffness composite panels: Buckling and first-ply failure improvements over straight-fibre laminates. Comput. Struct. 86 (2008) 897-907.
[249] Chiche A, Pareige P, Creton C. Role of surface roughness in controlling the adhesion of a soft adhesive on a hard surface. C.R. Acad. Sci., Ser. IV 1 (2000) 1197-1204.
[250] Ben-Zion O, Nussinovitch A. Testing the rolling tack of pressure-sensitive adhesive materials. Part II: Effect of adherend surface roughness. J. Adhes. Sci. Technol. 16 (2002) 599-619.
[251] Kinloch AJ. Adhesion and Adhesives: Science and Technology. Dordrecht: Springer Netherlands, 2012.
[252] Andrews D, Scholes G, Wiederrecht G. Comprehensive Nanoscience and Technology. Amsterdam: Elsevier Science, 2010.
[253] Stone A. The Theory of Intermolecular Forces. Oxford: Oxford University Press, 2013.
[254] Jones RW, Ng Y, McClelland JF. Monitoring ambient-temperature aging of a carbon-fiber/epoxy composite prepreg with photoacoustic spectroscopy. Compos. Part A: Appl. Sci. Manuf. 39 (2008) 965-971.
[255] Stark EB, Ibrahim AM, Munns TE, Seferis JC. Moisture effects during cure of high-performance epoxy matrices. J. Appl. Polym. Sci. 30 (1985) 1717-1731.

[256] Raponi OdA, Raponi RdA, Barban GB, Di Benedetto RM, Ancelotti Junior AC. Development of a Simple Dielectric Analysis Module for Online Cure Monitoring of a Commercial Epoxy Resin Formulation. Mat. Res. 20 (2017) 291-297.
[257] Shin JH, Kim D, Centea T, Nutt SR. Thermoplastic prepreg with partially polymerized matrix: Material and process development for efficient part manufacturing. Compos. Part A: Appl. Sci. Manuf. 119 (2019) 154-164.
[258] Agius SL, Magniez K, Fox BL. Cure behaviour and void development within rapidly cured out-of-autoclave composites. Compos. Part B: Eng. 47 (2013) 230-237.
[259] Grunenfelder LK, Nutt SR. Void formation in composite prepregs – Effect of dissolved moisture. Compos. Sci. Technol. 70 (2010) 2304-2309.
[260] Akay M, Ah Mun SK, Stanley A. Influence of moisture on the thermal and mechanical properties of autoclaved and oven-cured Kevlar-49/epoxy laminates. Compos. Sci. Technol. 57 (1997) 565-571.
[261] Moy P, Karasz FE. Epoxy-water interactions. Polym. Eng. Sci. 20 (1980) 315-319.
[262] Li L, Tirrell M, Korba GA, Pocius AV. Surface Energy and Adhesion Studies on Acrylic Pressure Sensitive Adhesives. J. Adhes. 76 (2001) 307-334.
[263] Sowa D, Czech Z, Byczyński Ł. Peel adhesion of acrylic pressure-sensitive adhesives on selected substrates versus their surface energies. Int. J. Adhes. Adhes. 49 (2014) 38-43.
[264] Tobing SD, Klein A. Molecular parameters and their relation to the adhesive performance of emulsion acrylic pressure-sensitive adhesives. II. Effect of crosslinking. J. Appl. Polym. Sci. 79 (2001) 2558-2564.
[265] Khan I, Poh BT. Natural Rubber-Based Pressure-Sensitive Adhesives: A Review. J. Polym. Environ. 19 (2011) 793.
[266] Czech Z, Pełech R. Thermal decomposition of polyurethane pressure-sensitive adhesives dispersions. Prog. Org. Coat. 67 (2010) 72-75.
[267] Webster I. Recent developments in pressure-sensitive adhesives for medical applications. Int. J. Adhes. Adhes. 17 (1997) 69-73.
[268] Lukaszewicz DH-JA, Potter K. Through-thickness compression response of uncured prepreg during manufacture by automated layup. Proc. Inst. Mech. Eng., Part B: J. Eng. Manuf. 226 (2012) 193-202.
[269] Cho KS. Viscoelasticity of Polymers: Theory and Numerical Algorithms. Dordrecht: Springer Netherlands, 2016.
[270] Ferry JD. Viscoelastic properties of polymers. New York, Chichester, Brisbane, Toronto, Singapore: John Wiley & Sons, 1980.
[271] Kaelble DH. Peel Adhesion: Influence of Surface Energies and Adhesive Rheology. J. Adhes. 1 (1969) 102-123.
[272] Tse MF, Jacob L. Pressure Sensitive Adhesives Based on Vector R SIS Polymers I. Rheological Model and Adhesive Design Pathways. J. Adhes. 56 (1996) 79-95.
[273] Chang EP. Viscoelastic Windows of Pressure-Sensitive Adhesives. J. Adhes. 34 (1991) 189-200.
[274] Chopin J, Villey R, Yarusso D, Barthel E, Creton C, Ciccotti M. Nonlinear Viscoelastic Modeling of Adhesive Failure for Polyacrylate Pressure-Sensitive Adhesives. Macromolecules 51 (2018) 8605-8610.
[275] Du J, Lindeman DD, Yarusso DJ. Modelling the peel performance of pressure-sensitive adhesives. J. Adhes. 80 (2004) 601-612.
[276] Mohammed IK, Charalambides MN, Kinloch AJ. Modeling the effect of rate and geometry on peeling and tack of pressure-sensitive adhesives. J. Non-Newtonian Fluid Mech. 233 (2016) 85-94.
[277] Forghani A, Hickmott C, Bedayat H, Wohl C, Grimsley BW, Coxon B, Poursartip A. A Physics-Based Modelling Framework for Simulation of Prepreg Tack in AFP Process. SAMPE North America Conference. Seattle (USA), 2017.
[278] Forghani A, Hickmott CW, Bedayat H, Wohl C, Grimsley BW, Coxon B, Poursartip A. Simulating Prepreg Tack in AFP Process, in: Yu W, Pipes RB, Goodsell J (Eds.) Proceedings of the American Society for Composites Conference. Lancaster: DEStech Publications, 2017.

[279] Forghani A, Hickmott C, Hutten V, Bedayat H, Wohl C, Grimsley BW, Coxon B, Poursartip A. Experimental Calibration of a Numerical Model of Prepreg Tack for Predicting AFP Process Related Defects. SAMPE North America Conference. Long Beach (USA), 2018.
[280] Hutten V, Forghani A, Silva P, Hickmott C, Sreekantamurthy T, Wohl C, Grimsley BW, Coxon B, Poursartip A. A Validation Study of a Physics-based Tack Model for an Automated Fiber Placement Process Simulation. SAMPE North America Conference. Charlotte (USA), 2019.
[281] Dillman SH, Seferis JC. Kinetic Viscoelasticity for the Dynamic Mechanical Properties of Polymeric Systems. Journal of Macromolecular Science: Part A - Chemistry 26 (1989) 227-247.
[282] Woo EM, Seferis JC, Schaffnit RS. Viscoelastic characterization of high performance epoxy matrix composites. Polym. Compos. 12 (1991) 273-280.
[283] ASTM D8336-21. Standard Test Method for Characterizing Tack of Prepregs Using a Continuous Application-and-Peel Procedure. West Conshohocken: ASTM International, 2021.
[284] De Focatiis D, Choong GYH, Joesbury A, Endruweit A. Development of the ASTM D8336 21: Standard Test Method for Characterizing Tack of Prepregs using a Continuous Application and Peel Procedure. European Conference on Composite Materials. Lausanne (Switzerland), 2022.
[285] Budelmann D, Schmidt C, Meiners D. Measuring techniques for prepreg tackiness: A comparative study. SAMPE Europe Conference. El Escorial Madrid (Spain), 2023.
[286] Smith AW, Endruweit A, Choong G, Focatiis D de, Hubert P. Adaptation of material deposition parameters to account for out-time effects on prepreg tack. Compos. Part A: Appl. Sci. Manuf. 133 (2020) 105835.
[287] Belhaj M, Dodangeh A, Hojjati M. Experimental investigation of prepreg tackiness in automated fiber placement. Compos. Struct. 262 (2021) 113602.
[288] Netzel C, Hoffmann D, Battley M, Hubert P, Bickerton S. Effects of environmental conditions on uncured prepreg characteristics and their effects on defect generation during autoclave processing. Compos. Part A: Appl. Sci. Manuf. 151 (2021) 106636.
[289] Heller K, Colin D, Drechsler K. Quantifying the Influence of Out-Time on Prepreg Material Properties and Out-Of-Plane Steering Defects During Automated Fiber Placement. Front. Mater. 9 (2022) 399.
[290] Heller K. Influence of Material Property Changes on Thermoset Automated Fiber Placement Processing. Doctoral Thesis. Munich: TU Munich, 2022.
[291] Pan H, Qu W, Di Yang, Li J, Ke Y. Analysis and characterization of interlaminar tack for different prepreg materials during automated fiber placement. Polym. Compos. 43 (2022) 4737-4748.
[292] Pan H, Di Yang, Qu W, Li J, Ke Y. Process-dependent wrinkle formation for steered tow during automated fiber placement: Modeling and experimental verification. Thin-Walled Struct. 180 (2022) 109928.
[293] Wang Y, Mahapatra S, Belnoue JP-H, Ivanov DS, Hallett SR. Understanding tack behaviour during prepreg-based composites' processing. Compos. Part A: Appl. Sci. Manuf. 164 (2023) 107284.
[294] Pouladvand AR, Mortezaei M, Fattahi H, Amraei IA. A novel custom-tailored epoxy prepreg formulation based on epoxy-amine dual-curable systems. Compos. Part A: Appl. Sci. Manuf. 132 (2020) 105852.
[295] Mbotto Tonye D, Buet Gautier K. Influence of the reinforcement on prepreg tack. Polym. Compos. 42 (2021) 4795-4803.
[296] Hübner F, Meuchelböck J, Wolff-Fabris F, Mühlbach M, Altstädt V, Ruckdäschel H. Fast curing unidirectional carbon epoxy prepregs based on a semi-latent hardener: The influence of ambient aging on the prepregs Tg0, processing behavior and thus derived interlaminar performance of the composite. Compos. Sci. Technol. 216 (2021) 109047.
[297] Kuliaei A, Amiri Amraei I, Mousavi SR. Investigating the relationship between tack and degree of conversion in DGEBA-based epoxy resin cured with dicyandiamide and diuron. J. Polym. Eng. 41 (2021) 537-545.

[298] Szpoganicz E, Demleitner M, Hübner F, Oh Y, Kweon Y, Lee H, Altstädt V, Ruckdäschel H. Phenolic prepregs for automated composites manufacturing – Correlation of rheological properties and environmental factors with prepreg tack. Compos. Sci. Technol. 218 (2022) 109188.
[299] Silva SO, Teixeira LA, Gontijo AB, Luz SM. Processing Characterization of Sisal/Epoxy Prepregs. J. Res. Updates Polym. Sci. 10 (2021) 42-50.
[300] Malakhovskii SS, Kostromina NV, Olikhova YV, Kravchenko TP, Gorbunova IY. Sticking Control of Prepregs Based on ED-20 Resin. Polym. Sci. Ser. D 16 (2023) 94-97.
[301] Rajan S, Sutton MA, McMakin W, Compton E, Kidane A, Gurdal Z, Wehbe R, Farzana Y. Characterization of Mode I and Mode II traction–separation laws for cohesive separation of uncured thermoset tows. Int. J. Fract. 221 (2020) 25-38.
[302] Choong G, Endruweit A, Focatiis D de. Analysis of contact area in a continuous application-and-peel test method for prepreg tack. Int. J. Adhes. Adhes. 107 (2021) 102849.
[303] Das A, Choong GY, Dillard DA, Focatiis DS de, Bortner MJ. Characterizing friction for fiber reinforced composites manufacturing: Method development and effect of process parameters. Compos. Part B: Eng. 236 (2022) 109777.
[304] Zu L, Xia X, Zhang Q, Jia X, Wang H, Zhang G, Lu J. Influence and optimization of parameters of prepreg viscosity during placement. Chin. J. Aeronaut. 35 (2022) 438-449.
[305] Xiao R, Wang W, Shi J, Xiao J. Two-stage model of prepreg bonding interface formation in automated fiber placement process. J. Reinf. Plast. Compos. 41 (2022) 583-601.
[306] Del Retuerta Rey G, Fernández Gorgojo A, Fernández Blázquez JP, Chacón Tanarro E. Calculation of Williams-Landel Ferry Shift Factors via Probe Tack Testing for Uncured Prepreg Materials. Ibero-American Congress of Mechanical Engineering. Las Vegas (USA), 2022.
[307] Osswald TA. Understanding Polymer Processing. Munich: Hanser, 2017.
[308] Gay D. Composite Materials: Design and Applications. Boca Raton: CRC Press, 2014.
[309] Heider D, Piovoso MJ, Gillespie Jr JW. Application of a neural network to improve an automated thermoplastic tow-placement process. J. Proc. Contr. 12 (2002) 101-111.
[310] Wang R, Zheng S, Zheng Y. Polymer matrix composites and technology. Oxford, Philadelphia, Beijing: Woodhead Publishing, 2011.
[311] Beakou A, Cano M, Le Cam J-B, Verney V. Modelling slit tape buckling during automated prepreg manufacturing: A local approach. Compos. Struct. 93 (2011) 2628-2635.
[312] Akay M. Effects of prepreg ageing and post-cure hygrothermal conditioning on the mechanical behaviour of carbon-fibre/epoxy laminates. Compos. Sci. Technol. 38 (1990) 359-370.
[313] Schmidt C, Weber P, Hocke T, Denkena B. Influence of Prepreg Material Quality on Carbon Fiber Reinforced Plastic Laminates Processed by Automated Fiber Placement. Procedia CIRP 67 (2018) 422-427.
[314] Blass D, Kreling S, Dilger K. The impact of prepreg aging on its processability and the postcure mechanical properties of epoxy-based carbon-fiber reinforced plastics. Proc. Inst. Mech. Eng., Part L: J. Mater.: Des. Appl. 231 (2017) 62-72.
[315] Denkena B, Schmidt C, Werner S. Continuous Draping of Double Curved Geometries – A Geometrical Approach to Describe an Automated Layup Process of Fabrics on Complex Surfaces. SAMPE Europe Conference. Southhampton, 2018.
[316] Aized T, Shirinzadeh B. Robotic fiber placement process analysis and optimization using response surface method. Int. J. Adv. Manuf. Technol. 55 (2011) 393-404.
[317] Aguirreurreta Z, Dimmer J-A, Willerich I, Leiza JR, La Cal JC de. Improving the properties of water-borne pressure sensitive adhesives by using non-migratory surfactants. Int. J. Adhes. Adhes. 70 (2016) 287-296.
[318] Karyu N, Noda M, Fujii S, Nakamura Y, Urahama Y. Effect of adhesive thickness on the wettability and deformability of polyacrylic pressure-sensitive adhesives during probe tack test. J. Appl. Polym. Sci. 133 (2016).

[319] Nakamura Y, Imamura K, Ito K, Nakano S, Sueoka A, Fujii S, Sasaki M, Urahama Y. Contact Time and Temperature Dependencies of Tack in Polyacrylic Block Copolymer Pressure-Sensitive Adhesives Measured by the Probe Tack Test. J. Adhes. Sci. Technol. 26 (2012) 231-249.
[320] Wisanrakkit G, Gillham JK. The glass transition temperature (Tg) as an index of chemical conversion for a high-Tg amine/epoxy system: Chemical and diffusion-controlled reaction kinetics. J. Appl. Polym. Sci. 41 (1990) 2885-2929.
[321] Grunenfelder LK, Nutt SR. Prepreg age monitoring via differential scanning calorimetry. J. Reinf. Plast. Compos. 31 (2012) 295-302.
[322] Juarez PD, Cramer KE, Seebo JP. Advances in in situ inspection of automated fiber placement systems. SPIE Commercial + Scientific Sensing and Imaging. Baltimore (USA), 2016.
[323] Creton C. Pressure-Sensitive Adhesives: An Introductory Course. MRS Bull. 28 (2003) 434-439.
[324] Czech Z, Wilpiszewska K, Tyliszczak B, Jiang X, Bai Y, Shao L. Biodegradable self-adhesive tapes with starch carrier. Int. J. Adhes. Adhes. 44 (2013) 195-199.
[325] Lee L-H. Fundamentals of Adhesion. Boston: Springer, 1991.
[326] HexPly 8552: Epoxy matrix (180°C/356°F curing matrix). Data sheet. Stamford (USA): Hexcel Corporation, 2020.
[327] Paiva JMF de, Santos ADNd, Rezende MC. Mechanical and morphological characterizations of carbon fiber fabric reinforced epoxy composites used in aeronautical field. Mat. Res. 12 (2009) 367-374.
[328] Young T. An essay on the cohesion of fluids. Phil. Trans. R. Soc. 95 (1805) 65-87.
[329] Owens DK, Wendt RC. Estimation of the surface free energy of polymers. J. Appl. Polym. Sci. 13 (1969) 1741-1747.
[330] ASME B46.1-2019. Surface Texture (Surface Roughness, Waviness, and Lay). Washington: American National Standards Institute, 2019.
[331] Synytska A, Michel S, Pleul D, Bellmann C, Schinner R, Eichhorn K-J, Grundke K, Neumann AW, Stamm M. Monitoring the surface tension of reactive epoxy-amine systems under different environmental conditions. J. Adhes. 80 (2004) 667-683.
[332] Page SA, Mezzenga R, Boogh L, Berg JC, Månson J-AE. Surface Energetics Evolution during Processing of Epoxy Resins. J. Colloid Interface Sci. 222 (2000) 55-62.
[333] Ma Y, Nutt S. Chemical treatment for recycling of amine/epoxy composites at atmospheric pressure. Polym. Degrad. Stab. 153 (2018) 307-317.
[334] Zhu Y-F, Zhang Z, Litt MH, Zhu L. High Dielectric Constant Sulfonyl-Containing Dipolar Glass Polymers with Enhanced Orientational Polarization. Macromolecules 51 (2018) 6257-6266.
[335] Kim J-H, Rothstein JP. Dynamic contact angle measurements of viscoelastic fluids. J. Non-Newtonian Fluid Mech. 225 (2015) 54-61.
[336] Kajiya T, Daerr A, Narita T, Royon L, Lequeux F, Limat L. Advancing liquid contact line on visco-elastic gel substrates: stick-slip vs. continuous motions. Soft Matter 9 (2013) 454-461.
[337] Nase J, Creton C, Ramos O, Sonnenberg L, Yamaguchi T, Lindner A. Measurement of the receding contact angle at the interface between a viscoelastic material and a rigid surface. Soft Matter 6 (2010) 2685.
[338] Lee JH, Lee DW. Contact-induced molecular rearrangement of acrylic acid-incorporated pressure sensitive adhesives. Appl. Surf. Sci. 500 (2020) 144246.
[339] Packham DE. Work of adhesion: contact angles and contact mechanics. Int. J. Adhes. Adhes. 16 (1996) 121-128.
[340] Fuensanta M, Martin-Martínez JM. Thermoplastic polyurethane pressure sensitive adhesives made with mixtures of polypropylene glycols of different molecular weights. Int. J. Adhes. Adhes. 88 (2019) 81-90.
[341] Droesbeke MA, Simula A, Asua JM, Du Prez FE. Biosourced terpenoids for the development of sustainable acrylic pressure-sensitive adhesives via emulsion polymerisation. Green Chem. 22 (2020) 4561-4569.

[342] Wolff H-M, Irsan, Dodou K. Investigations on the viscoelastic performance of pressure sensitive adhesives in drug-in-adhesive type transdermal films. Pharm. Res. 31 (2014) 2186-2202.
[343] Maassen W, Meier MA, Willenbacher N. Unique adhesive properties of pressure sensitive adhesives from plant oils. Int. J. Adhes. Adhes. 64 (2016) 65-71.
[344] Peykova Y, Guriyanova S, Lebedeva OV, Diethert A, Müller-Buschbaum P, Willenbacher N. The effect of surface roughness on adhesive properties of acrylate copolymers. Int. J. Adhes. Adhes. 30 (2010) 245-254.
[345] Ciavarella M, Papangelo A. A Generalized Johnson Parameter for Pull-Off Decay in the Adhesion of Rough Surfaces. Phys. Mesomech. 21 (2018) 67-75.
[346] Mangalgiri PD. Composite materials for aerospace applications. Bull. Mater. Sci. 22 (1999) 657-664.
[347] Paiva JMF, Costa ML, Rezende MC. Evaluation of Thermal Stability and Glass Transition Temperature of Different Aeronautical Polymeric Composites. Polym.-Plast. Technol. Mater. 45 (2006) 157-164.
[348] Galos J. Thin-ply composite laminates: a review. Compos. Struct. 236 (2020) 111920.
[349] Kim D, Nutt SR. Processability of DDS isomers-cured epoxy resin: Effects of amine/epoxy ratio, humidity, and out-time. Polym. Eng. Sci. 58 (2018) 1530-1538.
[350] Hassan MK, Tucker SJ, Abukmail A, Wiggins JS, Mauritz KA. Polymer chain dynamics in epoxy based composites as investigated by broadband dielectric spectroscopy. Arab. J. Chem. 9 (2016) 305-315.
[351] Sun Z, Xu L, Chen Z, Wang Y, Tusiime R, Cheng C, Zhou S, Liu Y, Yu M, Zhang H. Enhancing the Mechanical and Thermal Properties of Epoxy Resin via Blending with Thermoplastic Polysulfone. Polymers (Basel) 11 (2019).
[352] Rosetti Y, Alcouffe P, Pascault J-P, Gérard J-F, Lortie F. Polyether Sulfone-Based Epoxy Toughening: From Micro- to Nano-Phase Separation via PES End-Chain Modification and Process Engineering. Materials (Basel) 11 (2018).
[353] Park S-J, Kim H-C. Thermal stability and toughening of epoxy resin with polysulfone resin. J. Polym. Sci. B Polym. Phys. 39 (2001) 121-128.
[354] Essmeister J, Taublaender MJ, Koch T, Cerrón-Infantes DA, Unterlass MM, Konegger T. High modulus polyimide particle-reinforcement of epoxy composites. Mater. Adv. 2 (2021) 2278-2288.
[355] Cho JB, Hwang JW, Cho K, An JH, Park CE. Effects of morphology on toughening of tetrafunctional epoxy resins with poly(ether imide). Polymer 34 (1993) 4832-4836.
[356] Chen Q, Wang S, Qin F, Liu K, Liu Q, Zhao Q, Wang X-Y, Hu Y-H. Soluble Polyimide-reinforced TGDDM and DGEBA Epoxy Composites. Chin. J. Polym. Sci. 38 (2020) 867-876.
[357] Brooker RD, Kinloch AJ, Taylor AC. The Morphology and Fracture Properties of Thermoplastic-Toughened Epoxy Polymers. J. Adhes. 86 (2010) 726-741.
[358] Jones AR, Watkins CA, White SR, Sottos NR. Self-healing thermoplastic-toughened epoxy. Polymer 74 (2015) 254-261.
[359] Asaro L, Rivero G, Manfredi LB, Alvarez VA, Rodriguez ES. Development of carbon fiber/phenolic resin prepregs modified with nanoclays. J. Compos. Mater. 50 (2016) 1287-1300.
[360] Amirova L, Schadt F, Grob M, Brauner C, Ricard T, Wille T. Properties and structure of high temperature resistant cyanate ester/polyethersulfone blends using solvent-free toughening approach. Polym. Bull. 79 (2022) 213-225.
[361] Flynn JH, Wall LA. A quick, direct method for the determination of activation energy from thermogravimetric data. J. Polym. Sci. B Polym. Lett. 4 (1966) 323-328.
[362] Flynn JH, Wall LA. General Treatment of the Thermogravimetry of Polymers. J. Res. Natl. Bur. Stand. A Phys. Chem. 70A (1966) 487-523.
[363] Ozawa T. A New Method of Analyzing Thermogravimetric Data. BCSJ 38 (1965) 1881-1886.
[364] Budelmann D, Schmidt C, Meiners D. Adhesion-cohesion balance of prepreg tack in thermoset automated fiber placement. Part 1: Adhesion and surface wetting. Compos. Part C: Open Access 6 (2021) 100204.

[365] Yousefi A, Lafleur PG, Gauvin R. Kinetic studies of thermoset cure reactions: A review. Polym. Compos. 18 (1997) 157-168.
[366] Wazalwar R, Raichur AM. Model-free cure kinetics of tetra-functional epoxy reinforced with GO and p-Phenylenediamine modified GO. Thermochim. Acta 697 (2021) 178857.
[367] Pramanik M, Fowler EW, Rawlins JW. Another look at epoxy thermosets correlating structure with mechanical properties. Polym. Eng. Sci. 54 (2014) 1990-2004.
[368] Deng X. Progress on rubber-based pressure-sensitive adhesives. J. Adhes. 94 (2018) 77-96.
[369] Eschen H, Harnisch M, Schüppstuhl T. Flexible and automated production of sandwich panels for aircraft interior. Procedia Manuf. 18 (2018) 35-42.
[370] Zhang L, Wang X, Pei J, Zhou Y. Review of automated fibre placement and its prospects for advanced composites. J. Mater. Sci. 55 (2020) 7121-7155.
[371] Donough MJ, Shafaq, St John NA, Philips AW, Gangadhara Prusty B. Process modelling of In-situ consolidated thermoplastic composite by automated fibre placement – A review. Compos. Part A: Appl. Sci. Manuf. 163 (2022) 107179.
[372] Brasington A, Francis B, Godbold M, Harik R. A review and framework for modeling methodologies to advance automated fiber placement. Compos. Part C: Open Access 10 (2023) 100347.
[373] Yadav N, Schledjewski R. Review of in-process defect monitoring for automated tape laying. Compos. Part A: Appl. Sci. Manuf. (2023) 107654.
[374] Heathman N, Koirala P, Yap T, Emami A, Tehrani M. In situ consolidation of carbon fiber PAEK via laser-assisted automated fiber placement. Compos. Part B: Eng. 249 (2023) 110405.
[375] Anay R, Miller D, Tessema A, Wehbe R, Ziehl P, Tatting B, Gurdal Z, Harik R, Kidane A. An experimental investigation concerning the effect of AFP defects on progressive damage in CFRP coupons. Compos. Struct. 279 (2022) 114725.
[376] Friedel A, Heimbs S, Horst P, Schmidt C, Timmermann M. Representative structural element approach for assessing the mechanical properties of automated fibre placement-induced defects. Compos. Part C: Open Access (2023) 100350.
[377] Wang H, Wang W, Wang H, Dong H, Ke Y. Thermal management for thermoset automated fiber placement based on infrared heater structure arrangement. Chin. J. Aeronaut. 35 (2022) 173-183.
[378] Wehbe R, Sacco C, Baz Radwan A, Albazzan M, Harik R. Influence of process parameters in AFP fiber steering on cylinders: Constant curvature paths. Compos. Part C: Open Access 2 (2020) 100036.
[379] Budelmann D, Schmidt C, Meiners D. Tack of epoxy resin films for aerospace-grade prepregs: Influence of resin formulation, B-staging and toughening. Polym. Test. 114 (2022) 107709.
[380] Awaja F. Autohesion of polymers. Polymer 97 (2016) 387-407.
[381] Khodaei A, Shadmehri F. Intimate contact development for automated fiber placement of thermoplastic composites. Compos. Part C: Open Access 8 (2022) 100290.
[382] Levy A, Heider D, Tierney J, Gillespie JW. Inter-layer thermal contact resistance evolution with the degree of intimate contact in the processing of thermoplastic composite laminates. J. Compos. Mater. 48 (2014) 491-503.
[383] Çelik O, Peeters D, Dransfeld C, Teuwen J. Intimate contact development during laser assisted fiber placement: Microstructure and effect of process parameters. Compos. Part A: Appl. Sci. Manuf. 134 (2020) 105888.
[384] Chu Q, Li Y, Xiao J, Huan D, Zhang X, Chen X. Processing and characterization of the thermoplastic composites manufactured by ultrasonic vibration–assisted automated fiber placement. J. Thermoplast. Compos. Mater. 31 (2018) 339-358.
[385] Stokes-Griffin CM, Compston P. Investigation of sub-melt temperature bonding of carbon-fibre/PEEK in an automated laser tape placement process. Compos. Part A: Appl. Sci. Manuf. 84 (2016) 17-25.
[386] Gutowski TG, Bonhomme L. The Mechanics of Prepreg Conformance. J. Compos. Mater. 22 (1988) 204-223.
[387] Wool RP, O'Connor KM. A theory crack healing in polymers. J. Appl. Phys. 52 (1981) 5953-5963.

[388] Kendall K. Thin-film peeling-the elastic term. J. Phys. D: Appl. Phys. 8 (1975) 1449-1452.
[389] Lee WI, Springer GS. A Model of the Manufacturing Process of Thermoplastic Matrix Composites. J. Compos. Mater. 21 (1987) 1017-1055.
[390] Szcesny M, Heieck F, Carosella S, Middendorf P, Sehrschön H, Schneiderbauer M. The advanced ply placement process – an innovative direct 3D placement technology for plies and tapes. Adv. Manuf. Polym. Compos. Sci. 3 (2017) 2-9.
[391] Mantell SC, Springer GS. Manufacturing Process Models for Thermoplastic Composites. J. Compos. Mater. 26 (1992) 2348-2377.
[392] Butler CA, Mccullough RL, Pitchumani R, Gillespie JW. An Analysis of Mechanisms Governing Fusion Bonding of Thermoplastic Composites. J. Thermoplast. Compos. Mater. 11 (1998) 338-363.
[393] Gohl JA, Thiele-Sardina TC, Rencheck ML, Erk KA, Davis CS. A Modular Peel Fixture for Tape Peel Tests on Immovable Substrates. Exp. Mech. 61 (2021) 1209-1213.
[394] Mai V-D, Shin S-R, Lee D-S, Kang I. Thermal Healing, Reshaping and Ecofriendly Recycling of Epoxy Resin Crosslinked with Schiff Base of Vanillin and Hexane-1,6-Diamine. Polymers (Basel) 11 (2019).
[395] Wu X, Yang X, Yu R, Zhao X-J, Zhang Y, Huang W. A facile access to stiff epoxy vitrimers with excellent mechanical properties via siloxane equilibration. J. Mater. Chem. A 6 (2018) 10184-10188.
[396] Khan MA, Mitschang P, Schledjewski R. Identification of some optimal parameters to achieve higher laminate quality through tape placement process. Adv. Polym. Technol. 29 (2010) 98-111.
[397] Meiners D. Beitrag zur Stabilität und Automatisierung von CFK-Produktionsprozessen. Doctoral Thesis. Clausthal-Zellerfeld: Clausthal University of Technology, 2007.
[398] Permadi, Castro JM. Development of an environmentally friendly solventless process for electronic prepregs. J. Appl. Polym. Sci. 91 (2004) 1136-1146.